Dissertation

submitted to the

Combined Faculties for the Natural Sciences and for Mathematics

of the Ruperto-Carola University of Heidelberg, Germany

for the degree of

Doctoral of Natural Sciences

Presented by

M. Sc. (Medical Biotechnology) **Stephanie S. Kapel**

Born in: Paramaribo, Suriname

Oral-examination: 19.04.2018

Regulation of blood pressure, VSMC function and atherosclerosis by Tie2-expressing non-endothelial mesenchymal cells

Referees:

Prof. Dr. Peter Angel

Prof. Dr. Hellmut G. Augustin

Die vorliegende Arbeit wurde in der Abteilung „Vaskuläre Onkologie und Metastasierung“ am Deutschen Krebsforschungszentrum (DKFZ) in Heidelberg zwischen März 2012 und April 2018 durchgeführt.

Acknowledgements

I would like to thank everyone who has supported me through this challenging journey and contributed towards the successful completion of my thesis.

A heartfelt thank you to my supervisor **Prof. Dr. Hellmut G. Augustin** for giving me the opportunity to work on this intriguing and challenging topic and for sculpting me into the young scientist that I am today.

I would like to thank **Prof. Dr. Peter Angel** and **Prof. Dr. Ingrid Fleming** for their input during my Thesis Advisory Committee meetings and for diversifying and guiding my thinking.

I would also like to thank my collaborators **Prof. Dr. Thomas Korff**, **Dr. Oliver Drews**, **Dr. Caroline Arnold,** and **Felix Trogisch** for the cooperation, advice, and guidance that I received during my research.

I am especially grateful to **Anja Runge** and **Nicolas Gengenbacher** for constructive and meticulous corrections of my thesis. Many thanks to **Anja Runge**, **Jingjing Shi**, **Zulfiyya Hasanov**, **Laura Milde** and **Mahak Singhal** for their invaluable discussions and continuous support.

Thanks to my past and present **A190 family** for the support, patience, encouragement, lively discussions and for all the scientific and non-scientific experiences together. Soniya Savant, Claudia Korn, Beate Scholz, Junhao Hu, Kshitij Srivastava, Sila Appak-Baskoy, Zulfiyya Hasanov, Martin Teichert, Martin Augsten, Tina Heumann, Courtney König, Lise Roth, Anja Runge, Moritz Jakob, Silvia La Porta, Evangelia Giannakouri, Ashik Abdul Pari, Laura Milde, Katharina Schlereth, Nicolas Gengenbacher, Mahak Singhal, Jingjing Shi, Donato Inverso, Corinne Bauer, Ki Hong Lee, Maximilian Kriegmair, Jessica Wojtarowicz, Stella Hertel, Eva Besemfelder, Dorothee Terhardt, Benjamin Schieb, Maria Riedel, Carleen Spegg, Maike Deckers, Daniela Dietz and Barbara Böck, thanks for the cheerful and friendly atmosphere and for brightening my days at work. It has been a pleasure to work with all of you.

My sincere thanks go to **Jessica Wojtarowicz**, **Stella Hertel**, **Maria Riedel** and **Carleen Spegg** for their excellent technical support.

My appreciation and thanks go to **Dr. Damir Krunic**, **Dr. Felix Bestvater** and **Manuela Brom** for introducing me to the world of imaging and data processing.

I am grateful for '**The girls**', Tina Heumann, Silvia La Porta, Evangelia Giannakouri, Anja Runge, Lise Roth, Soniya Savant, Claudia Korn, Beate Scholz, Courtney König, Katharina Schlereth, Aida Freire Valls, Maike Deckers, Laura Milde and Jingjing Shi, who became true friends and with whom I shared wonderful times with, both inside and outside the lab. From the funny discussions during lunch-time, great times at Eckstein, Christmas-market, Karneval in Bonn/Köln 'Kölle Alaaf', to my bachelorette party in Vasto and trips to Stockholm, Kopenhagen, and Cambridge. May our friendship and our craziness never end!

I would especially like to thank my amazing (immediate, extended, in-laws) family for their years of unconditional love, support, and constant encouragement. In particular, I would express a deep sense of gratitude to my lovely parents, **Lucia Kapel-Etnel** and **Hedwig Kapel**, who have always stood by me through thick and thin and who have always believed in me. You are my rock and I undoubtedly could not have done this without you. **Gabriela**, my sweet sister, thank you for sending me messages like 'I miss you' and 'U got this', at the right moment. **Dion**, my dear brother, thank you for being my 'Bigzie'.

Last but not least, I would like to thank my beloved husband **Gunnar Picht** for his relentless faith, unconditional love, support, and understanding. Without your help and patience, I would not have managed to get this far. Thank you for being by my side through good and bad times. Thank you for making me a happy wife and giving me a happy life. I love you to the moon and back to infinity and beyond forever and ever!

Table of Contents

ACKNOWLEDGEMENTS V

TABLE OF CONTENTS VII

LIST OF FIGURES XII

LIST OF TABLES XIV

SUMMARY 1

ZUSAMMENFASSUNG 3

1 INTRODUCTION 5

1.1 THE VASCULAR SYSTEM 5

1.1.1 ARCHITECTURE AND FUNCTION OF BLOOD VESSELS 5

1.1.2 VASCULAR DEVELOPMENT 6

1.1.3 PHYSIOLOGICAL ANGIOGENESIS 6

1.1.3.1 PHASES OF ANGIOGENESIS 6

1.1.3.2 SIGNALING PATHWAYS IN ANGIOGENESIS 7

1.2 ANGPT/TIE SYSTEM 8

1.2.1 STRUCTURE OF TIE RECEPTORS AND ANGPT LIGANDS 8

1.2.2 EXPRESSION OF TIE RECEPTORS AND ANGPT LIGANDS 9

1.2.3 ANGPT/TIE SYSTEM: LOSS-AND GAIN-OF FUNCTION STUDIES 10

1.2.4 ANGPT1-INDUCED TIE2 SIGNALING 11

1.2.5 ANGPT2-MEDIATED TIE2 SIGNALING: AGONIST VS. ANTAGONIST PARADOX 13

1.3 VASCULAR SMOOTH MUSCLE CELLS 14

1.3.1 ORIGIN 14

1.3.2 LOCATION AND MORPHOLOGY 14

1.3.3 MOLECULAR SIGNATURE OF VSMC 16

1.3.4 ENDOTHELIAL-VSMC INTERACTION 17

1.3.5 REGULATORS OF VSMC PHENOTYPE 18

1.3.6 VSMC FUNCTION: FROM CARDIOVASCULAR HEALTH TO DISEASE 21

1.4 CARDIOVASCULAR DISEASES 22

1.4.1 EC DYSFUNCTION AND REACTIVE OXYGEN SPECIES 22

1.5 HYPERTENSION 23

1.5.1 VSMC REMODELING IN HYPERTENSION 23

1.5.1.1 LEFT VENTRICULAR HYPERTROPHY 24

1.5.1.2 CARDIOMYOCYTES 25

1.5.2 REGULATORS OF CM AND VSMC REMODELING IN HYPERTENSION 25
1.6 ATHEROSCLEROSIS 27
1.6.1 PHASES OF ATHEROSCLEROSIS 27
1.6.2 EC DYSFUNCTION AND ATHEROSCLEROSIS 29
1.6.3 INFLAMMATORY CELLS AND ATHEROSCLEROSIS 30
1.6.4 VSMC REMODELING AND ATHEROSCLEROSIS 30
1.6.5 LINK BETWEEN HYPERTENSION AND ATHEROSCLEROSIS 31
1.7 ANGPT/TIE SYSTEM IN CARDIOVASCULAR DISEASES 32
1.7.1 ANGPT/TIE SYSTEM DURING HYPERTENSION 32
1.7.2 ANGPT/TIE SYSTEM DURING ATHEROSCLEROSIS 32
1.7.3 ANGPT/TIE SYSTEM IN VSMC 33
1.8 AIM OF THE STUDY 33

2 RESULTS 34

2.1 VSMC-SPECIFIC EXPRESSION OF TIE2 34
2.2 SMC-SPECIFIC DELETION OF TIE2 36
2.3 VSMC-EXPRESSED TIE2 REGULATES PHENOTYPIC MODULATION OF ACTIVATED VSMC 39
2.4 VSMC-SPECIFIC TIE2 DELETION DOES NOT AFFECT BASELINE *IN VIVO* VSMC PHENOTYPE 41
2.5 VSMC-SPECIFIC TIE2 DELETION LEADS TO ENHANCED CONTRACTILE CAPACTITY OF FEMORAL ARTERIES UPON PRESSURE-CONTROLLED PERFUSION 42
2.6 SM22α-DRIVEN TIE2 DELETION AFFECTS BASELINE BLOOD PRESSURE 43
2.7 SM22α-DRIVEN TIE2 DELETION AFFECTS CARDIAC SIZE 45
2.8 SM22α-DRIVEN TIE2 DELETION REDUCES LEFT VENTRICULAR WALL- AND INTERVENTRICULAR SEPTUM THICKNESS 46
2.9 TIE2 IS EXPRESSED IN ADULT CARDIOMYOCYTES 48
2.10 SM22α-DRIVEN TIE2 DELETION DOES NOT HAVE A MAJOR IMPACT ON BLOOD PRESSURE UPON DOCA-SALT TREATMENT 55
2.11 SM22α-DRIVEN TIE2 DELETION AFFECTS CARDIAC SIZE UPON DOCA-SALT TREATMENT 58
2.12 SM22α-DRIVEN TIE2 DELETION AFFECTS VSMC PHENOTYPE AND FUNCTION UPON DOCA-SALT TREATMENT 59
2.13 SM22α-DRIVEN TIE2 DELETION AFFECTS THE COMPENSATORY POTENTIAL OF THE HEART UPON ANGII-INDUCED HYPERTENSION 61
2.14 VSMC-EXPRESSED TIE2 REGULATES PHENOTYPIC MODULATION OF ACTIVATED VSMC 63
2.15 VSMC-SPECIFIC TIE2 DELETION REDUCES ATHEROSCLEROSIS PROGRESSION 65
2.16 ANGIOPOIETIN 2-DEFICIENT MICE DISPLAY INCREASED ATHEROSCLEROSIS 68

3 DISCUSSION 71

3.1 VSMC-EXPRESSED TIE2 CONTROLS THE BALANCE BETWEEN THE CONTRACTILE AND SYNTHETIC VSMC PHENOTYPE 71

3.2 SM22α-DRIVEN TIE2 DELETION IN THE HEART AFFECTS BASELINE BLOOD PRESSURE AND CARDIAC SIZE 72
3.3 TIE2 EXPRESSION IN CARDIOMYOCYTES 73
3.4 SM22α-DRIVEN TIE2 DELETION DELAYS AN ADAPTIVE CARDIAC RESPONSE UPON HYPERTENSION 73
3.5 MODELS: SM22α-DRIVEN TIE2 DELETION IN THE HEART AND ARTERIES 75
3.6 FUNCTION OF VSMC-EXPRESSED TIE2 DURING ATHEROSCLEROSIS PROGRESSION 76
3.7 FUNCTION OF ANGPT2 DURING ATHEROSCLEROSIS PROGRESSION 76
3.8 MODEL: THE ROLE OF VSMC-EXPRESSED TIE2 ON VSMC PHENOTYPE AND FUNCTION DURING ATHEROSCLEROSIS PROGRESSION 77
3.9 CROSS-TALK BETWEEN VSMC-EXPRESSED TIE2 AND ANGPT2-PRODUCING EC 78
3.10 PLAQUE COMPOSITION IN THE PRESENCE AND ABSENCE OF VSMC-EXPRESSED TIE2 79
3.11 TIE2 SIGNALING IN VSMC 79
3.12 TIE2 AS A THERAPEUTIC TARGET AND FUTURE DIRECTIONS 79
3.13 CONCLUSION 80

4 METHODS 81

4.1 ANIMALS 81
4.1.1 ANIMAL WELFARE 81
4.1.2 RADIOTELEMETRY SYSTEM 81
4.1.3 ECHOCARDIOGRAPHY 82
4.1.4 DOCA-INDUCED HYPERTENSION MODEL 82
4.1.5 ANGIOTENSIN-INDUCED HYPERTENSION MODEL 82
4.1.6 *EX-VIVO* PERFUSION OF MESENTERIC AND FEMORAL ARTERIES 83
4.1.7 VSMC ISOLATION 83
4.1.8 CHARACTERIZATION OF ISOLATED AORTIC VSMC 83
4.1.9 MACROPHAGE ISOLATION 83
4.2 IMMUNOHISTOCHEMICAL METHODS 83
4.2.1 PREPARATION OF ZINC-FIXED PARAFFIN-EMBEDDED SECTIONS 83
4.2.1.1 DEPARAFFINIZATION AND REHYDRATION OF PARAFFIN 84
4.2.1.2 HEMATOXYLIN AND EOSIN (H&E) STAINING OF PARAFFIN-EMBEDDED SECTIONS 84
4.2.1.3 IMMUNOHISTOCHEMISTRY (IHC) 85
4.2.1.4 IMMUNOFLUORESCENCE OF PARAFFIN-EMBEDDED ARTERIES 85
4.2.1.5 PICRO SIRIUS RED STAINING 85
4.2.1.6 OIL RED O (ORO) STAINING OF WHOLE MOUNT AORTA 86
4.2.2 PREPARATION OF CRYOBLOCKS AND SECTIONS 86
4.2.2.1 IMMUNOFLUORESCENCE STAINING 86
4.2.2.2 WHOLE MOUNT RETINA STAINING 87
4.2.2.3 STAINING OF ATHEROSCLEROTIC LESION SIZE 87
4.3 CELL CULTURE METHODS 87
4.3.1 CELL CULTURE MAINTENANCE 87

4.3.2 CRYOPRESERVATION AND THAWING OF CELLS 88
4.3.3 TRANSFECTION WITH SMALL INTERFERING RNA (SIRNA) 88
4.3.4 STIMULATION ASSAYS 88
4.4 CELLULAR ASSAYS 88
4.4.1 SCRATCH WOUND ASSAY 88
4.5 MOLECULAR BIOLOGY METHODS 89
4.5.1 GENOTYPING PCR 89
4.5.1.1 PCR-POLYMERASE CHAIN REACTION 89
4.6.1.2 AGAROSE GEL ELECTROPHORESIS 90
4.5.2 RNA ISOLATION 90
4.5.3 CDNA GENERATION 91
4.5.4 QUANTITATIVE REALTIME-PCR (QRT-PCR) 91
4.5.5 MICROARRAY 92
4.6 PROTEIN CHEMICAL METHODS 93
4.6.1 PREPARATION OF PROTEIN LYSATES 93
4.6.2 PROTEIN CONCENTRATION MEASUREMENTS 93
4.6.2.1 BCA-ASSAY 93
4.6.3 IMMUNOPRECIPITATION AND IMMUNOBLOTTING 93
4.6.4 PROTEOME PROFILER ARRAY 94
4.6.5 MEASUREMENT OF PLASMA LIPID CONTENT 94
4.6.6 ENZYME-LINKED IMMUNOSORBENT ASSAY (ELISA) 94
4.6.7 FLUORESCENCE ACTIVATED CELL SORTING (FACS) 94
4.6.7.1 LUNG ENDOTHELIAL CELL ISOLATION 94
4.6.7.2 SM22α-POSITIVE CELL ISOLATION 94
4.7 STATISTICAL ANALYSIS 95

5 MATERIALS 96

5.1 CHEMICALS 96
5.2 CELLS 96
5.3 CELL CULTURE AND REAGENTS 96
5.4 PCR AND QRT-PCR REAGENTS 97
5.5 WESTERN BLOT REAGENTS 97
5.6 PRIMERS 98
5.7 SIRNA 99
5.8 GROWTH FACTORS, PROTEINS AND EMZYMES 100
5.9 KITS 100
5.10 MISCELLANEOUS 100
5.11 CONSUMABLES 101
5.12 EQUIPMENT 101
5.13 ANTIBODIES 102

5.13.1 PRIMARY ANTIBODIES 102
5.13.2 SECONDARY ANTIBODIES 103
5.14 ADDITIONAL STAINING REAGENTS 103
5.15 SOLUTIONS AND BUFFERS 103
5.16 SOFTWARE 104

6 ABBREVIATIONS 105

7 PUBLICATIONS 109

8 REFERENCES 110

List of Figures

Figure 1. Structure of Tie receptors and angiopoietins 9
Figure 2. Angiopoietin-Tie signaling in resting endothelial cells 12
Figure 3. Phenotypic modulation of VSMC 15
Figure 4. Regulators of VSMC phenotype 19
Figure 5. Types of vascular remodeling in hypertension 24
Figure 6: Onset and progression of atherosclerosis 28
Figure 7. Vascular smooth muscle cells express Tie2 34
Figure 8. Vascular smooth muscle cells express functional Tie2 receptor 35
Figure 9. Tie2 expression in isolated mouse aortic vascular smooth muscle cells 36
Figure 10. Characterization of retinal vascularization and mural cell coverage in *Tie2*$^{+/+}$ and *Tie2*$^{SMC-KO}$ mice 37
Figure 11. Tie2 expression in isolated mouse aortic vascular smooth muscle cells 38
Figure 12. Purity of isolated aortic VSMC 38
Figure 13. Evaluation of Tie2 expression in isolated lung EC and peritoneal macrophages from *Tie2*$^{+/+}$ and *Tie2*$^{SMC-KO}$ mice 39
Figure 14. Gene expression analysis in isolated aortic VSMC from *Tie2*$^{+/+}$ and *Tie2*$^{SMC-KO}$ mice 40
Figure 15. Contractile VSMC markers increased in isolated aortic VSMC from *Tie2*$^{SMC-KO}$ mice 40
Figure 16. Tie2 deficiency in VSMC impairs VSMC activation 41
Figure 17. *In vivo* analysis of contractile VSMC marker expression in arteries from *Tie2*$^{+/+}$ and *Tie2*$^{SMC-KO}$ mice 42
Figure 18. Hypercontractile response of isolated blood vessels from *Tie2*$^{SMC-KO}$ mice upon increasing intraluminal pressure 43
Figure 19. Radiotelemetric tracing of blood pressure and heart rate 44
Figure 20. Sm22α-driven Tie2 deletion reduces baseline blood pressure 45
Figure 21. Sm22α-driven Tie2 deletion reduces cardiac size 46
Figure 22. Sm22α-driven Tie2 deletion reduces left ventricular wall- and interventricular septum thickness 47
Figure 23. Sm22α-driven Tie2 deletion reduces cardiomyocyte dimensions 48
Figure 24. Sm22α-driven Tie2 deletion reduces cardiac size in mice after 4 weeks of age 49
Figure 25. Sm22α-driven Tie2 deletion does not affect proliferation or apoptosis 50
Figure 26. Tracing Sm22α expression using a Sm22α knockin fate-tracing mouse model 52
Figure 27. Tracing Tie2 expression in the aorta using a Tie2 knockin fate-tracing model 53

Figure 28. Tracing Tie2 expression in the heart using a Tie2 knockin fate-tracing model 54
Figure 29. Tie2 is not expressed in cardiomyocytes from 8-week-old *Tie2*$^{+/+}$ and *Tie2*$^{SMC-KO}$ mice 55
Figure 30. Experimental protocol for DOCA-induced hypertension 56
Figure 31. Analysis of SBP, DBP and MAP in *Tie2*$^{+/+}$ mice upon DOCA-salt treatment 56
Figure 32. Sm22α-driven Tie2 deletion does not have a major impact on blood pressure during hypertension 57
Figure 33. Sm22α-driven Tie2 deletion reduces cardiac size upon DOCA-salt treatment 58
Figure 34. Sm22α-driven Tie2 deletion reduces cardiac fibrosis upon DOCA-salt treatment 59
Figure 35. VSMC-specific Tie2 deletion maintains the contractile VSMC phenotype in DOCA-salt treated arteries 60
Figure 36. Experimental protocol for Angiotensin II-induced hypertension 61
Figure 37. Sm22α-driven Tie2 deletion delays the compensatory potential of the heart upon AngII-induced hypertension 62
Figure 38. Sm22α-driven Tie2 deletion delays an increase in cardiac output upon AngII-induced hypertension 62
Figure 39: Reduced proliferation of Tie2-deficient and Tie2-silenced aortic VSMC 63
Figure 40. Reduced migration of HAoSMC upon Tie2 silencing 64
Figure 41. Tie2 deficiency in VSMC reduces atherosclerosis in mice 65
Figure 42. Tie2 deficiency in VSMC reduces atherosclerosis in mice 66
Figure 43. Characterization of isolated aortic VSMC from *ApoE*^{KO} and *Tie2*$^{SMC-KO}$ mice 67
Figure 44. Angpt2 serum concentrations are increased in the absence of VSMC-expressed Tie2 68
Figure 45. Angpt2 deficiency promotes atherosclerosis in *ApoE* null mice 69
Figure 46. Angpt2 deficiency promotes atherosclerosis in *ApoE null* mice 70
Figure 47. Sm22α-driven Tie2 deletion in the heart and arteries 75
Figure 48. Model demonstrating the role of VSMC-expressed Tie2 on VSMC phenotype and function during atherosclerosis progression 78

List of Tables

Table 1: Paraffin section preparation 84
Table 2: Deparaffinization and rehydration of paraffin 84
Table 3. *Tie2fl/fl* PCR reaction mix 89
Table 4. *Sm22α-Cre* PCR reaction mix 89
Table 5. *Angpt2* PCR reaction mix 89
Table 6. *ApoE* PCR reaction mix 89
Table 7. *Sm22α-Cre* and *ApoE* genotyping PCR program 90
Table 8. *Tie2*$^{fl/fl}$ and *Angpt2* genotyping PCR program 90
Table 9. cDNA reaction mix 91
Table 10. Taqman qRT-PCR reaction mix 92
Table 11.Taqman qRT-PCR program 92
Table 12. List of cells used in this study 96
Table 13. List of cell culture media 96
Table 14. List of reagents used in cell culture 97
Table 15. PCR and qRT-PCR reagents 97
Table 16. Western blot reagents 97
Table 17. Taqman probes for qRT-PCR 98
Table 18. Mouse genotyping primers 99
Table 19. Human RT-qPCR primers 99
Table 20. siRNA used in this study 99
Table 21. Growth factors, proteins and enzymes 100
Table 22. Kits 100
Table 23. Miscellaneous 100
Table 24. Consumables 101
Table 25. Equipment 101
Table 26. Primary antibodies 102
Table 27. Secondary antibodies 103
Table 28. Staining reagents 103
Table 29. Solutions and buffers 103
Table 30. Software 104

Summary

Angiopoietin (Angpt)/Tie signaling in microvascular endothelial cells (EC) controls vascular development, remodeling and maturation[1,2]. Biomarker studies also imply a role of macrovascular Angpt/Tie signaling in the pathogenesis of hypertension and atherosclerosis[354-356]. Importantly, experimental studies on the role of the Angpt ligands and the Tie receptors in hypertension and atherosclerosis have yielded conflicting results suggesting spatiotemporally context-dependent pro- and anti-atherosclerotic/hypertensive functions in different experimental settings.

Reports of scattered observations have shown Tie2 expression by vascular smooth muscle cells (VSMC)[370-372]. VSMC contribute to hypertension and atherosclerosis progression either through VSMC hypertrophy and/or switching from a contractile quiescent to a synthetic and activated phenotype[248,302]. Yet, the functional role of VSMC-expressed Tie2 during these pathological conditions has not been analyzed. Therefore, in this study Tie2 was conditionally deleted in VSMC (*Tie2*$^{SMC\text{-}KO}$) using a mural cell-specific *Sm22α-Cre* driver line. These mice were crossed with atherosclerosis-prone *ApoE*-deficient mice (*ApoE*^{KO} *Tie2*$^{SMC\text{-}KO}$). VSMC marker expression did not differ in freshly isolated and lysed aortas, mesenteric and femoral arteries from *Tie2*$^{+/+}$ and *Tie2*$^{SMC\text{-}KO}$ mice. Transcriptionally, cultivated Tie2-deficient VSMC show an increased contractile and reduced synthetic phenotype-specific gene expression, suggesting that VSMC from *Tie2*$^{SMC\text{-}KO}$ mice fail to switch towards a synthetic phenotype upon activation. Correspondingly, migration and proliferation was significantly reduced in Tie2-deficient cultured VSMC. Long-term telemetric tracing identified significantly reduced basal systolic blood pressure (SBP) in *Tie2*$^{SMC\text{-}KO}$mice, indicative of a baseline cardiac phenotype that is independent of Sm22α-driven Tie2 deletion in VSMC. *Tie2*$^{SMC\text{-}KO}$ mice also display a significantly reduced left ventricular posterior wall thickness (LVPWT) and interventricular septum (IVS), which is in line with a reduced cardiomyocyte (CM) cross-sectional area observed in these mice. Notably, GFP-positive cardiomyocytes (CMs) and GFP-positive VSMC were detected in heart and aortic tissue, respectively, obtained from adult *Tie2*^{MCM} x *Rosa26*^{YFP} mice, suggesting that Tie2 may be deleted in CMs in the time frame of Sm22α expression in these cells during embryonic development. Furthermore, DOCA-salt-induced hypertension experiments revealed a significant decrease in cardiac size with a slightly reduced blood pressure in *Tie2*$^{SMC\text{-}KO}$ mice. Moreover, AngII-treated *Tie2*$^{SMC\text{-}KO}$ mice demonstrated a decrease in heart rate (HR), cardiac output (CO) and stroke volume (SV) that was compensated over time. Thus, the baseline cardiac phenotype in *Tie2*$^{SMC\text{-}KO}$ mice transiently compromises an adequate cardiac response upon hypertension.

Next, ApoE^{KO} *Tie2*$^{SMC\text{-}KO}$ mice were fed a Western-type diet for 14 weeks and showed significantly reduced atherosclerotic lesion progression with less VSMC content. Additionally, serum Angpt2 as well as the Angpt2/Angpt1 ratio were significantly increased in *ApoE*^{KO} *Tie2*$^{SMC\text{-}KO}$ mice. Consistent with the increased systemic Angpt2 levels and the reduced atherosclerosis in *ApoE*^{KO} *Tie2*$^{SMC\text{-}KO}$ mice, a pro- atherosclerotic phenotype was observed in *ApoE*^{KO} *Angpt2*^{KO} double knockout (KO) mice.

The data propose a remarkable role of Tie2 receptor in regulating cardiac size and blood pressure, which is most likely a consequence of Sm22α-driven Tie2 deletion in CMs. Moreover, the data

identified a cell autonomous function of VSMC-specific Tie2 in controlling VSMC phenotype and function. In the context of atherosclerosis, the data expand and revise the endotheliocentric Tie2 signaling concept to show that mural cell-expressed Tie2 is involved in regulating macrovascular functions. VSMC-expressed Tie2 acts pro-atherosclerotic to control the phenotypic switch towards a proliferative and migratory synthetic VSMC phenotype. The Tie2 ligand Angpt2 acts anti-atherosclerotic, which is compatible with an antagonistic mode of action of Angpt2 on Tie2.

Zusammenfassung

Der Angiopoietin (Angpt)/Tie Signalweg steuert die vaskuläre Entwicklung und Reifung mikrovaskulärer Endothelzellen (EC)[1,2]. Biomarker-Studien bringen den Angpt/Tie-Signalwegs auch im Kontext makrovaskulärer Gefäße in Zusammenhang mit der Pathogenese von Hypertonie und Atherosclerose[354-356]. Experimentelle Studien zur Rolle der Angpt-Liganden und der Tie-Rezeptoren bei Hypertonie und Atherosklerose haben zu widersprüchlichen Ergebnissen geführt, was auf kontextabhängige pro- und anti-atherosklerotische/hypertensive Funktionen in verschiedenen experimentellen Aufbauten schließen lässt.

Vereinzelte Studien haben gezeigt, dass Tie2 in vaskulären glatten Muskelzellen (VSMC) produziert wird[370-372]. VSMC tragen zur Entwicklung von Bluthochdruck und Arteriosklerose bei, entweder durch VSMC-Hypertrophie und/oder durch den Wechsel von einem kontraktilen ruhenden Zustand zu einem synthetischen und aktivierten Phänotypen[248,302]. Die funktionelle Rolle von VSMC-exprimiertem Tie2 während dieser pathologischen Zustände wurde jedoch noch nicht analysiert. Daher wurde in dieser Arbeit Tie2 in VSMC unter der Verwendung einer muralzellenspezifischen *Sm22α-Cre*-Linie konditionell deletiert (*Tie2*$^{SMC-KO}$). Diese Mäuse sind mit Atherosklerose-anfälligen *ApoE*-defizienten Mäusen (*ApoE*^{KO} *Tie2*$^{SMC-KO}$) gekreuzt worden. Unterschiede in der Markergenexpression in frisch isolierten VSMC aus Aorta, Mesenterial und Femoralarterie von *Tie2*$^{+/+}$- und *Tie2*$^{SMC-KO}$-Mäusen sind nicht festgestellt worden. Jedoch zeigen auf transkriptionaler Ebene kultivierte Tie2-defiziente VSMC eine verstärkte kontraktile und reduzierte synthetische Phänotyp-spezifische Genexpression, was darauf hindeutet, dass VSMC aus *Tie2*$^{SMC-KO}$-Mäusen, sobald sie aktiviert sind, nicht zu einem synthetischen Phänotyp wechseln. Dementsprechend sind Migration und Proliferation in Tie2-defizienten kultivierten VSMC signifikant reduziert. Eine längerfristige telemetrische Kontrolle ergab einen signifikant reduzierten basalen systolischen Blutdruck (SBP) in *Tie2*$^{SMC-KO}$-Mäusen, was auf einen kardialen Ausgangsphänotyp hinweist, der unabhängig von der Sm22α-gesteuerten Tie2-Deletion in VSMC ist. *Tie2*$^{SMC-KO}$-Mäuse zeigen auch eine signifikant reduzierte Dicke der linken ventrikulären posterioren Wand (LVPWT) und des interventrikulären Septums (IVS), was mit einer reduzierten Kardiomyozyten (CM)- Querschnittsfläche übereinstimmt, die bei diesen Mäusen beobachtet wird. Bemerkenswerterweise wurden GFP-positive Kardiomyozyten (CMs) und GFP-positive VSMC in Herz- und Aortengewebe von erwachsenen *Tie2*^{MCM} x *Rosa26*^{YFP}-Mäusen nachgewiesen, was nahelegt, dass Tie2 in CMs im Zeitrahmen der Sm22α-Expression in diesen Zellen während der embryonalen Entwicklung deletiert sein könnte. Darüber hinaus zeigten DOCA-Salz-induzierte Hypertonie-Experimente eine signifikante Abnahme der Herzgröße sowie eine Tendenz zu einem reduzierten Blutdruck in *Tie2*$^{SMC-KO}$-Mäusen. Zudem zeigten AngII-behandelte *Tie2*$^{SMC-KO}$-Mäuse eine Verringerung der Herzfrequenz (HR), des Herzzeitvolumens (CO) und des Schlagvolumens (SV), welche im

Laufe der Zeit ausgeglichen wurden. Somit führt der Herz-Phänotyp in *Tie2*$^{SMC-KO}$-Mäusen zu einer transienten Beeinträchtigung einer adäquate Herzreaktion bei Bluthochdruck.

Als nächstes erhielten *ApoE*^{KO} *Tie2*$^{SMC-KO}$-Mäuse 14 Wochen lang eine „Western"-Diät und zeigten anschließend eine signifikant verringerte atherosklerotische Läsionsprogression mit einem geringeren VSMC-Anteil. Darüber hinaus waren im Serum von *ApoE*^{KO} *Tie2*$^{SMC-KO}$-Mäusen der Angpt2-Spiegel sowie das Angpt2/Angpt1-Verhältnis signifikant erhöht. In Übereinstimmung mit den erhöhten systemischen Angpt2-Spiegeln und reduzierter Atherosklerose bei *ApoE*^{KO}*Tie2*$^{SMC-KO}$-Mäusen wurde ein proatherosklerotischer Phänotyp in *ApoE*^{KO}*Angpt2*^{KO}-Doppel-Knockout (KO)-Mäusen beobachtet.

Diese Daten zeigen eine fundamentale Rolle des Tie2-Rezeptors in der Regulierung der Herzgröße und des Blutdruck, was höchstwahrscheinlich eine Folge der Sm22α-gesteuerten Tie2-Deletion in CMs ist. Darüber hinaus identifizierten sie eine zellautonome Funktion des VSMC-spezifischen Tie2 bei dessen Kontrolle von VSMC Phänotyp und Funktion. Im Rahmen der Atherosklerose erweitern und korrigieren diese Daten das endothelzellenzentrische Tie2-Signalgebungskonzept, und zeigen, dass muralzellenproduziertes Tie2 an der Regulation makrovaskulärer Funktionen beteiligt ist. VSMC-spezifisches Tie2 wirkt proatherosklerotisch und kontrolliert den phänotypischen Wechsel zu einem proliferativen und migratorischen synthetischen VSMC-Phänotypen. Der Tie2-Ligand Angpt2 hingegen wirkt anti-atherosklerotisch, was kompatibel mit einer antagonistischen Wirkungsweise von Angpt2 auf Tie2 ist.

1 Introduction

1.1 The vascular system

The vertebrate vascular system is comprised of two highly branched, tree-like tubular networks: the blood vessels and a blind-ended network of lymphatic vessels. Both are formed by endothelial cells (EC) and are crucial in regulating tissue fluid homeostasis[3]. The vascular system consists of the heart and a hierarchical architecture of arteries, arterioles, capillaries, venules and veins. Capillaries, arterioles and venules are the smaller vessels, whereas veins and arteries are larger vessels. Arteries transport O_2- and nutrient-rich blood from the heart to capillaries, where exchange from gases, nutrients and waste between the blood vasculature and adjacent tissues occurs[4]. Deoxygenated CO_2-rich blood and metabolic waste products are removed via venous capillary beds and returned to the heart by venules and veins. In contrast, lymphatic vessels drain excessive interstitial fluid, proteins and macromolecules from the periphery through a conduit system of capillaries, collecting vessels, lymph nodes, lymphatic trunks and ducts back into the blood vasculature[3,5,6]. Lymphatic vessels also play an essential role in immune surveillance and the uptake of dietary fatty acids. About 75 % of all deaths are directly or indirectly associated with dysfunctions of the vascular system, including diabetes, aneurysm, atherosclerosis, myocardial infarction, stroke, neurodegenerative disorders and cancer, underlying its importance[7,8].

1.1.1 Architecture and function of blood vessels

The inner lining of a blood vessel, called tunica intima, is formed by a single cobble-stone-like monolayer of EC[6]. Although EC share common functional and morphological features, they show remarkable heterogeneity and display site-specific functions in different organs[9]. Three different organ-specific endothelia are described as adaptation to meet the anatomical and physiological demands of the underlying tissue: continuous, fenestrated and discontinuous endothelium[10]. Continuous endothelia, embedded in an elaborate basement membrane (BM), can be found in the brain and maintains the blood brain barrier through specialized tight junctions. Fenestrated endothelia are characterized by intercellular gaps and a continuous BM and are found in organs with high fluid exchange like kidney and intestine. The discontinuous sinusoidal endothelium is found in organs, such as liver, spleen and bone marrow that require extensive cell trafficking and fluid exchange. The discontinuous sinusoidal endothelium in these organs is characterized by even larger gaps and a lack of BM[10].

EC of the microvasculature (capillaries, small arterioles and venules) are loosely covered by pericytes. Pericytes are mural cells that are embedded in the BM to directly interact with EC thereby exerting vessel-stabilizing functions. In contrast, the tunica intima in large caliber blood vessels is covered by two additional layers, namely the tunica media and tunica externa/adventitia. The tunica media is separated from the intima by a dense elastic membrane (internal elastic lamina) and contains vascular smooth muscle cells (VSMC) (along with pericytes called mural cells), proteoglycans, elastin

fibers and collagen. The tunica adventitia, separated from the media by the eternal elastic lamina, consists of a mixture of extracellular matrix (ECM), fibroblasts, and nerve cells[6,10]. Arteries contain the highest mural cell (VSMC and pericytes) and fiber coverage, which is necessary for tight control of blood flow and pressure. Veins, on the other hand, contain specialized valves to ensure the directional blood flow from the periphery back to the heart[4,6,11].

1.1.2 Vascular development

The cardiovascular system is the first functional organ that develops during vertrebate embryogenesis and is critical for nutrients and O_2 supply to the embryo[12]. Vascular development in vertebrates occurs via two distinct processes: vasculogenesis and angiogenesis[13]. During vasculogenesis, blood vessels develop by the *de novo* formation of a primitive vascular plexus from angioblast progenitors. The angioblasts in the periphery of blood islands give rise to EC, whereas hematopoietic progenitor cells located in the center of these blood islands give rise to blood cells. These islands subsequently fuse into cord-like structures and give rise to a primitive luminized vascular plexus in the yolk sac and embryo[13]. Upon formation of the primary vascular plexus, blood vessels undergo arterial or venous specification. The Notch pathway is essential in regulating arterial differentiation, whereas the orphan nuclear receptor chicken ovalbumin upstream promoter-transcription factor II (Coup-TFII) regulates venous differentiation[14]. Subsequently, the primitive vascular plexus remodels into a mature vascular network during angiogenesis and requires the recruitment of mural cells to mediate vascular stabilization[4,15].

1.1.3 Physiological angiogenesis

Angiogenesis is a fundamental biological process leading to the formation of new blood vessels from preexisting vessels[13,16]. In the embryo, angiogenesis is essential for organ development and continues to contribute to organ growth after birth[13,16,17]. However, the adult vasculature remains quiescent and angiogenesis is limited to the cycling ovary and the placenta during pregnancy. Yet, quiescent EC maintain a high plasticity to sense and respond to (patho-)physiological stimuli, such as hypoxia, and angiogenesis is reactivated during wound healing and repair[13,16,17]. In contrast, inadequate angiogenesis or excessive angiogenesis contributes to pathological diseases such as cancer, diabetic retinopathy, obesity-associated disorders, ischemic heart diseases, and atherosclerosis[15,18]. Thus, adequate formation of new blood vessels demands to be tightly regulated[15].

1.1.3.1 Phases of angiogenesis

The recruitment of new blood vessels is mainly triggered by hypoxia, a reduction in the normal tissue oxygen levels. Initially, hypoxia inducible factor 1 (HIF1) is stabilized, which leads to upregulation of vascular endothelial growth factor-a (VEGFA)[19,20]. VEGFA/VEGFR2 signaling activates the endothelium and primes selected EC to become tip cells, the guiding cells of newly forming sprouts. VEGFA further induces internalization of the junctional molecule vascular endothelial (VE)-cadherin, which leads to

weakening of EC junctions. Moreover, VEGFA promotes the secretion of matrix metalloproteinases (MMPs) from EC to facilitate EC liberation. By inducing filopodia formation in tip cells, VEGFA facilitates a coordinated tissue invasion of tip cells towards the angiogenic stimulus and vessel sprouting into avascular areas[3,15,21,22]. The tip cells are followed by the stalk cells, which are more proliferative thereby promoting sprout extension. Stalk cells form a lumen in newly formed vessels[15], produce the BM, shape EC junctions and associate with mural cells to ensure sprout integrity[15]. The onset of perfusion, oxygen and nutrient delivery inhibits VEGF signaling and shifts the active EC behavior towards a quiescent phenotype[15]. Junctions of the quiescent EC (phalanx cells) are further strengthened and vessels are stabilized by the recruitment of mural cells[15,23]. Finally, a hierarchical vascular network is formed by regulating vessel density, either through the formation of new vessel sprouts or by formation of an immature vasculature, which leads to selective regression of redundant branches[24,25].

1.1.3.2 Signaling pathways in angiogenesis

The VEGF family consist of VEGFA, VEGFB, VEGFC, VEGFD, placental growth factor (PIGF), parapoxvirus VEGFE and snake venom VEGFF[19]. The importance of VEGFA in vascular development was demonstrated by employing genetic models in which the loss of one allele of *Vegfa* leads to embryonic lethality due to impaired vasculogenesis and angiogenesis[26]. VEGF was first described as vascular permeability factor, due to its ability to induce vascular leakage[19,27-29]. VEGFA promotes proliferation, migration and survival of EC[30-32]. Binding of VEGFA to VEGFR2 leads to receptor dimerization and auto-phosphorylation and subsequent activation of mitogen-activated protein kinase (MAPK), phosphoinositide 3-kinase (PI3K)/AKT, phospholipase Cγ (PLCγ), Src, focal adhesion kinase (FAK) and small GTPase downstream signaling[33]. Neuropillin (NRP) 1 and 2, the co-receptors for VEGFA, facilitate VEGFA-induced VEGFR2 signaling by increasing the affinity to VEGFR2[34]. However, NRP1 is able to signal independently of VEGFR2[35]. VEGFA also binds to VEGFR1, which has only weak kinase activity but higher affinity for VEGFA than VEGFR2. Hence, VEGFR1 as well as the inactive soluble isoform of VEGFR1 act as VEGFA trap antagonizing VEGFR2 signaling[36,37]. While VEGFR1 and VEGFR2 are predominantly expressed in EC, lymphangiogenesis is mainly regulated by VEGFC binding to VEGFR3 and primarely expressed by lymphatic EC[38].

The Notch pathway mediates tip cell versus stalk cell fate, which is of major importance for effective sprouting and network formation. EC express four different Notch receptors, Notch1 to Notch4[39,40], and corresponding Notch ligands Delta-like 1 (DLL1), DLL4, JAG1 and JAG2[41,42]. While tip cells mainly express DLL4, stalk cells express JAG1. DLL4 activates the Notch receptor in neighboring cells, which leads to the induction of the stalk cell phenotype by downregulation of VEGFR2 and upregulation of VEGFR1[2,43]. JAG1 interacts with Notch receptors on tip cells to suppress the Notch-induced stalk cell phenotype in tip cells[44].

The Angiopoietin (Angpt)/Tie system is another important signaling pathway involved in angiogenesis. This signaling pathway will be discussed in more detail in the next chapter 1.2.

1.2 Angpt/Tie system

The Angpt/Tie system is the second major EC specific ligand receptor signaling system. The Angpt/Tie system is comprised of two receptor tyrosine kinases, Tie1 (Tie) and Tie2 (Tek), and four Angpt ligands; Angpt1-Angpt4[45-49]. This system is essential for embryonic lymphatic and cardiovascular development[50]. The Angpt/Tie system also controls postnatal angiogenesis, vascular remodeling, vascular permeability and inflammation to retain vessel homeostasis in adult physiology[1]. Dysregulation of the Angpt/Tie system is associated with the pathogenesis of several human diseases.

1.2.1 Structure of Tie receptors and Angpt ligands

Tie1 and Tie2, whose acronym Tie stands for tyrosine kinase with immunoglobin and EGF homology, belong to a distinct family of tyrosine kinase receptors[17,47]. They are single transmembrane molecules with an extracellular ligand-binding domain and a split intracellular Tyrosine kinase domain (Figure 1). Tie1 and Tie2 show a high degree of structural homology, sharing 33% similarity in their extracellular domain and 76% in their intracellular domain[1,17,51]. The extracellular domain is composed of two immunoglobuline (Ig)-like domains, followed by three EGF-like domains, a third Ig-like domain and three fibronectin type III repeats that are adjacent to the transmembrane domain. The intracellular domain harbors tyrosine kinase domains including a number of phosphorylation and protein interaction sites.

Angiopoietins (Angpts) are secreted glycoproteins that function as ligands for Tie2[1,17,51]. Angpt1 and Angpt2 are the best characterized ligands for Tie2 and share 60% amino acid sequence homology. In contrast, less is known about Angpt3 (the mouse orthologue of Angpt4) and Angpt4. Angpts have opposing actions in EC. While Angpt1 and Angpt4 act as agonist of Tie2, Angpt2 and Angpt3 act as context-dependent antagonists. Structurally, angiopoietins consist of an N-terminal domain that promotes high-order clustering of the molecules, followed by a coiled-coiled domain required for multimerization, a linker peptide, and a carboxyl-terminal fibrinogen homology domain that contains the Tie2 binding site (Figure 1)[52,53]. Moreover, the short N-terminal region forms ring-like structures that serve to cluster dimers into variable oligomers. Electron microscopy experiments of Angpt proteins have demonstrated that Angpt1 and Angpt2 form heterogenous multimers with trimeric, tetrameric and pentameric oligomers[1]. Angpt1 primarily forms tetramer or higher order multimers[54], whereas Angpt2 exists mostly as dimers[1,2,51]. The oligomerization status of these ligands may have a direct functional impact on the receptor binding and activation. In particular, multimeric structures of Angpt1 can bind to both ligand-binding sites of extracellular Tie2 homodimers and in turn induce potent Tie2 receptor activation[55]. On the other hand, Angpt2 dimers fail to bridge the receptors and therefore limit dimerization and Tie2 receptor activation. Hence, Angpt2 acts as antagonist of Angpt1-mediated Tie2 signaling. However, it can also act as partial agonist[55].

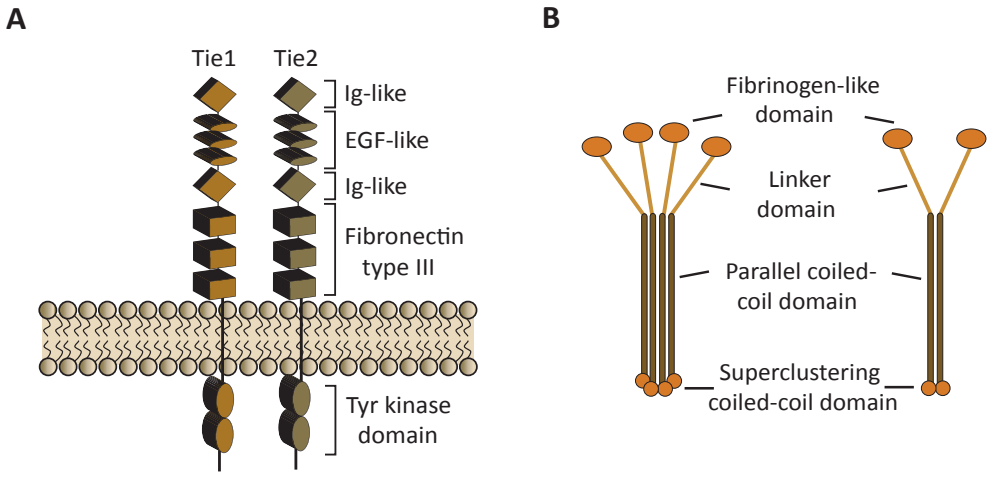

Figure 1. Structure of Tie receptors and angiopoietins

A, The Tie receptors are transmembrane receptor Tyr kinases, sharing a similar overall domain structure. Their extracellular ligand-binding domain consist of two immunoglobuline (Ig)-like domains, followed by three EGF-like domains, a third Ig-like domain and three fibronectin type III repeats. The carboxy- terminal intracellular domain is composed of a split Tyrosine kinase domain**. B**, The Angpt ligands are secreted glycoproteins that comprise of an amino-terminal coiled-coiled domain and a carboxyl-terminal fibrinogen homology domain. Ang ligand-monomers oligomerize via the parallel coiled-coil domain and the superclustering domain to form higher order multimers. Angpt1 primarily forms tetramer or higher order multimers, whereas Angpt2 exists mostly as dimers.

1.2.2 Expression of Tie receptors and Angpt ligands

The Tie receptors are almost exclusively expressed by blood vascular and lymphatic EC[50]. Tie1 and Tie2 are ubiquitously expressed in EC during embryonic development[56,57]. Tie2 expression was first detected in EC at E7.5 and continues to be expressed in these cells throughout development. Tie1 expression is detected at a slightly later embryonic day E8.0[58]. Tie2 plays important roles during vascular development, remodeling and maturation[1]. It exerts its angiogenesis-regulating functions through its EC-specific expression. Yet, Tie2 is not exclusively expressed by EC. Hematopoietic stem cells (HSC) express Tie2 controlling HSC dormancy[59,60]. Tie2 is also expressed by a subpopulation of monocytes, which exert important pro-tumorigenic functions[61-64]. Moreover, Tie2 has been suggested to control satellite cell function[65], neural cell behaviour[66], and growth-promoting functions of tumor cells[67,68]. Recently, pericyte-expressed Tie2 has been shown to regulate vessel maturation[69]. In the adult endothelium, Tie2 is uniformly expressed and constitutively activated in stalk and phalanx cells. However, it is transcriptionally downregulated following EC activation in sprouting tip cells[1,70]. Moreover, Tie2 cell surface presentation in tip cells is counter-regulated by Tie1 expression[71].

Tie1 remains an orphan receptor without any specific ligand. Yet, studies have reported that Tie1 heterodimerizes with Tie2, upon Angpt1 stimulation, and in turn regulates its activity[72-74]. In particular, the agonistic actions of Angpt1 and Angpt2 promote a direct interaction of Tie1 and Tie2, which is mediated by integrin β1[75]. Tie1 expression has also been detected in megakaryocytes, hematopoietic stem cells and osteoblast in the bone marrow niche[1,76].

The Angpt ligands have a distinct expression pattern. Angpt1 is critical for cardiac development and for correct organization and maturation of newly formed vessels. Following maturation, Angpt1 maintains the quiescence and stability of the mature vasculature. Angpt1 is abundantly expressed in the myocardium, while Tie2 is expressed in the developing epicardium and endocardium during cardiac development[77]. Myocardial Angpt1 mediates the developing epicardium and endocardium in a paracrine manner[77]. Furthermore, Angpt1 is expressed by perivascular cells (pericytes, VSMC and fibroblast) as well as tumor cells[78,79]. In healthy adults, Angpt1 is constitutively produced and released by mural cells and activates Tie2 receptor in a paracrine manner. Unlike Angpt2, Angpt1 is incorporated into the ECM through its linker peptide region[80]. In contrast, the autocrine-acting Angpt2, is produced in EC, stored in the Weibel-Palade bodies and interferes antagonistically with constitutive Angpt1/Tie2 signaling to destabilize the endothelium and prime it to respond to exogenous cytokines[81]. However, as a partial agonist, Angpt2 has also been shown to contextually activate Tie2 either in the absence of Angpt1 or in stressed EC[82-84]. Under physiological conditions, Angpt2 expression is restricted to sites of vascular remodeling (e.g. placenta, ovaries and uterus). However, Angpt2 expression is dramatically increased in many inflammatory and angiogenic diseases such as tumor angiogenesis, malaria and sepsis[85]. Angpt2 is rapidly released from the endothelium upon inflammatory stimuli, providing fast responses to inflammation, permeability and coagulation[86,87]. Numerous factors like shear stress, VEGF and hypoxia transcriptionally regulate Angpt2 expression. Importantly, laminar flow regulated transcription factor (TCF) kruppel-like factor 2 (KLF2) negatively regulates Angpt2 expression, which contributes to endothelial quiescence[88].

1.2.3 Angpt/Tie system: Loss-and gain-of function studies

Several studies have demonstrated the functional role of the Angpt/Tie system through the generation of knockout (KO) and overexpression mice for Angpt ligands and Tie receptors. These studies have highlighted the important biological functions of Tie1 and Tie2 receptors as well as Angpt1 and Angpt2 during physiological angiogenesis.

Tie2 deficiency leads to embryonic lethality and the mice die between E10.5 and 12.5 due to severe cardiac defects, hemorrhage and other vascular defects[89,90]. These mice proceed through the early steps of primary capillary plexus formation. However, the plexus fails to remodel or mature and remains poorly organized with fewer EC and branches[89]. Additionally, Tie2-deficient mice show a pronounced lack of pericytes and VSMC[89]. Further studies have demonstrated that Tie2 also plays an essential role in hematopoiesis and cardiac development[91]. By contrast, a constitutively active Tie2 mutant, resulting from a missense mutation in the kinase domain of the receptor tyrosine kinase, causes venous malformations with enlarged veins, pronounced EC proliferation, and irregular VSMC coverage[92]. Moreover, overexpression of Tie2 in EC and keratinocytes causes a psoriasis-like phenotype characterized by epidermal hyperplasia, altered dermal angiogenesis and inflammation[93].

Tie1-deficient embryos show no significant perturbations in the initial steps of developmental angiogenesis, but they die between E13.5 and postnatal day 1 (P1) due to loss of EC integrity thereby resulting in edema and hemorrhage[90,94]. Unlike Tie2-deficient mice, hematopoiesis is not disturbed in

Tie1-deficient mice[95]. The double KO of Tie1 and Tie2 resembles the phenotype observed in Tie2-deficient mice, highlighting the essential role of Tie2 in the endocardium[94].

Angpt1-deficient mice phenocopy Tie2-deficient mice and gene targeting of Angpt1 leads to embryonic lethality at E12.5[77]. These mice have growth-retarded hearts with poorly developed ventricular trabeculae. The endocardium is retracted from the myocardial wall and the endothelial lining in the atria is collapsed. Moreover, the atria display a lack of trabeculae. The importance of Angpt1 during heart development was further demonstrated by Angpt1 gain-of-function studies. Myocardial overexpression of Angpt1 led in 90% of the cases to embryonic lethality between E12.5 and E15.5 as a result of cardiac haemorrhage[96]. The remaining ten percent of the mice survives with cardiac hypertrophy and a dilated right atrium. Thus, Angpt1 overexpression has a dramatic impact on early heart development. Furthermore, Angpt1-deficient mice also exhibit defects in vascular development. The mice show a poorly formed and less complex vascular network and periendothelial cells appear to be dissociated from endothelial cells[77]. However, overexpression of Angpt1 in the skin leads to hypervascularization with larger, highly branched vessels, which are excessively covered by pericytes[97] and decreased vessel permeability[98].

Angpt2-deficient mice are born phenotypically normal, but develop chylous ascites soon after birth[99], suggesting that Angpt2 is dispensable for normal embryonic development. Nevertheless, the mice show defects in vascular sprouting and remodeling during postnatal-retinal angiogenesis with a lack of hyaloid vessel regression[99]. Furthermore, depending on the genetic background, Angpt2-deficient mice have defects in their lymphatic vasculature[99]. Angpt2 overexpression, on the other hand, leads to mid-gestational lethality similar to Angpt1 and Tie2-deficiency, supporting the antagonistic function of Angpt2 on Angpt1/Tie2 signaling[100].

In summary, Angpt/Tie system acts as a gatekeeper to control the quiescent EC phenotype in adults and plays a key role in remodeling and maturation of blood vessels during active angiogenesis.

1.2.4 Angpt1-induced Tie2 signaling

In the quiescent adult endothelium, Angpt1 is constitutivily secreted by mural cells and binds to Tie2 receptor thereby inducing its dimerization and phosphorylation. Angpt1-bound Tie2 is translocated to cell-cell junctions and forms trans-endothelial complexes with other Tie2 molecules from adjecent EC (Figure 2). Tie2 activation by Angpt1 leads to the recruitment of adaptor proteins such as growth factor receptor-bound protein 2 (GRB2), and the p85 regulatory subunit PI3K, which subsequently activates the AKT pathway[1,101-104]. AKT signaling, in turn, activates survival-promoting pathways including endothelial nitric oxide synthase (eNOS) and survivin, while suppressing pro-apoptotic molecules such as Bad and caspase 9. Furthermore, Angpt1/Tie2-mediated AKT signaling also represses Angpt2 expression by phosphorylation of the TCF forkhead box protein O1 (FOXO1) resulting in its nuclear exclusion, ubiquitination and degradation[105].

In contrast, inhibition of the AKT survival pathway activates FOXO1 and promotes its nuclear translocation, which leads to increased production of Angpt2 and consequently drives endothelial

destabilization[106]. Thus Angpt1/Tie2 signaling controls the quiescent endothelium by negatively regulating Angpt2 expression. Angpt1-induced Tie2 is also directly involved in limiting EC permeability by mediating the sequestering of the non-receptor Tyr kinase Src[107]. Moreover, the formation of Tie2 trans-complexes at cell-cell junctions is accompanied by vascular endothelial phosphoTyr phosphatase (VE-PTP), which signals via AKT to eNOS thereby inhibiting paracellular permeability. Conversely, in non-resting EC (in the absence of EC junctions), Angpt1 controls EC migration and proliferation. This process seems to be dependent on the receptor presentation on the cell surface. In particular, Angpt1-mediates translocation of Tie2 to cell-substratum contacts, triggering DOK-R, ERK1/2 and FAK signaling, which are all involved in EC migration[108]. Lastly, Angpt1-induced Tie2 stimulation exerts anti-inflammatory effects via the recruitment of intracellular protein ABIN2, which interferes with the nuclear factor κB (NF-κB) pathway[109,110].

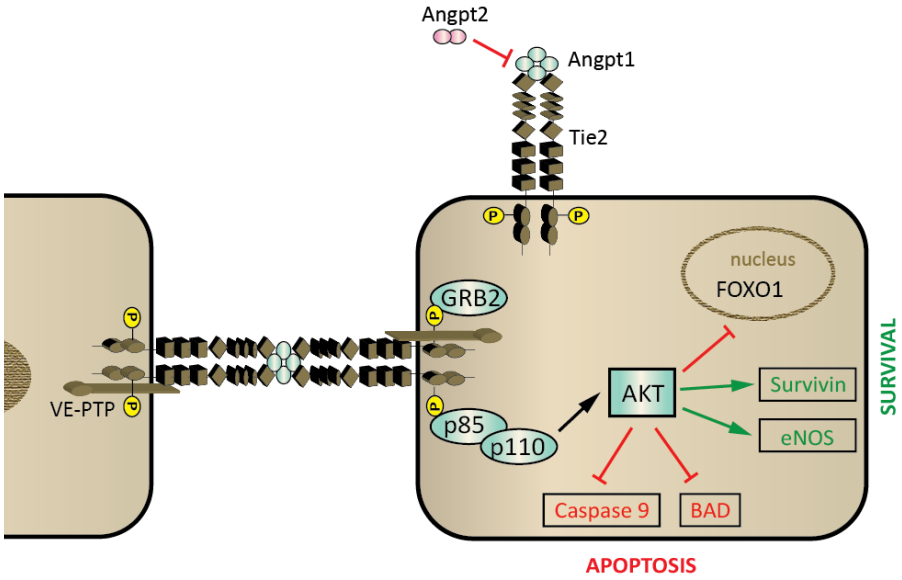

Figure 2. Angiopoietin-Tie signaling in resting endothelial cells

Angpt1 mediated phosphorylation of Tie2 leads to translocation of Tie2 to inter-endothelial cell junctions. Tie2 *trans*-complexes are established by Angpt1, which also contains VE-PTP. Angpt1-induced phosphorylation of Tie2 leads to the recruitment of adaptor proteins, such as GRB2 and the p85 regulatory subunit PI3K resulting in the activation of AKT signaling. AKT activates survival-promoting pathways while suppressing apoptotic genes.

The Angpt1/Tie2 signaling pathway is involved in the recruitment of mural cells, which surround the vessel wall and play an important role in vessel maturation, stabilization and quiescence. However, the mechanism involved in the recruitment of mural cells remains poorly understood. One possible mechanims of mural cell recruitment is via heparin binding EGF-like growth factor (HB-EGF). HB-EGF expression in EC is upregulated by Angpt1-mediated Tie2 signaling, albeit only in close contact with mural cells. Consequently, HB-EGF-mediated receptor activation, through the epidermal growth factor receptors ERBB1 and ERBB2, induces VSMC migration[111]. There is also evidence that hepatocyte growth factor (HGF) leads to Angpt1-mediated VSMC recruitment to the endothelium[112]. In addition, serotonin has also been implicated to play a role in Angpt1/Tie2-mediated VSMC

recruitment to the vasculature[113]. In contrast, transforming growth factor beta (TGFβ)-mediated downregulation of Angpt1 is required for VSMC differentiation and to restore the vasculature in its quiescent state[114]. Up to date, no molecular evidence has been established for a possible crosstalk between the Angpt1/Tie2 and platelet derived growth factor b (PDGFB)/platelet derived growth factor receptor β (PDGFRβ) pathway.

Angpt1 signaling has also been described to exert its functions independent of Tie2. It stimulates fibronectin production via astrocyte-expressed αvβ5 intergrin, thereby promoting EC migration in the developing retinal vasculature[115]. In EC, αvβ5 intergrin is crucial for Angpt1-induced formation of Tie1-Tie2 receptor complexes at the EC-EC junctions as well as Tie2 phosphorylation and downstream FOXO1 phoshorylation[75].

1.2.5 Angpt2-mediated Tie2 signaling: Agonist vs. antagonist paradox

As opposed to Angpt1, Angpt2-mediated Tie2 signaling promotes vessel destabilization, sprouting angiogenenesis, remodeling and vessel regression[87]. In the prescence of proangiogenic stimuli, Angpt2 binds to Tie2 and exerts antagonistic effects by blocking the ability of Angpt1 to activate Tie2 in EC[100]. However, in the abscence of pro-angiogenic stimuli Angpt2 contributes to vessel regression. Angpt2-mediated vessel stabilization induces complex formation between Tie2, αvβ3 and FAK followed by internalization and degradation of αvβ3, which primes EC for apoptosis[92]. Nevertheless, in stressed EC Angpt2 has been reported to function as Tie2 agonist[81,82,102]. Angpt2 production, rapidly induced by FOXO1, can activate Tie2/AKT signaling, which leads to the negative feedback regulation of FOXO1-mediated transcription and apoptosis. Correspondingly, Angpt2 has been reported to play a protective role in tumor endothelial cells[116]. Other studies have shown that Angpt2 overexpression (using different administration methods) reduced atherosclerosis progression in *Apolipoprotein E* KO (*ApoE*^{KO}) mice[117,118]. More recent studies have underlined the agonistic versus antagonistic role in basal and inflammatory conditions[75,84]. In pathogen-free conditions, Angpt2 acts as a Tie2 agonist and promotes high phosphorylation of Tie2, low nuclear FOXO1 activation and no leakage. The agonistic action of Angpt2 on Tie2 requires the presence of Tie1. In contrast, upon inflammation, the cleavage of Tie1 prevents Angpt2 agonistic activity and instead favors Angpt2 antagonism of Tie2 and thereupon vessel destabilization[75,84]. Thus, like Angpt1, Angpt2-mediated Tie2 signaling stabilizes the vasculature under physiological conditions, whereas Angpt2 promotes vessel destabilization and remodeling in pathological settings.

Angpt2 is also known to exert vascular effects in a Tie2-independent manner. Endothelial tip cells of sprouting vessels express high levels of Angpt2 and integrins and low levels of Tie2[70,119]. In this Tie2-low scenario, Angpt2 binds to αvβ3, αvβ5 and α5β1 integrins and stimulates FAK phosphorylation on Tyr 397 via integrins, thereby promoting cell migration and sprouting angiogenesis at the tip cell front via Rac activation[70]. Angpt2 also plays a central role in promoting pericyte dropout in diabetic mouse retina, associated with loss of integrity of the retinal vasculature, endothelial hyperplasia and increased vascular permeability[120,121]. Correspondingly, Angpt2 is described to induce pericyte apoptosis via α3β1 integrin under high glucose conditions[121].

1.3 Vascular smooth muscle cells

In 1967, Robert Wissler postulated that VSMC of the arterial media represent a single cell type[122]. Before this time, many histology textbooks stated that both VSMC and fibroblast exist in the arterial media. Yet, it was already in 1960 that Pease and Paule provided evidence for this unicellular concept using electron microscopy[123]. VSMC are highly specialized and differentiated cells in adult mammals. They are located in the wall of larger vessels and their main function is to regulate vascular tone thereby controlling blood pressure and blood flow. Under healthy vascular physiology, VSMC exhibit a quiescent contractile phenotype characterized by an unique repertoire of contractile VSMC-specific markers and an extremely low synthetic activity and proliferation rate[124-126]. Like pericytes, VSMC are classified as mural cells because of their perivascular basal membrane embedded position[127]. Moreover, both cell types are involved in the formation and stabilization of mature blood vessels, thereby maintaining vessel integrity. Although VSMC and pericytes are distinct cell types, they show overlapping similarities in origin, location, marker expression and function.

1.3.1 Origin

VSMC progenitors originate from different embryonic sources including neural crest, somatic mesoderm (lateral plate mesoderm derivative), proepicardium (lateral plate mesoderm derivative), splanchnic mesoderm, and other embryonic cell types. As such, the variation in VSMC population can in part be explained by the diverse embryological origins of VSMC[128,129]. VSMC of the ascending aorta, the aortic arch, and pulmonary trunk are neural crest-derived[130], whereas VSMC of the descending aorta arise from somatic mesoderm[131]. Coronary VSMC have been reported to originate from progenitors found in the proepicardium[132]. Furthermore, VSMC at the base of the aorta and pulmonary trunk develop from the second heart field[133,134]. Other VSMC precursors such as Nkx2.5+ and Isl1+ cardiovascular progenitors are able to differentiate into mature VSMC[135]. Moreover, pericytes have been described to differentiate into VSMC or vice versa during vessel growth and remodeling. Finally, Sca1+ and Flk1+ progenitor cells have also been shown to differentiate into VSMC via PDGFRβ-mediated signaling[136] and culture on collagen IV[137,138].

1.3.2 Location and morphology

The distribution of VSMC in the vessel wall is not stochastic. Large vessels, like the aorta, have multiple layers of VSMC intertwined with an elaborate elastin and collagen-based matrix that is required to withstand the higher blood pressure of the circulatory system[127]. Veins, on the other hands, serve as a low-pressure reservoir, are irregularly covered by VSMC and pericytes, facilitate the return of blood from the organs and contain valves to prevent the backflow of blood. The smallest vessels, the capillaries, have limited pericyte coverage, with EC that are highly permeable, to allow gas exchange and nutrient delivery to cells via tiny pores or fenestrations[6,10]. Nevertheless, the differential distribution of pericytes and VSMC is not absolute. Mural cells that share characteristics

with both VSMC and pericytes have been reported to cover intermediate-size vessels, arterioles and venules[127,139,140].

VSMC are heterogeneous and exhibit distinct morphological and functional properties within the same blood vessel, as well as in different types of vessels, e.g. arteries and veins[141-145]. Unlike skeletal or cardiac muscle cells, VSMC are not terminally differentiated and exhibit a diversity of VSMC phenotypes ranging from a contractile to a synthetic phenotype. Environmental cues, including biochemical factors, ECM components and physical forces (stretch and shear stress) modulate VSMC phenotype from a contractile to a synthetic (proliferative) state, or vice versa, a process known as phenotypic modulation/switching. Due to phenotypic switching, synthetic VSMC can take part in long-term maintenance and vascular repair, while contractile VSMC are the major phenotype for short-term regulation of the vessel diameter. As such, this plasticity of VSMC could be regarded as a survival advantage, which enables blood vessels to withstand changes in the circulatory system. Contractile or differentiated VSMC are characterized by an elongated spindle-shaped morphology, with a high concentration of contractile filaments and a low proliferation rate (Figure 3). Moreover, these cells display increased expression of contractile VSCM markers, collagen I and IV and several integrin's such α1β1 and α7β1, which all contribute to the quiescent contractile phenotype of VSMC[125,126,145]. Synthetic VSMC, on the other hand, acquire a rhomboid morphology and display decreased expression of contractile VSMC markers with concomitant increase in synthetic VSMC markers (Figure 3). Other characteristics of synthetic VSMC include increased proliferative and migratory activity, increased ECM deposition, increased cell size and increased expression of α4β1[125,126,145]. VSMC undergoing phenotypic switching can also acquire macrophage markers and properties.

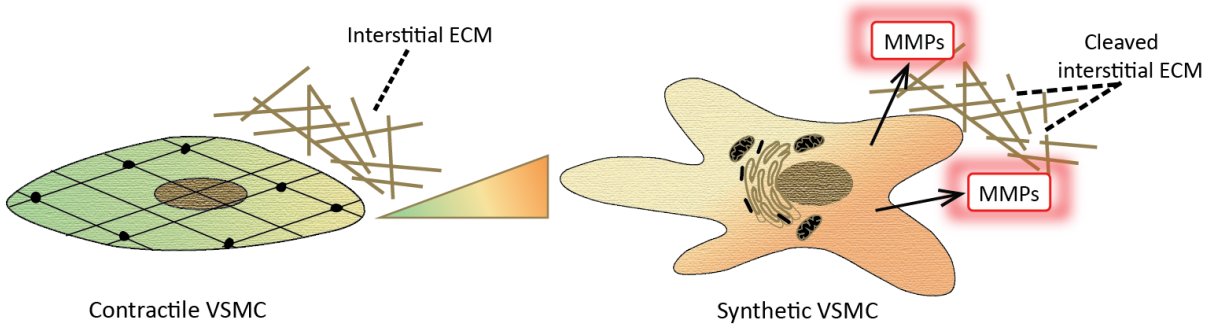

Figure 3. Phenotypic modulation of VSMC

Contractile VSMC are characterized by an elongated spindle-shape morphology, a low prolifertation rate, increased expression of contractile VSMC markers, collagens (I and IV) and integrins (α1β1 and α7β1). Synthetic VSMC exhibit a rhomboid morphology and these cells lose the expression of contractile VSMC marker expression while expressing synthetic VSMC markers. These cells also display increased proliferative and migratory activity, increased ECM deposition includings MMPs and increased expression of α4β1 integrin.

1.3.3 Molecular signature of VSMC

Since there is no definitive marker for VSMC, a large repertoire of VSMC-selective marker genes are available to characterize VSMC differentiation[124-126,146]. PDGFRβ is a well-established receptor marker for mural cells, which include VSMC. VSMC-contraction markers include myosin heavy chain 11 (MYH11), myosin light chain 9 (MYL9) and tropomyosin 1 (TPM1). In addition, differentiated VSMC express a number of proteins that are part of the cytoskeleton and are involved in the regulation of the differentiated VSMC phenotype such as alpha smooth muscle actin 2 (αSMA/ACTA2), smoothelin (SMTN), transgelin (SM22α/TAGLN), calponin (CNN1), caldesmon (CALD1). Most of the VSMC markers, except MYH11, can also be expressed in non-VSMC under certain conditions. In particular, MYH11 is the only marker protein that is VSMC-specific during embryogenesis[124,126,147]. Thus, a combination of several VSMC markers is state-of-the-art to identify VSMC. Furthemore, myosin heavy chain 10 (MYH10), retinol-binding protein 1 (RBP1), vimentin (VIM), matrix g1a protein (MGP) and tropomyosin 4 (TPM4) are described as suitable synthetic VSMC markers since these proteins are markedly upregulated in proliferating VSMC[148,149]. As such, assessment of the differentiated VSMC phenotype depends on the analysis of multiple marker genes, including the analysis of proliferation marker genes. Yet, it has been reported that differentiation and proliferation are not necessarily mutually exclusive and other factors than the VSMC proliferation status may influence differentiation[126,150].

PDGFRβ

PDGFRβ is an essential receptor expressed in VSMC. The interplay of PDGFB, expressed by EC, and PDGFRβ, expressed on mural cells, is an important process for mural cell recruitment during angiogenesis[16,151-154]. KO of PDGFB- and PDGFRβ leads to mural cell deficiency and embryonic lethality[155-157]. PDGFRβ is expressed by mesenchymal cells, myofibroblasts, pericytes and neuronal progenitor cells[157,158]. Despite the fact that PDGFRβ is expressed by other cells, it is considered as a suitable marker for mural cells.

αSMA

αSMA is a contractile protein of the cell cytoskeleton. It is mainly expressed in smooth muscle cell lineages and myofibroblasts[159]. αSMA was first detected in the heart at E8.0 and gradually decreased after E10.5[160]. Its expression was detected in skeletal muscle at 9.5 and gradually increased to a high level by E15.5. Furthermore, αSMA expression is also expressed in VSMC between E9.5 and E10.5 and continues to be expressed into adulthood. αSMA is the first known marker of VSMC differentiation during development, and is highly selective for mature VSMC or VSMC-related cells such as pericytes[161,162]. Moreover, it is involved in the regulation of vascular contractility and blood pressure[163]. αSMA is by far the single most abundant protein in mature fully differentiated VSMC making up to 40% total cell protein and over 70% of the total actin[164].

SM22α/TAGLN

SM22α, like αSMA, is part of the cell cytoskeleton and is abundantly expressed in VSMC. It is a 22-kDa calponin-related protein that interacts with other contraction-associated proteins such as F-actin and tropomyosin[165,166]. SM22α is considered to be a VSMC-specific protein and is one of the earliest markers of differentiated VSMC. However, its expression has also been shown in a portion of myeloid cells including neutrophils, monocytes and macrophages (MΦ)[167]. SM22α is known to co-localize to actin filament bundle and stress fibers[168]. Moreover, purified SM22α protein can even bind directly to actin filaments at a ratio of 1:6 actin monomers, suggesting that it may serve to organize the spatial relationships of actin filaments in VSMC[166,169,170]. Correspondingly, SM22α gene expression is dramatically downregulated when VSMC acquire a synthetic phenotype, which also involves cytoskeletal rearrangements[171,172]. There is also evidence that SM22α mediates calcium (Ca^{2+})-independent vascular contractility[173]. During embryonic development, SM22α is expressed in VSMC at E9.5 and continues to be expressed in all SMC into adulthood[160]. SM22α is also expressed in the heart and skeletal muscle in the early stages of development, however only transiently between E8.0 and E12.5.

MYH11

MYH11, also known as smooth muscle myosin heavy chain (SMMHC), is a smooth muscle myosin that belongs to the myosin heavy chain family[174]. It is a major component of the contractile apparatus in VSMC involved in VSMC contraction and the conversion of chemical energy into mechanical energy via ATP hydrolysis[174]. Unlike αSMA and SM22α, MYH11 is expressed in VSMC at a later stage during embryonic development, E10.5, and is not expressed in cardiac or skeletal muscle cells[147,160].

1.3.4 Endothelial-VSMC interaction

The interaction between EC and VSMC is essential for maintaining vascular tone in mature vessels. Communication between the two cell types is critical during embryonic development and for physiological angiogenesis in the adult, which is required for tissue repair and remodeling processes. During late embryonic development, the formation of mature and fully functional vessels requires the recruitment and differentiation of VSMC, which is tightly regulated by growth factor gradients and tissue hypoxia[175-177]. In mature vessels, developmental signals continue to be required for the maintanance of blood vessels, but additional communication also takes place to regulate vascular tone and blood pressure[178,179]. There are several key regulators involved in EC and VSMC communication and/or VSMC differentiation, which can be devided into two categories: i) those that demand physical contact between the two cell types (e.g. gap junctions, myoendothelial junctions), and ii) those that occur via a soluble or secreted molcule (e.g. PDGFB, TGFβ, Angiotensin II [AngII]).

PDGF was first identified as a serum growth factor for fibroblasts, glia cells and VSMC[180-182]. The PDGF family consists of four ligands, PDGFA, PDGFB, PDGFC and PDGFD. While PDGFC and PDGFD are able to form homodimers, PDGFA and PDGFB build either homodimers or heterodimers[183]. PDGFs bind

and signal via two cell surface receptor tyrosine kinases, PDGFRα and PDGFRβ. PDGFRβ binds PDGFB and PDGFD, whereas PDGFRα binds PDGFA, PDGFB and PDGFC[183]. Binding of the ligand leads to autophosphorylation and subsequent activation and signaling of downstream intracellular pathways including RAS-MAPK, PI3K, FAK and PLCγ. PDGFB is able to form a concentration gradient, which is sensed by surrounding mural cells through the PDGFRβ and is critical for their recruitment and proliferation for blood vessel maintenance. The expression of PDGFB is mainly induced by hypoxia, thrombin and various growth factors[184]. During angiogenesis, PDGFB is expressed by tip cells and binds to heparin-sulfate proteoglycans through its C-terminal retention motifs, composed of a stretch of positively charged amino acid residues[140,185]. Subsequently, PDGFRβ-positive mural cells proliferate and migrate along new angiogenic sprouts through a temporal and spatial PDGFB gradient[151]. Deletion of either *Pdgfb* or *Pdgfrβ* causes embryonic lethality resulting from mural cell dysfunction and vascular dysfunction, including micro-aneurysms, vascular leakage and hemorrhage[155,156,186]. Correspondingly, deletion of the retention motif leads to partial detachment of mural cells[187]. Moreover, EC-specific deletion of PDGFB results in pericyte deficiency, proving that EC provide the major source of PDGFB and that PDGFB is critical for mural cell coverage of the vasculature[188]. Furthermore, the crosstalk of PDGFB/PDGFRβ signaling with other signaling pathways may alter the response of VSMC to EC-secreted PDGFB. In particular, the ratio between PDGFB and VEGF plays a critical role during blood vessel growth and maturation. VEGF signaling interacts with PDGFB/PDGFRβ signaling through regulation of PDGFB expression and suppression of PDGFRβ signaling. Intriguingly, a positive feedback loop between VEGFC/VEGFR3 and PDGFB/ PDGFRβ regulates vessel maturation through the induction of PDGFB[189]. VEGFA, on the other hand, is described to be a negative regulator of vessel maturation. VEGFR2 and PDGFRβ assemble a receptor complex in mural cells upon VEGFA stimulation, which leads to the suppression of PDGFRβ signaling[190]. Additionally, specific blocking of VEGFA and PDGFB in age-related macular degeneration suppresses subretinal neovascularization and might be a potential therapeutic approach[191].

In the adult vasculature, the communication between EC and VSMC is established through secreted or diffusible factors. EC-derived factors including nitric oxide (NO), prostacyclin, and hyperpolarizing agents diffuse to VSMC to cause vasodilation[178,179,192]. Similarly, EC-derived vasoactive agents such as endothelin 1 (ET1) and AngII act on VSMC to increase vascular tone[178,179,192]. Thus, both the secreted developmental factors as well as the cell-cell contact mediators seem to function in the adult vasculature to control blood vessel function.

1.3.5 Regulators of VSMC phenotype

There are several factors and signaling pathways that determine the contractile or synthetic phenotypic fate of VSMC (Figure 4). PDGFB/PDGFRβ signaling is described to have a negative effect on mature VSMC, and induces profound suppression of contractile VSMC marker genes such as *Myh11* and *αSMA and Tagln/Sm22α*[193]. In particular, PDGFB binds to a *cis*-acting DNA sequence known as CArG box (CC(A/T6GG), which is located in the regulatory regions of VSMC specific genes, to antagonize myocardin (MYOCD)-serum response factor (SRF) induced differentiation of VSMC.

Conversely, TGFβ-induced Smad2 and Smad3 signaling promotes the contractile phenotype of adult VSMC by increased expression of *αSMA, Myh11* and *Cnn1*[194]. Importantly, Smad2 and Smad3 also interact with SMC-specific promoters at putative Smad binding elements (SBE)[195]. The vasoactive agent AngII exerts a dual role regulating both the contractile and synthethic VSMC phenotype depending on cell-context and location within the artery. In particular, AngII has been described to promote the contractile VSMC via L-type Ca^{2+} channels (LTCCs) and Prx[196,197] and the synthetic phenoype of VSMC by inducement of authophagy[198]. Furthermore, AngII is also responsible for mediating VSMC contraction[199,200].

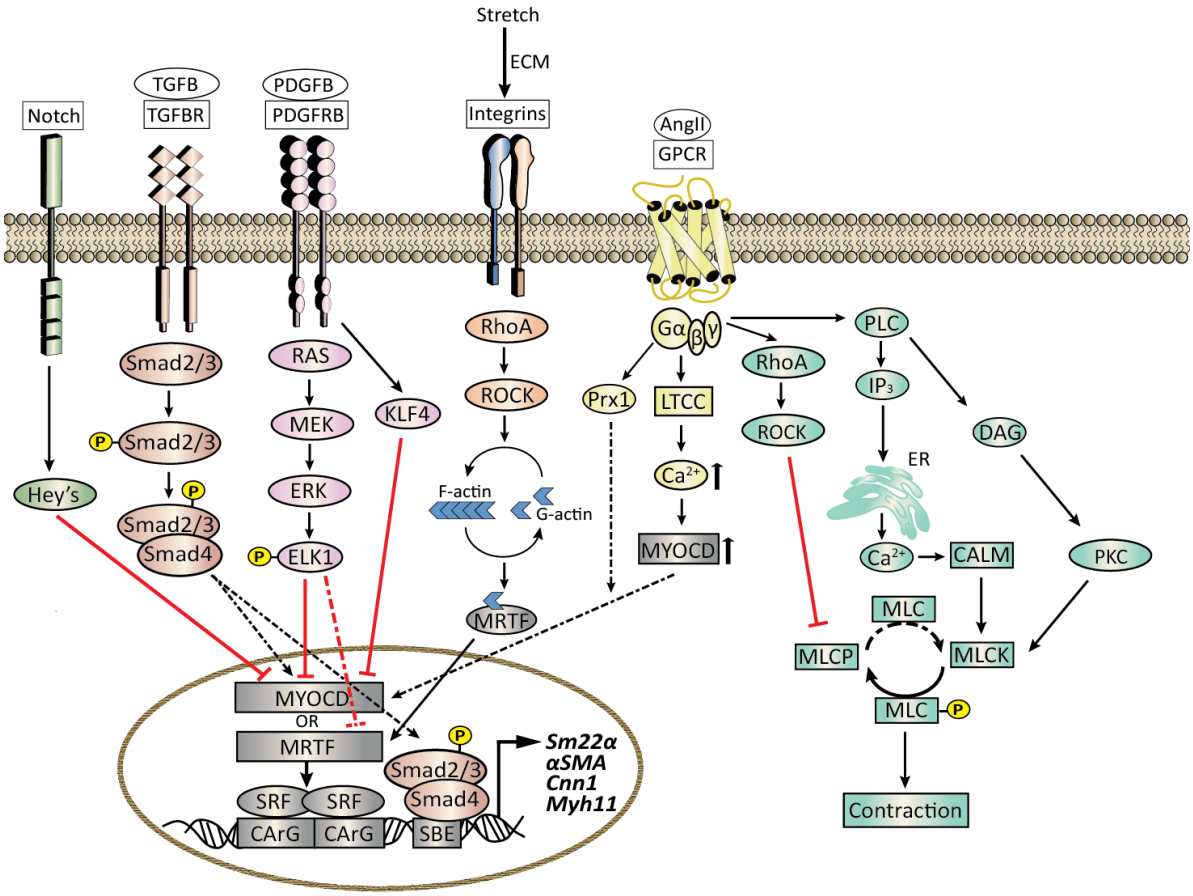

Figure 4. Regulators of VSMC phenotype

Schematic model illustrating important molecular pathways that control VSMC growth or differentiation. The MYOCD-SRF-CarG-axis plays an essential role in maintaining the contractile VSMC phenotype. Its activity is antagonized by PDGFB and Notch via the action of the repressor factors, Hey's, KLF4 and ELK1, thereby promoting the synthetic VSMC. TGFβ, Notch and AngII exert dual effects on VSMC phenotype and depending on the environmental stimuli they can either promote the contractile VSMC phenotype or the synthetic VSMC. The ECM has a major impact on VSMC phenotype and promotes VSMC differentiation through the integrin-RhoA-ROCK-mediated signaling pathway. AngII also regulates VSMC contraction by promoting downstream signaling, via IP_3 and PKC, the release of intracellular Ca^{2+}, followed by the phosphorylation of myosin light chain (MLC) and subsequent cytoskeletal reorganization. Many of these molecular pathways are also implicated in cardiovascular diseases, and contribute to the synthetic VSMC phenotype and/or contraction.

Transcription factors (TCFs) also play key roles in regulating phenotypic switching of VSMC. In quiescent and mature VSMC, the expression of contractile VSMC-specific genes is regulated by the increased expression of SRF and its VSMC- and cardiomyocyte (CM)-specific cofactors MYOCD and myocyte enhancer factor 2 (MEF2). This complex binds to the CArG box, to promote gene activation and expression of contractile VSMC markers[195,201-203]. Moreover, the two MYOCD-related TCFs, MRTA and MRTB have similar transcriptional properties to MYOCD and induce VSMC differentiation by binding to SRF. These TCFs are mediated by the RhoA/Rho-associated coiled-coil containing protein kinase (ROCK) signaling pathways[204].

KLF4, which is normally not detected in quiescent VSMC, is rapidly upregulated upon vascular inury. KLF4 is induced by PDGFB stimulation and functions as a transcriptional repressor to prevent gene-activation of contractile VSMC markers through the inhibition of MYOCD expression and inhibition of SRF binding to intact chromatin[205-207]. Like PDGFB, KLF4 is able to inhibit SRF binding to CArG boxes, thereby downregulating transcription of VSMC contractile genes[126]. Additionally, the TCF ELK1 (a ternary complex of Ets domain proteins) also suppresses transcription of contractile VSMC marker genes by inhibiting the binding of MYOCD-SRF complexes to CArG boxes[193,208]. ELK1 is phosphorylated by PDGFB stimulation and signals downstream via a MAPK signaling cascade, ultimately cleaving MYOCD-SRF.

The ECM, in which VSMC are embedded, plays a pivotal role in mediating VSMC differentiation, proliferation, migration, survival, and cytoskeletal organization[209]. Modulation of VSMC phenotype by ECM components seems to be regulated by their binding to specific integrin receptors[145]. The medial ECM is predominantly composed of collagen isoforms (type I, III and IV), elastin, and proteoglycans. Among those, the proteoglycan heparin has proven to be an essential ECM component for the regulation of VSMC phenotype by promoting the contractile phenotype and detaining VSMC proliferation[210]. In contrast, the proteoglycan fibronectin promotes modulation towards a synthetic VSMC phenotype[211]. Other ECM components such as fibrillar collagen type I promote the contractile phenotype of VSMC, whereas monomeric collagen type I activates VSMC proliferation[212]. Just like fibrillar collagen type I, collagen type IV and laminin have been shown to be important for the induction of the contractile VSMC phenotype.

Finally, VSMC within the vessel wall are continuously exposed to mechanical stretch and shear stress resulting from blood pressure and blood flow, respectively. While shear stress is mainly sensed by EC, mechanical stretch affects all cell types in the vessel wall including VSMC[213]. Mechanical stress modulates cell shape, cellular organization and intracellular processes resulting in migration, proliferation or contraction[214]. As such, both mechanical stretch and shear stress induce vessel wall remodeling by changing VSMC phenotype, thereby maintaining vascular tone and homeostasis. Mechanical stretch has been reported to increase the expression of ECM components as well as contractile VSMC marker genes by VSMC within the vessel wall[215,216]. However, in response to excessive mechanical stretch as a consequence of high blood pressure, the expression of contractile VSMC marker genes diminishes while VSMC undergo phenotypic remodeling towards a synthetic phenotype. Hence, these cells loose their ability to contract. Consequently, VSMC secrete growth

factors (e.g. PDGFB; VEGF, basic fibroblast growth factor [bFGF], AngII), which act in an autocrine or paracrine loop to influence VSMC and EC growth and function[217-219]. This process further stimulates medial VSMC hypertrophy and/or intimal hyperplasia of the arterial walls. The response of VSMC to shear stress is coordinated by EC as these cells recognize and mediate the effects of this type of mechanical stress. This occurs not only via the production of NO but also through direct cell-cell interactions[210].

Phenotypic switching of VSMC is associated with proliferation and migration of these cells. After the transition from a contractile to a synthetic VSMC phenotype, VSMC migrate and proliferate in the vascular wall to promote healing following vessel injury. This process is regulated by growth promoting factors such as PDGFB[146,220], bFGF[146,221] and AngII[199,222] within the injured vascular wall, which regulate downstream signal transduction in VSMC. Moreover, VSMC proliferation and migration are two important processess in the pathogenesis of atherosclerosis, which will be discussed in more detail in section 1.6.

1.3.6 VSMC function: From cardiovascular health to disease

Quiescent, contractile VSMC alter the luminal diameter by vasoconstriction and dilation, which enables blood vessels to maintain an appropriate blood pressure[223]. VSMC of resistance arteries mainly participate in the regulation of blood pressure, while conduit arteries supply blood to visceral organs and limbs[224,225]. VSMC contraction and dilation are regulated by two main signaling pathways: i) Ca^{2+}-dependent signaling pathways via Phospholipase C (PLC), and inositol trisphosphate (IP_3), ii) Ca^{2+}-independent signaling pathways through diacylglycerol (DAG) and protein kinase C (PKC) (Figure 4)[223]. Binding of vasoactive agents, such as AngII or ET1, to their respective receptors on VSMC leads to PLC activation[226-228]. In turn, PLC cleaves the membrane lipid phosphoinositide 4, 5- bisphosphate (PIP2), resulting in the generation of IP_3 and DAG. Subsequently, IP_3 increases Ca^{2+} release into the cytosol from the sacroplasmatic reticulum by binding to ryanodine receptors. Ca^{2+} forms complexes with calmodulin, which is then able to activate myosin light chain kinase (MLCK), resulting in phosphorylation of myosin light chain (MLC), allowing myosin to interact with actin, and subsequent contraction of VSMC. Furthermore, activated RhoA leads to activation of ROCK, which in turn phosphorylates and inhibits the regulatory myosin-binding subunit of myosin phosphatase (MLCP). On the contrary, removal of Ca^{2+} from cytosol leads to relaxation. In pathological cases, deregulated Ca^{2+} levels triggers constricted vessels and sustained blood pressure levels[223].

In summary, VSMC, located in the walls of blood vessels, exert multiple functions to maintain vascular tone, homeostasis and integrity. However, VSMC do not only play important roles in the physiological scenario, but are also described in various pathological conditions such as hypertension and atherosclerosis, which will be discussed in the following chapters, 1.4 - 1.6.

1.4 Cardiovascular diseases

Cardiovascular diseases (CVD) encompass a range of pathological conditions including hypertension, atherosclerosis and myocardial infarction, and nowdays still constitute the major cause of death globally. As reported by the World Health Organization (WHO), more people die annually from CVD than from any other cause. In 2015, 17.7 million people died from CVD representing 31% of all global deaths. Of these deaths 7.4 million were due to coronary heart diseases and 6.7 million were due to stroke. Coronary heart disease, also known as ischaemic heart disease, causes 46% of cardiovascular deaths in men and 38% in women. Cerebrovascular disease is the form of CVD with the second highest mortality, leading to 34% of cardiovascular deaths in men and 37% in women. Despite progress, the overall mortality of CVD is estimated to rise to 23.6 million by 2030 (http://www.who.int/cardiovascular_diseases/about_cvd/en/).

1.4.1 EC dysfunction and reactive oxygen species

Endothelial dysfunction is an early event that signals the onset of CVD. This alteration in endothelial function is characterized by decreased vasodilation, decreased production/ availability of NO, and increased proinflammatory and prothrombotic activity of the EC. NO is generated by eNOS (found in EC and CMs), neuronal nitric oxide (nNOS, found in CM) and inducible NO synthase (iNOS), found in VSMC, EC, CM and macrophages[229-231]. eNOS and nNOS are expressed under normal physiological conditions, whereas iNOS is induced by stress or inflammatory cytokines. Under normal physiological conditions, NO exerts multiple effects that are essential for maintenance of vessel wall homeostasis and cardiac function. These include vasodilation of VSMC, inhibition of VSMC proliferation and migration, and down regulation of inflammatory and adhesion molecules[231,232]. Similarly, NO in the heart affects the onset of ventricular relaxation, which is required for a precise optimization of cardiac pump function. Under pathological stress, risk factors for CVD induce oxidative stress, which plays a critical role in endothelial dysfunction. Moreover, eNOS and nNOS promote the production of reactive oxygen species (ROS) due to malfunctioning of the substrate L-arginine or cofactors such as tetrahydrobiopterin (BH4)[233-235]. This process is called ‘‘NOS uncoupling’’ and implies that the physiological activity of the enzyme for NO production is decreased and switch to NOS-dependent (O_2^-) generation. Moreover, endothelial-induced injury can either activate VSMC proliferation and/or hypertrophy, a phenomenon found in hypertension or VSMC migration and proliferation, a phenomenon found in atherosclerosis.

ROS are ubiquitous, highly diffusible and reactive derivatives of O2 metabolism (as a result of reduction of molecular oxygen), such as hydrogen peroxide (H2O2), superoxide anion ($\bullet O2^-$), hydroxyl radical ($\bullet HO^-$) and reactive nitrogen species peroxynitrite (ONOO-)[236,237]. ROS play a critical role in the initiation and progression of CVD[231,232,238]. They are produced in controlled manners at low concentrations and function as signaling molecules controlling vascular constriction, relaxation and growth. In contrast, under pathological conditions, such as hypertension and atherosclerosis, ROS are produced at levels that cannot be controlled by usual protective antioxidant mechanism employed

by the cells, which in turn promote a state of oxidative stress. Major sources of ROS include xanthine oxidase, uncoupled endothelial NO synthase, NAPD(P)H oxidase, and cyclooxygenase (COX)[231,237]. ROS signaling between cardiac EC and CM occurs in three ways: i) via direct diffusion of ROS and NO, ii) through changes in ECM composition, which in turn affects CM function[239], and iii) via ROS-dependent alteration of paracrine release of multiple cytokines and growth factors from EC[240].

1.5 Hypertension

Hypertension is a complex multifactorial disease that involves alterations in cardiac function and blood vessels[241]. It results from the intricate interactions between genetic and environmental factors, many of which are not completely understood[242]. Hypertension remains a major health problem and a significant risk factor for coronary heart disease and stroke, the leading causes of death worldwide. It is described as a chronic increase in systolic blood pressure (BP, ≥140mmHg) or diastolic BP (≥90 mmHg)[126]. Hypertension is associated with, pressure overload-induced concentric, left ventricular hypertrophy (LVH), which normally occurs as a compensatory mechanism to maintain wall stress[243]. However, sustained pressure-overload can ultimately lead to maladaptive LVH, which is accompanied by cardiac remodeling[243]. Hence, remodeling of arterial resistance vessels with increased peripheral vascular resistance is an independent risk factor for established hypertension[244,245]. Furthermore, although hypertension is considered to be a major contributor to coronary heart diseases, the fundamental disturbance in coronary disease is atherosclerosis, which will be discussed later[246,247].

1.5.1 VSMC remodeling in hypertension

The predominant hemodynamic alteration in hypertension is increased peripheral vascular resistance, which is primarily determined by enhanced VSMC-mediated constriction in resistance arteries (< 500µm) and arterioles and VSMC remodeling[248]. At physiological pressures, these vessels typically exhibit a level of contraction (myogenic tone) independent of neurohormonal influences, and are able to mediate autoregulation of blood flow and stabilize capillaries pressure[249]. In hypertension, VSMC is attributable to arterial remodeling through various processes, including hyperplasia (increase in cell number), hypertrophy (increase in cell size), apoptosis, elongation of cells, reorganization of cells and/or altered ECM composition. According to Poiseuille's law, flow resistance is inversely proportional to the fourth power of vessel radius[250-252]. Consequently, minor decreases in the lumen of resistance arteries will significantly increase peripheral resistance leading to the development of hypertension. In hypertension, the resistance arteries undergo vascular remodeling characterized by reduced outer and lumen diameters, unaltered media cross-sectional area, and increased media to lumen (M/L) ratio (Figure 5). Although the media cross-sectional area is maintained, VSMC rearrange around a smaller lumen, which leads to an increase in media and subsequently to an increased M/L ratio without precipitating hypertrophy[245,249,250]. This type of remodeling is known as eutrophic inward remodeling. In experimental animal models, eutrophic

inward remodeling is often observed in hypertension associated with involvement of the renin-angiotensin system (RAS). In other types of hypertension such as renovascular hypertension, the remodeling process is characterized by increased media cross-sectional area (VSMC hypertrophy and possible hyperplasia). In turn, VSMC growth encroaches on the lumen to increase the M/L ratio (Figure 5). This process is referred to as hypertrophic remodeling. Hypertrophic remodeling is often seen in hypertension induced by administration of deoxycorticosterone acetate (DOCA)[244,252,253]. Conduit arteries (large elastic arteries) do not contribute to peripheral vascular resistance, but are important in damping the pulsatile flow created by the heart[241]. In hypertension, the diameter of conduit arteries, such as aorta or carotid artery, is increased. There is also an increase in wall thickness and VSMC may undergo phenotypic switching towards a synthetic/proliferative phenotype[254]. The increase in vessel diameter is most likely passive as a result of the rise in blood pressure that distends the vessel while the increase in wall thickness normalizes media stress[241]. Furthermore, activation of transcriptional regulatory pathways triggers alterations in the components of the cytoskeleton, contractile apparatus and ECM, ultimately leading to VSMC stiffness. The structural vascular changes in resistance and conduit arteries with increased arterial stiffness leads to increased wave reflection and blood pressure, which ultimately promote the development of LVH[241].

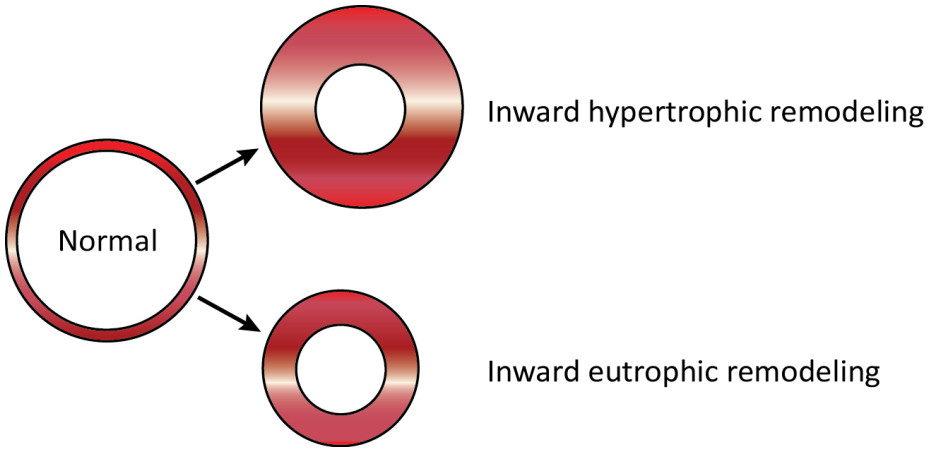

Figure 5. Types of vascular remodeling in hypertension
Hypertension is associated with structural changes of resistance arteries. These arteries undergo inward eutrophic and/or hypertrophic remodeling. Inward eutrophic remodeling is characterized by reduced outer and lumen diameters, unaltered media cross-sectional area and increased M/L ratio. In inward hypertrophic remodeling, medial growth, due to VSMC hyperplasia and/or hypertrophy and ECM deposition, encroaches on the lumen to increase M/L ratio.

1.5.1.1 Left ventricular hypertrophy

The myocardium has three morphological compartments: i) the muscular compartment composed of cardiomyocytes (CMs), the dominant type occupying approximately 50% of the heart weight, ii) the interstitial compartment formed by fibroblast and collagen and iii) the vascular compartment with VSMC and EC[255]. LVH is a major maladaptive response to chronic pressure overload and an important

risk factor in patients with hypertension[255,256]. LVH is associated with cardiac remodeling characterized by endothelial dysfunction, interstitial fibrosis, and alterations in sarcomere organization and CMs. Complications of LVH include atrial fibrillation, diastolic dysfunction, systolic dysfunction, and sudden death[255,256]. Both early recognition and a better understanding of LVH may lead to more effective therapeutic measures for this cardiovascular risk factor[256].

1.5.1.2 Cardiomyocytes

CMs are mainly responsible for generating contractile force in the heart and their proliferation is important for development, function, and regeneration of the heart[257-259]. CMs rapidly proliferate during fetal life, but exit the cell cycle irreversibly soon after birth in mammals. During fetal development, heart growth is mediated by CM proliferation and they respond to increased hemodynamic load of the developing cardiovascular system by undergoing hypertrophic growth, remodeling and contractility accompanied by activation of the immediate early genes (c-JUN, c-MYC, c-FOS), and fetal genes (atrial natriuretic factor (ANF/ANP), beta-myosin heavy chain (β-MHC), and skeletal alpha actin (SKA)[258,260]. During cardiac injury, the same adaptive hypertrophic response occurs in adult CM, leading to the notion that CM respond to pressure-overload by calling upon the fetal hypertrophic growth program to provide compensatory growth and increased contractility. However, adult CMs fail to re-enter the cell cycle, which is considered to be the primary limiting factor in restoring function to the damaged heart[258,260]. Therefore the generation of novel CMs within the cardiac milieu to replace the injured myocardium is warranted to design adequate therapeutic applications for patients with heart failure and limited treatment options[261]. An increasing number of studies have reported induction of CM proliferation and cardiac regeneration, either by fetal or neonatal CM transplantation, skeletal myoblast transplantation or stem cell transplantation[262-265]. However, the improvements are minor and may be only transient[266,267]. Hence, it is still disputed to what extent CM proliferation can be induced and whether it can be utilized therapeutically. Other studies have reported that adult zebrafish and newts regenerate their hearts after cardiac injury, and in both cases regeneration is based on CM proliferation[268-270]. Yet, the mechanism that drives cardiac proliferation in zebrafish and newts is still under investigation.

1.5.2 Regulators of CM and VSMC remodeling in hypertension

Hypertension is associated with cardiac remodeling and vascular remodeling. The mechanism regulating these processes involves multiple signaling cascades and downstream TCFs that function in a coordinated fashion to activate genes involved in the regulation of growth, apoptosis and ECM metabolism. These signaling cascades are activated by different stimuli including mechanical stress (shear stress or stretch), ROS, neurohormonal factors, growth factors and cytokines, and are also critically involved in pathological cardiac remodeling and vascular remodeling[231,249]. While stretch of the vessel wall acts on all layers of the vessel wall, stretch on the myocardium predominantly acts on CM[271]. Moreover, shear stress affects primarily the endothelium in response to changes in blood

flow[213]. Integrin's and respective downstream signaling are important regulators during adaptive as well as maladaptive cardiac and VSMC remodeling. The ECM-integrin-cytoskeleton axis enables VSMC to detect and respond to changes in intraluminal pressure allowing remodeling of resistance arteries during hypertension[231,271-273]. In the heart, this axis is also able to promote hypertrophic growth of CMs in hypertension. Substantial evidences indicate that ablation of β3 or β1 integrin inhibits pressure-induced hypertrophic signaling, thereby resulting in reduced cardiac output with increased mortality and heart failure[274,275]. Furthermore, anti-α5- or anti-β1-integrin antibodies significantly inhibited the capacity of arterioles to contract in response to increments in intraluminal pressure[276].

The MAPK pathway is the primary signaling mechanism by which mechanical stress, neurohormonal factors and ROS regulate expression of genes involved in growth and remodeling. Activation of the three major subfamilies of MAPKs (ERK1/2, JNK, p38MAPK) have been demonstrated in animal models of cardiac injury as well as in humans with heart failure[277-279]. In addition, increased AngII-stimulated MAPK activity has also been observed in VSMC derived from spontaneously hypertensive rats (SHR) compared to those from normotensive (WKY) controls[280].

Structural changes in CMs and VSMC are mediated not only by mechanical stress but also by neurohormonal factors such as RAS, Aldosterone and ET1. ET1 is a potent vasoconstrictor produced and released by EC, CMs and VSMC[281-284]. In the myocardium, ET1 may act in an autocrine and paracrine fashion, where it binds to ET_B receptors on cardiac EC and ET_A receptors on CMs. Binding of ET1 to ET_B receptors leads to the release of other signaling molecules (NO and prostaglandin I_2), which regulate vasodilation. In contrary, when binding to the ET_A receptors on CMs, ET1 causes CM constriction and hypertrophic actions. Similarly, ET_A and ET_B receptors mediate the vasoconstrictive, proliferative and hypertrophic effects of ET1 in VSMC[281,282,284].

AngII is the active component of the RAS, formed from enzymatic cleavage of angiotensinogen to angiotensin 1 (AngI) by aspartyl preotease renin, with subsequent conversion of AngI to AngII by angiotensin converting enzyme (ACE)[285-287]. It is produced both systemically and locally via tissue-specific renin-angiotensin systems[285]. AngII is involved in the regulation of blood pressure and plasma volume via aldosterone-regulated sodium excretion, and sympathetic nervous system activation[285,288,289]. Furthermore, it contributes to the regulation of several cellular processes such as proliferation, differentiation, regeneration and apoptosis[285]. The multiple actions of AngII are mediated via specific, highly complex, intracellular signaling pathways that are stimulated upon receptor binding; AngII type 1 receptor and AngII type 2 receptor[285,288,289]. The importance of the RAS, and the benefit of its inhibition, in cardiac and vascular remodeling are well-established[290]. Numerous studies have shown that activation of the (local) RAS contributes to myocardial hypertrophy, fibrosis, and dysfunction[291,292]. Accordingly, a large number of animal experiments[293-296] and clinical trials in humans[297,298] have documented the beneficial effects of AngII receptor blockade or ACE blockade in preventing or reversing ventricular remodeling in patients with heart failure. Increasing evidence suggest a direct link between the RAS and TGFβ, indicating that TGFβ acts downstream of AngII. AngII stimulation induces TGFβ expression in CMs and cardiac fibroblast, in

turn promoting CM hypertrophy and fibrosis, respectively. In addition, TGFβ1-overexpressing mice displayed significant cardiac hypertrophy accompanied by interstitial fibrosis[290]. RAS also contributes to vessel remodeling in the aorta and other vascular beds in hypertension[299]. AngII causes systemic vasoconstriction by activation of AngII type 1 receptors in VSMC. Along with vasoconstriction, Binding of AngII to its respective receptor may also stimulate growth and hypertrophy of VSMC, thereby directly contributing to vascular remodeling in hypertension[300]. Moreover, the AngII type 1 receptor anatagonist Losartan reversed vascular remodeling in patients with hypertension[300].

1.6 Atherosclerosis

Atherosclerosis is a chronic inflammatory disease of the arterial wall that is responsible for nearly 50% of all deaths in the Western world[301]. The major clinical complications of atherosclerosis, such as myocardial infarction and stroke, are the consequences of thrombotic events associated with acute rupture or erosion of an unstable plaque[302]. Atherosclerosis plaques are characterized by asymmetric focal thickening of the intima, the innermost layer of the artery, that encroach on the lumen of medium-sized and large arteries[303]. These plaques contain lipids, inflammatory cells, VSMC, connective-tissue elements, and debris[303]. Atherosclerosis can remain asymptomatic for decades, highlighting the need for preventive cardiology in the early stage of life. In humans, arterial stiffness and atherosclerosis can start as early as childhood. There are a number of genetic and environmental risk factors for atherosclerosis[301]. The genetic factors include hypertension, obesity and diabetes, whereas the environmental factors include life-style (smoking, lack of exercise, high-fat diet), infectious agents and low antioxidant levels.

1.6.1 Phases of atherosclerosis

The earliest changes that precede atherosclerosis formation take place in the endothelium, with resultant endothelial dysfunction triggered by high levels of low-density lipoprotein (LDL), in particular oxidized low-density lipoprotein (oxLDL), low levels of high-density lipoprotein (HDL) and low levels of NO (Figure 6)[303-307]. Endothelial dysfunction allows circulating LDL infiltration into the vascular intima, which subsequently leads to formation on oxLDL through enzymatic and non-enzmatic oxidation[303-307]. Additionally, oxLDL activates endothelial cells and resident immune cells leading to the expression of chemokines (e.g. M-CSF, MCP1, CCL5 (RANTES), CX3CL1) and adhesion molecules (e.g. VCAM1, PCAM1 and ICAM1, E-selectin, P-selectin) that attract circulating monocytes and lymphocytes to the vessel wall. This process supports infiltration of these inflammatory cells in the intima through adhesion, rolling, and transendothelial migration. Once in the intima, M-CSF stimulates entering monocytes to differentiate into MΦ. Subsequently, MΦ ingest oxLDL and transform into foam cells, which eventually leads to fatty streak formation[308].

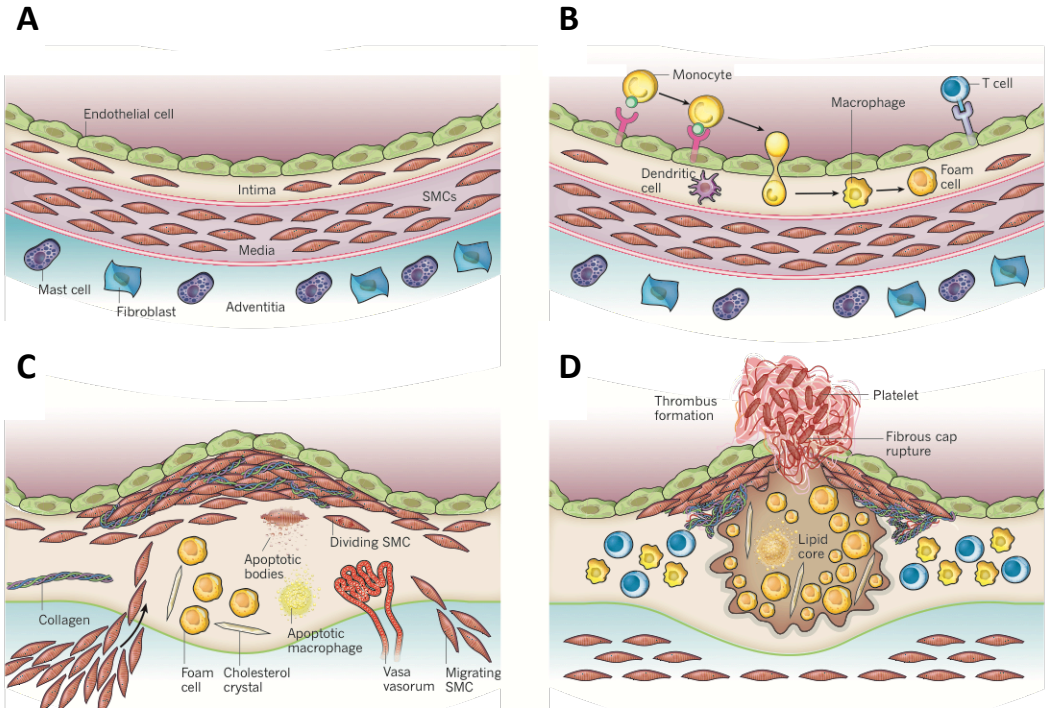

Figure 6: Onset and progression of atherosclerosis

A, The normal artery consists of three layers: the tunica intima, tunica media and the adventitia. The inner layer, the tunica intima, is the monolayer of EC that are in contact with blood flow. In contrast to many mammals, the human intima contains resident VSMC. The middle layer, the tunica media, contains VSMC embedded in an intricate ECM made up of (mostly) elastin between the VSMC, which gives elasticity to the vessel. The adventitia, the outer layer of the vessel wall, consists of mast cells, fibroblasts, nerve endings and microvessels. **B**, At early stages of atherosclerosis progression, leukocytes adhere to the activated endothelial monolayer, migrate into the intima and mature into MΦ. Subsequently, MΦ ingest oxLDL and transform into foam cells. **C**, Progression of atherosclerotic lesions involves the migration of VSMC from the media to the intima. The intimal VSMC proliferate and synthesize ECM macromolecules such as collagen, elastin and proteoglycans. In addition to all these events, MΦ and VSMC die and generate apoptotic bodies in advancing plaques. Extracellular lipids derived from dead cells accumulate and form a lipid or necrotic core. Cholesterol crystals and microvessels are also found in the advancing plaques**. D**, Thrombosis is often the ultimate complication of atherosclerosis due to rupture of the fibrous cap. Reprinted with permission[306].

Along with excessive lipid accumulation, uncontrolled monocyte infiltration and phagocytosis results in MΦ apoptosis and, when not adequately disposed of, necrosis. This progressively promotes the formation of a necrotic atherosclerotic plaque core, which is surrounded by a cap of VSMC and collagen-rich matrix, in advanced stages of lesion progression[303,308]. The inflammatory response of EC promotes migration and proliferation of VSMC, from the media to the intima, which in turn become intermixed with the area of inflammation to form an intermediate lesion progression[303]. These responses proceed uninhibited and are accompanied by production and accumulation of synthesized ECM and inflammatory chemokines by VSMC[309,310]. VSMC are essential in the pathogenesis of atherosclerosis and plaque rupture[302,303]. The stability of the atherosclerotic plaque relies on the thickening of the fibrous cap and the

degree of cap inflammation[302,303]. VSMC in advanced atherosclerotic plaques exhibit a very low rate of proliferation and produce high amounts of collagen leading to a stable atherosclerotic plaque. In contrary, plaque instability is associated with cap thinning characterized by increased MΦ accumulation and VSMC death in the shoulder area of the plaque. Moreover, MΦ are able to sensitize VSMC to apoptosis by secreting different cytokines (IL1β, TNFα and IFNγ)[311-313]. In addition, activated T-cells stimulate MΦ to produce MMPs, which degrade the fibrous cap and support plaque instability ultimately leading to plaque rupture. Apoptotic VSMC are evident in advanced human plaques, supporting the notion that VSMC apoptosis in advanced atherosclerotic plaques may promote plaque rupture[303]. Thus, the balance of VSMC proliferation and migration versus VSMC apoptosis and senescence determines the population of VSMC within the atherosclerotic plaque and stability of the plaque[302].

The phases of atherosclerosis have been studied in detail in animal models including genetically modified mouse models[301,304]. Mice deficient in *ApoE* or *low-density lipoprotein receptor* (*LDLR*) develop advanced lesions and are the models of choice to explore the role of inflammatory cells, VSMC and EC, and their complex interactions, during atherosclerosis progression[301,304].

1.6.2 EC dysfunction and atherosclerosis

Diabetes mellitus, hypertension, modified LDL and other injuries to the EC monolayer initiate a chronic inflammatory response of the vessel wall. The earliest step of atherosclerosis progression occurs in an injured endothelium, resulting in increased infiltration of immune cells, LDL particles, leukocyte adhesion and thrombotic potential[310,314]. Moreover, injury to the endothelium limits the bioavailability of eNOS. Numerous oxidative stress biomarkers show strong associations with the development and progression of coronary artery disease (CAD) and predict cardiovascular events[315]. In particular, oxLDL is part of the 'downstream markers' of oxidative stress. It has been reported that the oxLDL/LDL cholesterol ratio may be the best indicator of the risk associated with oxLDL levels[316]. Several studies have confirmed endothelial dysfunction to be an early stage event of atherosclerosis[317,318]. The study of Ludmer and colleagues provided the first line of evidence, in humans, of impaired endothelium-dependent vasodilation in the presence of atherosclerosis[319]. They observed, upon acetylcholine administration, paradoxical constriction in the arteries of patient with mild CAD as well as in those with advanced CAD, indicating that endothelial dysfunction is present in the early stages of atherosclerosis[319]. Moreover, in studies using either acetylcholine administration[320] or flow-mediated dilation[317] endothelial dysfunction was detected in both conduit and microvascular vessels of patients with coronary risk factor. However, no angiographic or ultrasound evidence of structural CAD was observed, confirming that endothelial dysfunction occurs in the preclinical stage of atherosclerosis.

1.6.3 Inflammatory cells and atherosclerosis

The complex interaction of inflammatory cells with VSMC and EC promotes atherosclerosis progression and its clinical complications. Monocytes MΦ exert pro-inflammatory functions in the atherosclerotic plaque. They are able to secrete ROS that oxidizes LDL, which in turn boost the inflammatory milieu[321,322]. They also produce IL1β and TNFα, thereby promoting leukocyte adhesion to EC[323] and VSMC apoptosis[311-313]. Furthermore, MΦ secrete monocyte chemotactic protein (MCP1) that increases leukocytes infiltration into the intima[324]. In addition, they degrade collagen by producing MMPs. Moreover, MΦ express procoagulant activity, which contributes to fibrin formation and subsequently mediates leukocyte adhesion and trafficking[325]. Along with monocytes and MΦ other immunce cells cells such as lymphocytes, mast cells, T cells and dendritic cells enter into the intima.

Taken together, immune cells influence the behavior of EC and VSMC and create a positive feedback-loop leading to further recruitment of these cells into the atherosclerotic lesion, thereby promoting the onset and progression of atherosclerosis. Hence, regulators of immune cell accumulation and trafficking play a key role during atherosclerosis.

1.6.4 VSMC remodeling and atherosclerosis

Endothelial dysfunction and immune cell accumulation mark the initial stages of atherosclerosis, whereas the later stages of disease progression are highly dependent on synthetic VSMC characterized by enhanced migration, proliferation and ECM deposition[306]. VSMC phenotypic switching plays a key role during atherosclerosis progression and ultimately determines the fate of plaque stability in advanced atherosclerotic lesions.

Under normal physiological conditions, VSMC express contractile genes, however during atherosclerosis progression these genes are temporarily silenced while the synthetic genes are active[326-328]. In the initial stages of atherosclerosis VSMC lose their contractile phenotype and switch towards a synthetic phenotype with increased proliferation, migration and ECM production[124,126]. In contrary, VSMC at later stages of disease progression show reduced proliferation, migration and ECM synthesis in vulnerable lesions. The ability of VSMC to switch back to a contractile state correlates with lesion stabilization at advanced stages of atherosclerosis progression. Regulation of VSMC phenotypic switching has been extensively studied and inhibiting this switch might be beneficial in advanced atherosclerosis[126,329-332]. More specifically, MYOCD is regarded as a promising therapeutic target for atherosclerosis. It exerts several anti-atherosclerotic functions by abolishing lipid uptake of VSMC, inflammation in the vessel wall, macrophage interaction and chemotaxis[126,329-332,333]. Furthermore, there is also evidence demonstrating the involvement of VSMC-expressed PDGFRβ in atherosclerosis progression. Blockade of the PDGFB/ PDGFRβ signaling pathway, using neutralizing antibodies or chemical inhibitors, reduced VSMC participation in atherosclerosis[334,335]. Another study

demonstrated that VSMC-specific overexpression of PDGFRβ in *ApoE*^{KO} mice, on a high-fat diet, leads to increased atherosclerosis and macrophage accumulation[336].

The synthesis and degradation of the ECM in advanced atherosclerotic plaques play a critical role in plaque stabilization[337]. While large amounts of ECM are produced in the fibrous cap, with the characteristics of a stable plaque, ECM degradation is enhanced in the lipid core, leading to plaque vulnerability[337]. Plaque vulnerability in turn may predispose to plaque rupture. Importantly, degradation of the ECM by the actions of Mmps derived from MΦ prompts VSMC to interact with interstitial matrix proteins (collagen I, collagen III, fibronectin, ostepontin) that facilitates the switch towards a synthetic phenotype[145,338]. Increased collagen I in plaques leads to the release of monomeric collagen 1. While collagen IV and polymerized collagen I inhibit VSMC growth and promote the contractile VSMC phenotype, monomeric collagen I reduces the contractile phenotype and promotes VSMC proliferation[339].

VSMC are also actively involved in propagating inflammation, through their regulation of cytokine secretion and membrane receptors, during atherosclerosis progression[340]. Studies have shown that endothelial dysfunction, inflammatory cytokines (TNFα, IL1β and IL8) and oxLDL promote the transition of VSMC toward a proinflammatory phenotype[341-344].

1.6.5 Link between hypertension and atherosclerosis

Hypertension and atherosclerosis are distinct diseases that cause similar, yet distinguishable biochemical and pathological alterations in arteries[345,346]. Atherosclerosis predominantly affects large and medium-sized vessels, whereas hypertension is primarily a disease of small arteries and arterioles. However, hypertension can also affects large vessels. Atherosclerosis, when associated with hypertension may also involve small arteries like those in the brain or heart. One major discrepancy between the two diseases is the accumulation of lipids that is only observed in atherosclerotic lesions[345,346]. Epidemiology studies and clinical trials have shown that hypertension contributes significantly to atherosclerosis progression[305,347-349]. In particular, these studies have reported that atherosclerosis of the aorta, coronary artery, cerebral arteries and other major vessels is more severe in hypertensive as compared to normotensive subjects[349]. The mechanism by which hypertension accelerates atherosclerosis are not fully explored. However, several possibilities are discussed in literature: i) serum lipids are carried into the vessel wall by ultrafiltration via the arterial intima. As such, an increase in filtration pressure during hypertension will alter the equilibrium across the intimal surface to favour a greater lipid deposition[345,350,351], ii) experimental coarction of the aorta leads to an increase in mucopolysaccharides in the wall of the aorta prior to lipid accumulation[345], iii) increasing evidence indicate that hypertension, through the vasoactive peptides ET1 and AngII, promotes atherosclerosis progression through inflammatory mechanisms[352,353]. Hence, these possibilities, interrelated or not, may serve as a bridge linking hypertension and atherosclerosis.

1.7 Angpt/Tie system in cardiovascular diseases

Growing evidence implicates the involvement of the Angpt/Tie system in hypertension as well as atherosclerosis. Interestingly, controversial roles of Angpt1 and Angpt2 have been reported for both pathological conditions.

1.7.1 Angpt/Tie system during hypertension

Biomarker studies imply a role of Angpt/Tie signaling in the pathogensis of hypertension. These studies reported increased Angpt2 concentrations in the serum of patients with essential hypertension[354-356], particularly those associated with atherosclerosis[355]. Correspondingly, elevated Angpt2 levels in these patients correlate with inflammation and adhesion molecules (IL6, VCAM1, and ICAM1)[355]. Interestingly, next to Angpt2 plasma levels, levels of Angpt1 and sTie2 were also increased in hypertensive patients[354]. In addition, plasma levels of Angpt1, Angpt2 and Tie2 are also increased in patients with pulmonary arterial hypertension (PAH)[357]. There is evidence that overexpression of Angpt1 in rodents leads to a PAH-like phenotype[358,359]. In contrast, other studies have shown that the Angpt1-Tie2 signaling protects against PAH[360,361].

1.7.2 Angpt/Tie system during atherosclerosis

The Ang/Tie system has been proposed to play essential roles in the pathogenesis of atherosclerosis[362-367]. Biomarker studies suggest a role of the Ang/Tie system in macrovascular functions related to atherosclerosis. Elevated levels of circulating Angpt2, have been associated with hypertension and atherosclerosis[362,365]. Moreover, *LDLR-/-* mice vaccinated against Tie2 significantly reduced atherosclerotic plaque formation in carotid arteries and aortic root, supporting a pro-atherosclerotic role of Tie2[364]. Additionally, adventitial angiogenesis was reduced significantly upon vaccination against Tie2, suggesting a possible mechanism via which vaccination against Tie2 inhibits lesion formation. Like Angpt2, Tie1 has shown to be expressed at regions of non-laminar flow in the mouse aorta[368]. Tie1 plays an essential role in endothelial cell activation associated with inflammation[368]. Overexpression of Tie1, *in vitro,* increased the expression of inflammatory markers such as of VCAM1, ICAM1 and E-selectin, potentially through a p38-dependent mechanism[368]. In addition, partial deletion of Tie1 reduced the number of atherosclerotic plaques and MΦ in the distal aorta in a mouse model of atherosclerosis[367], supporting that Tie1 mediates inflammation during atherosclerosis progression. The role of Angpt1 and Angpt2 in atherosclerosis remains controversial. Angpt1 has been shown to protect against atherosclerosis[369] and Angpt2 blocking antibodies reduce early atherosclerotic lesion formation[366]. Likewise, adenoviral systemic overexpression of Angpt2 or recombinant Angpt2 protein have in two independent studies been shown to act atheroprotective[117,118]. These apparently conflicting results likely suggest that Angpt/Tie signaling during atherosclerosis exerts spatiotemporally context-dependent pro- and anti-atherosclerotic

effects that cannot exclusively be explained by the stabilizing effects of Angpt1 and the destabilizing effects of Angpt2 on EC.

1.7.3 Angpt/Tie system in VSMC

Tie2 expression has also been reported in VSMC[370-372]. There is evidence that Angpt1 induces migration of mural precursor cells in a Tie2-dependent manner[370]. Moreover, MCF-7 cells overexpressing Angpt1 in a tumor xenograft led to reduced tumor growth, by recruiting VSMC expressing Tie2[372]. Another study compared normal and arthritic synovial tissues and observed high levels of Tie2 in VSMC from rheumatoid arthritis patients as compared to normal synovial tissue[371]. Although these scattered observations have reported Tie2 expression by VSMC, the functional role of VSMC-expressed Tie2 has not been investigated.

1.8 Aim of the study

The tyrosine kinase receptor Tie2 (Tek) plays important roles during vascular development, remodeling and maturation[1,2]. Tie2 exerts its angiogenesis-regulating functions through its almost exclusive EC-specific expression. In fact, EC-specific deletion of Tie2 phenocopies the embryonic lethal phenotype of globally Tie2-deficient mice, which die during midgestation (E10.5) as a result of perturbed vessel maturation[69]. Yet, Tie2 is not solely expressed by EC[59,60,62,64-68]. Scattered reports have suggested that VSMC may also express Tie2[370-372]. However, a functional role of VSMC-expressed Tie2 has not yet been established. Importantly, Angpt/Tie signaling has also been implicated in the pathogenesis of cardiovascular diseases including hypertension and atherosclerosis. Therefore, the aim of the study is to i) investigate the role of VSMC-expressed Tie2 in regulating blood pressure and cardiac function in hypertension and ii) investigate the role of VSMC-expressed Tie2 in regulating phenotypic remodeling of VSMC during atherosclerosis progression.

2 Results

2.1 VSMC-specific expression of Tie2

In order to confirm previous reports on the expression of Tie2 in VSMC[370-372], Tie2 (*TEK*) expression was comparatively assessed in cultured human aortic smooth muscle cells (HAoSMC), human umbilical artery smooth muscle cells (HUaSMC), human aortic endothelial cells (HAoEC) and human umbilical vein endothelial cells (HUVEC). Real-time quantitative PCR (RT-qPCR) and semi-quantitative PCR revealed low, but consistently detectable levels of Tie2 (*TEK*) in HAoSMC and HUaSMC as compared to HAoEC and HUVEC (Figure 7A and 7B). Moreover, HAoSMC and HUaSMC expressed *ANGPT1*, but not the EC-specific markers *ANGPT2* and *VEGFR2* (Figure 7B). Western blot analysis confirmed Tie2 along with Tagln and a lack of Vegfr2 expression on protein level in HAoSMC and HUaSMC (Figure 7C).

The detectable but comparatively lower expression of Tie2 in VSMC raised the question whether the receptor is functional and plays a role in cell signaling. The Angpt1 ligand is the most prominent inducer of Tie2, which is known to bind to the extracellular domain of Tie2, thereby leading to its dimerization and consequent phosphorylation[101]. Therefore, the functional capability of the VSMC-expressed Tie2 receptor was validated by stimulation of HuASMC with recombinant human Angpt1 for 20 min. HUVEC were used as a positive control. To detect Tie2 recepter phosphorylation, Tie2 was immunoprecipitated from protein extracts and detected by western blotting using a pan-phosphotyrosine antibody. Angpt1 stimulation led to a significant increase in Tie2 phosphorylation,

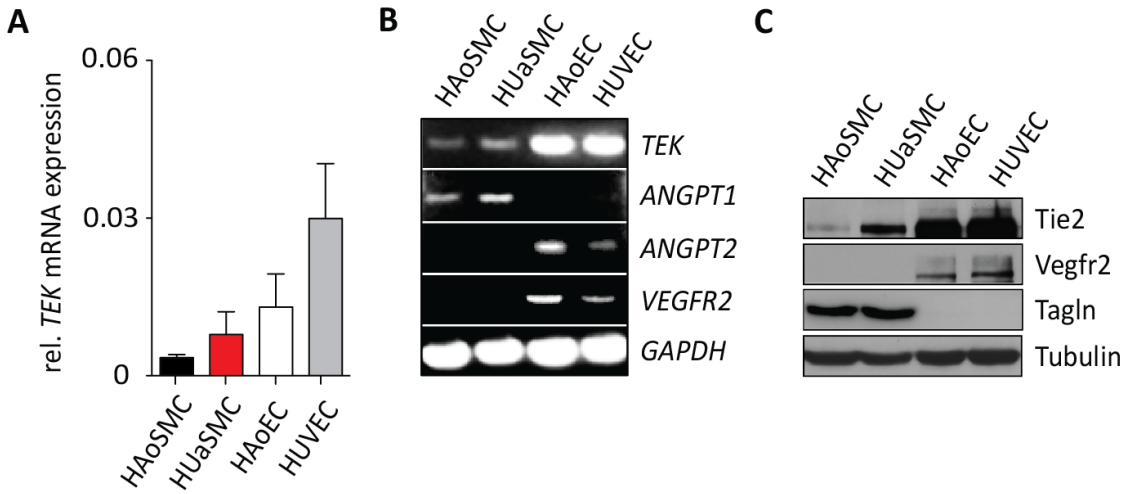

Figure 7. Vascular smooth muscle cells express Tie2

A, Gene expresssin analyses by RT-qPCR of Tie2 (*TEK*) in HAoSMC, HUaSMC, HAoEC and HUVEC. **B**, Tie2 *(TEK), ANGPT1, ANGPT2, VEGFR2 and GAPDH* expression in HAoSMC, HUaSMC, HAoEC and HUVEC were detected by semi-quantitative PCR. **C**, Tie2, Vegfr2, Tagln (transgelin/Sm22α) and Tubulin expression in HAoSMC, HUaSMC, HAoEC and HUVEC were detected by Western blot. Cells were analyzed at passage 2 (n=3). Expression is normalized to *B2m* mRNA expression. Data are shown as mean ± S.D.

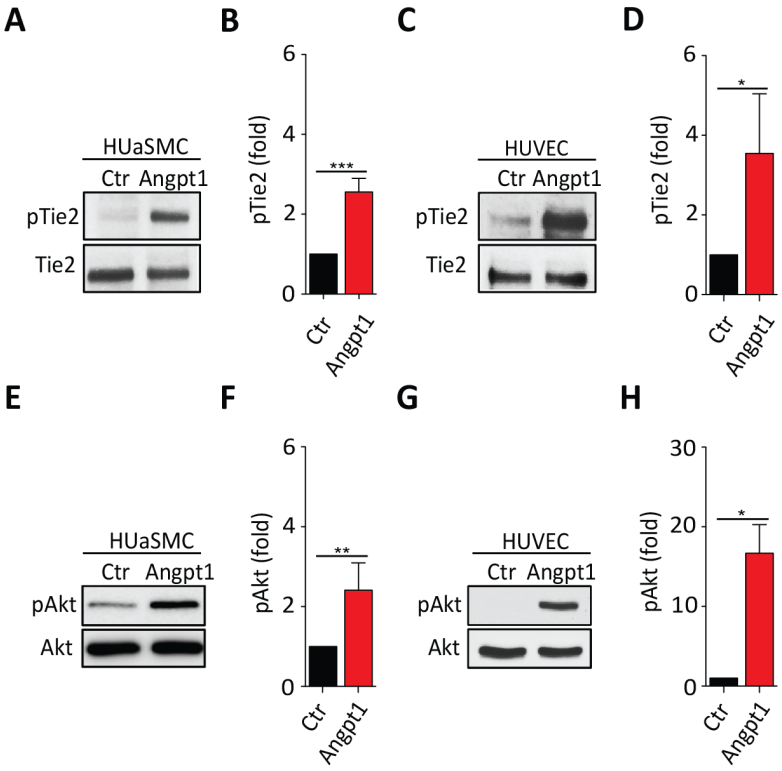

Figure 8. Vascular smooth muscle cells express functional Tie2 receptor

A-D, Representative Western blots and corresponding densitometric analyses of pTie2 and Tie2 in HUaSMC (**A-B**) and HUVEC (**B-C**) stimulated with or without recombinant human Angpt1 (400 ng/ml) for 20 min. Cell lysates were immunoprecipitated with anti-Tie2 antibody and immunoblotted sequentially with anti-phophotyrosine (pTie2) and anti-Tie2 (Tie2) antibodies. Tie2 phosphorylation represents the ratio of phosphorylated Tie2 to total Tie2, normalized to unstimulated controls. **E-H**, Representative Western blots and corresponding densitometric analyses of pAkt and Akt in HUaSMC (**E-F**) and HUVEC (**G-H**) stimulated with or without recombinant human Angpt1 (400 ng/ml) for 20 min. Akt phosphorylation represents the ratio of phosphorylated Akt to total Akt normalized to unstimulated controls (n=3-4). Data are shown as mean ± S.D. of 3-4 independent experiments. *$p < 0.05$, **$p < 0.001$, ***$p < 0.0001$. Student´s *t-test*.

albeit Tie2 phosphorylation was less in HUaSMC (Figure 8A and 8B) compared to HUVEC (Figure 8C and 8D). Correspondingly, Angpt1 induced phosphorylation of the Tie2 downstream effector Akt (Figure 8E-8H), which are important pathways controlling cell survival and proliferation.

To assess VSMC-specific Tie2 expression *in vivo*, *Sm22α-Cre* mice were crossed to *Rosa26* yellow fluorescent protein (YFP) reporter (*Rosa26*^{YFP}) mice[373] and CD31$^-$CD45$^-$YFP$^+$ and CD31$^+$CD45$^-$YFP$^-$ cells were isolated from the heart for subsequent gene expression analysis. Therefore, hearts from 12-weeks-old adult mice were resected and digested for single cell suspensions. Cells were resuspended in ACK-lysis buffer and subsequently labelled for the EC and leukocyte marker CD31 and CD45, respectively. Dead cells were excluded by staining with FxCycle. Viable CD31$^-$ CD45$^-$ YFP$^+$ and CD31$^+$CD45$^-$YFP$^-$ cells were isolated using fluorescent-activated cell sorting (FACS) (Figure 9A). RT-qPCR analyses demonstrated that Sm22α-positive cells expressed Tie2 (*Tek*) and were devoid of Pecam1 expression (Figure 9B and 9C).

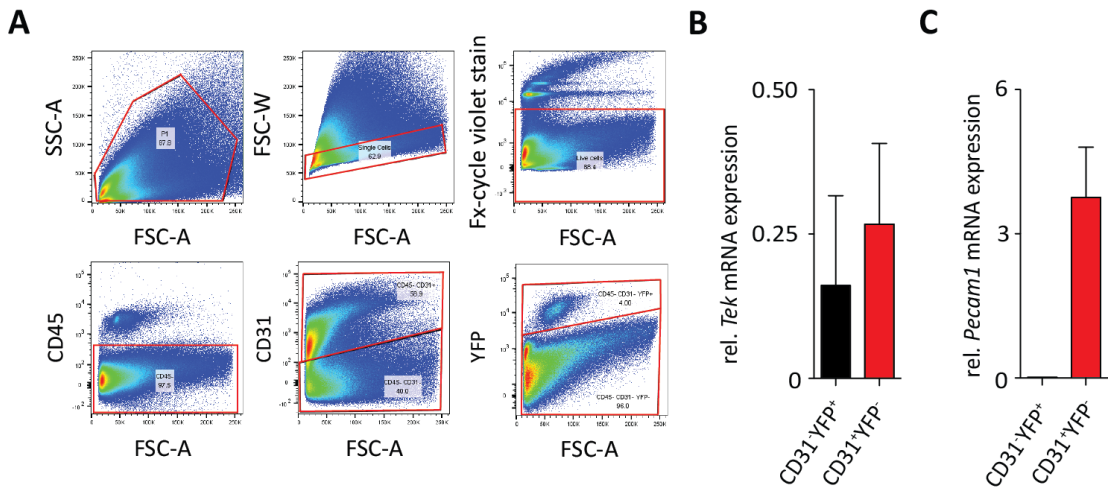

Figure 9. Tie2 expression in isolated mouse aortic vascular smooth muscle cells

A, Representative FACS sorting scheme for the isolation of viable Sm22α-positive cells from the heart of *Sm22α-Cre x Rosa26*^{YFP} mice. **B-C**, CD31$^-$ CD45$^-$ YFP$^+$ and CD31$^+$ CD45$^-$ YFP$^-$ cells were isolated from the heart of *Sm22α-Cre x Rosa26*^{YFP} mice for gene expression analysis (n=3-4). RT-qPCR analysis of Tie2 (*Tek*) (**B**) and *Pecam1* (**C**) in isolated CD31$^-$ CD45$^-$ YFP$^+$ and CD31$^+$ CD45$^-$ YFP$^-$ cells. Expression is normalized to *B2m* mRNA expression. Data are shown as means ± S.D.

2.2 SMC-specific deletion of Tie2

To investigate the functional role of VSMC-expressed Tie2 *in vivo*, *Tie2*$^{flox/flox}$ mice were crossed to *Sm22α-Cre* driver mice to generate mice with constitutively deleted Tie2 in SMC (*Tie2*$^{SMC-KO}$). *Tie2*$^{flox/flox}$ (*Tie2*$^{+/+}$) mice were used as controls. As described previously, mice with a global deletion of Tie2 or EC-specific deletion of Tie2 die within the first 10.5 days postpartum[69,374]. Notably, *Tie2*$^{SMC-KO}$ mice are born phenotypically normal and according to Mendelian ratio. To explore the impact of VSMC-specific Tie2 deletion on vessel growth and morphology during physiological angiogenesis, developing retinal vessels at postnatal day 4 (P4) were analysed in *Tie2*$^{SMC-KO}$ and *Tie2*$^{+/+}$ mice. The retinal vasculature was stained using isolectin B-4 (IB-4), Desmin (for PC coverage) and αSMA (for VSMC coverage) antibodies (Figure 10A). Images were obtained using confocal microscopy and analyzed using Fiji software. Analysis of P4 retinas identified no significant alterations in vessel structure, smooth muscle cell or pericyte coverage in *Tie2*$^{SMC-KO}$ mice (Figure 10B-10D), suggesting that VSMC-specific Tie2 deletion does not alter postnatal retinal angiogenesis or mural cell coverage.

To study the efficiency of VSMC-specific Tie2 deletion, VSMC were isolated from the aorta of *Tie2*$^{+/+}$ and *Tie2*$^{SMC-KO}$ mice and maintained in short-term culture. Tie2 deletion was confirmed by RT-qPCR in short-term cultured aortic VSMC from *Tie2*$^{+/+}$ and *Tie2*$^{SMC-KO}$ mice (Figure 11A). Tie2 high-expressing MS1 cells (immortalized mouse endothelial cell line) and low-expressing NIH3T3 cells (fibroblast cell line) were used as positive and negative controls, respectively. Correspondingly, semi-quantitative PCR revealed Tie2 (*Tek*) deletion in short-term cultured aortic VSMC from *Tie2*$^{SMC-KO}$ mice (Figure 11B) as well as in femoral arteries, mesenteric arteries, aortas and hearts from *Tie2*$^{SMC-KO}$ mice (Figure 11C).

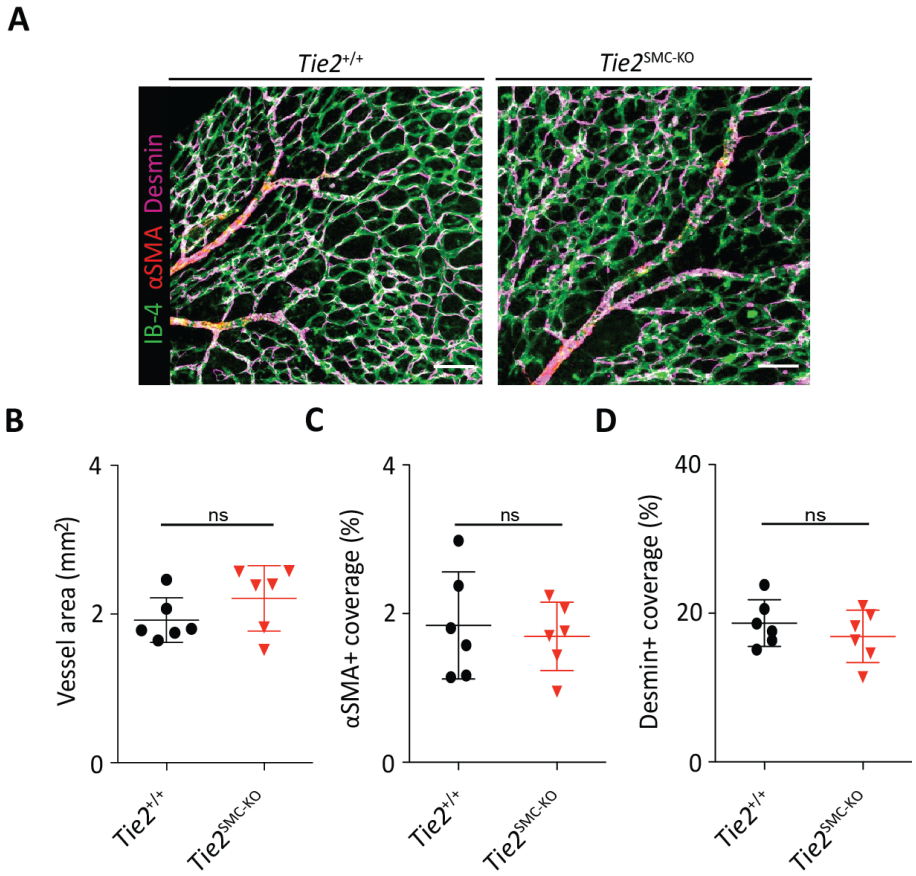

Figure 10. Characterization of retinal vascularization and mural cell coverage in *Tie2*$^{+/+}$ and *Tie2*$^{SMC-KO}$ mice

A, Representative images of the total retinal vasculature (P4) of *Tie2*$^{+/+}$ and *Tie2*$^{SMC-KO}$ mice stained with IB-4 (green), αSMA (red) and Desmin (violet). Scale bar: 200 µm. **B-D**, Quantitative analyses of vessel area (**B**) αSMA-positive coverage (VSMC coverage) (**C**) Desmin-positive coverage (pericyte coverage) (**D**) in retinas from *Tie2*$^{+/+}$ and *Tie2*$^{SMC-KO}$ mice; n=6. Data are shown as mean ± S.D. Student´s *t-test.* ns=non-significant.

The purity of VSMC was analyzed at passage 1 by gene expression analysis. EC and fibroblast are possible contaminations during VSMC isolation. Therefore, MS1 (pancreatic islet endothelial cell line) and NIH3T3 cells (mouse embryomic fibroblast cell line) were used as positive controls. *Pdgfrβ* and Desmin (*Des*) are mural cell markers, whereas *Pecam1 and S100a4* are abundantly expressed by EC or fibroblast, respectively. The purity of VSMC was confirmed by abundant *Pdgfrβ* and *Des* mRNA expression and consistently low levels of EC-specific *Pecam1* transcripts and fibroblast transcript *S100a4* (Figure 12A-12C). These data confirm the homogeneity and purity of isolated aortic VSMC. Hence, isolation of aortic VSMC is applicable to study the functional role of VSMC-expressed Tie2.

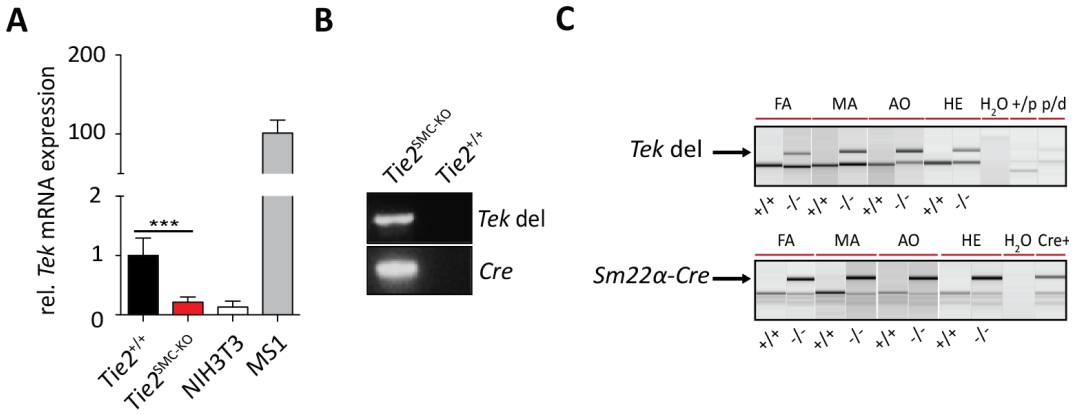

Figure 11. Tie2 expression in isolated mouse aortic vascular smooth muscle cells

A-B, Tie2 *(Tek)* expression in isolated aortic VSMC from *Tie2*$^{+/+}$ and *Tie2*$^{SMC-KO}$ mice detected by quantitative RT-qPCR **(A)** (n=4) and semi-quantitative PCR **(B)** (n=3). **C,** Semi-quantitative PCR analysis of isolated femoral arteries (FA), mesenteric arteries (MA), total aorta (AO) and heart (HE) from *Tie2*$^{+/+}$ and *Tie2*$^{SMC-KO}$ mice for Tie2 deletion; n=3. Tie2 del indicates Tie2 deletion in FA, MA, AO and HE of *Tie2*$^{SMC-KO}$ mice. +/+ is used as symbol for *Tie2*$^{+/+}$ and -/- for *Tie2*$^{SMC-KO}$ mice. p/d is used as control for a floxed homozygous sample with deletion via Cre, and +/p as control for a floxed heterozygous sample without deletion. Mouse EC line MS1 and fibroblast cell line NIH3T3 were used as controls to exclude possible contaminations (n=4). Data are shown as means ± S.D. of 3-4 independent experiments. ***$p < 0.0001$. Student´s *t-test*.

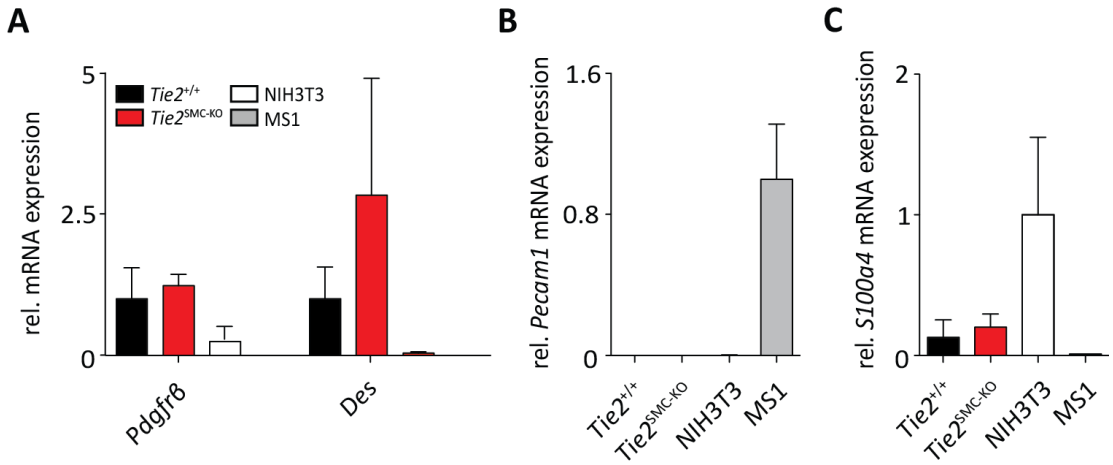

Figure 12. Purity of isolated aortic VSMC

A, Gene expression analysis of mural cell-specific genes *Pdgfrβ* and *Des*. **B-C,** *Pecam1* (EC-specific marker) gene expression **(B)** and *S100a4* (fibroblast-marker) gene expression **(C)** in isolated VSMC of *Tie2*$^{+/+}$ and *Tie2*$^{SMC-KO}$ mice. Expression is normalized to *B2m* mRNA expression. Mouse EC line MS1 and fibroblast cell line NIH3T3 were used as controls to exclude possible contaminations (n=4). Data are shown as means ± S.D. of 3-4 independent experiments.

To determine whether EC-specific Tie2 expression remained unaffected in *Tie2*$^{SMC-KO}$ mice, lung EC were isolated and analyzed for relative marker gene expression. Lungs from adult mice (8-12 weeks old) were resected and digested for preparation of single cell suspensions. Cells were stained for CD45 (leukocytes), Ter119 (erythrocytes), Lyve1 (lymphatic endothelial cells), Podoplanin, ([Pdpn], alveolar epithelial cells) for depletion by magnetic beads. Dead cells were excluded by staining with FxCycle. EC were labelled by co-staining for CD31 (Figure 13A). Relative gene expression analysis

identified no alterations in EC- specific *Pecam1, Cdh5 and Tie2* (*Tek*) expression between *Tie2*$^{+/+}$ and *Tie2*$^{SMC\text{-}KO}$ mice (Figure 13B), suggesting that EC-specific Tie2 expression was unaffected in *Tie2*$^{SMC\text{-}KO}$ mice. Correspondingly, expression levels of VSMC-markers *Tagln/Sm22*, *Cnn1* and *Pdgfrβ* and the fibroblast marker *S100a4* were hardly detected in the two EC populations (Figure 13B). Futhermore, gene expression analysis revealed Tagln mRNA expression levels in isolated peritoneal macrophages from *Tie2*$^{+/+}$ and *Tie2*$^{SMC\text{-}KO}$ mice, whereas Tie2 (*Tek*) mRNA levels were undetected (Figure 13C). In conclusion, these findings demonstrate an efficient and specific deletion of VSMC-expressed Tie2 in *Tie2*$^{SMC\text{-}KO}$ mice.

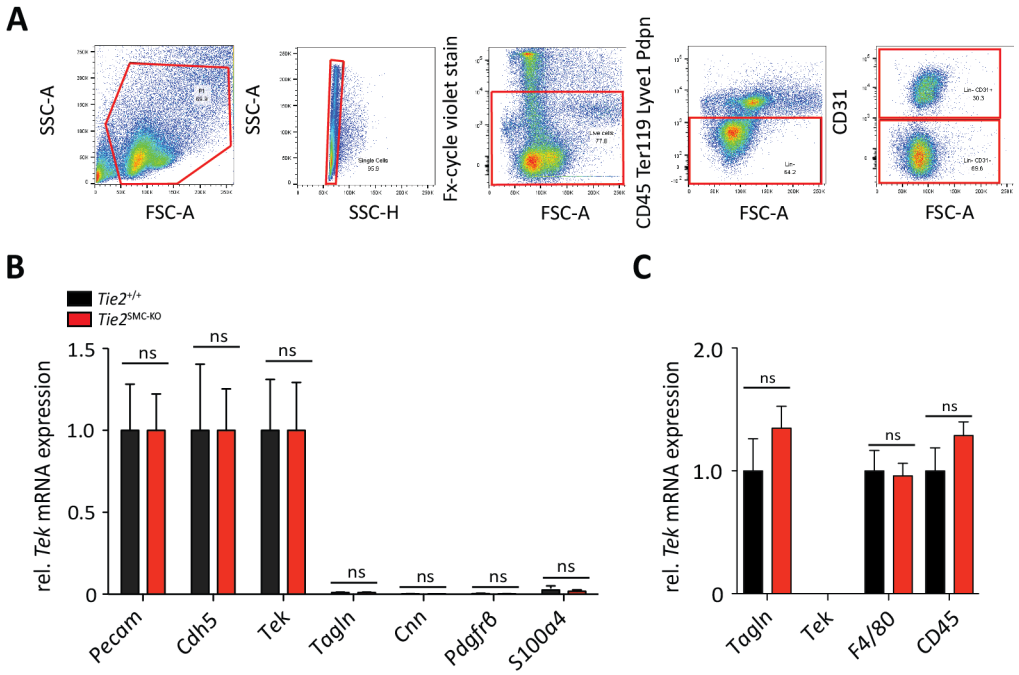

Figure 13. Evaluation of Tie2 expression in isolated lung EC and peritoneal macrophages from *Tie2*$^{+/+}$ and *Tie2*$^{SMC\text{-}KO}$ mice

A, Representative FACS sorting scheme for the isolation of viable lung EC. **B**, Gene expression analysis by RT-qPCR of FACS-sorted CD45$^-$Ter119$^-$Lyve1$^-$Pdpn$^-$CD31$^+$ cells for Tie2 (*Tek*), *Pecam1* (EC-specific marker), and *Cdh5* (EC-specific marker, *Tagln*, *Cnn1*, *Pdgfrβ* (VSMC-specific markers) and *S100a4* (fibroblast marker); n=5. **C**, Quantitative analyses of *Tagln, Tek, F4/80 and CD45* in isolated peritoneal macrophages; n=3. Data are shown as mean ± S.D. Student´s *t-test*. ns=non-significant.

2.3 VSMC-expressed Tie2 regulates phenotypic modulation of activated VSMC

To study whether VSMC-specific Tie2 deletion affects VSMC phenotype and function, gene expression profiling was performed on isolated, short-term cultured aortic VSMC from *Tie2*$^{+/+}$ and *Tie2*$^{SMC\text{-}KO}$ mice. Short-term cultured aortic VSMC from *Tie2*$^{+/+}$ and *Tie2*$^{SMC\text{-}KO}$ mice showed only a minor subset of differentially expressed genes (Figure 14A). Therefore, the Gene Set Enrichment Analysis (GSEA) was employed to elucidate which gene sets were significantly associated with

changes in VSMC phenotypes. GSEA confirmed a downregulation of *Tie2* (*Tek*) in *Tie2*$^{SMC-KO}$ mice (Figure 14B).

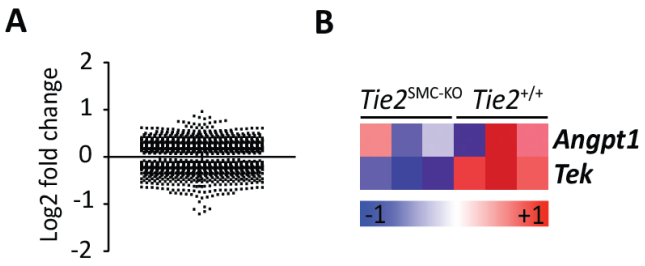

Figure 14. Gene expression analysis in isolated aortic VSMC from *Tie2*$^{+/+}$ and *Tie2*$^{SMC-KO}$ mice
A, Identification of differential gene expression in isolated aortic VSMC (passage 1) from *Tie2*$^{+/+}$ and *Tie2*$^{SMC-KO}$ mice, represented as $\log_2$ fold-change. **B**, Heatmap showing the downregulation of *Angpt1* in the absence of VSMC-expressed Tie2 (n=3).

GSEA revealed that downregulated *Tie2* (*Tek*) and *Angpt1* expression (Figure 14B) in *Tie2*$^{SMC-KO}$ mice significantly correlated with upregulated contractile VSMC-specific gene expression of *Actn4* (actinin 4), *Rock1, Smtn*, *Cald1*, *Tagln* and VSMC contraction-related gene expression of *Myl9*, *Lmod1* (leiomodin 1), *Mylk* (myosin light chain kinase) and *Myl6* (Figure 15A and 15B). In contrast, the proliferation-related gene *Pcna* (proliferating cell nuclear antigen) was downregulated in VSMC from *Tie2*$^{SMC-KO}$ mice as compared to *Tie2*$^{+/+}$ mice (Figure 15C).

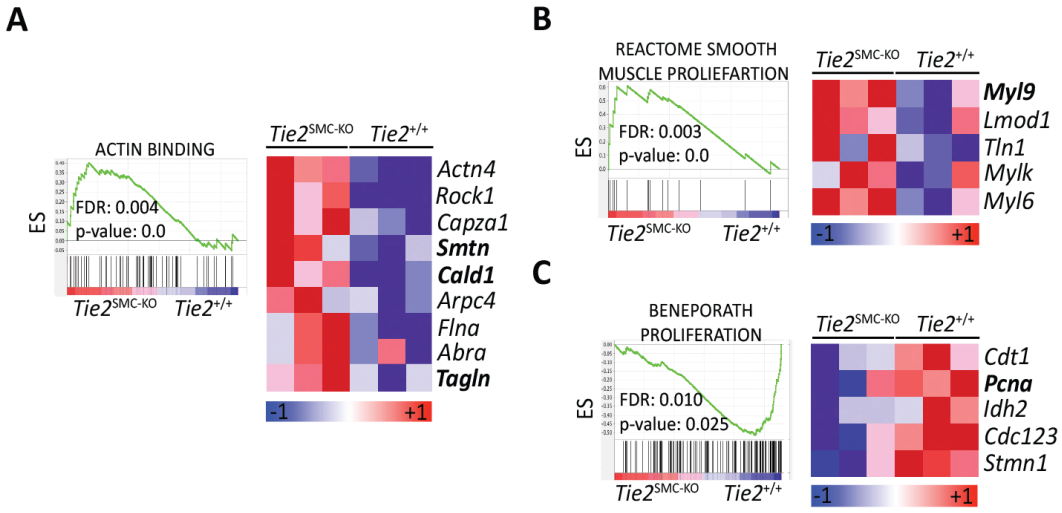

Figure 15. Contractile VSMC markers increased in isolated aortic VSMC from *Tie2*$^{SMC-KO}$ mice
A-C, Heatmap showing the upregulation of contractile VSMC marker genes (*Actn4*, *Rock1*, *Smtn*, *Cald1, Tagln*) **(A)** and VSMC-contraction related genes (*Myl9*, *Lmod1, Mylk*, *Myl6*) **(B)** and the downregulation of proliferation genes (*Pcna*) **(C)** in the absence of VSMC-expressed Tie2 (n=3, ES stands for Enrichment Score).

Validation of the GSEA findings by RT-qPCR confirmed a significant increase in contractile VSMC markers of *Cnn1*, *Tagln*, *Smtn*, *Cald1, Acta2* (αSMA), *Myh11* and *Myl9* in aortic VSMC in the absence of Tie2 (*Tek*) (Figure 16A and 16B). *Angpt1* as well as *Pcna* and the synthetic VSMC markers genes

Rbp1, Vim and *Mgp1* were significantly downregulated (Figure 16A-16C). The expression of other synthetic VSMC-specific genes *Myh10* and *Tpm4* was not altered (Figure 16C).

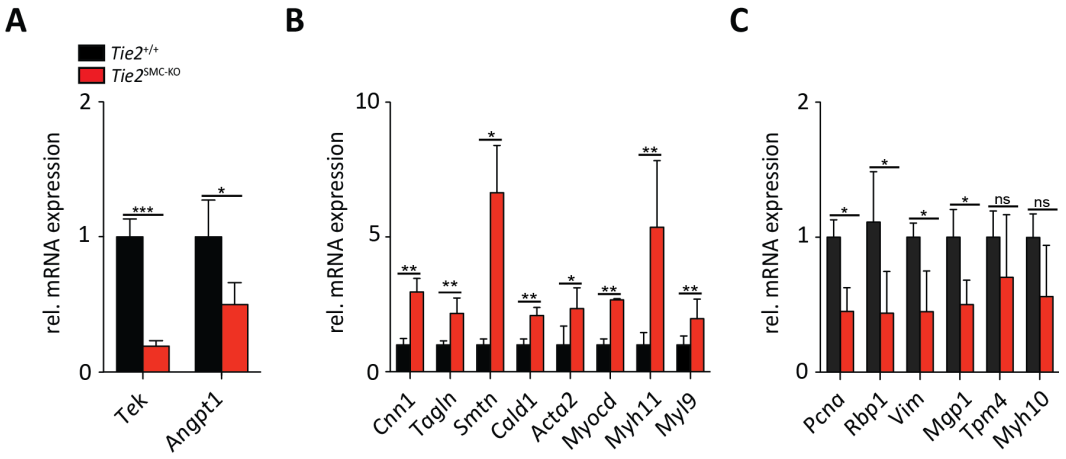

Figure 16. Tie2 deficiency in VSMC impairs VSMC activation

A, Gene expression analysis by RT-qPCR of Tie2 (*Tek*) and *Angpt1* in isolated aortic VSMC from *Tie2*$^{+/+}$ and *Tie2*$^{SMC\text{-}KO}$ mice. **B**, Expression of contractile VSMC-specific marker genes *Cnn1*, *Tagln*, *Smtn*, *Cald1*, *Acta2*, *Myocd* and VSMC-contraction-related genes *Myh11* and *Myl9* by RT-qPCR (n=3-5). **C**, Gene expression analysis by RT-qPCR of *Pcna* and synthetic VSMC markers *Rbp1*, *Vim*, *Mgp1, Tpm4 and Myh10*. n=5-6. Data are shown as mean ± S.D. of 3 independent experiments. *p < 0.05, **p < 0.001, ***p < 0.0001. Student´s *t-test*. ns=non-significant.

2.4 VSMC-specific Tie2 deletion does not affect baseline *in vivo* VSMC phenotype

In order to analyze VSMC phenotype *in vivo*, cross-section of mesenteric arteries and femoral arteries were stained for EC markers (CD31) and contractile VSMC markers (αSMA and Calponin) (Figure 19 A and 19C). Mesenteric arteries (Figure 17A and 17B) and femoral arteries (Figure 17C and 17D) from *Tie2*$^{+/+}$ and *Tie2*$^{SMC\text{-}KO}$ mice did not reveal changes in αSMA- and Calponin-positive area. Correspondingly, protein levels of αSMA and Calponin were not altered in mesenteric arteries, femoral arteries and aortas from *Tie2*$^{+/+}$ and *Tie2*$^{SMC\text{-}KO}$ mice (Figure 17E-17G). These results demonstrate that the baseline *in vivo* VSMC phenotype was not altered among the groups and the changes observed *in vitro* in aortic VSMC from *Tie2*$^{+/+}$ mice were most likely due to an activated status of these cells upon culture. Indeed, it has been reported that cultured VSMC fail to maintain their contractile quiescent phenotype and shift towards a synthetic VSMC phenotype in response to serum, a process known as phenotypic modulation to acquire characteristics found in vascular lesions[375,376].

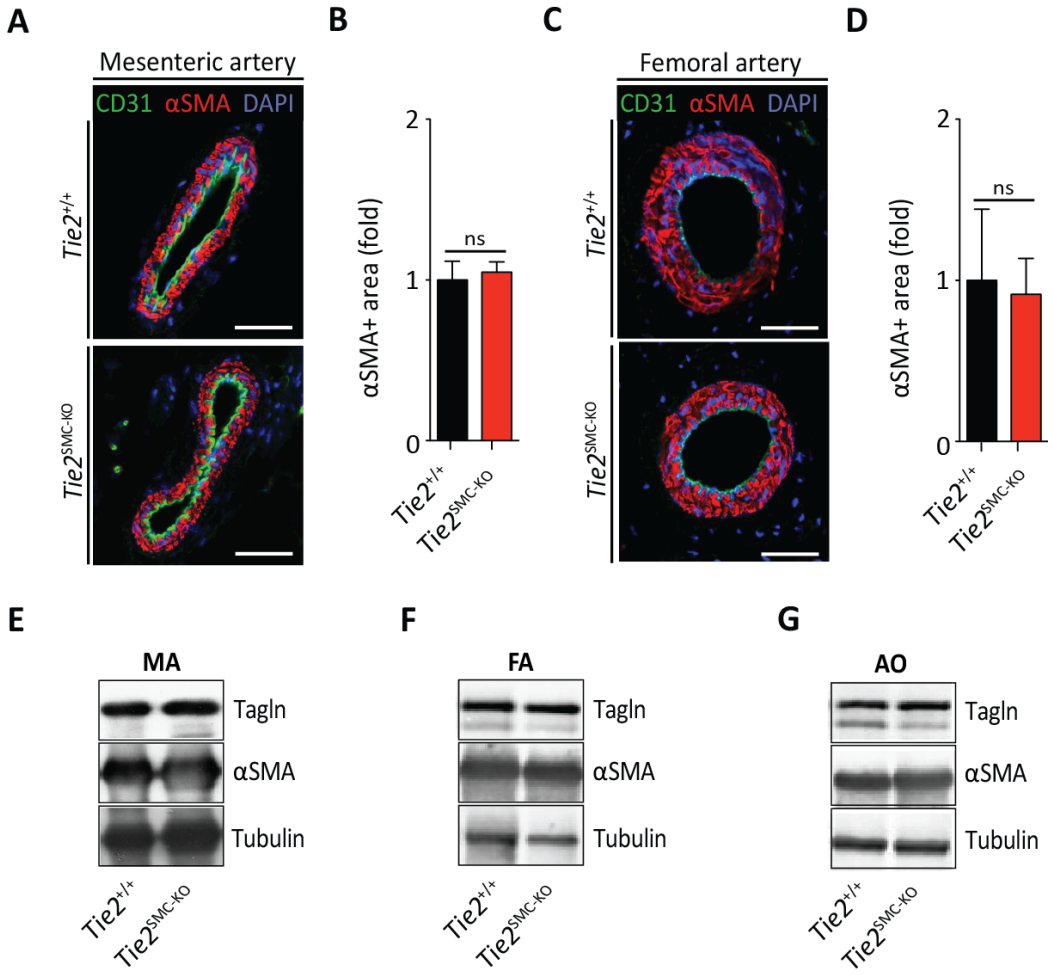

Figure 17. *In vivo* analysis of contractile VSMC marker expression in arteries from *Tie2*$^{+/+}$ and *Tie2*$^{SMC-KO}$ mice

A, **B**, Isolated mesenteric arteries (MA) stained and quantified for αSMA-positive area for VSMC content. **C**, **D**, Isolated femoral arteries (FA) stained and quantified for αSMA-positive area for VSMC content; n=4-6. Scale bar: 50 µm. **E-G**, Representative Western blots of Tagln, αSMA and Tubulin protein expression in isolated MA **(E)**, FA **(F)** and total aortas (AO) **(G)**; n=3-5. Data are shown as mean ± S.D. Student´s *t-test.* ns=non-significant.

2.5 VSMC-specific Tie2 deletion leads to enhanced contractile capactity of femoral arteries upon pressure-controlled perfusion

To determine whether the phenotype observed in *in vitro* activated VSMC holds true, an *ex vivo* perfusion model mimicking hypertension was employed. Isolated mesenteric arteries and femoral arteries were subjected to increasing intraluminal pressure, and hence passively distended. It is known that arterioles (e.g. mesenteric arteries) and arteries (e.g. femoral arteries) compensate for such a pressure-dependent distenstion through active constriction and to pressure reduction with dilation. This myogenic response is crucial in mesenteric arteries as they are involved in the regulation of arterial blood pressure[377]. Mesenteric arteries and femoral arteries from *Tie2*$^{SMC-KO}$ mice displayed a decrease in vessel diameter upon increasing intraluminal pressure, indicating a (hyper-) contractile phenotype (Figure 18A and 18B). However, the differential response was more

pronounced in femoral arteries from *Tie2*$^{SMC-KO}$ as compared to mesenteric arteries. From a functional and morphological point of view the mesenteric arteries and femoral arteries are very distinct, leading to the rationale that mesenteric arteries are from itself more adaptive to changes in blood pressure. In conclusion, the data suggest that VSMC-specific Tie2 control the contractile response of mesenteric arteries and femoral arteries.

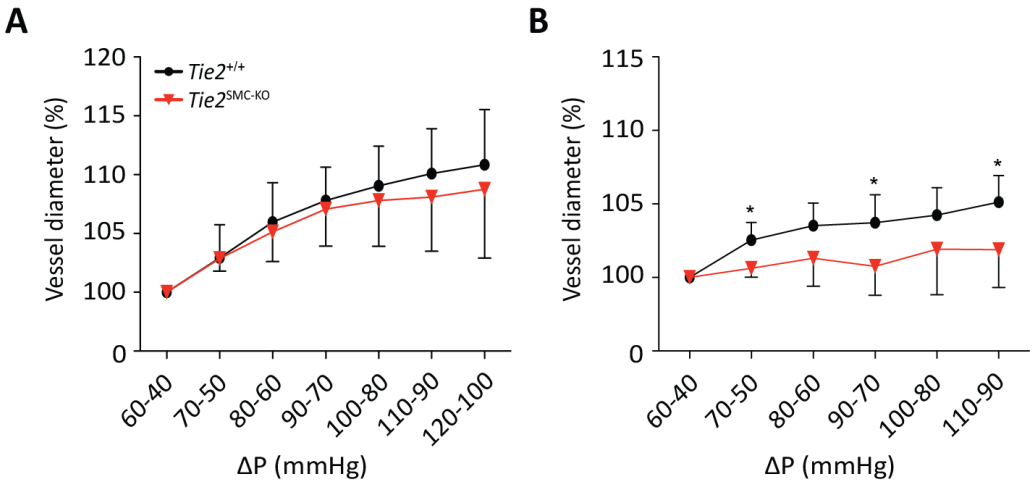

Figure 18. Hypercontractile response of isolated blood vessels from *Tie2*$^{SMC-KO}$ mice upon increasing intraluminal pressure

A-B, Relative increase in diameter of mesenteric arteries (**A**) and femoral arteries (**B**) segments from *Tie2*$^{+/+}$ and *Tie2*$^{SMC-KO}$ mice subjected to increasing intraluminal pressure; n=3 (4-7 segments were used per group). Diameter of unchallenged arteries was set to 100%. 60 to 40 mmHg represents a physiological pressure gradient. 120 to 100 mmHg represents a supra-physiological (hypertensive) pressure gradient. ΔP is the pressure difference at which segments were perfused. Data are shown as mean ± S.D. *p < 0.05. Student´s t-test. ns=non-significant.

2.6 Sm22α-driven Tie2 deletion affects baseline blood pressure

To evaluate*, in vivo,* whether VSMC-specific Tie2 deletion affects baseline blood pressure, 12 weeks-old *Tie2*$^{+/+}$ and *Tie2*$^{SMC-KO}$ mice were subjected to blood pressure measurement using radio-telemetry. The use of radio-telemtry is considered to be a 'state of the art' technique and the most reliable cardiovascular measurement[378,379]. The radio-telemetry system consists of two primary components; i) a blood pressure sensor (BPS) that is made up of a catheter and a transmitter device, which transfers the data wirelessly to a nearby (ii) receiver (Figure 19). The receiver in turn converts the telemetry information into a form readily accessible by a computerized data acquisition system. The RTS was implanted into *Tie2*$^{+/+}$ and *Tie2*$^{SMC-KO}$ mice via catherization of the carotid artery. The mice were allowed to recover for 7 days from transmitter implantation surgery to return cardiac function and animal activity to normal. Thereafter, baseline systolic blood pressure (SBP), diastolic blood pressure (DBP), mean arterial pressure (MAP) and heart rate (HR) were recorded for 7 days.

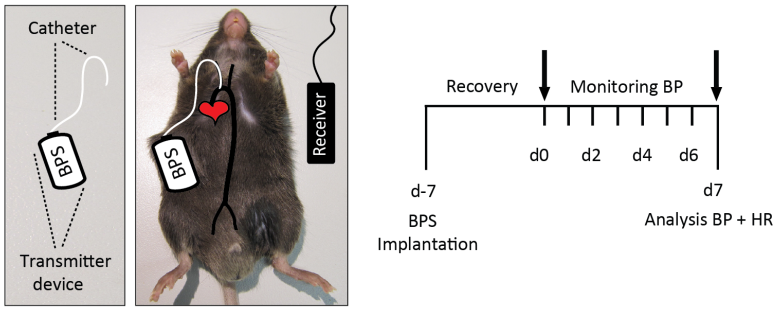

Figure 19. Radiotelemetric tracing of blood pressure and heart rate

Schematic representation of the experimental model: A catheter was implanted into *Tie2*$^{+/+}$ and *Tie2*$^{SMC\text{-}KO}$ mice by cannulating the carotid artery. The transmitter device was impanted subcutaneously into the right flank of the mice. Mice were subsequently allowed to recover for 7 days from transmitter implantation surgery. Baseline systolic blood pressure (SBP), diastolic blood pressure (DBP), heart rate (HR) and mean arterial pressure (MAP) was monitored for 7 days.

The SBP reading is defined as the pressure in the arteries when the heart beats, and pushes blood through the arteries to perfuse the rest of the body[380]. The DBP reading indicates the pressure in the arteries when the heart relaxes between beats[380]. The SBP depends on the frequency and force of heart contractions, whereas the DBP is dependend on the resistance of the peripheral arteries[381]. Comparitive analysis of resting (day-time) and active (night-time) conditions, revealed a significant decrease in SBP in resting and active *Tie2*$^{SMC\text{-}KO}$ mice as compared to their *Tie2*$^{+/+}$ controls (Figure 20A), suggesting a possible heart dysfunction in *Tie2*$^{SMC\text{-}KO}$ mice. During physical activity (comparison of resting mice vs active mice), SBP was increased in *Tie2*$^{+/+}$ as well as *Tie2*$^{SMC\text{-}KO}$ mice. Interestingly, DBP did not differ between resting *Tie2*$^{+/+}$ and *Tie2*$^{SMC\text{-}KO}$ mice (Figure 20B), which corresponds with the observation that VSMC-specific Tie2 deletion does not affect VSMC function at baseline. However, a significant decrease was observed in DBP in active *Tie2*$^{SMC\text{-}KO}$ mice as compared to active *Tie2*$^{+/+}$ mice. Similar results were observed for HR in *Tie2*$^{SMC\text{-}KO}$ mice (Figure 20C). While no significant differences were observed in HR between resting *Tie2*$^{+/+}$ and resting *Tie2*$^{SMC\text{-}KO}$ mice, active *Tie2*$^{SMC\text{-}KO}$ mice displayed a significantly lower HR as compared to active *Tie2*$^{+/+}$ mice. Moreover, both *Tie2*$^{+/+}$ and *Tie2*$^{SMC\text{-}KO}$ mice displayed a significant increase in DBP and HR during physical activity. The significant decrease in DBP and HR in active *Tie2*$^{SMC\text{-}KO}$ mice could be the result of i) adaptation of the cardiac outflow to increased peripheral resistance and/or to the central nervous effects and ii) to the adaptive response of VSMC in response to NO and/or more rapid responses[382,383]. Furthermore, baseline MAP was significantly reduced in resting *Tie2*$^{SMC\text{-}KO}$ mice as compared to *Tie2*$^{+/+}$ controls (Figure 20D). Similary, MAP was significantly reduced in active *Tie2*$^{SMC\text{-}KO}$ mice as compared to their controls. Concordingly, MAP was increased in *Tie2*$^{+/+}$ as well as *Tie2*$^{SMC\text{-}KO}$ mice during physical activity. Taken together, the data suggest that the baseline blood pressure phenotype might be a consequence of Sm22α-driven Tie2 deletion in the heart that is independent from Sm22α-driven Tie2 deletion in VSMC.

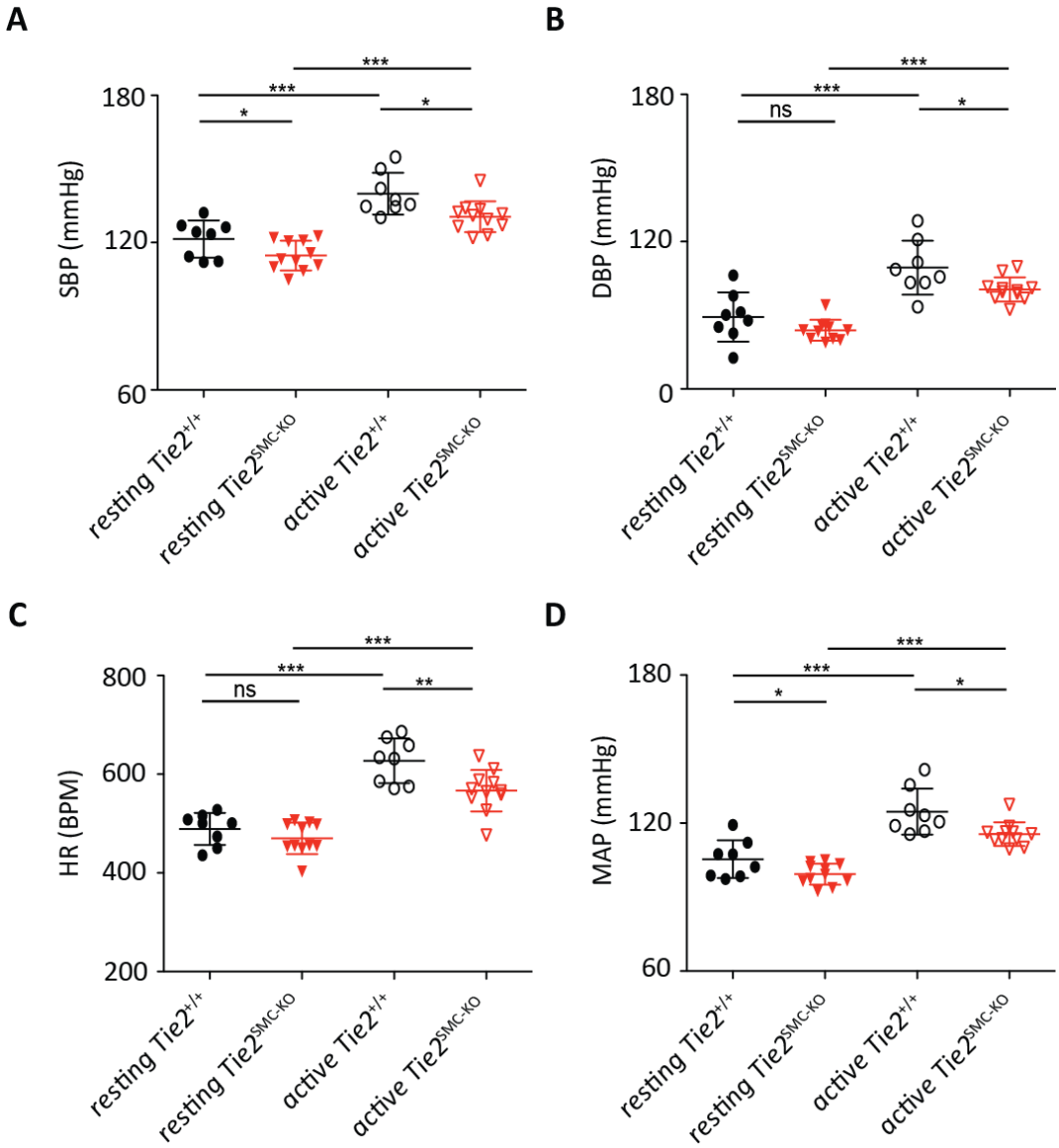

Figure 20. Sm22α-driven Tie2 deletion reduces baseline blood pressure

A-D, Radiotelemetric tracing and quantitative analyses of systolic blood pressure (SBP) (**A**), diastolic blood pressure (DBP) (**B**), heart rate (HR) (**C**), and mean arterial pressure (MAP) (**D**) in resting (day-time) and active (night-time) *Tie2*$^{+/+}$ and *Tie2*$^{SMC-KO}$ mice, assessed by 7 days radiotelemetric system; n=8-11. Data are shown as mean ± S.D. **p* < 0.05, ***p* < 0.001, ****p* < 0.0001. Student´s *t-test*. ns=non-significant.

2.7 Sm22α-driven Tie2 deletion affects cardiac size

Morphometric analysis of the heart was performed by measuring heart weight (HW) and heart weight to tibia length (HW/TL) in *Tie2*$^{+/+}$ and *Tie2*$^{SMC-KO}$ mice at baseline. No differences were observed in body weight (BW) between *Tie2*$^{+/+}$ and *Tie2*$^{SMC-KO}$ mice (Figure 21A). Interestingly, HW and HW/TL were significantly lower in *Tie2*$^{SMC-KO}$ mice as compared to *Tie2*$^{+/+}$ mice (Figure 21B and 21C), which correlates with the reduced BP in these mice.

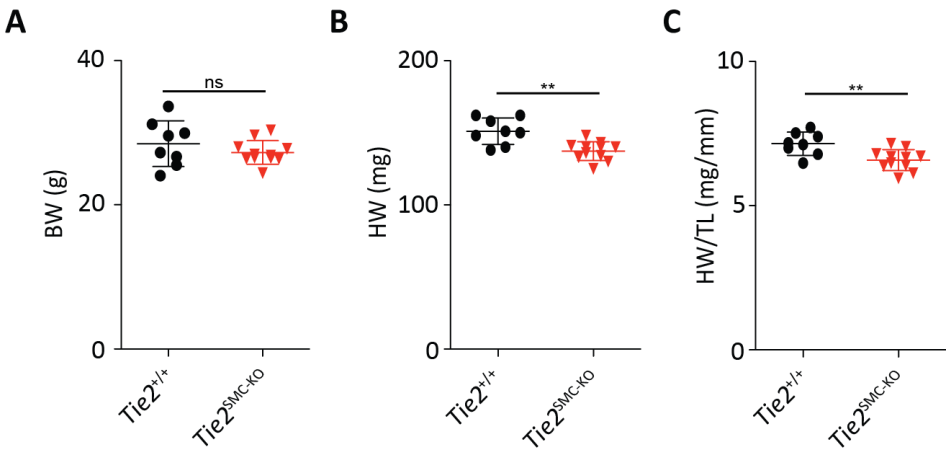

Figure 21. Sm22α-driven Tie2 deletion reduces cardiac size

A-C, Quantitative analyses of body weight (BW), heart weight (HW) and heart weight to tibia length (HW/TL) in *Tie2*$^{+/+}$ and *Tie2*$^{SMC-KO}$ mice; n=8-11. Data are shown as mean ± S.D. ** $p < 0.001$, *** $p < 0.0001$. Student´s *t-test*. ns=non-significant.

2.8 Sm22α-driven Tie2 deletion reduces left ventricular wall- and interventricular septum thickness

To assess function *in vivo*, echocardiography was performed on 12 weeks-old *Tie2*$^{+/+}$ and *Tie2*$^{SMC-KO}$ mice (Figure 22A-22C). The motion-mode (M-mode) imaging was utilized to capture an image of the left ventricle in one dimension over time (Figure 22C). Subsequently, the Vevo 2100-imaging system software was applied to allow various measurements including left ventricular posterior wall (LVPW) thickness, interventricular septum (IVS) thickness, left ventricular internal diameter (LVID) at diastole and systole. Echocardiographic recordings at baseline demonstrated a significant reduction in LVPWd and IVSd in *Tie2*$^{SMC-KO}$ mice as compared to *Tie2*$^{+/+}$ mice (Figure 22D and 22E). Hence, *Tie2*$^{SMC-KO}$ mice may not be able to increase force as much as *Tie2*$^{+/+}$ mice. Furthermore, no obvious differences were detected for LIVDd between the two groups (Figure 22F).

To test whether the reduced cardiac size was also present on the cellular level, CM cross-sectional lenght, width and area was analysed in heart sections from *Tie2*$^{+/+}$ and *Tie2*$^{SMC-KO}$ mice (Figure 23A). No significant differences were obtained in fibrotic area between *Tie2*$^{+/+}$ and *Tie2*$^{SMC-KO}$ mice, by quantification of Picro-sirius red area (Figure 23B). Furthermore, CM width was significantly reduced in the hearts of *Tie2*$^{SMC-KO}$ mice as compared to *Tie2*$^{+/+}$ mice, whereas CM length did not differ between the two groups (Figure 23C and 23D). As a result CM area was significantly decreased in the hearts of *Tie2*$^{SMC-KO}$ mice (Figure 23E).

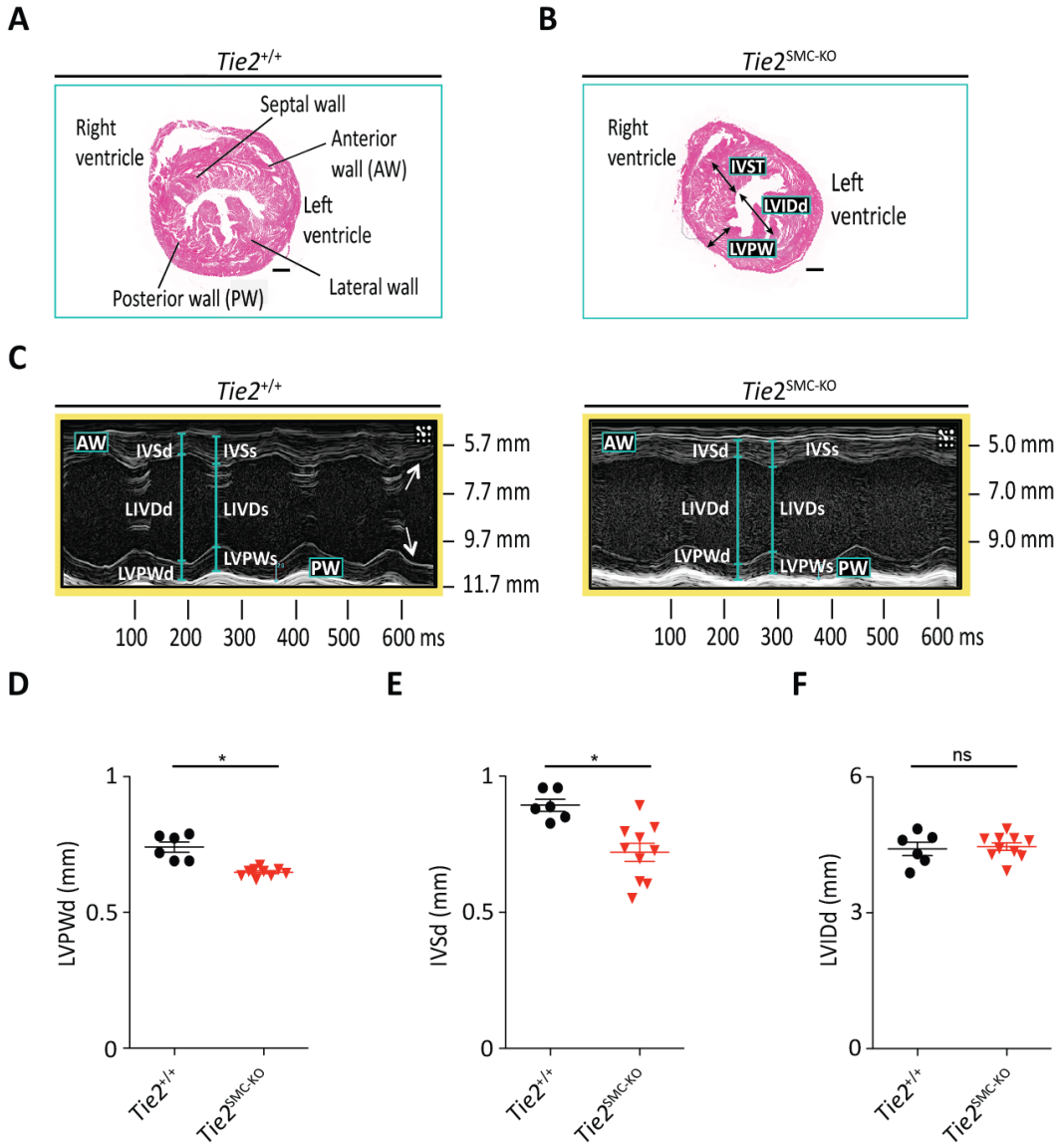

Figure 22. Sm22α-driven Tie2 deletion reduces left ventricular wall- and interventricular septum thickness

A, Representative HE images showing the cross-sectional dimensions of the mouse heart, including the right ventricle, left ventricle, lateral, septal, anterior and posterior wall. The septal wall separates the left ventricle from the right ventricle. Scale bar=500 µm. **B**, Interventricular septum (IVS), left ventricular internal diameter (LVID) and left ventricular wall thickness (LVPW) were examined at baseline in both *Tie2*$^{+/+}$ and *Tie2*$^{SMC-KO}$ mice. **C**, Representative M-mode echocardiographic recordings illustrate the assessement of IVS, LVID and LVPW at diastole and systole in *Tie2*$^{+/+}$ and *Tie2*$^{SMC-KO}$ mice (right). **D-F**, Quantitative baseline echocardiographic analysis of LVPWd (**C**), IVSd (**D**) LVIDd (**E**) at diastole; n=6-9. Data are shown as mean ± S.D. *$p < 0.05$. Student´s *t-test*. ns=non-significant.

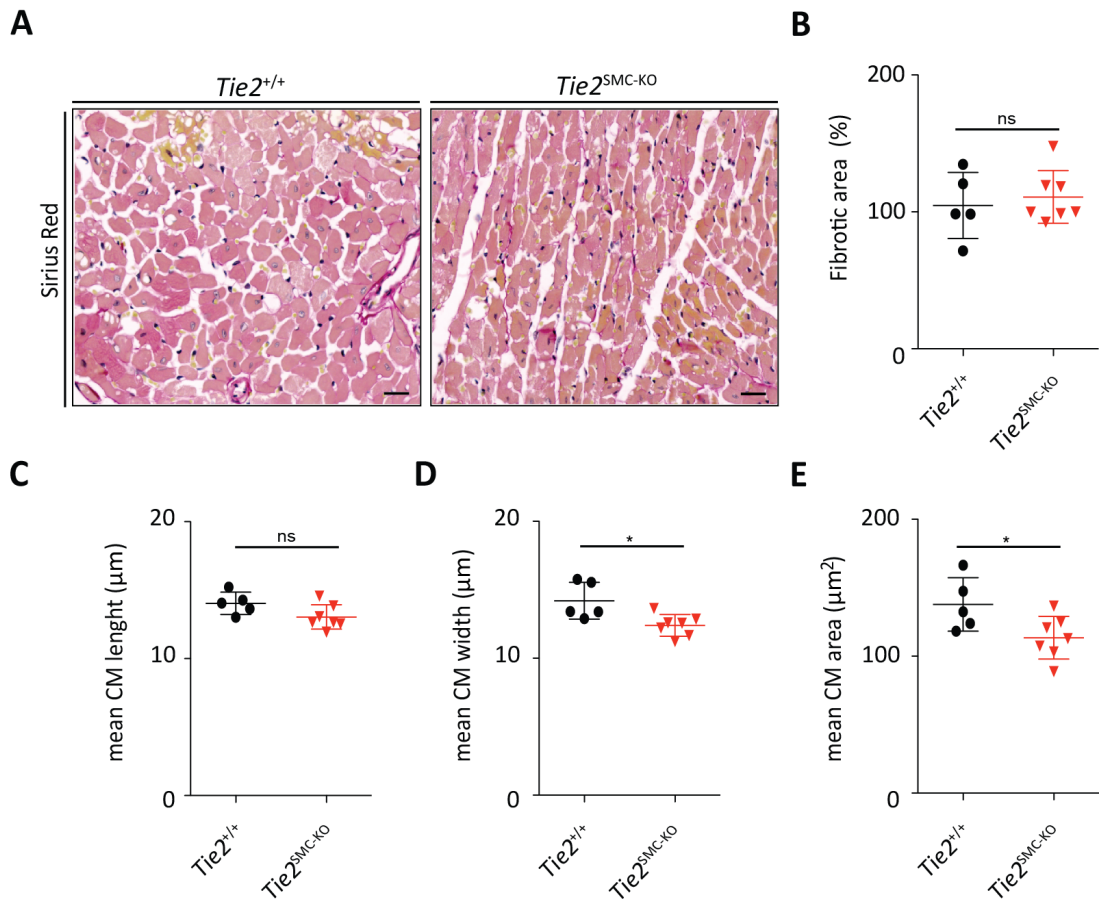

Figure 23. Sm22α-driven Tie2 deletion reduces cardiomyocyte dimensions

A, Representative image of heart sections from *Tie2*$^{+/+}$ and *Tie2*$^{SMC-KO}$ mice stained with Picro-sirius red. Scale bar= 20 µm. **B**, Quantitative analyses of fibrotic area in the hearts of *Tie2*$^{+/+}$ and *Tie2*$^{SMC-KO}$ mice. **C-D**, Quantitative analyses of cardiomyocyte (CM) length (**C**), CM width (**D**) and CM area (**E**) in the left heart chamber of *Tie2*$^{+/+}$ and *Tie2*$^{SMC-KO}$ mice; n=5-7. Data are shown as mean ± S.D. *$p < 0.05$. Student´s *t-test*. ns=non-significant.

2.9 Tie2 is expressed in adult cardiomyocytes

To determine the time frame in which the baseline heart phenotype takes place, HW and HW/TL were analysed in *Tie2*$^{+/+}$ and *Tie2*$^{SMC-KO}$ mice at the age of 4, 6 and 12 weeks. While 6-week- (Figure 24B and 24E) and 12-week-old (Figure 24C and 24F) *Tie2*$^{SMC-KO}$ mice displayed a significant reduction in HW and HW/TL as compared to *Tie2*$^{+/+}$ mice, 4-week-old (Figure 24A and 24D) *Tie2*$^{SMC-KO}$ mice did not differ significantly from *Tie2*$^{+/+}$ mice, suggesting that Sm22α-driven Tie2 deletion affects cardiac growth/development between the age of 4 and 6 weeks.

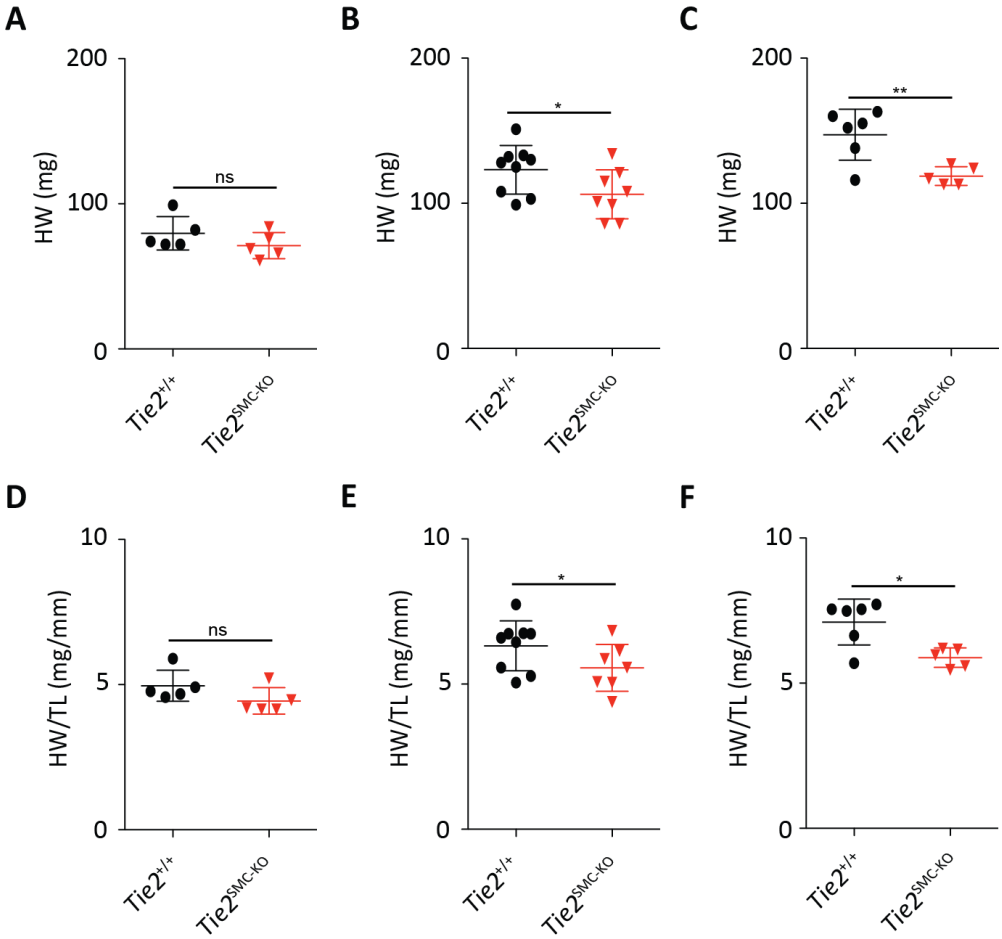

Figure 24. Sm22α-driven Tie2 deletion reduces cardiac size in mice after 4 weeks of age

A-C, Quantitative analyses of heart weight (HW) in 4-week-old *Tie2*$^{+/+}$ and *Tie2*$^{SMC-KO}$ mice (**A**), 6-week-old *Tie2*$^{+/+}$ and *Tie2*$^{SMC-KO}$ mice (**B**) and 12-week-old *Tie2*$^{+/+}$ and *Tie2*$^{SMC-KO}$ mice (**C**). **D-F**, Quantitative analyses of heart weight to tibia length (HW/TL) in 4-week-old *Tie2*$^{+/+}$ and *Tie2*$^{SMC-KO}$ mice (**D**), 6-week-old *Tie2*$^{+/+}$ and *Tie2*$^{SMC-KO}$ mice (**E**) and 12-week-old *Tie2*$^{+/+}$ and *Tie2*$^{SMC-KO}$ mice (**F**). n=5-9. Data are shown as mean ± S.D. *p < 0.05, **p < 0.001. Student´s *t-test*. ns=non-significant.

To determine whether the decrease in cardiac size was associated witch changes in cell number, proliferation and apoptosis was assessed in heart sections of 6-week-old *Tie2*$^{+/+}$ and *Tie2*$^{SMC-KO}$ mice. Comparitive analysis of heart sections stained for Ki67 or Cleaved Caspase 3 (Figure 25A and 25C) revealed that neither proliferation nor apoptosis, respectively, were significantly altered in in the hearts of 6-week-old *Tie2*$^{+/+}$ and *Tie2*$^{SMC-KO}$ mice (Figure 25B and 25D). These results suggest that the decrease in cardiac size was most likely not the cause of a decrease in cell number, but rather the result of poor development of the heart.

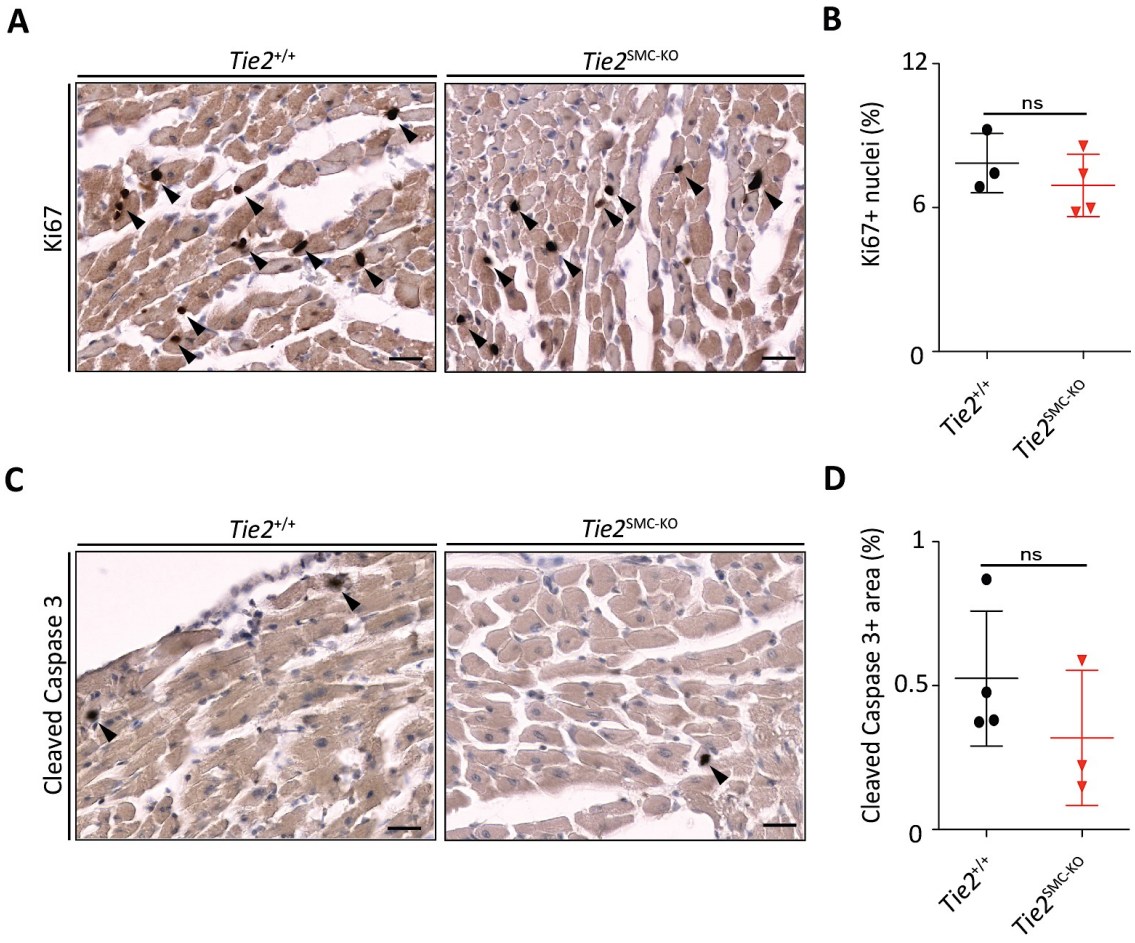

Figure 25. Sm22α-driven Tie2 deletion does not affect proliferation or apoptosis
A, **C**, Heart sections form 6-week-old *Tie2*$^{+/+}$ and *Tie2*$^{SMC-KO}$ mice stained for the proliferation marker Ki67 (**A**) and the apoptosis marker Cleaved Caspase 3 (**C**). Scale bar= 20 µm **B**, **D**, Quantitative analyses of Ki67+ cells normalized to total nuclei (**B**), and Cleaved Caspase 3+ area, normalized to total area (**D**), in the hearts of *Tie2*$^{+/+}$ and *Tie2*$^{SMC-KO}$ mice; n=3-5. Data are shown as mean ± S.D. Student´s *t-test*. ns=non-significant.

CMs are the major components of the heart and are responsible for their contractile force[384]. The heart also consist of several other cell types including, fibroblast, EC and VSMC. Since EC-specific Tie2 expression was unaltered in lungs of *Tie2*$^{+/+}$ and *Tie2*$^{SMC-KO}$ mice and since primary mouse fibroblast showed almost undetectable levels of Tie2, these cells could be excluded as potential candidates for the observed baseline heart phenotype. Moreover, VSMC phenotype was not altered at baseline in *Tie2*$^{+/+}$ and *Tie2*$^{SMC-KO}$ mice, leading to the rationale that Tie2 might be deleted in CMs under the control of the Sm22α-promoter. This rationale further prompted the investigation of Tie2 expression in CMs. During embryonic development, Sm22α is only transiently expressed in CMs (between E8.0-E12.5)[160]. After E12.5, its expression is not observed in skeletal and cardiac muscle from adult mouse tissue, but is instead localized to the vasculature. As such, the impaired cardiac function at baseline may be a consequence of Sm22α-driven Tie2 deletion in CMs during embryonic development.

To study the expression pattern of Sm22α in aortic and heart tissue, sections from adult *Sm22α-Cre x mT/mG* mice were co-stained with anti-GFP and CD31 antibodies (Figure 26). Once the Cre is active

in Sm22α-positive cells, the GFP protein is switched on and proceeds to be expressed in all daughter cells[385]. In the aorta, GFP expression was restricted to VSMC in the tunica media, whereas CD31-positive-GFP-negative cells (EC) were localized in the tunica intima. Furthermore, the overall expression pattern in the tunica media was similar to the expression of endogenous Sm22α and αSMA. In the heart, CD31 was found in close proximity to GFP-positive cells (Figure 26), which defines the vasculature covered by mural cells. However, GFP expression was also abundantly expressed in CD31-negative cells, hinting that, next to mural cells, Cre-mediated recombination also occurred in other cell-types in the heart. Moreover, only a subset of GFP-positive cells truly express endogenous Sm22α in the adult heart. The diminished expression of endogenous Sm22α in the adult heart was most likely the result of the transient nature of Sm22α-expression in CMs. Endogenous αSMA expression was restricted to the cardiac macrovasculature VSMC.

In order to trace Tie2 expression in aortic and heart tissue from *Tie2MerCreMer (MCM)* x *Rosa26*^{YFP} mice, 5 consecutive doses of tamoxifen (1 mg) were administered intraperitoneally in 6 week-old mice[386]. This model provides permanent YFP-tagging of Tie2-positive cells that exist at the time of tamoxifen injection. Aortic sections from *Tie2*^{MCM} x *Rosa26*^{YFP} mice were stained with anti-GFP and αSMA antibody (Figure 27). In the aorta, GFP expression was detected in the tunica media and tunica intima, while endogenouse αSMA expression was restricted to VSMC in the tunica media. Moreover, αSMA immunostaining colocalized with GFP expression in the tunica media. Furthermore, heart sections stained with anti-GFP antibody demonstrated GFP expression in the CMs (Figure 27), identified by the sarcomere arrangement. However, the GFP expression in the heart is lower as compared to the aorta. In conclusion, CMs and VSMC from 6-week-old *Tie2*^{MCM} x *Rosa26*^{YFP} mice undergo recombination, which confirms that the *Tie2*^{MCM} transgene is expressed by these cells, and that tamoxifen administration efficiently leads to DNA recombination in these cells.

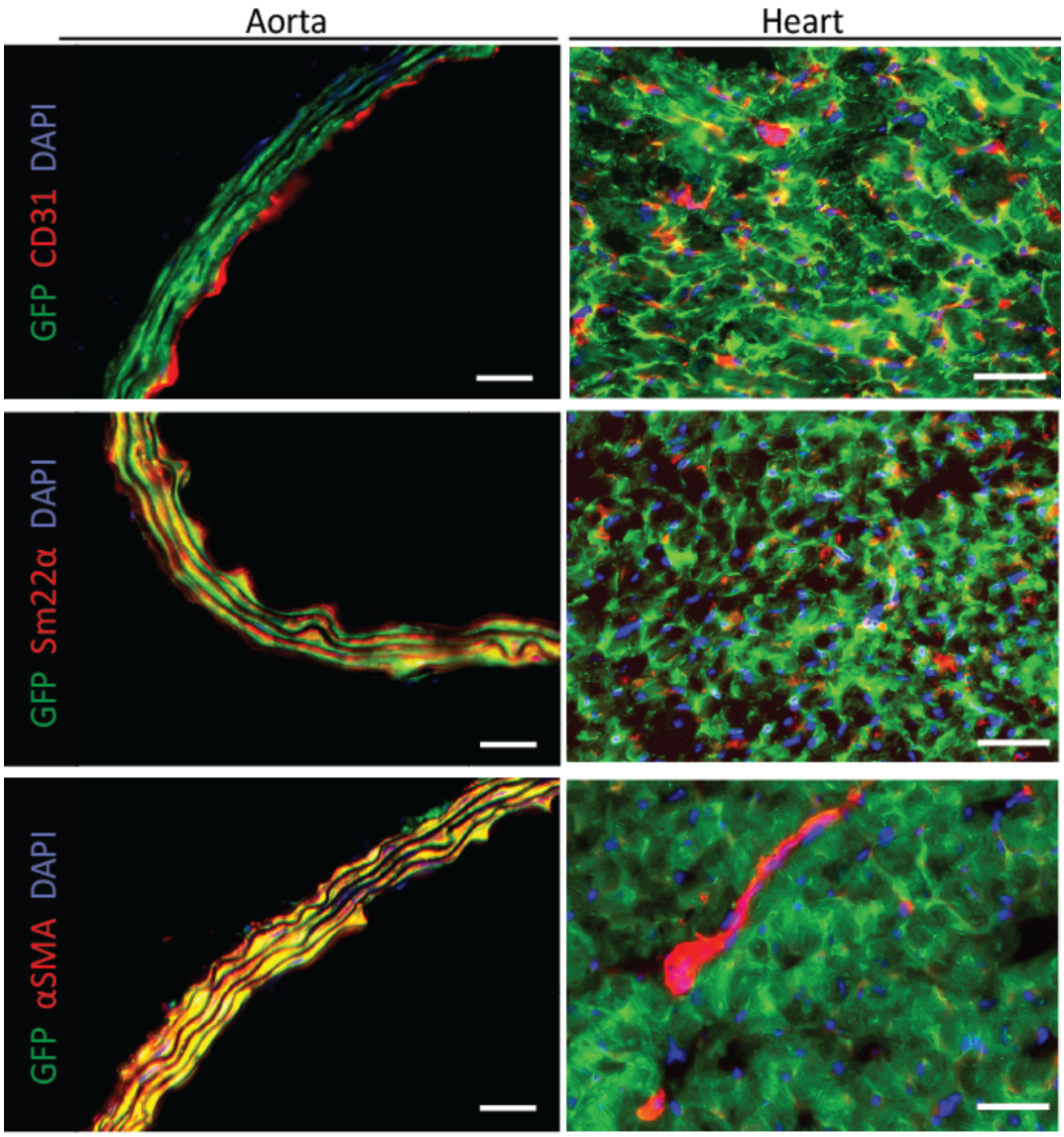

Figure 26. Tracing Sm22α expression using a Sm22α knockin fate-tracing mouse model

Representative images of GFP staining (green) in heart and aortic cryosections from *Sm22α/Tagln-Cre* x *mT/mG* mice co-stained with CD31, SM22α and αSMA (red); n= 3. Scale bar= 25 µm. This experiment was done in cooperation with Annegret Holm, DKFZ.

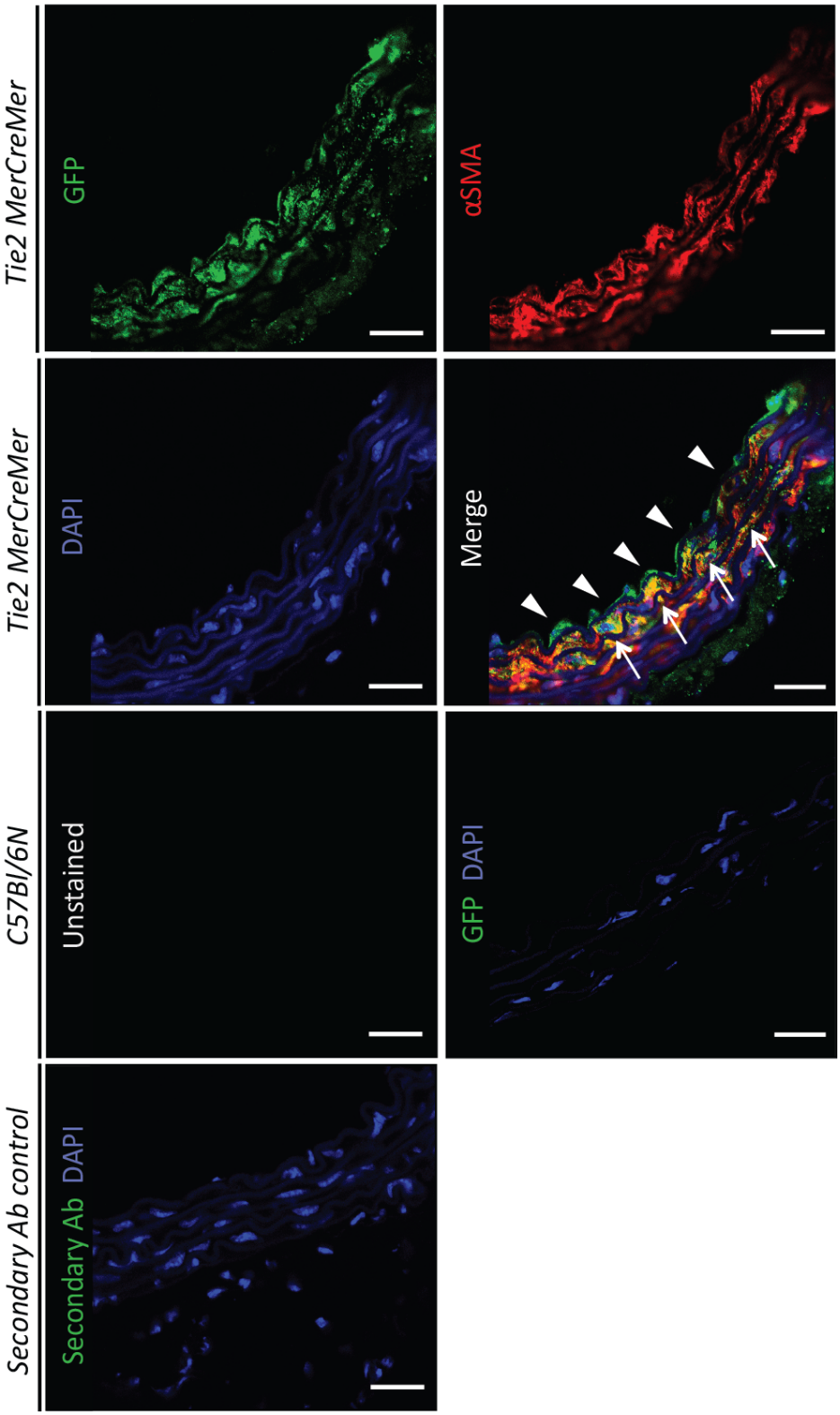

Figure 27. Tracing Tie2 expression in the aorta using a Tie2 knockin fate-tracing model

Tie2 expression was analyzed in aortic tissue derived from 6-week-old *Tie2*^{MCM} x *Rosa26*^{YFP} mice, which are Tie2 knock in reporter mice. Upon tamoxifen induction, promoter activity of Tie2 induces Cre-mediated excision of the floxed-stop cassette resulting in YFP expression at the *Rosa26* locus. YFP expression permits tracing Tie2 expression. Aortic cryosections were stained for GFP (green) and αSMA (red). Arrows show Tie2 expression in medial VSMC. Arrowheads show Tie2 expression in intimal EC; n= 3. Scale bar= 25 µm. Aortic samples from *Tie2*^{MCM} x *Rosa26*^{YFP} were provided by Dr. Katrin Busch and Prof. Dr. Hans-Reimer Rodewald, DKFZ.

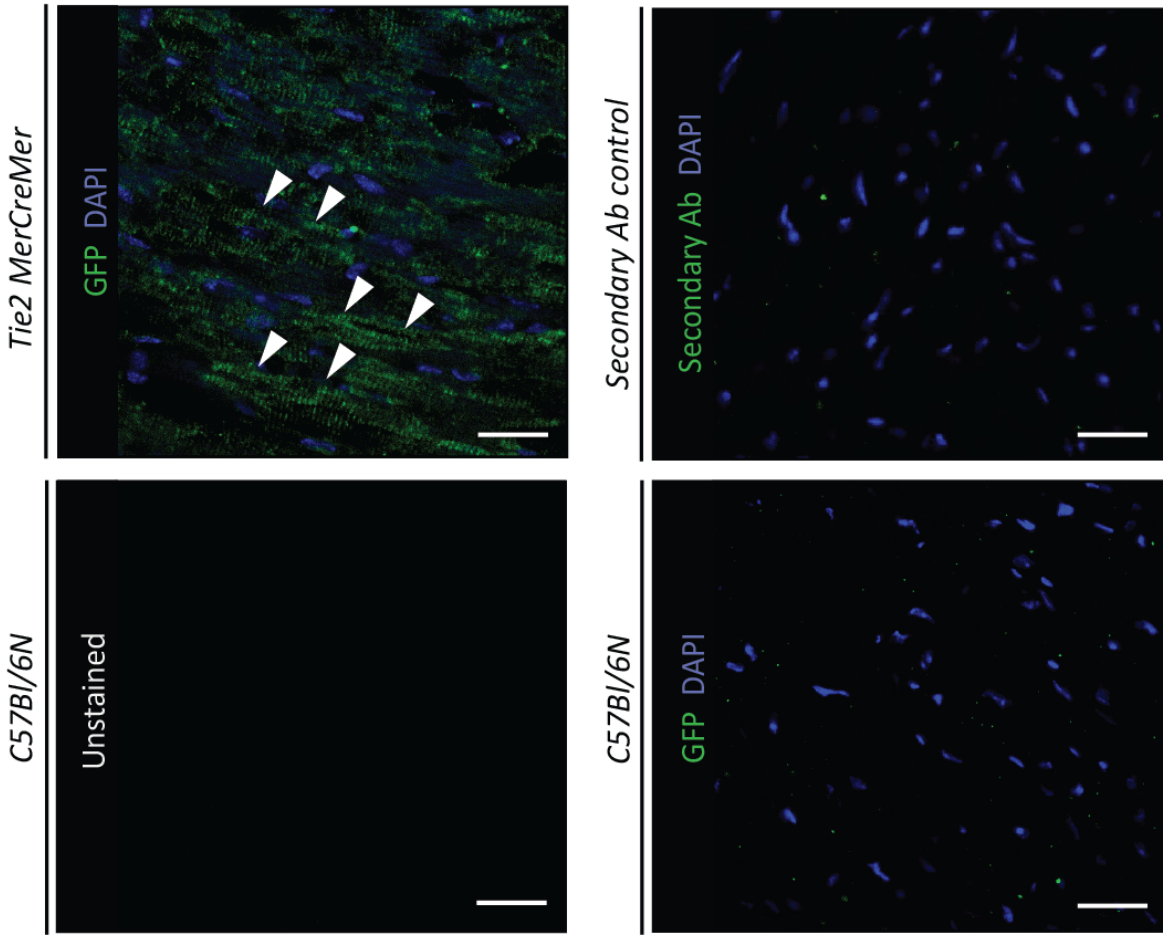

Figure 28. Tracing Tie2 expression in the heart using a Tie2 knockin fate-tracing model
Tie2 expression was analyzed in heart tissue derived from 6 week-old *Tie2*^{MCM} x *Rosa26*^{YFP} mice. Heart cryosections were stained for GFP (green). Arrowheads show the sarcomere arrangement of CMs; n= 3. Scale bar= 25 µm. Heart samples from *Tie2*^{MCM} x *Rosa26*^{YFP} were provided by Dr. Katrin Busch and Prof. Dr. Hans-Reimer Rodewald, DKFZ.

To determine whether Tie2 is expressed by CMs, CMs were isolated from 8-week-old *Tie2*$^{+/+}$ and *Tie2*$^{SMC-KO}$ mice. Isolated CMs from *Tie2*$^{+/+}$ and *Tie2*$^{SMC-KO}$ mice expressed high mRNA levels of *Tnnt2* (Troponin 2, CM-specific marker) (Figure 29A), whereas the mRNA expression of *Sm22α/Tagln* and Tie2 (*Tek)* was at almost undetectable levels in isolated CMs from *Tie2*$^{+/+}$ and *Tie2*$^{SMC-KO}$ mice as compared to non-CMs from *Tie2*$^{+/+}$ and *Tie2*$^{SMC-KO}$ mice (Figure 29B and 29C). The isolated non-CMs from *Tie2*$^{+/+}$ and *Tie2*$^{SMC-KO}$ mice represent other cell-types present in the heart such as EC, VSMC and fibroblast. Correspondingly, Western blot analysis confirmed undetectable levels of Tie2 in isolated CMs from *Tie2*$^{+/+}$ and *Tie2*$^{SMC-KO}$ (Figure 29D). Together, the data indicate that Tie2 is not expressed in CMs from 8-week-old mice, hinting that Tie2 might be required at an earlier time-point for normal development of the heart.

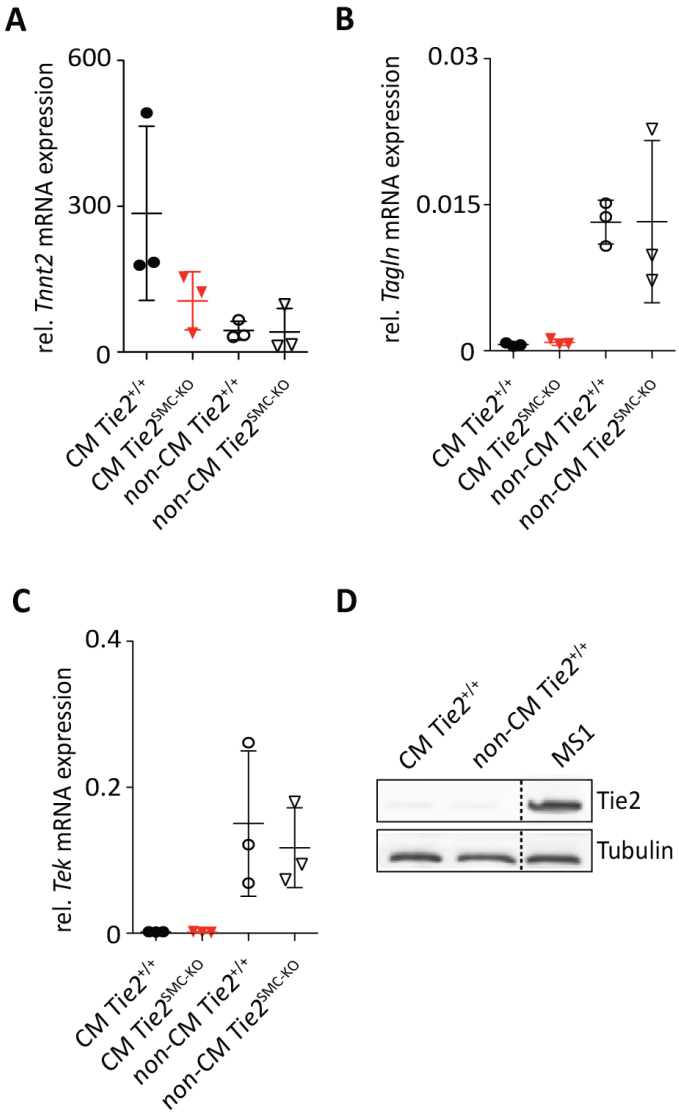

Figure 29. Tie2 is not expressed in cardiomyocytes from 8-week-old *Tie2*$^{+/+}$ and *Tie2*$^{SMC\text{-}KO}$ mice

A-C, Gene expression analyses by RT-qPCR of *Tnnt2* (**A**), *Tagln* (**B**) and *Tek* (**C**) in isolated adult cardiomyocytes (CMs) and non-cardiomyocytes (non-CMs) from *Tie2*$^{+/+}$ and *Tie2*$^{SMC\text{-}KO}$ mice; n=3. Expression is normalized to *B2m* mRNA expression. **D**, Representative Western blots of Tie2 and Tubulin in isolated adult cardiomyocytes (CMs) and non-cardiomyocytes (non-CMs) from *Tie2*$^{+/+}$ and *Tie2*$^{SMC\text{-}KO}$ mice; n=3. Data are shown as mean ± S.D. Student´s *t-test*. ns=non-significant. CM isolation was done in collaboration with Dr. Lorenz Lehmann, University of Heidelberg.

2.10 Sm22α-driven Tie2 deletion does not have a major impact on blood pressure upon DOCA-salt treatment

To explore the role of Sm22α-driven Tie2 deletion upon hypertension, the DOCA-induced hypertension model was employed. DOCA pellets were implanted subcutaneously into the back of the mice (Figure 30). Subsequently, the mice received drinking water containing 1% NaCl. Changes in arterial blood pressure and HR were monitored over a period of 10 days following DOCA-salt administration.

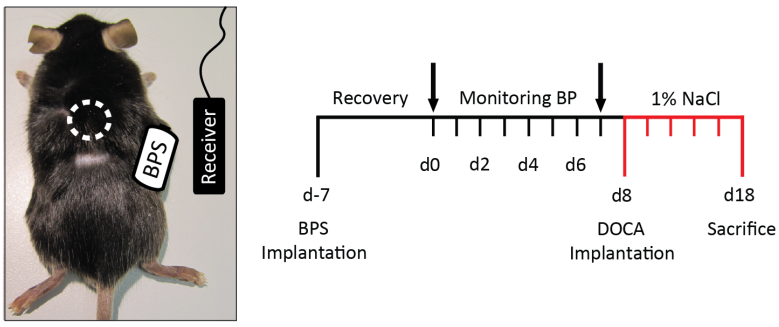

Figure 30. Experimental protocol for DOCA-induced hypertension

Deoxycorticosterone acetate *(*DOCA*)* pellets were implantated subqutaneously at the back of the mice. At the same day mice received isotonic saline water (1% NaCl). SBP, DBP, HR and MAP were monitored by radiotelemtry for 10 days following DOCA-implantation.

Upon DOCA-salt treatment, SBP, DPB and MAP were significantly increased in resting *Tie2*$^{+/+}$ mice as compared to untreated resting controls (Figure 31A-31C). Correspondingly, active *Tie2*$^{+/+}$ mice displayed marked increase in SBP, DPB as well as MAP upon DOCA-salt treatment in comparison to untreated active control mice (Figure 31A-31C). Collectively, the data established a successful induction of hypertension upon DOCA-salt treatment.

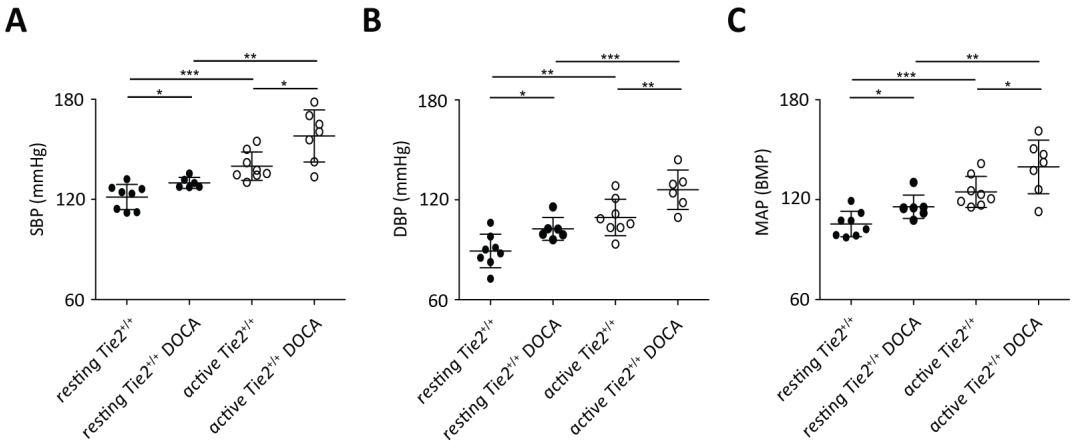

Figure 31. Analysis of SBP, DBP and MAP in *Tie2*$^{+/+}$ mice upon DOCA-salt treatment

A-C, Quantitative analyses of SBP (**A**), DBP (**B**) and MAP (**C**) in resting (day-time) and active (night-time) *Tie2*$^{+/+}$ mice, assessed by 10 days radiotelemetric system (n=6-11). Data are shown as mean ± S.D. **p* < 0.05, ***p* < 0.001, ****p* < 0.0001. Student´s *t-test*. ns=non-significant.

Comparative analysis of resting and active *Tie2*$^{+/+}$ and *Tie2*$^{SMC-KO}$ mice upon DOCA-salt treatment revealed no significant differences in SBP in resting *Tie2*$^{SMC-KO}$ mice as compared to resting *Tie2*$^{+/+}$ mice (Figure 32A). However, a slightly lower SBP was observed in active *Tie2*$^{SMC-KO}$ mice upon DOCA-salt treatment in comparison to *Tie2*$^{+/+}$ mice. Similarly, DBP did not differ in resting active *Tie2*$^{SMC-KO}$ mice as compared to resting, whereas active *Tie2*$^{SMC-KO}$ mice demonstrated a reduction in DBP as compared to active *Tie2*$^{+/+}$ mice following DOCA-salt treatment (Figure 32B). Furthermore, resting and active *Tie2*$^{SMC-KO}$ mice did not differ in HR upon DOCA-salt treatment as compared to resting and active *Tie2*$^{+/+}$ mice (Figure 32C). While resting *Tie2*$^{SMC-KO}$ mice displayed no significant differences in

MAP in comparison to resting *Tie2*$^{+/+}$ mice upon DOCA-salt treatment, active *Tie2*$^{SMC-KO}$ mice showed a slight reduction in MAP compared to active *Tie2*$^{+/+}$ mice (Figure 32D), albeit not significant. Moreover, DOCA-salt treatment induced a significant increase in SBP, DBP, MAP and HR in *Tie2*$^{+/+}$ and *Tie2*$^{SMC-KO}$ mice during physical activity (Figure 32A-32D).

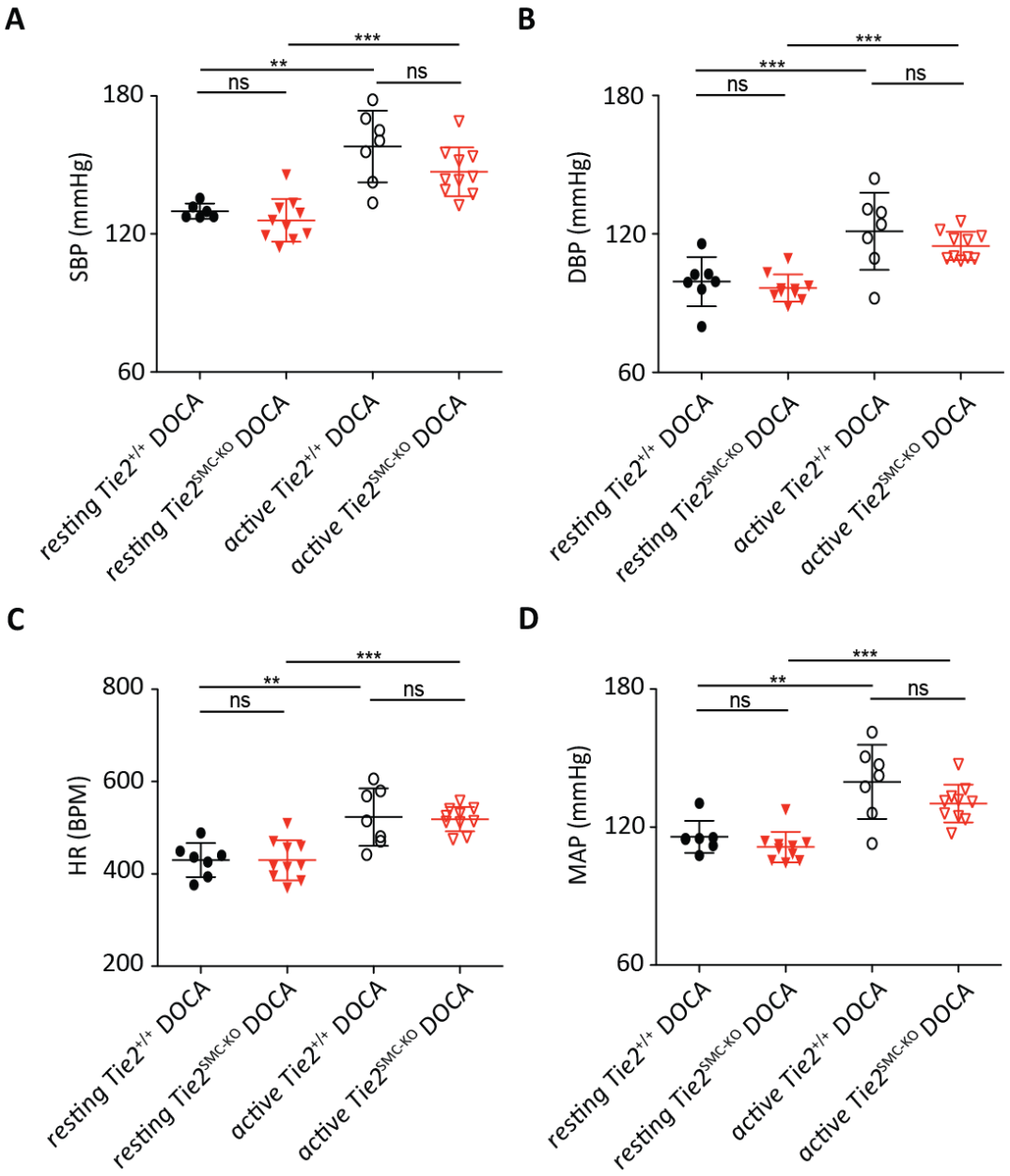

Figure 32. Sm22α-driven Tie2 deletion does not have a major impact on blood pressure during hypertension

A-D, Quantitative analyses of SBP (**A**), DBP (**B**), HR (**C**) and MAP (**D**) in resting (day-time) and active (night-time) *Tie2*$^{+/+}$ and *Tie2*$^{SMC-KO}$ mice, assessed by 10 days radiotelemetric system (n=6-11). Data are shown as mean ± S.D. $^{**}p < 0.001$, $^{***}p < 0.0001$. Student´s *t-test*. ns=non-significant.

2.11 Sm22α-driven Tie2 deletion affects cardiac size upon DOCA-salt treatment

Morphometric analysis of the heart was performed by measuring HW and HW/TL in *Tie2*$^{+/+}$ and *Tie2*$^{SMC\text{-}KO}$ mice at baseline and following DOCA-salt treatment. HW and HW/TL were significantly lower in untreated *Tie2*$^{SMC\text{-}KO}$ mice as compared to untreated *Tie2*$^{+/+}$ mice (Figure 33A and 33B). Analysis of cardiac hyperthrophy upon DOCA-salt treatment demonstrated a significant increase in HW and HW/TL in *Tie2*$^{+/+}$ mice as compared to untreated *Tie2*$^{+/+}$ controls. In contrast, no significant differences were observed in HW and HW/TL in *Tie2*$^{SMC\text{-}KO}$ mice upon DOCA-salt treatment as compared to their untreated *Tie2*$^{SMC\text{-}KO}$ controls (Figure 33A and 33B). Moreover, HW and HW/TL were markedly reduced in *Tie2*$^{SMC\text{-}KO}$ mice upon DOCA-salt treatment when compared to *Tie2*$^{+/+}$ mice. Kidney weight (KW) was analyzed in *Tie2*$^{+/+}$ and *Tie2*$^{SMC\text{-}KO}$ mice upon DOCA-salt treatment as an additional measurement for the induction of hypertension. *Tie2*$^{+/+}$ and *Tie2*$^{SMC\text{-}KO}$ mice showed significantly greater KW upon DOCA-salt treatment as compared to their untreated controls, whereas a significantly reduced KW was observed in *Tie2*$^{SMC\text{-}KO}$ mice upon DOCA-salt treatment as compared to the *Tie2*$^{+/+}$ mice (Figure 33C). Taken together, the reduced BP at baseline in *Tie2*$^{SMC\text{-}KO}$ mice dampens the hypertrophic cardiac response in *Tie2*$^{SMC\text{-}KO}$ mice upon DOCA-salt treatment.

Immunohistochemical analysis of Picro-sirius red stained fibrotic area revealed a significant increase in fibrosis in the hearts of *Tie2*$^{+/+}$ and *Tie2*$^{SMC\text{-}KO}$ mice upon DOCA-salt treatment. However, the fibrotic area is less pronounced in the hearts of DOCA-salt treated *Tie2*$^{SMC\text{-}KO}$ as compared to DOCA-salt treated *Tie2*$^{+/+}$ mice (Figure 34A and 34B). To coroborate these findings, gene-expression analysis was perfomed on heart samples from untreated *Tie2*$^{+/+}$ and *Tie2*$^{SMC\text{-}KO}$ mice, and DOCA-salt-treated *Tie2*$^{+/+}$ and Tie2$^{SMC\text{-}KO}$ mice. Indeed, *Collagen 1* (*Col 1*) and *Mmp2* mRNA expression levels where

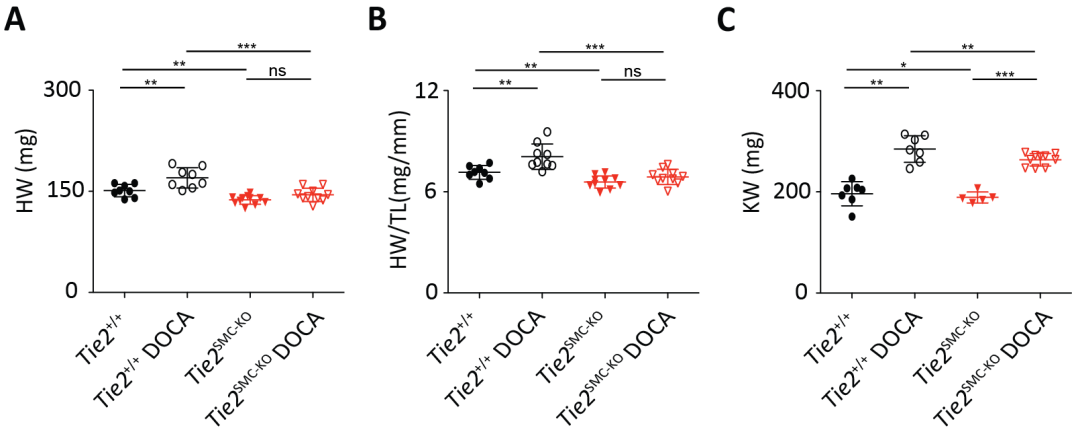

Figure 33. Sm22α-driven Tie2 deletion reduces cardiac size upon DOCA-salt treatment

A-C, Quantitative analyses of heart weight (HW) (**A**), heart weight to tibia length (HW/TL) (**B**), and kidney weight (KW) (**C**) in *Tie2*$^{+/+}$ and *Tie2*$^{SMC\text{-}KO}$ mice at baseline and following DOCA-salt treatment; n=5-11. Data are shown as mean ± S.D. $^{**}p < 0.001$, $^{***}p < 0.0001$. Student´s *t-test*. ns=non-significant.

significantly higher in *Tie2*$^{+/+}$ mice upon DOCA-salt treatment as compared to their untreated controls, whereas no significant differences were observed between untreated *Tie2*$^{SMC-KO}$ and DOCA-salt-treated *Tie2*$^{SMC-KO}$ mice (Figure 34C and 34D). Morover, *Col 1* and *Mmp2* expression levels were markedly reduced in the hearts of *Tie2*$^{SMC-KO}$ mice as compared to *Tie2*$^{+/+}$ mice upon DOCA-salt treatment (Figure 34C and 34D). In conlusion, the hindered cardiac remodeling response in *Tie2*$^{SMC-KO}$ mice upon DOCA-salt treatment most likely originates from the reduced baseline heart phenotype (decrease in cardiac size, and BP).

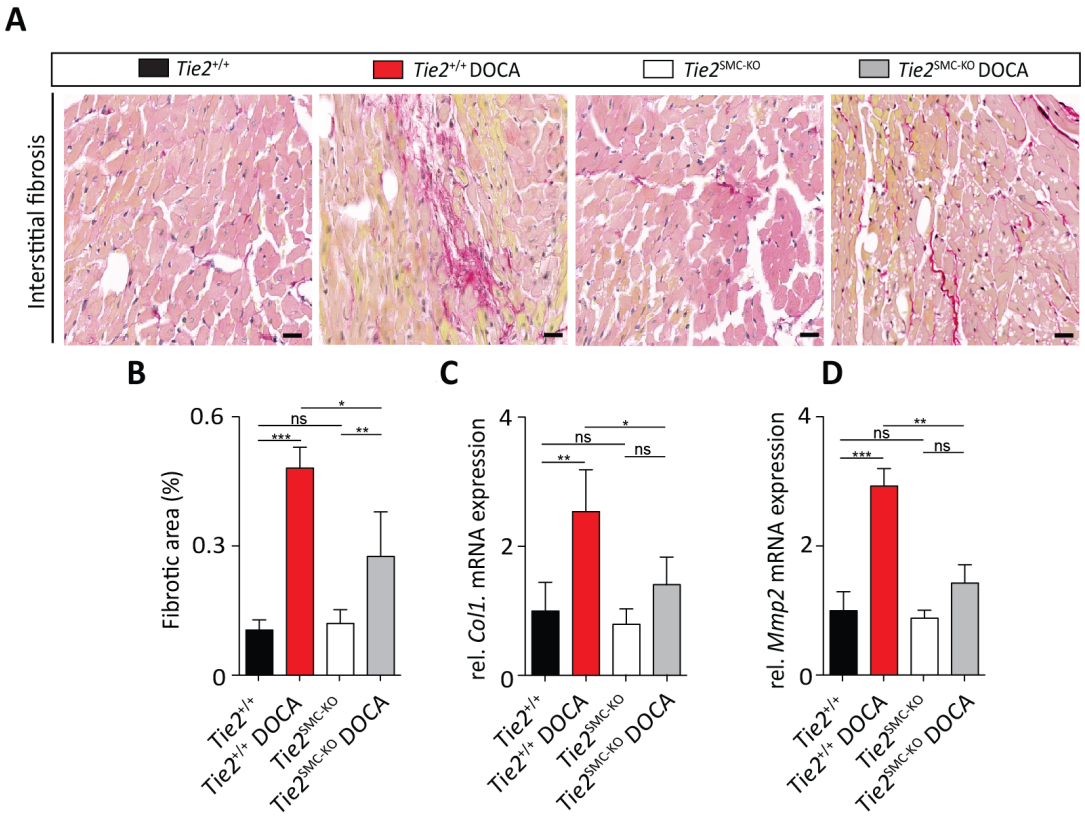

Figure 34. Sm22α-driven Tie2 deletion reduces cardiac fibrosis upon DOCA-salt treatment

A, Representative image of heart sections derived from untreated and DOCA-salt treated *Tie2*$^{+/+}$ and *Tie2*$^{SMC-KO}$ mice and stained with Picro-sirius red for the assessment of fibrosis. **B**, Quantitative analyses of fibrotic area in heart sections of *Tie2*$^{+/+}$ and *Tie2*$^{SMC-KO}$ mice. Fibrotic area was normalized to total area; n=5-8. Scale bar: 20 µm **C-D**, *Collagen 1* (*Col1*) (**C**) and *matrix metalloproteinase 2* (*Mmp2*) (**D**) gene expression in isolated hearts of untreated and DOCA-salt treated *Tie2*$^{+/+}$ and *Tie2*$^{SMC-KO}$ mice; n=3-8. Data are shown as mean ± S.D. **p* < 0.05, ***p* < 0.001, ****p* < 0.0001. Student´s *t-test*. ns=non-significant.

2.12 Sm22α-driven Tie2 deletion affects VSMC phenotype and function upon DOCA-salt treatment

To investigate changes in VSMC phenotype in DOCA-salt mice, mesenteric arteries were isolated and stained for the distinct VSMC-markers αSMA and Calponin, and for the proliferation marker PCNA

(Figure 35A). No differences were detected in αSMA- and Calponin-positive area or PCNA-positive nuclei between untreated *Tie2*$^{+/+}$ and *Tie2*$^{SMC-KO}$ mice (Figure 35A-35D).

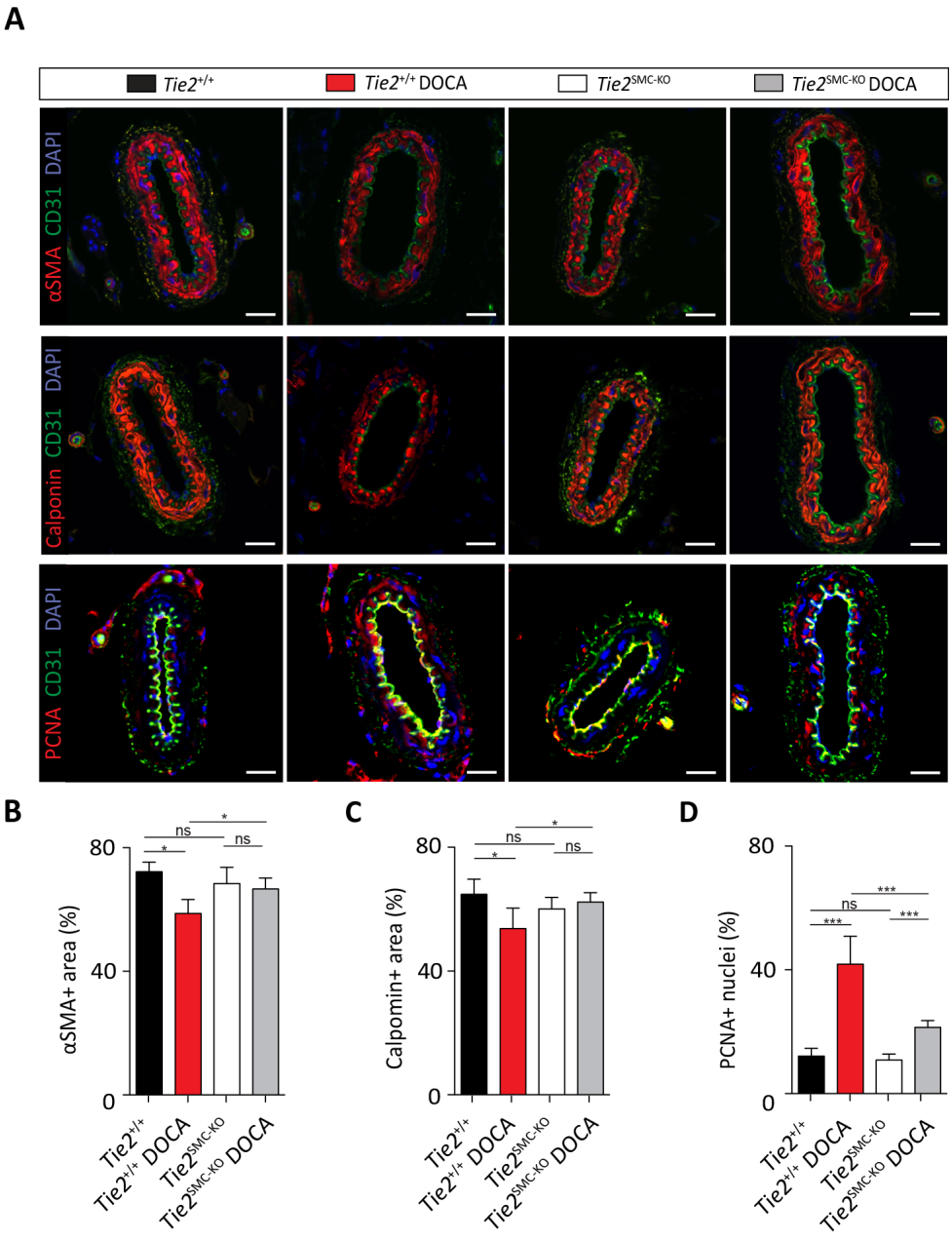

Figure 35. VSMC-specific Tie2 deletion maintains the contractile VSMC phenotype in DOCA-salt treated arteries

A, **B**, Isolated mesenteric arteries (MA), from untreated and DOCA-treated *Tie2*$^{+/+}$ and *Tie2*$^{SMC-KO}$ mice, stained and quantified for αSMA-positive area for VSMC content. **A**, **C**, Isolated MA, from untreated and DOCA-treated *Tie2*$^{+/+}$ and *Tie2*$^{SMC-KO}$ mice, stained and quantified for Calponin-positive area for VSMC content; Scale bar: 50 µm. **A**, **D**, Isolated MA, from untreated and DOCA-treated *Tie2*$^{+/+}$ and *Tie2*$^{SMC-KO}$ mice, stained and quantified for PCNA-positive VSMC nuclei; n=4-7. Data are shown as mean ± S.D. Student´s *t-test*. *$p < 0.05$, **$p < 0.001$, ***$p < 0.0001$. Student´s *t-test*. ns=non-significant.

Mesenteric arteries derived from *Tie2*$^{+/+}$ mice displayed a significant decrease in αSMA- and Calponin-positive area as compared to *Tie2*$^{+/+}$ mice upon DOCA-salt treatment (Figure 35A-35C), supporting an active vascular remodeling process. Interestingly, no differences were observed between untreated mesenteric arteries from *Tie2*$^{SMC\text{-}KO}$ mice and DOCA-salt treated *Tie2*$^{SMC\text{-}KO}$ mice. In addition, a significant increase in PCNA expression was observed in mesenteric arteries of DOCA-salt-treated *Tie2*$^{+/+}$ and *Tie2*$^{SMC\text{-}KO}$ mice as compared to their untreated controls (Figure 35D), whereas *Tie2*$^{SMC\text{-}KO}$ mice displayed a reduction in PCNA expression as compared to *Tie2*$^{+/+}$ mice upon DOCA-salt treatment. Hence, the data suggest that the effect of VSMC-expressed Tie2 is cell autonomous.

2.13 Sm22α-driven Tie2 deletion affects the compensatory potential of the heart upon AngII-induced hypertension

To validate cardiac function in a second hypertension model targeting cardiac hypertrophy, the AngII-induced hypertension model was applied. Osmotic minipumps were implanted subcutaneously into the back of *Tie2*$^{+/+}$ and *Tie2*$^{SMC\text{-}KO}$ mice to infuse AngII (1.5 mg/ kg/ day) (Figure 36A). The short-term effect of AngII-treatment on cardiac hypertrophy was examined on day 4 and day 7. BP was non-invasively measured by tail cuff method before pump implantation and at endpoint. On infusion of AngII, blood pressure increased in both *Tie2*$^{+/+}$ and *Tie2*$^{SMC\text{-}KO}$ mice as compared to untreated controls, indicative of a successful induction of hypertension by AngII (Figure 36B). However, no differences were observed in blood pressure between *Tie2*$^{+/+}$ and *Tie2*$^{SMC\text{-}KO}$ mice upon AngII treatment.

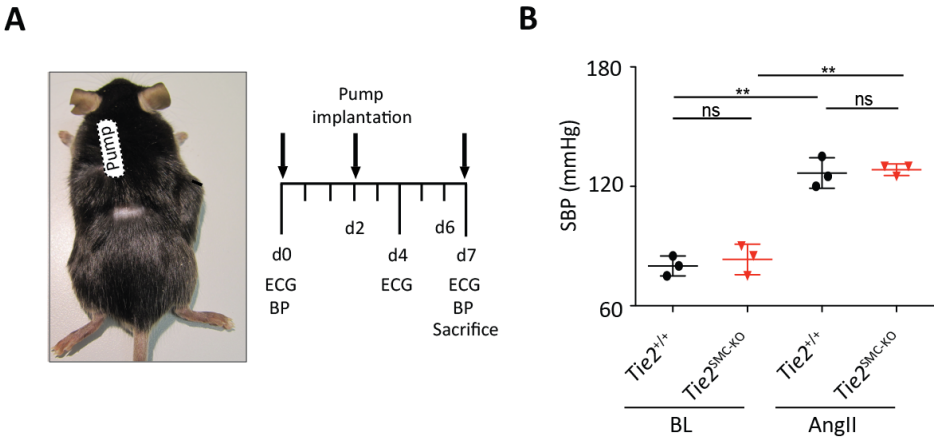

Figure 36. Experimental protocol for Angiotensin II-induced hypertension

A, Schematic representation of the experimental model: Baseline (BL) echocardiography was performed on *Tie2*$^{+/+}$ and *Tie2*$^{SMC\text{-}KO}$ mice 2 days prior to Angiotensin II (AngII) treatment and 4 and 7 days following AngII treatment. SBP was measured by tail cuff method at baseline and at endpoint. Osmotic minipumps containing AngII (1.5 mg/ kg/ day) were implanted subcutaneously at the back of *Tie2*$^{+/+}$ and *Tie2*$^{SMC\text{-}KO}$ mice. Mice were sacrificed at day 7 following AngII treatment. **B**, Quantitative analyses of SBP in *Tie2*$^{+/+}$ and *Tie2*$^{SMC\text{-}KO}$ mice before and after AngII treatment; n=4-7. Data are shown as mean ± S.D. Student´s *t-test*. $^{**}p < 0.001$. Student´s *t-test*. ns=non-significant.

HW and HW/TL were significantly increased in untreated *Tie2*$^{+/+}$ and *Tie2*$^{SMC-KO}$ mice (Figure 37A and 37B), which is in agreement with previous observations. Analysis of cardiac hypertrophy revealed a reduction, although not significant, in HW and HW/TL in AngII-treated *Tie2*$^{SMC-KO}$ mice in comparison to untreated mice. While LVPW thickness was decreased in untreated *Tie2*$^{SMC-KO}$ mice as compared to untreated *Tie2*$^{+/+}$ mice at baseline (Figure 37C), no gross differences were detected in heart rate (HR), stroke volume (SV), and cardiac output (CO) between the two untreated groups (Figure 38A-38C).

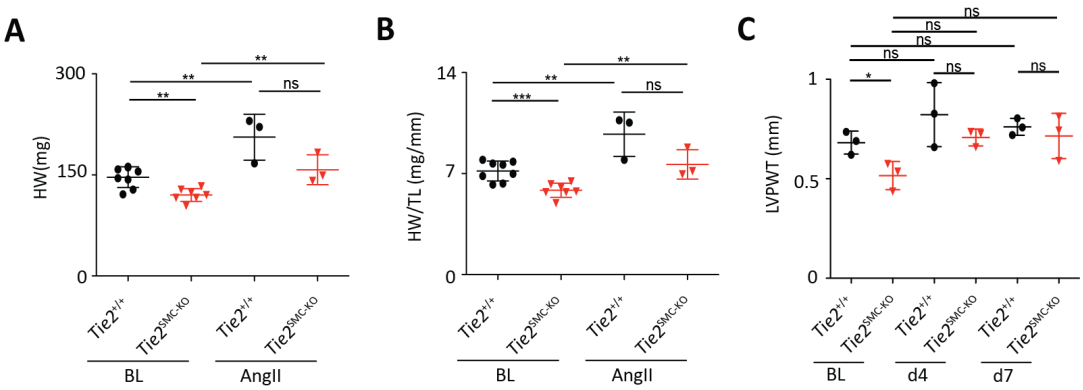

Figure 37. Sm22α-driven Tie2 deletion delays the compensatory potential of the heart upon AngII-induced hypertension

A-B, Quantitative analyses of HW (**A**) and HW/TL (**B**) in untreated *Tie2*$^{+/+}$ and *Tie2*$^{SMC-KO}$ mice at baseline (BL) and after AngII treatment; n=3-7. **C**, Quantitative analyses of left ventricular posterior wall thickness (LVPWT) in *Tie2*$^{+/+}$ and *Tie2*$^{SMC-KO}$ mice at BL and after AngII treatment; n=3. Data are shown as mean ± S.D. **p* < 0.05, ***p* < 0.001, ****p* < 0.0001. Student´s *t-test*. ns=non-significant.

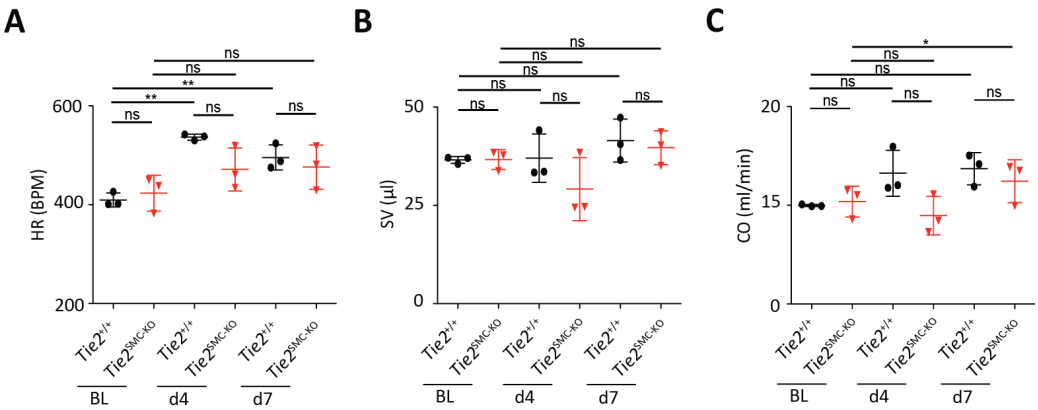

Figure 38. Sm22α-driven Tie2 deletion delays an increase in cardiac output upon AngII-induced hypertension

A, Quantitative analyses of heart rate (HR) in untreated and AngII-treated *Tie2*$^{+/+}$ and *Tie2*$^{SMC-KO}$ mice. **B**, Quantitative analyses of stroke volume (SV) in untreated and AngII-treated *Tie2*$^{+/+}$ and *Tie2*$^{SMC-KO}$ mice. **C**, Quantitative analyses of cariac output (CO) in untreated and AngII-treated *Tie2*$^{+/+}$ and *Tie2*$^{SMC-KO}$ mice; n=3. Data are shown as mean ± S.D. **p* < 0.05, ***p* < 0.001. Student´s *t-test*. ns=non-significant.

On day 4 and day 7 following AngII treatment, HR was significantly increased in *Tie2*$^{+/+}$ mice as compared to untreated controls, whereas no differences were detected in HR between AngII-treated *Tie2*$^{SMC-KO}$ mice and their untreated controls (Figure 38A). Furthermore, *Tie2*$^{SMC-KO}$ mice

revealed a reduced LVPW, HR, SV and CO as compared to *Tie2*$^{+/+}$ mice upon day 4 of AngII infusion (Figure 37C and 38A-38C). However, the reduction in LVPW, HR, SV and CO in *Tie2*$^{SMC-KO}$ mice is compensated at day 7 of AngII treatment. Thus, *Tie2*$^{SMC-KO}$ mice exhibit a delay in adaptive cardiac responses upon AngII-induced hypertension.

2.14 VSMC-expressed Tie2 regulates phenotypic modulation of activated VSMC

Phenotypic modulation of activated VSMC is an important process during atherosclerosis progression[375,376]. Since phenotypic modulation is associated with changes in VSMC proliferation and migration, it was investigated whether VSMC-specific Tie2 deletion could attenuate these processes in isolated short-term cultured VSMC. Indeed, FACS analysis of 5-ethynyl-2'-deoxyuridine-(EdU)-positive cells showed significantly reduced proliferation of isolated, short-term cultured aortic VSMC from *Tie2*$^{SMC-KO}$ mice as compared to *Tie2*$^{+/+}$ mice (Figure 39A). Similar results were obtained in Tie2-silenced HAoSMC, using two siRNA constructs as compared to non-silenced controls (NS) (Figure 39B). Tie2 (*Tek*) deletion in isolated aortic VSMC was confirmed by RT-qPCR (Figure 39C). Comparative analysis of HAoSMC migratory activity in lateral scratch wound assays demonstrated a significant reduction in migration of Tie2-silenced HAoSMC as compared to control siRNA (Figure 40A and 40B). Taken together, these data highlight the importance of Tie2 in controlling proliferation and migration of activated VSMC.

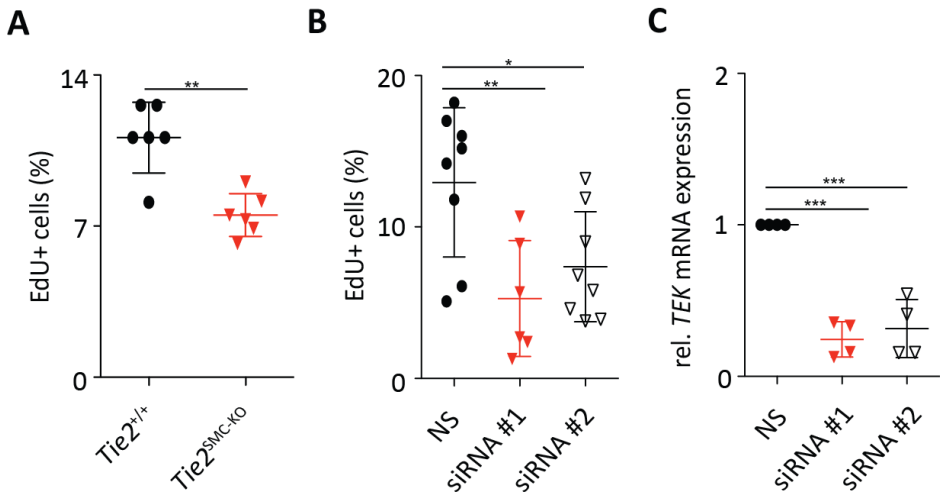

Figure 39: Reduced proliferation of Tie2-deficient and Tie2-silenced aortic VSMC

A, EdU-FACS analysis of isolated aortic VSMC from *Tie2*$^{+/+}$ and *Tie2*$^{SMC-KO}$ mice; n=5-6. **B**, EdU-FACS analysis of Tie2-silenced (transfected with either siRNA#1 or siRNA#2) and non-silenced HAoSMC; n=7-8. **C**, Tie2 (*Tek*) expression analyzed by RT-qPCR of Tie2-silenced and non-silenced HAoSMC; n=4. Data are shown as mean ± S.D. of 3 independent experiments. *$p < 0.05$, **$p < 0.001$, ***$p < 0.0001$. Student´s *t-test*.

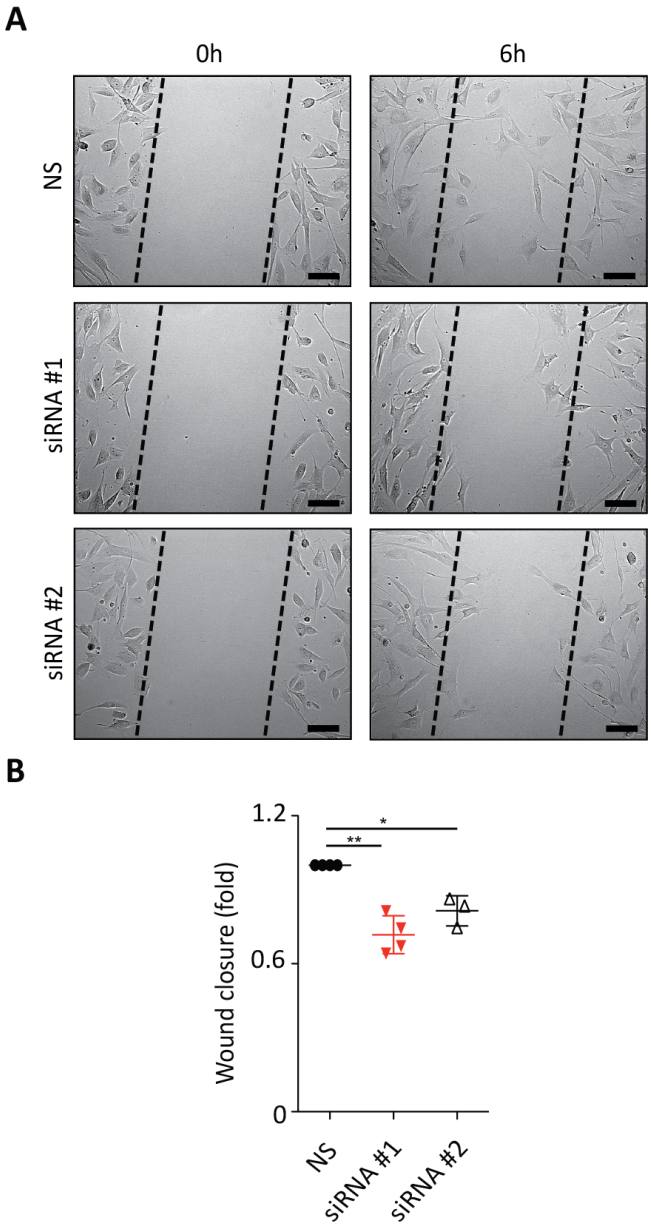

Figure 40. Reduced migration of HAoSMC upon Tie2 silencing

A, Representative images of Tie2-silenced and non-silenced HAoSMC at the beginning (t=0 h) and end (t=6 h) of time-lapse microscopy (3 regions per wound) during lateral-scratch wound assay. Scale bar: 200 µm. **B**, The migration of HAoSMC transfected with either siRNA#1, siRNA#2 or NS was determined as the ratio of filled area with migrated cells to total wounded area normalized to NS controls. NS = non-silenced; n=4. Data are shown as mean ± S.D. *$p < 0.05$, **$p < 0.001$. Student´s *t-test*.

2.15 VSMC-specific Tie2 deletion reduces atherosclerosis progression

Since VSMC proliferation and migration are two important processes for atherosclerosis, the role of VSMC-expressed Tie2 on atherosclerosis progression was investigated. To this end, constitutive *ApoE*^{KO} *Tie2*$^{SMC-KO}$ double KO and *ApoE*^{KO} *Tie2*$^{+/+}$ (*ApoE*^{KO}) control mice were generated. *ApoE* null mice spontaneously develop atherosclerosis and feeding them a cholesterol-rich diet accelerates the development of lesions[387].

Male *ApoE*^{KO} and *ApoE*^{KO} *Tie2*$^{SMC-KO}$ mice, at the age of 10 weeks, were fed a Western-type diet for 14 weeks. VSMC-specific Tie2 deletion did not alter body weight, plasma cholesterol, and triglyceride profile in *ApoE* null mice. Analysis of Oil red O (ORO)-positive area revealed a significant reduction in atherosclerotic lesions in aortic sinus of *ApoE*^{KO} *Tie2*$^{SMC-KO}$ mice (Figure 41A and 41B).

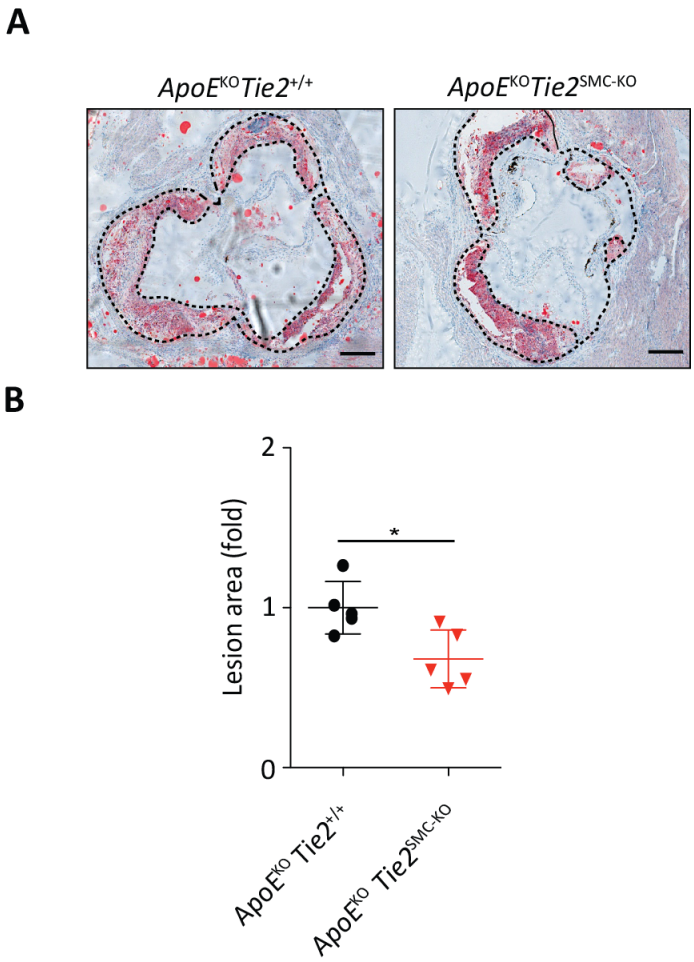

Figure 41. Tie2 deficiency in VSMC reduces atherosclerosis in mice

A-B, Representative images (**A**) and quantification (**B**) of ORO-stained aortic sinus from 24-week-old *ApoE*^{KO} and *ApoE*^{KO} *Tie2*$^{SMC-KO}$ mice fed a Western-type diet for 14 weeks, n=5. Dashed lines mark the atherosclerotic lesions within the intima. Scale bar: 200 µm. Data are shown as mean ± S.D. *$p < 0.05$. Student´s *t-test*.

To investigate the contribution of VSMC-expressed Tie2 on macrophage infiltration in atherosclerotic lesions, aortic-sinus sections were stained with anti-Mac3 antibody (Figure 42A and 42B). *ApoE*^{KO} *Tie2*$^{SMC-KO}$ mice showed no significant differences in Mac3+ area as compared to *ApoE*^{KO} mice,

suggesting that VSMC-expressed Tie2 has no major effect on macrophage infiltration into the atherosclerotic lesions. Furthermore, atherosclerotic lesions from *ApoE*^{KO} *Tie2*$^{SMC-KO}$ mice showed a marked decrease in αSMA+ smooth muscle cell area as compared to *ApoE*^{KO} mice (Figure 42A and 42C), suggesting that VSMC-specific Tie2 deletion attenuated VSMC content in the lesions. Morover, analysis of ORO-positive area also demonstrated a significant reduction in atherosclerotic lesions in total aorta of *ApoE*^{KO} *Tie2*$^{SMC-KO}$ mice (Figure 42D and 42E).

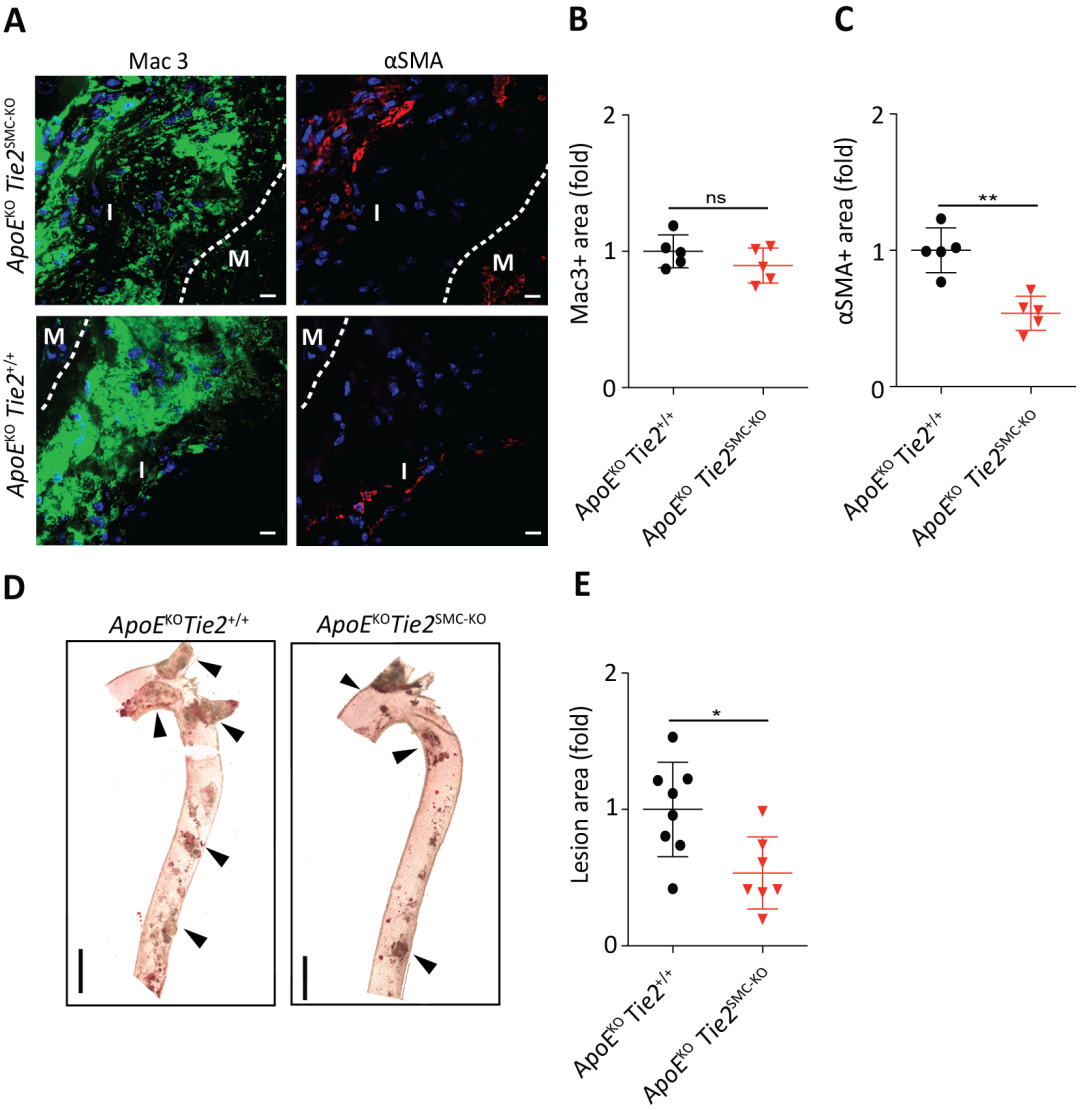

Figure 42. Tie2 deficiency in VSMC reduces atherosclerosis in mice

A, Representative images of Mac3- and αSMA-stained aortic sinus from 24-week-old *ApoE*^{KO} and *ApoE*^{KO} *Tie2*$^{SMC-KO}$ mice fed a Western-type diet for 14 weeks. Dashed lines mark the border between media (M) and intima (I). Scale bar: 10 µm. **B**-**C**, Quantification of Mac3+ area (**B**) and αSMA+ area (**C**) in the aortic sinus of 24-week-old *ApoE*^{KO} and *ApoE*^{KO} *Tie2*$^{SMC-KO}$ mice fed a Western-type diet for 14 weeks. **D-E**, Representative images (**D**) and quantification (**E**) of ORO-stained aortas from 24-week-old *ApoE*^{KO} and *ApoE*^{KO} *Tie2*$^{SMC-KO}$ mice fed a Western-type diet for 14 weeks. The ORO-positive lesion area, αSMA+ area and Mac3+ area were quantified as percentage of total area normalized to *ApoE*^{KO} littermates. Scale bar: 1 mm. Black arrows indicate atherosclerotic lesions. Data are shown as mean ± S.D. *$p < 0.05$, **$p < 0.001$. Student´s *t-test*. ns=non-significant.

To further validate these findings, mRNA expression of contractile VSMC markers and synthetic VSMC markers was analyzed in isolated, short-term cultured, aortic VSMC from *ApoE*^{KO} and *ApoE*^{KO} *Tie2*$^{SMC-KO}$ mice fed a Western-type diet for 14 weeks. *Tie2* (*Tek*) and *Angpt1* mRNA levels were significantly reduced in *ApoE*^{KO} *Tie2*$^{SMC-KO}$ mice (Figure 43A). The expression of contractile VSMC markers *Tagln*, *Acta2* and *Myl9* was significantly increased in VSMC from *ApoE*^{KO} *Tie2*$^{SMC-KO}$ mice, whereas synthetic VSMC markers *Rbp1*, *Vim* and *Myh10* were significantly decreased (Figure 43B and 43C), thereby supporting the GSEA data (Figure 14 and 15). No significant differences were detected for *Cnn1* and *Myh11* (Figure 43B). In conclusion, these data suggest that VSMC-expressed Tie2 regulates VSMC phenotypic modulation during atherosclerosis progression, thereby promoting VSMC content in the lesions.

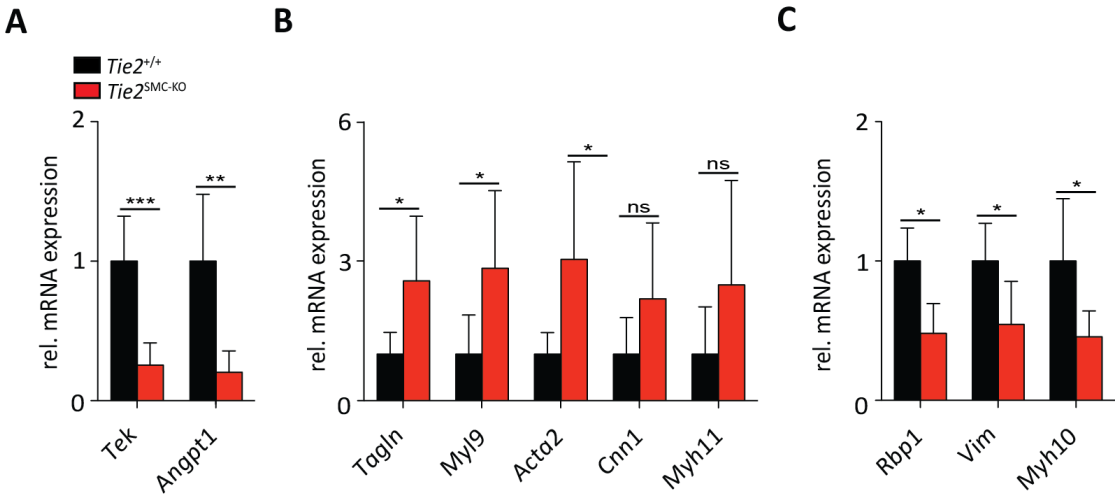

Figure 43. Characterization of isolated aortic VSMC from *ApoE*^{KO} and *Tie2*$^{SMC-KO}$ mice

A-C, Gene expression analysis by RT-qPCR of *Tie2* (*Tek*) and *Angpt1* (**A**), contractile VSMC-specific markers *Tagln*, *Myl9*, *Acta2*, *Cnn1*, *Myh11* (**B**) and synthetic markers *Rbp1*, *Vim* and *Myh10* (**C**) in isolated VSMC from *ApoE*^{KO} and *ApoE*^{KO}*Tie2*$^{SMC-KO}$ mice fed a Western-type diet for 14 weeks; n= 4-6. Data are shown as mean ± S.D. ***p* < 0.05, ***p*< 0.001, ****p* < 0.0001. Student´s *t-test.* ns=non-significant.

2.16 Angiopoietin 2-deficient mice display increased atherosclerosis

To trace possible systemic effects of VSMC-expressed Tie2 in atherosclerosis, a proteome profiler array was performed using serum samples of *ApoE*^{KO} and *ApoE*^{KO} *Tie2*$^{SMC\text{-}KO}$ mice fed a Western-type diet for 14 weeks. The array revealed slightly increased Angpt1 and Angpt2 expression in the serum from *ApoE*^{KO} *Tie2*$^{SMC\text{-}KO}$ as compared to *ApoE*^{KO} mice (Figure 44A). Validation of these findings by ELISA confirmed a significant increase in circulating levels of Angpt2 from *ApoE*^{KO} *Tie2*$^{SMC\text{-}KO}$ mice, whereas levels of Angpt1, the constitutive agonist of Tie2, were unaltered among the groups (Figure 44B and 44C). As a result Angpt2 to Angpt1 ratio was significantly increased in *ApoE*^{KO} *Tie2*$^{SMC\text{-}KO}$ as compared to *ApoE*^{KO} mice (Figure 44D).

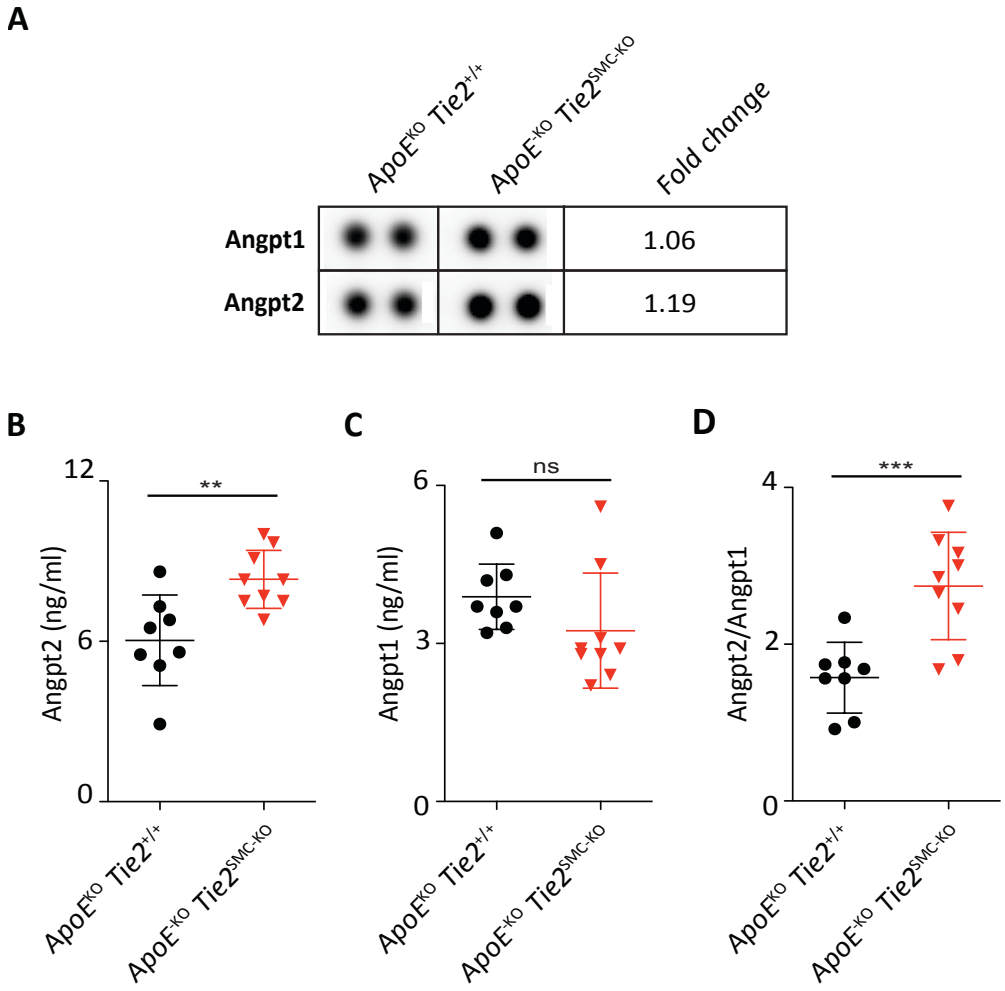

Figure 44. Angpt2 serum concentrations are increased in the absence of VSMC-expressed Tie2

A, Representative scans of the proteome profiler array performed on serum samples of 24-week-old *ApoE*^{KO} and *ApoE*^{KO}*Tie2*$^{SMC\text{-}KO}$ mice fed a Western-type diet for 14 weeks showing Angpt1 and Angpt2 proteins. Serum samples were pooled from 4 *ApoE*^{KO} mice and 4 *ApoE*^{KO}*Tie2*$^{SMC\text{-}KO}$ mice, respectively. Quantification was based on signal intensity measured on gray levels using FIJI imaging software. **B-C**, Quantification of circulating Angpt2 **(B)** and Angpt1 **(C)** by ELISA in serum samples of 24-weeks-old *ApoE*$^{-/-}$ *Tie2*$^{+/+}$ and *ApoE*$^{-/-}$ *Tie2*$^{\Delta}$SMC mice fed a Western-type diet for 14 weeks; n=8-9. **D**, Quantification of Angpt2 to Angpt1 ratio from **B** and **C** (n=8-9). Data are shown as mean ± S.D. *$p < 0.05$, **$p < 0.001$, ***$p < 0.0001$. Student´s *t-test*.

Systemic adenoviral Angpt2 overexpression has previously been shown to act atheroprotective[117]. In turn, Angpt2 blocking antibodies have been shown to particularly reduce early atherosclerotic lesion formation[366]. In order to shed further light on the role of Angpt2 in atherosclerosis, constitutive *ApoE*$^{-/-}$ *Angpt2*$^{-/-}$ (*ApoE*^{KO} *Angt2*^{KO}) double KO and *ApoE*^{KO} littermate control mice were generated and atherosclerosis experiments were performed by feeding a Western-type diet for 14 weeks. *ApoE*^{KO} *Angpt2*^{KO} mice had no altered body weight, cholesterol or triglyceride levels compared to *ApoE* null mice. *ApoE*^{KO} *Angpt2*^{KO} mice showed a significant increase in atherosclerotic lesion area in sinus (Figure 45A and 45B), as demonstrated by ORO staining. Analysis of Mac3+ and αSMA+ area revealed a significant increase in macrophage and VSMC content (Figure 46A-46C). Moreover, analysis of ORO-positive area also demonstrated a significant increase in atherosclerotic lesions in total aorta of *ApoE*^{KO} *Angpt2*^{KO} mice (Figure 46D and 46E).

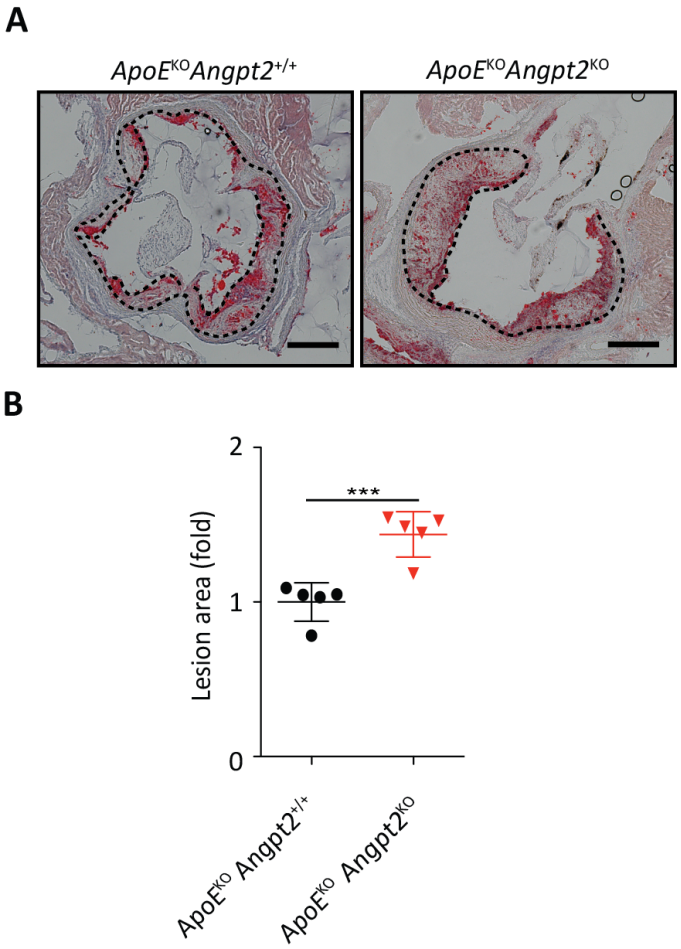

Figure 45. Angpt2 deficiency promotes atherosclerosis in *ApoE* null mice

A-B, Representative images (**A**) and quantification (**B**) of ORO-stained aortic sinus from 24-week-old *ApoE*^{KO} and *ApoE*^{KO} *Angpt2*^{KO} mice fed a Western-type diet for 14 weeks; n=5. Dashed lines mark the atherosclerotic lesions within the intima. Scale bar: 200 µm. Data are shown as mean ± S.D. ***$p < 0.001$. Student´s *t-test*.

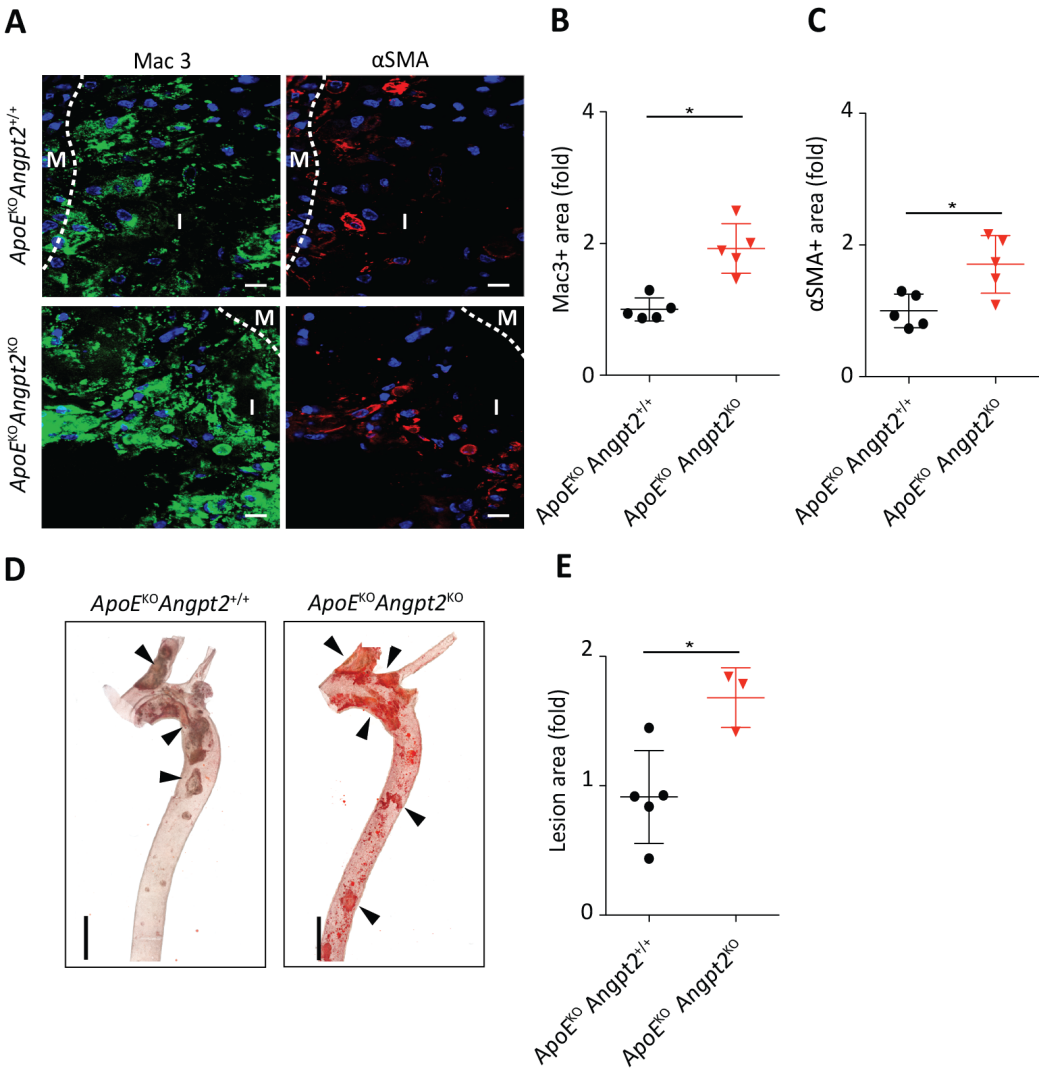

Figure 46. Angpt2 deficiency promotes atherosclerosis in *ApoE null* mice

A, Representative images of Mac3- and αSMA-stained aortic sinuses from 24-week-old *ApoE*^{KO} and *ApoE*^{KO}*Angpt2*^{KO} mice fed a Western-type diet for 14 weeks. Dashed lines mark the border between media (M) and intima (I). Scale bar: 10 µm. **B-C**, Quantification of Mac3+ (**B**) and αSMA+ area (**C**) in the aortic sinus of 24-week-old *ApoE*^{KO} and *ApoE*^{KO} *Angpt2*^{KO} mice fed a Western-type diet for 14 weeks. **D-E**, Representative images (**D**) and quantification (**E**) of ORO-stained aortas from 24-week-old *ApoE*^{KO} and *ApoE*^{KO} *Angpt2*^{KO}mice fed a Western-type diet for 14 weeks. The ORO-positive lesion area, αSMA+ area and Mac3+ area were quantified as percentage of total area normalized to *ApoE*^{KO} littermates. Scale bar: 1 mm. Black arrows indicate atherosclerotic lesions. Data are shown as mean ± S.D. *$p < 0.05$, **$p < 0.001$. Student´s *t-test*. ns=non-significant.

3 Discussion

The study was aimed at deciphering i) the role of VSMC-expressed Tie2 in regulating blood pressure and cardiac function during hypertension and ii) the role of VSMC-expressed Tie2 in regulating phenotypic remodeling of VSMC during atherosclerosis progression. Hypertension and atherosclerosis are the most common risk factors for CVD, which still constitute the major cause of death globally[126,388,389].

3.1 VSMC-expressed Tie2 controls the balance between the contractile and synthetic VSMC phenotype

Scattered reports have demonstrated Tie2 expression in VSMC[370-372]. In agreement with these findings, primary mouse and human VSMC express lower, but consistently detectable levels of functional Tie2 as compared to EC. Therefore, VSMC-specific Tie2-deficient mice (*Tie2*$^{SMC-KO}$) were generated, using a mural cell-specific *Sm22α-Cre* driver line. Tie2 deletion efficiency was confirmed in mesenteric arteries, femoral arteries, hearts, aortas and short-term cultured aortic VSMC isolated from *Tie2*$^{SMC-KO}$ mice. EC-specific deletion of Tie2 has been shown to phenocopy the embryonic lethal phenotype of globally Tie2-deficient mice, which die during midgestation (E10.5) as a result of perturbed vessel maturation[374,390]. In contrast, *Tie2*$^{SMC-KO}$ mice were born phenotypically normal and according to the Mendelian ratio. Moreover, VSMC-specific Tie2 deletion did not affect postnatal retinal angiogenesis or mural cell coverage.

VSMC express a repertoire of proteins involved in contractility including calcium regulatory and contractile proteins, receptors, ion channels, and signal transduction molecules[124]. However, expression of a single contractile VSMC marker gene alone is not sufficient, and the assessment of VSMC phenotype has to be conducted by a combination of various marker genes[126]. Therefore, multiple contractile (e.g. *Sm22α, αSMA, Cnn1, Myh11, Myl9, Cald1)* and synthetic *(e.g. Rbp1, Vim, Myh10, Tpm4)* VSMC-specific markers were analysed in the presence and absence of Tie2. Gene expression analysis of isolated short-term cultured aortic VSMC from *Tie2*$^{SMC-KO}$ mice identified an upregulation of contractile and a downregulation of synthetic VSMC markers, suggesting that Tie2 controls the phenotypic switch of VSMC. VSMC remodeling is associated with an increased proliferative and migratory rate[307,309]. These cells migrate into the intima and change their phenoyte from a contractile to a proliferative state. The reduced migration and proliferation in Tie2-deficient cultured VSMC in the present study supports a contractile, quiescent phenotype rather than a synthetic VSMC phenotype. However, *in vivo*, VSMC-specific Tie2 deletion did not result in any structural alterations in isolated mesenteric arteries, femoral arteries, or aortas at baseline. Hence, Tie2 gene disruption in VSMC alone is not sufficient to induce gross structural abnormalities in the vessels, suggesting that additional triggers are needed to induce the VSMC-phenotype observed upon culture. Indeed, *ex vivo* cultured isolated mesenteric arteries and femoral arteries obtained

from *Tie2*$^{SMC-KO}$ mice showed a decrease in vessel diameter upon increasing intraluminal pressure, indicating a (hyper-) contractile phenotype, which is in line with the contractile VSMC phenotype observed *in vitro*. Previous studies have also described that upon culture VSMC acquire a synthetic phenotype, which resemble an activated status upon vascular injury[375,376].

3.2 Sm22α-driven Tie2 deletion in the heart affects baseline blood pressure and cardiac size

The principal role of VSMC is to regulate vasoconstriction and dilation of blood vessels, thereby regulating vascular tone, blood flow and blood pressure[388,391]. Importantly, *αSMA-null* mice displayed significantly lower baseline blood pressure[163]. Therefore, the relative importance of VSMC-expressed Tie2 on baseline blood pressure was evaluated in *Tie2*$^{+/+}$ and *Tie2*$^{SMC-KO}$ mice. Telemetric tracing identified significantly reduced basal SBP in resting *Tie2*$^{SMC-KO}$ mice, whereas no differences were observed in DBP and HR. The findings indicate that *Tie2*$^{SMC-KO}$ mice are dealing with a baseline heart phenotype. Wang and colleagues demonstrated distinct roles of vascular EC- and VSMC-expressed peroxisome proliferators-activated receptor-γ (PPARγ) in regulating blood pressure and vascular tone[392]. Another study showed that loss of epidermal growth factor receptor (EGFR) in CMs as well as VSMC leads to hypotension and cardiac hypertrophy[393]. These examples emphasize that a 'yin-yang' relationship might exist in blood vessels to maintain vascular homeostasis. However, VSMC phenotype was not affected at baseline in *Tie2*$^{SMC-KO}$ mice, suggesting that the baseline heart phenotype is independent of Sm22α-driven Tie2 deletion in VSMC.

The MAP is defined as the average pressure in arteries during one cardiac cycle, and is calculated from SBP and DBP (MAP= SBP + 2 (DBP)/3)[394]. The MAP is considered to be a better alternative measurement than SBP as it serves as indicator of tissue and organ perfusion[394]. Moreover, SBP or DBP alone do not suffice as predictors for this critical cardiovascular parameter. Comparative analysis of baseline MAP revealed a significant reduction in resting *Tie2*$^{SMC-KO}$ mice as compared to resting *Tie2*$^{+/+}$ mice, indicating that perfusion may be reduced in these mice. Active *Tie2*$^{SMC-KO}$ mice and *Tie2*$^{+/+}$ mice displayed a significant increase in SBP, DBP, HR and MAP upon physical activity. Furthermore, SBP, DBP, HR and MAP were notably decreased in active *Tie2*$^{SMC-KO}$ mice as compared to active *Tie2*$^{+/+}$ mice. The significant decrease in DBP and HR in active *Tie2*$^{SMC-KO}$ mice could be explained by the fact that physical activity causes a beneficial adaptive response of the cardiovascular system, that is more prominent in the *Tie2*$^{SMC-KO}$ mice[382,383]. Furthermore, HW and HW/TL were measured in *Tie2*$^{+/+}$ and *Tie2*$^{SMC-KO}$ mice. HW were normalized to TL and used as measurement for cardiac size as TL remains constant after maturity, whereas BW fluctuates with aging, therefore making HW/BW an unreliable reference for normalizing HW[395]. The findings demonstrated that the decrease in blood pressure correlated with a decrease in HW and HW/TL, stating that *Tie2*$^{SMC-KO}$ mice have a reduced blood pressure as well as a reduced cardiac size. Echocardiographic recordings supported a significant reduction in LVPW and IVS thickness in the heart of *Tie2*$^{SMC-KO}$ mice. Further analysis of CM size revealed a sharp decrease in CM width and area

in *Tie2*$^{SMC-KO}$ mice with no differences in CM length. These findings suggest that cardiac development is impaired in *Tie2*$^{SMC-KO}$ mice. The decrease in cardiac size in *Tie2*$^{SMC-KO}$ mice could also be a consequence of a reduction in cell number. CMs in the mammalian heart loose their capacity to proliferate soon after birth, meaning that any differences in proliferation that occurs in the heart will be due to proliferation in other cell-types present in the heart, such as VSMC, fibroblasts and EC[258,260]. Proliferation (Ki67+ nuclei) and apoptosis (Cleaved Caspase 3+ area) did not differ between *Tie2*$^{+/+}$ and *Tie2*$^{SMC-KO}$ mice, indicating that the decrease in cardiac size is supposedly not the cause of decreased cell number in the heart, but rather the result of poor development of CMs, which is most likely the cause of Sm22α-driven Tie2 deletion in CMs.

3.3 Tie2 expression in cardiomyocytes

Analysis of HW and HW/TL implies that cardiac size is affected between 4 and 6 weeks of age in *Tie2*$^{SMC-KO}$ mice, suggesting that Tie2 might be required in this time frame for normal development of the heart. Previous studies have reported that Sm22α is only transiently expressed in CMs, between E8.5 and 12.5 during embryonic development[160]. In adult CMs, Sm22α expression is restricted to the vasculature. Hence, Sm22α-driven Tie2 deletion in CMs during embryonic development might lead to the reduction in BP and cardiac size observed in adult *Tie2*$^{SMC-KO}$ mice. Cre-mediated recombination was observed in VSMC in the media layer of the aorta as well as in CMs from 6-week-old *Tie2*^{MCM} x *Rosa26*^{YFP} mice, indicating that Tie2 is expressed by VSMC and CMs. In contrast, Tie2 expression was not detected in isolated CMs from 8-week-old *Tie2*$^{+/+}$ and *Tie2*$^{SMC-KO}$ mice by gene expression analysis or Western blot, hinting that Tie2 might be required at an earlier time-point for normal development of the heart. Further studies are needed to exploit the expression pattern of Tie2 in CMs, particularly during the transient expression of Sm22α in CMs during embryonic development and in young adults (6-week-old mice). Overall, Sm22α-driven Tie2 deletion in the heart did not impair blood pressure or heart development to a life-threatening condition. It could be that Sm22α targets only a small proportion of CMs, without affecting other CMs that develop normally and express Tie2. This would explain why the mice survive but still experience an impaired heart function. Importantly, Myh6, Desmin and Nkx2.5 are also expressed throughout the heart from E7.5[396-398]. While Desmin, Myh6 and Sm22α play an important role in maintaining the integrity of the contractile apparatus of the heart, Nkx2.5 is essential for cardiac development.

3.4 Sm22α-driven Tie2 deletion delays an adaptive cardiac response upon hypertension

The treatment with DOCA-salt, a synthetic mineralocorticoid derivative, is a widely used model in various animals, including mice, to induce heart failure mediated by volume overload[399,400]. DOCA-salt treatment mimics the effects of aldosteron by promoting salt retention and an increase in circulating blood volumes. Consequent salt retention ultimately gives rise to hypertension, cardiac

hypertrophy and vascular remodeling. The DOCA-induced hypertension model is regarded as an angiotensin-independent model as DOCA-salt treated animals show a markedly depressed renin-angiotensin system. In the present study, DOCA-salt treatment did not have a major impact on SBP, DBP, MAP and HR in resting *Tie2*$^{+/+}$ and *Tie2*$^{SMC-KO}$ mice, whereas a delay was observed in SBP, DBP and MAP in active *Tie2*$^{SMC-KO}$ mice as compared to active *Tie2*$^{+/+}$ mice, which could be a result of the prominent baseline reduction observed in active *Tie2*$^{SMC-KO}$ mice. In hypertension, the heart responds to increased hemodynamic stimuli by inititiating adaptive remodeling processes including cardiac hypertrophy and fibrosis[255,256]. While Sm22α-driven Tie2 deletion in the heart did not significantly reduce blood pressure upon DOCA-salt treatment, it significantly attenuated fibrotic area. This correlated with a decrease in *Col1* and *Mmp2* mRNA levels, evaluated as markers of extracellular cardiac matrix turnover. Hence, DOCA-salt treatment did not markedly promote fibrosis in *Tie2*$^{SMC-KO}$ mice, indicating a limited remodeling or a lower response due to the reduced blood pressure level. Likewise, DOCA-salt treatment did not elevate HW and HW/TL in *Tie2*$^{SMC-KO}$ mice.

Induction of hypertension leads to structural changes of arteries that include VSMC remodeling and thus the transition from a contractile to a synthetic and proliferative VSMC phenotype[249,401]. Upon DOCA-salt treatment, the contractile VSMC phenotype was maintained in mesenteric arteries from DOCA-salt treated *Tie2*$^{SMC-KO}$ mice as compared to DOCA-salt treated *Tie2*$^{+/+}$ mice. The contractile VSMC phenotype in arteries of DOCA-treated *Tie2*$^{SMC-KO}$ mice and the hypercontractile response of arteries upon intraluminal pressure could be responsible for the increases observed in blood pressure upon DOCA-salt treatment.

These findings were recapitulated in the AngII-induced hypertension model. This is another widely used model of experimental hypertension in which increased blood pressure is mediated by ligand stimulation of AT_1 receptors. This leads to end-organ damage, including cardiac hypertrophy[402]. CO, SV and HR were analysed as parameters for cardiac function in *Tie2*$^{+/+}$ and Tie2^{SMC-KO} mice before and after AngII-treatment. CO is described as the volume of blood that is pumped by the heart per minute. It is a product of HR, which is the number of beats per minute and SV, which is the amount of blood pumped by each heart beat[403,404]. Interestingly, Tie2^{SMC-KO} mice displayed a delay in SV, HR and CO at day 4 following AngII treatment. As such, AngII treatment did not elevate CO and HR in Tie2^{SMC-KO} mice while elevating blood pressure, indicating an impaired cardiac response. However, the reduced SV, HR and CO at day 4 and the subsequent normalization at day 7 suggest that these changes might be only transient. A limitation of this part of the study is that a relatively small number of mice (n=3 per group, trial experiment) were included for the AngII-treated groups. Moreover, 'state of the art' radiotelemetry should be applied instead of tail-cuff system to detect small and accurate changes in blood pressure. Future studies are required to investigate cardiac function in *Tie2*$^{+/+}$ and Tie2^{SMC-KO} mice in more detail upon AngII treatment.

Since both CMs and VSMC are targets of DOCA- and AngII-induced hypertension, it is recommended to investigate Tie2 function on blood pressure in either a VSMC-specific (αSMA, Myh11) mouse model or a CM-specific mouse model (Nkx2.5, Myh6).

3.5 Models: Sm22α-driven Tie2 deletion in the heart and arteries

Taken together, the findings reveal that Sm22α-driven Tie2 deletion in the heart i) reduces baseline blood pressure ii) reduces HW, HW/TL, LVPW thickness, IVS thickness, CM size and thus cardiac size iii) with no changes in cell number. The data proposes CM-expressed Tie2 as a regulator of blood pressure and cardiac size. Upon hypertension, Sm22α-driven Tie2 deletion delays the compensatory potential of the heart (Figure 47A). Furthermore, the data also identified a cell autonomous function of VSMC-expressed Tie2 (Figure 47B). VSMC-specific Tie2 deletion does not affect baseline VSMC phenotype and function. However, VSMC-specific Tie2 deletion limits the transition of VSMC towards a synthetic, proliferative phenotype in an activated status. Upon hypertension, VSMC-specific Tie2 deletion maintains the contractile VSMC phenotype. In conclusion, VSMC-expressed Tie2 promotes phenotypic modulation of activated VSMC.

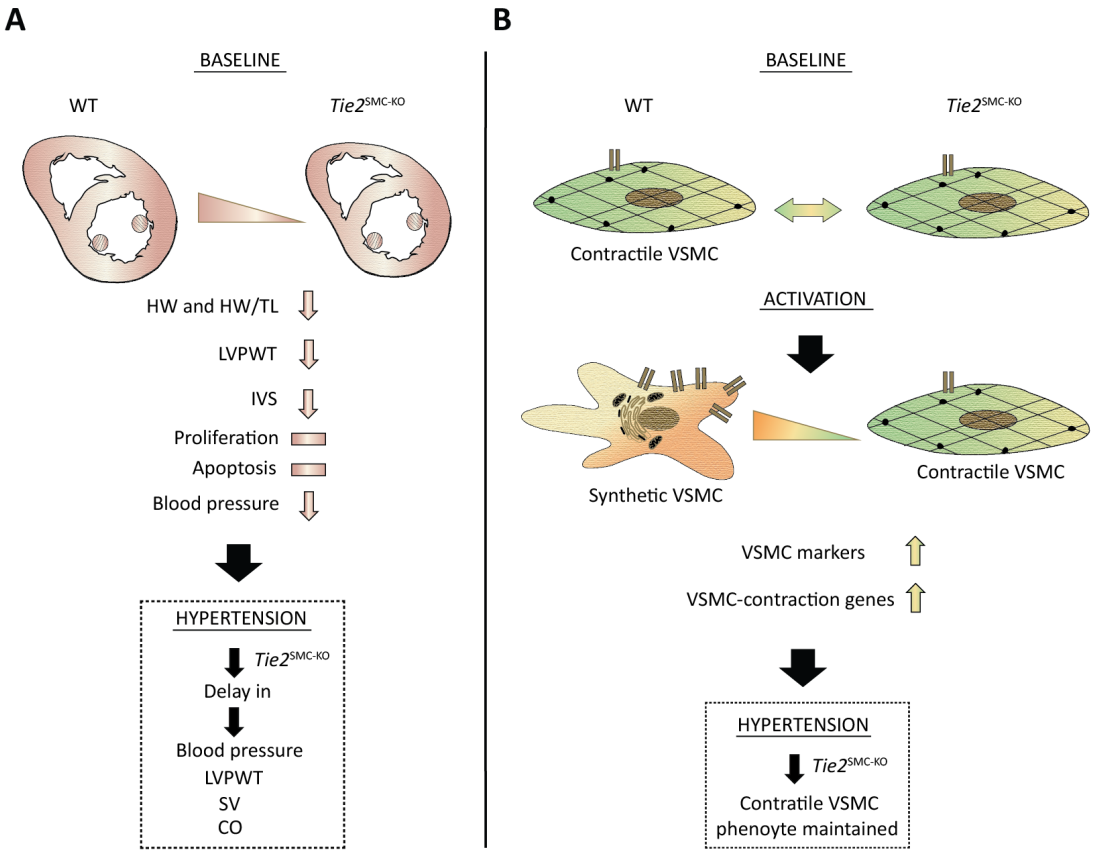

Figure 47. Sm22α-driven Tie2 deletion in the heart and arteries

A, At baseline, Sm22α-driven Tie2 deletion in the heart reduces HW, HW/TL, LVPW thickness, IVS thickness and thus cardiac size with no changes in proliferation and apoptosis. Additionally, blood pressure is also reduced upon Sm22α-driven Tie2 deletion in the heart. Upon hypertension, Sm22α-driven Tie2 deletion delays the compensatory potential of the heart. **B**, VSMC-specific Tie2 deletion does not affect baseline VSMC phenotype and function. In an activated status, VSMC-specific Tie2 deletion limits the transition of VSMC towards a synthetic, proliferative phenotype. Upon hypertension, VSMC specific Tie2 deletion maintains the contractile VSMC phenotype.

3.6 Function of VSMC-expressed Tie2 during atherosclerosis progression

The use of atherosclerosis prone mouse models via genetic and/or diet modifications over the past decades has helped to decipher the molecular and cellular mechanisms that give rise to atherosclerotic lesion progression[405]. The use of *ApoE*- and *LDLR*-deficient mice, the two mouse models best used, allows the study of relatively large number of animals under different environmental and diet condition. Most importantly, these models can be used to study the similarity between mouse lesion progression and human lesions. Atherosclerosis progression can also be studied from fatty streak to advanced lesions within some weeks in the above mentioned mouse models. Lesion progression in these genetically modified mouse models can first be detected at the aortic sinus, and as atherosclerosis progresses, lesions begin to appear in the ascending aorta, followed by the descending aorta[406]. Although the two experimental mouse models have similarities in lesion progression, *ApoE*-deficient mice on a chow diet develop more severe atherosclerotic lesions than *LDLR*-deficient mice[406,407]. Therefore, *ApoE*-deficient mice ($ApoE^{KO}$) were used in this study as atherosclerotic model and $ApoE^{KO}$ $Tie2^{SMC\text{-}KO}$ mice were generated on a C57Bl/6N background.

$ApoE^{KO}$ $Tie2^{SMC\text{-}KO}$ mice had a significant delay of atherosclerotic lesion formation in the aortic sinus (and the aorta) with a reduction of αSMA+ VSMC area. This was in line with an increased mRNA expression of contractile VSMC-specific markers in isolated aortic VSMC from $ApoE^{KO}$ $Tie2^{SMC\text{-}KO}$ mice, whereas the expression of synthetic VSMC-specific makers was markedly reduced. The findings establish a role of VSMC-expressed Tie2 in controlling the shift towards a proliferative and migratory VSMC phenotype and thereby atherosclerosis progression. Hypercholesterolemia plays a critical role in the progression of atherosclerosis and is induced by the accumulation of MΦ and the formation of foam cells in early lesions[408,409]. As a result, there is an increased adhesion of monocytes to the endothelium and infiltration of MΦ. Along with hypercholesterolemia, EC dysfunction and inflammation, phenotypic modulation of VSMC contributes to the development and progression of atherosclerosis[409-411]. Since plasma lipid levels and body weights were not affected by the presence or absence of VSMC-expressed Tie2, Tie2 deficiency in VSMC slowed atherosclerosis progression in $ApoE^{KO}$ $Tie2^{SMC\text{-}KO}$ mice in other ways than through regulation of lipid catabolism.

3.7 Function of Angpt2 during atherosclerosis progression

The loss of VSMC-expressed Tie2 was associated with a significant increase of circulating levels of Angpt2 in $ApoE^{KO}$ mice. Angpt2 is almost exclusively produced by EC[1,412]. Angpt2 has an autocrine mode of action as partial agonist, i.e., it inhibits Tie2 activation in the presence of the strong agonist Angpt1 but it weakly activates Tie2 in the absence of Angpt1[84,413]. Angpt2-mediated inhibition of Angpt1/Tie2 signaling leads to vascular destabilization and primes activated EC for other EC activating growth factors, including angiogenesis- and inflammation-inducing cytokines[1,84,412]. EC

destabilization would be expected to promote atherosclerosis. Concordingly, Angpt2 neutralizing antibodies have been shown to inhibit its progression[366]. Yet, the reported inhibiting effects appear to be transient and are mostly restricted to early stages of atherosclerosis[366]. In contrast, long-term systemic adenoviral overexpression of Angpt2 has been shown to exert anti-atherosclerotic effects[117]. Given the vascular destabilizing effects of Angpt2 on resting EC, this protective phenotype is indeed mechanistically difficult to relate to the current concepts of endothelial Angpt/Tie signaling. Employing a genetic model of constitutive Angpt2 deficiency, this study could in principle be fully compatible with the earlier findings of an atheroprotective effect of increased circulating Angpt2 by showing that *ApoE*^{KO} *Angpt2*^{KO} mice are not protected from atherosclerosis, but have in fact a pro-atherosclerotic phenotype. Above counterintuitive findings on the role of Angpt2 during atherosclerosis suggest that Angpt/Tie signaling in EC alone is not sufficient to account for the complexity of Angpt/Tie signaling during atherosclerosis. A transient pro-atherosclerotic effect of EC Angpt2 destabilization may be compatible with the blocking antibody experiments during early atherosclerosis[366], but the atheroprotective effects of increased circulating Angpt2 as well as the pro-atherosclerotic effect of *ApoE*^{KO} *Angpt2*^{KO} mice are likely due to other, possibly non-endothelial mechanisms.

In contrast to the findings in *ApoE*^{KO} *Angpt2*^{KO} mice, VSMC-specific Tie2 deletion did not significantly attenuate macrophage infiltration within the lesions of the aortic sinus. This may be due to the fact that inflammation in developing atherosclerotic lesions is not only regulated by VSMC but also by the complex interaction of EC and inflammatory cells, leading to accelerated atherosclerosis progression[409,411]. In EC, Angpt2 is solidly established as a pro-inflammatory mediator[87,414].

3.8 Model: The role of VSMC-expressed Tie2 on VSMC phenotype and function during atherosclerosis progression

In the context of atherosclerosis, the findings revealed that (i) VSMC-expressed Tie2 supports the synthetic VSMC phenotype, thereby enhancing migration, proliferation and VSMC content within atherosclerotic lesions, (ii) VSMC-specific Tie2 deletion shifts the ratio of circulating Angpt2 to Angpt1 towards Angpt2 in *ApoE*^{KO} mice, and (iii) constitutively *ApoE*^{KO} *Angpt2*^{KO} mice have a pro-atherosclerotic phenotype. Together, the data establish a role of VSMC-expressed Tie2 in the pathogenesis of atherosclerosis, thereby expanding and revising the endotheliocentric model of Angpt/Tie signaling towards a bi-directional signaling system involving EC and VSMC (Figure 48).

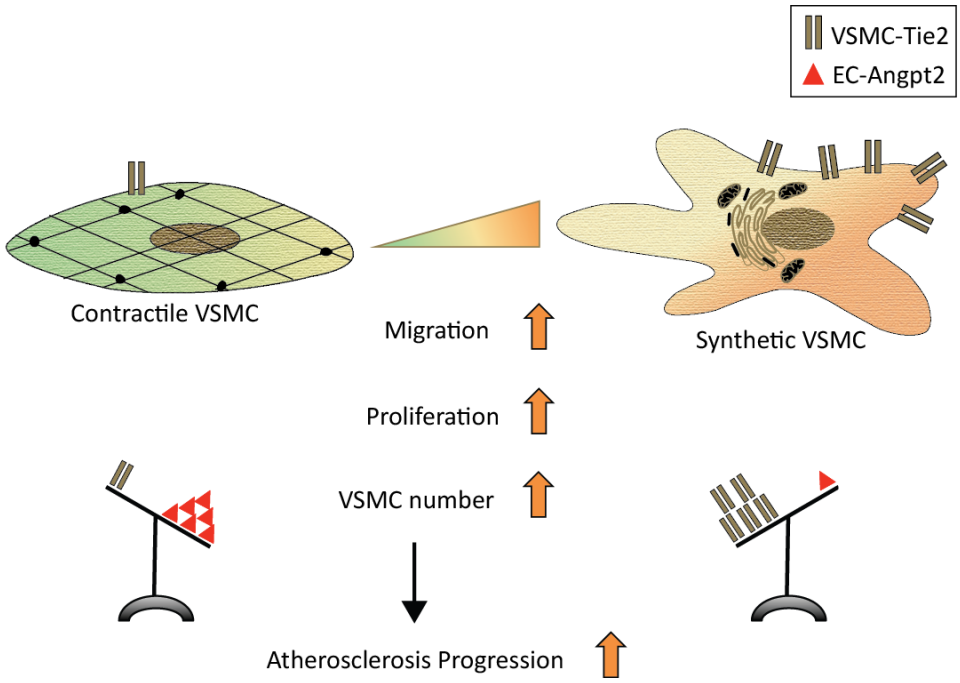

Figure 48. Model demonstrating the role of VSMC-expressed Tie2 on VSMC phenotype and function during atherosclerosis progression

Upon atherosclerosis progression, VSMC-expressed Tie2 shifts the balance from a contractile to a synthetic VSMC phenotype resulting in decreased contractile markers, increased migration and proliferation as well as an increase in the number of VSMC within the intima. In addition, VSMC-expressed Tie2 attenuates Angpt2 release by EC thereby sustaining atherosclerosis.

3.9 Cross-talk between VSMC-expressed Tie2 and Angpt2-producing EC

Angpt2 exerts atheroprotective functions by inhibiting atherosclerosis via the activation of eNOS and release of NO, leading to reduced LDL oxidation[117]. The protective effect of Angpt2 was abolished by Tie2-neutralizing antibodies and a Tie2-blocking peptide, confirming that Angpt2 acts in a Tie2-dependent manner. Furthermore, Angpt2 stimulated NO release without promoting inflammatory cell recruitment, giving it the characteristics of an atheroprotective factor. Yu and colleagues demonstrated that administration of recombinant Angpt2 reduces atherosclerosis progression and angiotensin II-induced aortic aneurysm by i) restricting inflammatory egress from the bone marrow and ii) regression of neovascularization[118]. Future work will need to unravel the mechanistic crosstalk between Tie2-expressing VSMC and Angpt2-producing EC and the contribution of Angpt2-mediated EC destabilization towards atherosclerosis. The feedback loop between Tie2-expressing VSMC and increased Angpt2 production in EC suggests that Angpt2 may contribute to confer atheroprotection in VSMC-specific Tie2-deficient mice. Moreover, this feedback loop is fully compatible with an antagonistic mode of action of EC-derived Angpt2 on VSMC expressed Tie2[100,415].

3.10 Plaque composition in the presence and absence of VSMC-expressed Tie2

The stability of atherosclerotic lesions is considered as important as the actual degree of stenosis[416]. About 75% of coronary thrombosis events originate from rupture of weakened atherosclerotic lesions. The importance of VSMC in plaque stability is based on the criteria that formation of a fibrous cap over the plaques necrotic core by proliferating and migrating VSMC lessens the risk of plaque rupture and the underlying acute events such myocardial infarction and stroke[410,417]. VSMC apoptosis is also linked to weakening of the plaque, resulting in plaque rupture and thrombosis. Furthermore, adventitial and plaque angiogenesis are associated with enhanced atherosclerosis and less stable lesions[364]. Therefore, plaque composition should be analysed in more detail in lesions from *Tie2*$^{+/+}$ and *Tie2*$^{SMC-KO}$ mice to unravel whether VSMC-expressed Tie2 is indeed 'pro-atherosclerotic' or not. Notably, a decreased lesion size characterized by reduced VSMC content and collagen deposition is considered to be more prone to plaque rupture.

3.11 Tie2 signaling in VSMC

Angpt1-mediated Tie2 signaling is essential for EC survival and quiescence[2]. *In vitro* experiments in this study demonstrated Angpt1-induced Tie2 phosphorylation in HUaSMC. Additionally, Angpt1 stimulation led to the activation of Akt, which is an important downstream effector pathway of Tie2 activation. Future studies are required to unravel the mechanistic role of Angpt/Tie2 signaling in regulating VSMC phenotype and to investigate which possible downstream effectors are involved. The role of RhoA for the regulation of VSMC phenotype and tone has been well described[204,226-228]. Likewise, the transcription factor Myocd plays a pivotal role in the regulation of the contractile VSMC phenotype, whereas Elk1 promotes the synthetic VSMC by inhibiting Myocd markers[195,201-203]. Angpt1 exert vascular protective effect by maintaining EC integrity and limiting permeability, which is mediated in a RhoA-dependent manner[1], highlighting the link between Angpt/Tie2 and RhoA. Furthermore, Anpt1/Tie2 dependent activation of Rac1 and RhoA is involved in EC motilitiy during vascular work assembly and angiogenesis[418].

3.12 Tie2 as a therapeutic target and future directions

In summary, Tie2 signaling exerts beneficial, vasoprotective functions contributing to maintaining the non-proliferative, quiescent phenotype of the resting vasculature[1,412]. In contrast, the present study revealed a disease-promoting role of Tie2 in VSMC during hypertension and atherosclerosis progression. Future work will need to address the physiological role of Angpt/Tie2 singnaling in VSMC. Gene expression analyses and cellular experiments in the present study revealed a role of VSMC-expressed Tie2 in controlling the balance between the contractile and the synthetic VSMC phenotype. This contributed under hypertensive conditions (i.e. DOCA-salt treatment, *ex vivo* perfusion assay) and pro-atherogenic conditions (i.e., Western diet in *ApoE* null mice) towards a less

contractile and more synthetic, proliferative VSMC phenotype. Under physiological conditions, this may possibly translate into a role of VSMC-expressed Tie2 in the control of vascular tone and thereby indirectly to blood pressure regulation. Future work will need to validate if Tie2 could serve as a therapeutic target for either hypertension or atherosclerosis. In fact, COMP-Angpt1 effectively prevents hypertension and ends organ damage in SHR by binding to its endothelial Tie2 receptor[419]. More precisely, *Tie2+/-* mice displayed a significant elevation in pulmonary arterial pressures induced with either 5-HT or IL6 as compared to WT mice[361]. Furthermore, *LDLR*-deficient mice vaccinated against Tie2 have been reported to display significantly reduced atherosclerotic lesion formation in the carotid arteries and the aortic root[364]. In turn, Angpt2 blocking antibodies are presently in development in the field of oncology and it consequently remains to be seen if long term Angpt2 antibody inhibition could turn out as a pro-atherogenic risk factor.

3.13 Conclusion

In conclusion, the current work proposes that Tie2 regulates blood pressure and cardiac size in a manner that is independent from VSMC-expressed Tie2, and most likely a consequence of Sm22α-driven Tie2 deletion in CMs. The work further demonstrated a cell autonomous effect of VSMC-expressed Tie2 in the regulation of VSMC remodeling from a contractile to a synthetic phenotype in hypertension. The study also established a surprising and mechanistically challenging pro-atherosclerotic function of VSMC-expressed Tie2. The genetic data expand and revise the established concept of endothelial Angpt/Tie signaling towards a complex bi-directional signaling network involving EC as well as VSMC. The data reconcile for some of the apparent discrepancies in the published literature and will stimulate important future avenues of mechanistic and potentially also translational research.

4 Methods

4.1 Animals

4.1.1 Animal welfare

Mice were bred on a C57Bl/6N background. *Tie2*$^{flox/flox}$ mice were generated by Ingenious targeting Laboratories (Ronkonkoma, NY, USA) as previously described[71]. *Tie2*$^{flox/flox}$ mice were crossed with *Sm22α-Cre* mice (The Jackson Laboratory, Bar, Harbor, ME, USA) for Tie2 deletion in smooth muscle cells. *Angpt2*-deficient mice crossbred into a C57Bl/6N background were used as previously described[87]. *Sm22α-Cre* mice were crossed to *Rosa26* yellow fluorescent protein (YFP) reporter (*Rosa26*^{YFP}) mice[373] for isolation of Sm22α-positive smooth muscle cells by fluorescence-activated cell sorting (FACS). Heart and aortic samples from *Tie2*^{MerCreMer} x *Rosa26*^{YFP} were kindly provided by Dr. Katrin Busch and Prof. Hans-Reimer Rodewald, DKFZ. Mice were injected daily on 5 consecutive days with 1 mg tamoxifen intraperitoneally[386].

For DOCA-induced and AngII-induced hypertension experiments, twelve-week-old *Tie2*$^{+/+}$ and *Tie2*$^{SMC-KO}$ mice were transferred to a mouse room at the Institute of Physiology and Pathophysiology, Heidelberg, Germany, and subsequently housed singly per cage. For atherosclerosis experiments, eight- to ten-week-old *ApoE*^{KO} *Tie2*$^{SMC-KO}$, *ApoE*^{KO} *Angpt2*^{KO} and their respective littermate controls were fed a Western-type diet (41% of calories from fat, 43% from carbohydrate, and 17% from protein (diet D12079B [Research Diets, New Brunswick, NJ, USA]) for 14 weeks to induce atherosclerosis as decribed previously[420].

Animals were housed in individually ventilated cages under sterile and temperature-controlled conditions. Mice had free access to autoclaved food and water and were kept in a 12h light-dark cycle. Mutant and control littermates were used for all experiments. All animal experiments were approved according to the ethical guidelines of the local animal welfare committee (Bezirkregierung Karlsruhe, Germany; permit number G77/14).

4.1.2 Radiotelemetry system

In order to monitor baseline blood pressure over a time-course of 7 days, the mouse radiotelemetry system (DSI PhysioTel® PA-C10, The Netherlands) was utilized according to the manufacturer's instructions. Briefly, the pressure sensor catheter was inserted by cannulating the carotid artery and the transmitter device was placed subcutaneously in the right flank of 12- week-old male *Tie2*$^{+/+}$ and *Tie2*$^{SMC-KO}$ mice. The mice were allowed to recover for 7 days. Thereafter, systolic blood pressure (SBP), diastolic blood pressure (DBP), heart rate (HR) and mean arterial pressure (MAP) were monitored for 7 days. SBP, DBP, MAP and HR were compared between the day-time resting period and the night-time active period of *Tie2*$^{+/+}$ and *Tie2*$^{SMC-KO}$ mice. Physical activity was defined by comparison of resting versus active.

4.1.3 Echocardiography

Mice were anesthesized with isoflurane and maintained at 37°C on a heating-pad. The localization of the left ventricle was obtained in M-mode. Cardiac function was measured by transthoracic echocardiograpy under anesthesia (isoflurane 1.5-2% in 1 Lpm O^2 using OxyCare EverFlo oxygenator) using the VisualSonics Vevo 2100 (VisualSonics, Toronto, Ontario, Canada) equipped with a MS550D linear transducer (40 Mhz). Electrocardiograms (ECGs) were obtained using built-in ECG electrode-contact pads (VisualSonics). The Vevo 2100-imaging sytem software was applied to acquire left ventricular wall thickness (LVPW), interventricular septum (IVS) and left ventricular internal diameter (LVID) at diastole and systole. Imaging and quantification was performed by Felix Trogisch and Dr. Oliver Drews, Institute of Physiology and Pathophysiology, Heidelberg, Germany.

4.1.4 DOCA-induced hypertension model

Hypertension was induced by subcutaneously implanting DOCA-salt slow-release pellets (Innovative Research of America, Sarasota, FL, USA) in 12-week-old male *Tie2*$^{+/+}$ and *Tie2*$^{SMC\text{-}KO}$ mice according to the manufacturer's instructions under anesthesia (isoflurane 3%, v/v) and providing 1% (w/v) sodium chloride in the drinking water. Adequate anesthesia was monitored by controling the footpad reflex. Blood pressure and HR was monitored 7 days prior and 10 days post DOCA-salt treatment, using the mouse radiotelemetry system (DSI PhysioTel® PA-C10, The Netherlands) according to the manufacturer's instructions. Untreated and DOCA-treated animals were euthanized after 10 days. Mice were anesthetized and hearts were perfused with PBS, weighted, and fixed in zinc-fixation for further processing. Kidneys were excised and weighted and isolated arteries were prepared for histological examination. Surgery, DOCA implantation and analysis were done in collaboration with Dr. Caroline Arnold and Prof. Thomas Korff, Institute of Physiology and Pathophysiology, Heidelberg, Germany. The Rout test was used to exclude possible outliers.

4.1.5 Angiotensin-induced hypertension model

Cardiac hypertension and hypertrophy was induced in *Tie2*$^{+/+}$ and *Tie2*$^{SMC\text{-}KO}$ mice by AngII-treatment (Sigma-Aldrich). Micro-osmotic pumps (alzet, model 1002), which release AngII at a rate of 1.5 mg/kg/day, were implanted subcutaneously at the back of the mice. Body temperature was maintained at 37°C using temperature controlled heat pads. Systolic blood pressure (SBP) was measured before treatment and 7 days after treatment by using a computerized, noninvasive, tail-cuff system (NIBP, NIBPchart software; Panlab/Harvard apparatus, Holliston, MA, USA). Mice were anesthetized and hearts were perfused with PBS, weighted and fixed in zinc-fixation for further processing. Imaging was performed by Felix Trogisch and Dr. Oliver Drews, Institute of Physiology and Pathophysiology, Heidelberg, Germany.

4.1.6 *Ex-vivo* perfusion of mesenteric and femoral arteries

Perfusion of isolated arteries was performed as previously described[401]. Briefly, animals were sacrificed by cervical dislocation. Subsequently, mesenteric and femoral arteries were isolated and inserted into the chamber of a myograph (Culture Myograph, DMT, Copenhagen, Denmark). The chambers were placed in an incubator at 37°C and 5% CO_2, and the arteries were continuously perfused with DMEM medium (Invitrogen, Darmstadt, Germany) containing 15% FCS at increasing intravascular pressure levels. The arteries were exposed to a supra-physiological transmural pressure gradient of 110 mmHg or to the physiological pressure gradient of 60 mmHg.

4.1.7 VSMC isolation

VSMC were isolated from *Tie2*$^{+/+}$ and *Tie2*$^{SMC\text{-}KO}$ mice, as described previously[420]. In brief, the right atrium of 24-week-old atherosclerotic mice was punctured. HBSS (5 ml) was perfused through the left ventricle to flush out blood. Whole aortas were excised and adventitia was removed. Aortas were digested at 37°C for 45 min using filtered 10 µg/ml collagenase type I (Sigma, C9891-1G). DMEM culture media, supplemented with 15% FCS and 1% Penicillin/ Streptomycin (P/S), was added to the cell suspension to stop the digestion process and subsequently centrifuged at 200 g for 5 min at 4°C. The cell suspension was then plated and cultured at 37°C with complete DMEM culture media in 5% CO_2 and high humidity.

4.1.8 Characterization of isolated aortic VSMC

RNA isolated from cultured aortic VSMC at passage 1 was tested for the VSMC-specific makers (*Pdgfrβ* and *Des*), endothelial cell-specific (*Pecam1* and *Cdh5*), and fibroblast-marker (*S100a4*) by qRT-PCR with the according TaqMan probes (Table 17). HUVEC and NIH3T3 cells were used as positive and negative controls, respectively.

4.1.9 Macrophage isolation

Peritoneal macrophages were obtained by flushing the peritoneal cavity with pre-warmed Roswell Park Memorial Institute medium (RPMI) (Life Technologies). Cells were plated in RPMI medium supplemented with 10% FCS and 1% P/S at 37 °C and 5% CO_2 for 45 min. After 45 min, cultures were washed three times with PBS to remove non-adherent cells and left in culture media overnight.

4.2 Immunohistochemical methods

4.2.1 Preparation of zinc-fixed paraffin-embedded sections

Following mouse dissection, hearts and arteries were fixed in zinc-fixative overnight. The next day, samples were washed with VE-water and further processed automatically with the spin processor

STP120 including incubations in graded ethanol series (70-85-96%), twice in isopropanol (Iso), twice in xylol, and stored in paraffin (Table 1). Subsequently, samples were manually embedded in paraffin blocks. 10 µm tissue sections were prepared using the rotary microtome HM355S. Sectioning was performed from at least three different regions of the tissue sample.

Table 1: Paraffin section preparation

Procedure	Reagent	Time
1	70% ethanol	2h
2	85% ethanol	1 h 45 min
3	99% ethanol	1 h 45 min
4	isopropanol	1 h 45 min
5	isopropanol	1 h 45 min
6	xylol	1 h 45 min
7	xylol	1 h 45 min
8	paraffin	2 h
9	paraffin	1 h 45 min

4.2.1.1 Deparaffinization and rehydration of paraffin

Zinc-fixated, paraffin sections (10 µm) were deparaffinized, dehydrated and rehydrated by passing them through graded alcohols.

Table 2: Deparaffinization and rehydration of paraffin

Procedure	Reagent	Time
1	Histo-Clear II	2 min
2	Histo-Clear II	2 min
3	99% ethanol	1 min
4	80% ethanol	10 sec
5	70% ethanol	10 sec
6	VE-water	1 min

4.2.1.2 Hematoxylin and eosin (H&E) staining of paraffin-embedded sections

Heart sections were stained with H&E for routine histological examination. Hematoxylin stains basophilic components including cell nuclei and ribosomal rough ER in blue, whereas eosin detects eosinophilic structures such are cytoplasmic proteins, mitochondria, smooth ER, keratin, erythrocytes and collagen in red. Sections were stained with filtered hemalaun for 4 min. The slides were washed with running tap water for up to 10 min, and then counterstained with 2% ethanoic eosin for 1 min. Subsequently, sections were washed three times with VE-water followed by dehydration via a graded series of alcohol (10 sec 70%, 10 sec 80%, 10 sec 90% and 1 min Iso) and cleared by xylol. Before mounting with histomount, sections were treated with histoclear for 90 sec. Bright field images were obtained with the Zeiss Axio Scan (20x objective).

4.2.1.3 Immunohistochemistry (IHC)

Antigen-retrieval of deparaffinized, de- and rehydrated sections was achieved by boiling the sections for 20 min in 0.01 M pH 6.0 citrate target retrieval buffer followed by cooling in VE-water for 20 min. In order to block the background activity of endogenous peroxidases, slides were treated with 3% H_2O_2 for 15 min and washed 2x 5 min with PBS-T or TBS-T. Unspecific binding sites were blocked with 10% rabbit serum for 1 h at room temperature (RT). Afterwards, slides were incubated overnight at 4°C with primary antibody in the appropriate buffer (Table 26). The next day, slides were washed 3x 5 min with TBS-T and incubated with the respective secondary antibody in the primary antibody buffer for 30 min at room temperature (Table 27). Slides were washed 3x 5 min with TBS-T. Detection was performed using a biotin-peroxidase complex, in form of Vectastain ABC solution according to manufacturers' protocol. To sum up, 1 drop of solution A was mixed into 2.5 ml PBS, followed by adding 1 drop of solution B, further mixing and incubation in the dark for 20 min at RT. The mix was added to sections for 40 min at RT. After 40 min, sections were rinsed with TBS-T for 3x 5 min, followed by diaminobenzidine substrate (DAB) treatment for 2-5 min. Sections, briefly washed with tap water, were counterstained with Hematoxylin for 2 min, rinsed with running tap water for 10 min, dehydrated through 99% ethanol and Iso, treated with Histoclear for 2x 2 min and mounted with Histomount. Bright field images were taken at the Zeiss Axio Scan (20x objective). Ki67-positive nuclei (as percentage of total nuclei) and Cleaved Caspase 3-positive area (as percentage of total area) were analysed with Fiji software.

4.2.1.4 Immunofluorescence of paraffin-embedded arteries

Paraffin cross-sections of mesenteric arteries and femoral arteries were deparaffinized in xylene and passed through graded alcohols. Antigen retrieval was performed with 8 µg/ml Proteinase K in Tris-EDTA (TE) buffer (10 mM Tris, 1 mM EDTA, pH 8.0) for 10 min at 37°C. The sections were blocked with 10% normal goat serum (Life Technologies) for 1 h at RT, and stained with CD31, αSMA and Desmin antibodies (Table 26) overnight at 4°C. The sections were subsequently washed 3x 5 min with TBS-T and incubated with the appropriate secondary antibody (Table 27) for 1 h at RT. Pictures were taken with a Zeiss LSM 700 (40x objective) and analyzed with Fiji software. For analysis, the αSMA- and Calponin-positive area was quantified and normalized to the total area.

4.2.1.5 Picro Sirius red staining

Picro-sirius red staining was used to detect the deposited collagen fibers type I and III in the extracellular space. Picrosirius red stains were performed according to the manufacturer's protocol (Poly Science). In brief, after dewaxing, de- and rehydration, sections were placed in Sirius red staining solution A for 2 min, followed by VE-water rinse. Next, sections were placed in Sirius red solution B for 60 min and additionally for 2 min in Sirius red solution C. Finally, sections were gradually dehydrated and mounted with Histomount. Bright field images were taken with the Zeiss

Axio Scan (20x objective). Fibrotic area was analysed with Fiji software by assessing the positively stained area normalized to total area.

Sirius red solution A: Phosphomolybdic acid hydrate in water

Sirius red solution B: Direct Red80 and 2,4,6-Trinitrophenol in water

Sirius red solution C: 0.1 N hydrochloride acid

4.2.1.6 Oil Red O (ORO) staining of whole mount aorta

Whole mount aortas were fixed in 4% paraformaldehyde (PFA) overnight. Aorta's were placed in absolute 1,2 Propanediol solution for 2-5 min and stained in prewarmed ORO solution (Sigma-Aldrich) for 8-10 min at 60°C. Next, aorta's were incubated in 85% 1,2-Propanediol solution for 2-5 min, followed by 2x washing with VE-water. The ORO-stained aorta's were counterstained with Hematoxylin for 30 s and further developed by washing thoroughly in running tap water for 3 min. The mounting was done with Aquatex. Bright field images were taken with the Cell Observer (ZEISS), objective 10x and analyzed with Fiji software. Quantification of ORO-positive area is expressed as percentage of total lesion area normalized to littermate average.

4.2.2 Preparation of cryoblocks and sections

Immediately after mouse dissection heart tissues were fixed overnight in 4% PFA at 4°C. Heart sections and aortic sections from *Tie2*^{MerCreMer} x *Rosa26* ^{YFP} were fixed overnight in 4% PFA at 4°C, followed by an additional overnight incubation in sucrose (30% sucrose in PBS) at 4°C. After overnight incubation, the samples were placed in cryomold immersed in O.C.T Cryo-medium on dry ice, and stored at -80°C. Sections (10 µm) were cut using the cryo microtome Hyrax C50 followed by drying for few minutes. The frozen sections were stored at -80 °C.

4.2.2.1 Immunofluorescence staining

Heart sections, aortic sections and aortic sinus sections were permeabilized and blocked with Ready-to-use-Zymed (Life Technologies) or PBS supplemented with 10% goat serum and 0.5% Triton X-100 for 1 h at RT. Slides were incubated overnight at 4°C with primary antibody in the appropriate buffer (Table 26). The next day, slides were washed 2x 10 min with PBS-T and incubated with the respective secondary antibody in the primary antibody buffer for 1 h at room temperature (Table 27). Images were taken with a Zeiss LSM 700 (40x objective) and analyzed with Fiji software. Quantification of Mac3- and αSMA-positive area is expressed as percentage of total lesion area normalized to littermate average.

4.2.2.2 Whole mount retina staining

For analysis of the retinal vasculature, mice were sacrificed by decapitation at P4 and the eyeballs were isolated using a stereo microscope. The eyes were fixed in methanol at -20°C overnight or in 4% or 2% PFA/PBS for 1h at RT. Long term storage of methanol fixed eyes was in methanol at -20°C and PFA fixed eyes were kept in PBS at 4°C. After isolation of the retinas, whole mount retina staining was performed to visualize the vasculature and related structures. Therefore, retinas were blocked and permeabilized with retina blocking buffer for 1h at RT. The retinal vasculature was stained with FITC-conjugated IB-4 (1:100) and the denoted primary antibodies (Table 26) overnight at 4°C in retina antibody dilution buffer followed by three washing steps with 0.2% Tween/PBS for 5min. Retinas were then incubated with the appropriate fluorescently labelled secondary antibodies (Table 27) in retina antibody dilution buffer for 1h at RT and subsequently washed three times with 0.2% Tween/PBS for 5min. Afterwards, retinas were flattened on glass slides by making four radial incisions and then mounted with Fluoromount G mounting medium. Pictures of retinas were taken with the confocal microscopes Zeiss LSM700 (10x objective) and image analysis was accomplished with Fiji software. The relative vessel area was calculated as IB-4^+ area per retina area. Pericyte and VSMC coverage was determined by measuring the desmin-positive and αSMA-positive area associated with the vasculature, and correlating it to the vessel area.

4.2.2.3 Staining of atherosclerotic lesion size

Heart sections (10 µm) were stained with ORO and counterstained with hematoxylin (see 4.2.1.6). The stained sections were imaged using Cell Observer (ZEISS), objective 10x, and quantified using Fiji software. Quantification of ORO-positive lesion area is expressed as percentage of total lesion area normalized to littermate average.

4.3 Cell culture methods

4.3.1 Cell culture maintenance

Cells were cultured at 37°C, 5% CO_2 and 100% humidity. Human aortic smooth muscle cells (HAoSMC) and human umbilical artery smooth muscle cells (HUaSMC) were purchased from PromoCell and cultured in Smooth Muscle Cell Growth Medium 2 kit, the corresponding supplement-mix and 1% Penicilin/Streptomycin (P/S). HAoEC were purchased from PromoCell and grown in Endothelial Cell Growth Medium MV, the corresponding supplement-mix and 1% P/S. HUVEC (PromoCell) and MS1 (ATCC) were cultured in Endopan 3 medium (PAN Biotech) supplemented with 3% FCS, the corresponding supplement-mix and 1% P/S. NIH3T3 were a kind provided by the Clinic for Tumor Biology, Freiburg and cultured in DMEM with 10% FCS and 1% P/S.

4.3.2 Cryopreservation and thawing of cells

Cells were resuspended in cell-type specific medium, containing 10% DMSO and 20% FCS. Cell suspension was transferred into cryostatic vials (1 ml/vial). The vials were slowly frozen in an isopropanol-containing container at -80°C overnight and then stored in a liquid nitrogen tank. For thawing, cells were placed in a water bath for 2 min at 37°C. Slightly thawed cells were immediately mixed with pre-heated medium and centrifuged at 1000 rpm for 3 min. Pellet was resuspended in fresh media and transferred into tissue culture plates. The medium was replaced with fresh medium the next day.

4.3.3 Transfection with small interfering RNA (siRNA)

For siRNA-mediated Tie2 silencing, $1x10^6$ cells were seeded in 6-well plates. After 24 h, cells were transfected with 200 nM Silencer select/Silencer siRNA or control siRNA (Thermo Fisher Scientific, #s224719 (#1) and #s13984 (#2) (Table 20) using Oligofectamine (Life Technologies) in Opti-MEM I + GlutaMAX-I (Life Technologies) according to manufacturer's instructions. Medium was exchanged to smooth muscle cell medium after 4 h. Gene expression and protein expression were analyzed after 48 h. For EdU incorporation experiments, EdU was added to subconfluent cells at a final concentration of 10 µM for 6 h. Harvesting, fixation, permeabilization and staining of cells were performed using the Click-iT™ EdU Alexa 488 Flow Cytometry Assay Kit (Life Technologies) according to the manufacturer's protocol.

4.3.4 Stimulation assays

For stimulation assays, cells were starved overnight with media containing 0.5% FCS. Prior to stimulation, medium was changed to basal medium without supplements. Cells were stimulated with recombinant human Angpt1, 400 ng/ml (R&D Systems) for 20 min at 37°C.

4.4 Cellular assays

4.4.1 Scratch wound assay

Cells were seeded in fibronectin-coated (10µg/ml, PromoCell) 24 well plates and grown overnight. The next day, cells were transfected with either NS, siRNA#1 or #2 using Oligofectamine (Life Technologies) in Opti-MEM I + GlutaMAX-I (Life Technologies) according to manufacturer's instructions. Medium was exchanged to smooth muscle cell medium after 4 h. After 48 h, cells were treated with 10 µg/ml Mitomycin C (Sigma) for 2 h prior to scratching the monolayer to prevent cell proliferation. Pictures were taken automatically every 30 min (at least 3 wells and 3 positions per well) at an Olympus Cell R Microscope with cell incubation chamber conditioned in a humid environment at 37°C and 5% CO_2. Images were analyzed using Fiji software.

4.5 Molecular biology methods

4.5.1 Genotyping PCR

Genotyping of mice was carried out by PCR of genomic DNA extracted from mouse tails. Tails (~0.5 cm) were lysed in 200 µl Direct PCR Lysis Reagent with 10 µg Proteinase K at 55°C overnight. The next day, tails were heated to 95°C for 15 min to inactivate Proteinase K. The lysate was centrifuged for 10 sec, and supernatant was used for subsequent PCRs.

4.5.1.1 PCR-Polymerase chain reaction

PCR was performed to analyse the genotype of Tie2 wildtype and knockout mice. *Tie2* genotyping generated a wild-type band of 320 bp, a floxed band of 389 bp and a mutant band of 526 bp. In case of *Sm22α-Cre* genotyping, a band approving *Cre* expression was detected at 350 bp, and the control band at 300 bp. *ApoE* genotyping generated an $ApoE^{-/-}$ band of 245 bp and an $ApoE^{+/+}$ of 155 bp. *Angpt2* genotyping generated an $Angpt2^{-/-}$ band of 259 bp and an $Angpt2^{+/+}$ of 400 bp. The following pipetting scheme was used for the PCR reaction mix:

Table 3. *Tie2fl/fl* PCR reaction mix

Reagent	1x
Q-solution	5.0 µl
H_2O (nuclease-free)	13.8 µl
10x buffer	2.5 µl
MgCl2	1.0 µl
dNTPs (5 mM)	0.5µl
Primer *TEKI3 (10 µM)*	0.5 µl
Primer *SDL2 (10 µM)*	0.5 µl
Primer *VERI (10 µM)*	0.5 µl
Taq polymerase	0.2 µl
Template (1 µg/µl)	1.0 µl

Table 4. *Sm22α-Cre* PCR reaction mix

Reagent	1x
H_2O (nuclease-free)	5.6 µl
10x buffer	1.2 µl
MgCl2	1.1 µl
dNTPs (5 mM)	1.1 µl
Primer *MB183F (10 µM)*	0.7 µl
Primer *MB183R (10 µM)*	0.7 µl
Primer *MB182R (Actin) (10 µM)*	0.7 µl
Primer *MB182F (Actin) (10 µM)*	0.7 µl
Taq polymerase	0.2 µl
Template (1 µg/µl)	1.0 µl

Table 5. *Angpt2* PCR reaction mix

Reagent	1x
H_2O (nuclease-free)	6.5 µl
RedTaq Mix	12.5 µl
MgCl2	0.5 µl
Primer *mL2-5`GTD (10 µM)*	2.00 µl
mL2-intron1US1 (10 µM)	2.00 µl
Primer *neo3`ds85 (10 µM)*	1.00 µl
Template (1 µg/µl)	1.0 µl

Table 6. *ApoE* PCR reaction mix

Reagent	1x
H_2O (nuclease-free)	9.15 µl
10x buffer	1.25 µl
MgCl2	0.5 µl
dNTPs (5 mM)	0.25 µl
Primer *Neo19*	0.25 µl
Primer *Anti-S 20*	0.25 µl
Primer *Sense 21*	0.25 µl
Taq polymerase	0.1 µl
Template (1 µg/µl)	1.0 µl

The PCR was performed with an Applied Biosystems thermocycler according to the PCR program depicted here:

Table 7. *Sm22α-Cre* and *ApoE* genotyping PCR program

Step	Temp°C (*Sm22α-Cre)*	Time (*Sm22α-Cre*)	Temp°C (*ApoE*)	Time (*ApoE*)	
1	94°C	2 min	94°C	4 min	
2	94°C	30 sec	94°C	30 sec	35x
3	58°C	45 sec	58°C	30 sec	
4	72°C	2 min	72°C	30 min	
5	72°C	2 min	72°C	5 min	
6	4°C	forever	4°C	forever	

Table 8. *Tie2*$^{fl/fl}$ and *Angpt2* genotyping PCR program

Step	Temp°C (*Tie2*$^{fl/fl}$*)*	Time (*Tie2*$^{fl/fl}$*)*		Temp°C (*Angpt2*)	Time (*Angpt2*)	
1	95°C	30 sec		98°C	4 min	
2	61°C	1 min	35x	98°C	30 sec	39x
3	72°C	1 min		98°C	5 sec	
4	72°C	10 min		63°C	10 sec	
5	15°C	forever		72°C	5 sec	
6				72°C	1 min	
7				72°C	forever	

The amplified DNA was analysed directly by 1% agarose gel electrophoresis or stored at 4°C until analysis.

4.6.1.2 Agarose gel electrophoresis

1% (w/v) agarose was dissolved in 0.5x TBE buffer by heating. Ethidium bromide (5 µl/100 ml) was added and the solution was poured into a cast tray for solidification. Samples were loaded onto the gel, which run at 140 V for 45 min. The 100 bp Generuler Plus DNA-Ladder (7 µl/well) was used as a size reference. DNA was visualized under UV-light and the band size was determined relative to the DNA ladder.

4.5.2 RNA isolation

RNA from cells was isolated using Rneasy Mini Kit (Qiagen) according to the manifacturer's protocol. The RNeasy spin column placed in a 2 ml collection tube was loaded with 700 µl of the sample, centrifuged at 10000 rpm for 15 sec and flow through was discarded. The column was washed with 700 µl of RW1 wash buffer, followed by centrifugation at 10000 rpm for 15 sec (flow-through was discarded). Further washing was performed by adding 500 µl of RPE and centrifugation at 10000 rpm for 15 sec (flow-through was discarded). This step was repeated and sample was centrifuged at 10000 rpm for 2 min (flow-through was discarded). The column was dried by centrifugation at full speed for 1 min. RNA was eluted from the column after adding 30 µl of RNase-free H_2O, incubation

for 1 min, and centrifugation at 10000 rpm for 1 min. Concentration and purity was measured by analysing 1 µl of sample with the RNA program of the Nanodrop. A 260/280 ratio of ≥2 represented protein-free RNA. Purified RNA was stored at -80°C or used directly for cDNA preparation.

RNA of FACS-sorted mouse EC and $CD31^{-}CD45^{-}YFP^{+}$ and $CD31^{+}CD45^{-}YFP^{-}$ cells was isolated with the Arcturus PicoPure RNA Isolation Kit. Cells were centrifuged at 500 g and 4°C for 5 min and the pellet was resuspended in 50 µl Arcturus PicoPure extraction buffer. RNA was isolated according to manufacturer´s instructions. RNA was eluted in 11 µl RNase free H_2O and RNA concentrations were measured using NanoPhotometer® N60.

4.5.3 cDNA generation

cDNA generation was performed with the Quantitect® Reverse Transcription Kit from Qiagen according to manufacturer's instructions. Template RNA was thawed on ice and 1 µg was mixed with 2 µl of gDNA Wipeout buffer. To reach a total volume of 14 µl RNase-free water was added. This reaction was incubated for 2 min at 42°C and immediately placed on ice afterwards.

Table 9. cDNA reaction mix

Component	Volume	Final concentration
Reverse-transcription master mix		
Quantiscript Reverse Transcriptase	1 µl	
Quantiscript RT Buffer, 5x	4 µl	1x
RT Primer Mix	1 µl	
Template RNA		
Entire genomic DNA elimination reaction	14 µl	
Total volume	**20 µl**	

To start the transcription reaction from RNA into cDNA, the reaction was incubated for 30 min at 42°C. In order to achieve inactivation of the Quantiscript Reverse Transcriptase the reaction tube was then incubated for 3 min at 95°C. cDNA was stored at -20 °C.

cDNA of FACS-sorted EC, $CD31^{-}CD45^{-}YFP^{+}$ and $CD31^{+}CD45^{-}YFP^{-}$ cells was amplified with QuantiTect Whole Transcriptome Kit (Qiagen) according to to manufacturer's instructions and cDNA was diluted in RNAse-free water 1:250. cDNA was stored at -20 °C.

4.5.4 Quantitative realtime-PCR (qRT-PCR)

Relative gene expression analysis was performed using qRT-PCR. The Taqman mono-color hydrolysis probe method (Applied Biosystems) was used to detect differences in the amount of mRNA transcription levels. This method is based on probes that are labelled with a fluorophore (6-carboxyfluorescein, FAM) at the 5´end and a fluorescence quencher at the 3´end. The exonuclease activity of the Taq polymerase cleaves the probe and thereby allows detection of the FAM

fluorescence. Reactions were performed in a 96 or 384-well plate. One reaction contained the following components:

Table 10. Taqman qRT-PCR reaction mix

Reagent	Volume
Taqman FAST Universal Master Mix (ABI)	5 µl
Taqman Probe/Primer	0.5 µl
H_2O (nuclease-free)	1.5 µl
Total	**7 µl**
+ cDNA (1:10 diluted)	3 µl
Total	**10 µl**

Each reaction was performed in technical triplicates. The qRT-PCR was performed using the Lightcycler® 480 System (for the 384-well plates) or the StepOnePlus Real-Time PCR System (for the 96-well plates) with the following temperature profile:

Table 11.Taqman qRT-PCR program

Step	Temperature	
Pre-denaturation	95°C	
Denaturation	95°C	45x
Amplification	60°C	

For analysis, the ΔΔCt method was applied as described previously[421]. This was done by comparing the Ct values of the samples of interest with a control. The Ct values of both the control sample and the samples of interest were normalized to a housekeeping gene ($\Delta Ct_{gene\ of\ interest} = Ct_{gene\ of\ interest} - Ct_{housekeeping\ gene}$). Here *B2m* was used as housekeeping genes. Next, internally normalized Ct values were further normalized to the mean value of all controls (*Tie2*$^{+/+}$ animals, or siNS samples) resulting in ΔΔCt values. Respective fold changes (FC) were calculated as follows: $FC = 2^{-\Delta\Delta Ctgene\ of\ interest}$.

4.5.5 Microarray

For gene expression analysis of isolated short-term cultured aortic VSMC, microarrays were performed by the DKFZ Genomics and Proteomics core facility (Heidelberg). In brief, RNA was isolated with RNeasy Mini Kit (Qiagen) and RNA quantity and quality were checked using the Agilent RNA 6000 Pico Kit on an Agilent 2001 Bioanalyzer. RNA was reverse transcribed into cDNA and cDNA was amplified according to the NuGen SPIA (Single Primer Isothermal Amplification) technology. Only RNA samples with a RIN value of > 6.0 were eligible for microarray analysis. cDNA was hybridized on Illumina Mouse Sentrix-6 arrays according to the manufacturer's protocol. Microarray data were normalized and analyzed with the Chipster software. Only genes with a significantly differential expression ($p \leq 0.05$) were considered for further analysis. Analysis was performed using Gene Set

Enrichment Analysis (GSEA) software. The raw microarray data are accessible through GEO accession number GSE100364.

4.6 Protein chemical methods

4.6.1 Preparation of protein lysates

Cells and isolated arteries (femoral and mesenteric arteries and aorta) were lysed on ice using RIPA buffer (1% NP-40, 0.1% sodium dodecyl sulphate, 0.5% sodium deoxycholate, 10% glycerol, 5 mM EDTA) supplemented with protease-inhibitor mix G (Serva) and 2 mM sodium orthovanadate (Na_3VO_4) (Sigma). Samples were incubated on ice for 20 min. To sediment cellular debris, cell suspension was centrifuged for 5 min at 14,000 rpm at 4°C. The cleared lysate was stored at -80°C.

4.6.2 Protein concentration measurements

Exact protein concentrations were determined by using the BCA-assay (Pierce).

4.6.2.1 BCA-assay

The BCA-assay from Pierce® with a working range from 20-200 µg/ml was performed according to manufacturer's instructions for microplate formats. For the preparation of the working reagent (WR), 50 parts of reagent A were mixed with 1 part of BCA reagent B, resulting in a mixture of 50:1. The reaction in the microplate was prepared as follows: 25 µl of standard or sample were mixed with 200 µl WR and shaken for 30 sec. The covered microplate was incubated for 30 min at 37°C. After that time, the microplate was measured at λ = 562 nm using a Photometer. Standard values with known concentrations were plotted in a graph and a standard curve was generated by linear extrapolation of the plotted standard values. The unknown concentration of the samples was then calculated as the following: x = (y-b)/a).

4.6.3 Immunoprecipitation and immunoblotting

For immunoprecipitation, cell lysates were incubated with protein G-sepharose beads (GE Healthcare) and 3 µg Tie2 antibody (Supplementary Table 2) overnight at 4°C on a rotator. Beads were washed by centrifugation at 100 g, 4°C for 2 min with lysis buffer containing 2 mM Na_3VO_4 and boiled with 2x protein sample buffer at 95°C for 10 min. Immunoprecipitates or lysates were separated on 10% or 12% polyacrylamide SDS gels and blotted on nitrocellulose membranes. Membranes were blocked with 3% BSA for 1 h at RT and subsequently incubated in 1% BSA/PBS-T with the indicated primary antibodies (Table 26) at 4°C overnight. Horseradish peroxidase-conjugated secondary antibodies (Table 27) were used for chemiluminescence detection. Signals were detected by exposing the membrane to a Fuji X-ray film. Tubulin was used as loading control.

4.6.4 Proteome profiler array

Mouse proteome profiler array (R&D Systems) was performed with serum obtained from *ApoE*^{KO} (4-pooled serum samples) and *ApoE*^{KO} *Tie2*$^{SMC\text{-}KO}$ (4-pooled serum samples) mice, fed a Western-type diet for 14 weeks, according to the manufacturer's instructions. Spots were quantified using Fiji software after background subtraction.

4.6.5 Measurement of plasma lipid content

Plasma was separated by centrifugation and stored at -80°C until further use. Lipoprotein profiles were determined after 5 weeks or 14 weeks of Western diet feeding using enzymatic methods (Diagnostic Center of Heidelberg University, Heidelberg).

4.6.6 Enzyme-linked immunosorbent assay (ELISA)

Plasma concentrations of Angpt1 (MyBioSource) and Angpt2 (R&D Systems) were measured by ELISA according to the manufacturer's instructions.

4.6.7 Fluorescence activated cell sorting (FACS)

4.6.7.1 Lung endothelial cell isolation

EC isolation was performed as described previously[422]. Briefly, mice were sacrificed and lungs were surgically removed and cut into small pieces. Lung pieces were digested with Dulbecco's Modified Eagle's medium (DMEM, Gibco), containing 1.25 mM $CaCl_2$, 200 U/ml Collagenase I and 10 µg/ml DNaseI (Roche) at 37°C for 1 h. Single-cell suspensions were prepared by passing the digestion mix through 18G and 19G cannula syringes and filtering through a 100 µm cell strainer. Cells were stained for negative markers CD45, Ter119, Lyve1 and podoplanin (Pdpn) (Table 26) for 30 min at 4°C in PBS/5% fetal calf serum (FCS). Negative stained cells were depleted by incubating them with magnetic Dynabeads (Life Technologies) in 750 µl PBS/5% FCS for 30 min at 4°C on a rotator. The remaining cells were positively stained with a CD31 antibody (Table 26) in PBS/5%FCS for 30 min at 4°C on the rotator. $CD45^-Ter119^-Lyve1^-Pdpn^-CD31^+$ cells were sorted with a BD Biosciences FACS Aria Cell Sorter.

4.6.7.2 Sm22α-positive cell isolation

Mice were sacrificed and hearts were surgically removed and cut into small pieces. Heart pieces were digested with DMEM (Gibco), containing 1.25 mM $CaCl_2$, 200 U/ml Collagenase I and 10 µg/ml DNaseI (Roche) at 37°C for 30 min. Single-cell suspensions were prepared by passing the digestion mix through a 19G cannula syringe and filtering through a 100 µm cell strainer. Cells were resuspended in ACK-lysis buffer and incubated at RT for 2-3 min. Cells were stained with CD31 and

CD45 antibodies (Table 26) in PBS/5%FCS for 20 min at 4°C. $CD31^{-}CD45^{-}YFP^{+}$ and $CD31^{+}CD45^{-}YFP^{-}$ cells were sorted with a BD Biosciences FACS Aria Cell Sorter.

4.7 Statistical analysis

All data are presented as mean ± S.D. Statistical significance was determined by two-tailed Student's *t-test*. For *in vitro* experiments, n represents the number of independent experiments. For mouse experiments, n represents the number of independent mice analyzed per group. Statistical comparisons were performed using GraphPad Prism 5 software. A *p*-value of less than 0.05 was considered statistically significant and marked by asterisks (*$p<0.05$, **$p<0.01$, ***$p<0.001$).

5 Materials

5.1 Chemicals

Bulk chemicals were purchased from the following companies:

- AppliChem (www.applichem.com)
- Carl Roth (www.carl-roth.de)
- Gerbu (www.gerbu.de)
- Merck (www.merck.de)
- Roche (www.roche-applied-science.com)
- Serva (www.serva.de)
- Sigma-Aldrich (www.sigmaaldrich.com)

5.2 Cells

Table 12. List of cells used in this study

Primer	Sequence
Human aortic smooth muscle cells (HAoSMC)	PromoCell
Human umbilical artery smooth muscle cells (HUaSMC)	PromoCell
Human aortic endothelial cells (HAoEC)	PromoCell
Human umbilical vein artery endothelial cells (HUVEC)	PromoCell
Mouse embryonic cell line (NIH3T3)	Clinic for Tumor Biology
Pancreatic islet endothelial cells (MS1)	ATCC

5.3 Cell culture and reagents

Table 13. List of cell culture media

Medium	Cell type	Company
Smooth Muscle Cell Growth Medium 2 kit	HAoSMC, HUaSMC	PromoCell
Endothelial Cell Growth Medium MV	HAoEC	PromoCell
Endopan 3	HUVEC, MS1	Pan Biotech
Dulbecco's modified eagle medium (DMEM) Glutamax1	NIH3T3, #mAoVSMC	Gibco
Opimem + Glutamax	HAoSMC	Life Technologies
Roswell Park Memorial Institute medium (RPMI)	#mPerit. macrophages	Life Technologies

[#] m stands for mouse, Perit. stands for peritoneal

Table 14. List of reagents used in cell culture

Reagent	Company
Accutase, 10x	PAA Laboratories
Dimethylsufoxide (DMSO)	Sigma-Aldrich
Dulbecco's phosphate buffered saline (PBS)	PAA Laboratories
Fetal calf serum (FCS), heat inactivated	PAA Laboratories
Penicillin/streptomycin (PS), 100x	PAA Laboratories
Trypan blue	PAA Laboratories
Trypsin-EDTA solution, 10x	PAA Laboratories
Mitomycin	Sigma Aldrich
Oligofectamine	Life technology

5.4 PCR and qRT-PCR reagents

Table 15. PCR and qRT-PCR reagents

Component	Company
100 bp DNA Ladder plus	Fermentas
10 x Coral Load PCR buffer	Qiagen
Direct PCR Lysis Reagent	PeqLab
DNase/RNase free H2O	Gibco
dNTP mix (10mM each)	Fermentas
Ethidium bromide	Roth
MgCl2 (25mM)	Qiagen
6x Orange DNA Loading Dye Solution	Fermentas
Taq DNA polymerase (5U/µl)	Qiagen
TaqMan Fast Advanced PCR Master Mix	Applied Biosystems
Trizol	Sigma-Aldrich

5.5 Western blot reagents

Table 16. Western blot reagents

Reagent	Company
Bovine Serum Albumine (BSA)	PAA laboratories
Nitrocellulose membrane	GE Healthcare
Orthovanadate	Sigma-Aldrich
PageRuler^{TM} Prestained Protein Ladder	Thermo Scientific
Pierce ECL Western blotting substrate	Thermo Scientific
Immobilon-P PVDF membrane	Millipore
ReBlot Plus Strong Solution	Merck
Rotiphorese Gel 30	Carl-Roth
Super RX X-ray films	Fuji
SuperSignal™ West Dura Extended Duration Substrate	Thermo Fisher Scientific

5.6 Primers

All Taqman probes were purchased from Applied Biosystems

Table 17. Taqman probes for qRT-PCR

Mouse probes	Ordering number	Human probes	Ordering number
Tie2 (Tek)	Mm00443254_m1	*Tie2 (TEK)*	Hs00945146_m1
Pecam1	Mm01242584_m1	*TAGLN*	Hs01038777_g1
Pdgfrβ	Mm00435546_m1	*MYL9*	Hs00697086_m1
Des	Mm00802455_m1	*CALD*	Hs00921982_m1
S100a4	Mm00803372_g1	*PECAM1*	Hs00169777_m1
Angpt1	Mm00456503_m1	*CDH5*	Hs00901463_m1
Cnn1	Mm00487032_m1	*ANGPT1*	Hs00375822_m1
Tagln	Mm00441661-g1	*ANGPT2*	Hs01048042_m1
Smtn	Mm00449973_m1	*TIE1*	Hs00892696_m1
Cald1	Mm00513996_m1	*B2M*	Hs00984230_m1
Acta2	Mm00725412_s1		
Myocd	Mm00455051_m1		
Myh11	Mm00443013_m1		
Myl9	Mm01251442_m1		
Pcna	Mm00448100_g1		
Rbp1	Mm00441119_m1		
Vim	Mm01333430_m1		
Mgp1	Mm00485009_m1		
Tpm4	Mm01245304_g1		
Myh10	Mm00805131_m1		
B2m	Mm00437762_m1		
Tnnt2	Mm01290256_m1		

Genotyping primers were purchased from MWG Biotech (www.mwg-biotech.com)

Table 18. Mouse genotyping primers

Primer	Sequence
**TEKI3*	5' CAGGCTATCACTGTGACACTGGTAC 3'
**SDL2*	5'AAATACGCAGTTTCAG GGCTGGGA 3'
**VERI*	5' ACCAATTCGGGGAATCCTATGGCA 3'
MB183 F (Sm22α-Cre)	5' CAGGGTGTTATAAGCAATCCC 3'
MB183 R (Sm22α-Cre)	5' CCTGGAAAATGCTTCTGTCCG 3'
MB182R (Actin)	5' CAATGGTAGGCTCACTCTGGGAGATGATA 3'
MB182F (Actin)	5' GCCTAGCCGAGGGAGAGCCG 3'
mROSA-YFP_1 HL15	5' AAG ACC GCG AAG AGT TTG TCC 3'
mROSA-YFP_2 HL54	5' TAA GCC TGC CCA GAA GAC TCC 3'
mROSA-YFP_3 HL152	5' AAG GGA GCT GCA GTG GAG TA 3'
mL2-5`GTD (Angpt2)	5' CTG GGA TCT TGT CTT GGC C 3'
mL2-intron1US1 (Angpt2)	5' CTT CTC TCT GTG ACT GCT TTG C 3'
neo3`ds85 (Angpt2)	5' GAG ATC AGC AGC CTC TGT TTC 3'

* Primers for genotyping Tie2-floxed mice

Table 19. Human RT-qPCR primers

Primer	Sequence
TEK F	5' CTCTTCACCTCGGCCTTCAC 3'
TEK R	5' GACTTGCATCCCTCTTGTCC 3'
ANGPT1 F	5' GGATGTCAATGGGGGAGGTT 3'
ANGPT1 R	5' AGGGGCCACAAGCATCAAA 3'
ANGPT2 F	5' TTGCCGGCTGTCCCTGTAAGTC 3'
ANGPT2 R	5' GACCCCACTGTTGCTAAAGAAGAA 3'
VEGFR2 F	5' AGCGGGGCATGTACTGACGATTAT 3'
VEGFR2 R	5' CTCTCCTCTCCCGACTTTGTTGAC 3'
GAPDH F	5' GACGCCTGCTTCACCACCTTCTTG 3'
GAPDH R	5' GGGGAGCCAAAAGGGTCATCATC 3'

5.7 siRNA

All Silencer® Select siRNAs were purchased from Life technologies

Table 20. siRNA used in this study

Enzymes	Company
(#1) s224719	4392422
(#2) s13984	4390826
NS	4390847

5.8 Growth factors, proteins and emzymes

Table 21. Growth factors, proteins and enzymes

Growth factors, proteins and enzymes	Company
Collagenase I	Sigma-Aldrich
DNase I	Roche
Proteinase K	Gerbu
RNase free DNAse	Qiagen
Recombinant Angpiopietin 1	R&D Systems
Angiotensin II	Sigma-Aldrich

5.9 Kits

Table 22. Kits

Reagent	Company
Arcturus PicoPure RNA Isolation Kit	Life Technologies
Pierce Bicinchoninic acid (BCA) Protein Assay Kit	Thermo Fischer
Quantitect Reverse Transcription Kit for cDNA Synthesis	Qiagen
RNeasy Mini Kit	Qiagen
Angpt1 ELISA	MyBioSource
Angpt1 ELISA	R&D systems

5.10 Miscellaneous

Table 23. Miscellaneous

Reagent	Company
Bepanthen eye cream	Roche
Betadine	MundiPharma
Ketavet	Pfizer
Paraffin (low melting 56°C)	Merck
Rompun	Bayer
Tissue freezing medium (Tissue TEK)	Sakura
DOCA-pellets	Innovative Research of America, USA

5.11 Consumables

Table 24. Consumables

Consumables	Company
6-well plates	Beckton Dickinson
Cannula (18G, 19G, 27G)	BD
Cell culture dishes (5cm, 10cm)	TPP
Cryotubes	Carl-Roth
Embedding cassettes	Medim Histotechnologie
FACS tubes	BD Falcon
Filter containing pipette tips	Biozym
Freezing box	Thermo Scientific
Insulin syringe	BD
Microscope cover glasses	VWR international
Microscope glass slides	Menzel-Gläser
Pipette tips	Nerbe
PDVF filter (0.22 µm, 0.45 µm)	Millipore
Polyamid suture (4.0)	ETHICON/ETHILON
Polyamid suture (5.0)	ETHICON/ETHILON
qPCR plates (96-well)	Biozyme
qPCR plates (384-well)	Roche
Reaction tubes (0.5ml, 1.5ml, 2ml)	Eppendorf
Reaction tubes (15ml, 50 ml)	Greiner
Round bottom 96 well plate	Greiner
Sealing foil	Applied Biosystems
Sterile pipettes	Corning
Sterile filters	Renner
Suture clip	Braun
Syringes	Dispomed
Tissue cultures 6-well plates	Greiner
Transwell permeable supports 6.5mm, 8.0µm	Costar

5.12 Equipment

Table 25. Equipment

Product	Company
Agarose gel documentation system	Peqlab
Axio Scan	Zeiss
Canto FACS Analyzer	BD
Cell culture hood	Thermo Scientific
Cell culture incubator	Thermo Scientific
Cell Observer	Zeiss
Centrifuge	Beckman Coulter
Countess Automated Cell Counter	Invitrogen
Cryotome	Zeiss
Elisa reader (Multiskan)	Thermo Scientific
Freezing box	Thermo Scientific
Heating block	Eppendorf
Heating mat	ThermoLux
Inverted fluorescence microscope IX71	Olympus
Light cycler 480	Roche
Microm HM3555	Thermo Scientific
Multistep pipette	Eppendorf

Product	Company
Nanodrop 1000 spectrophotometer	Thermo Scientific
Neubauer Cell Counting Chamber	Marienfeld
Pipettes	ErgoOne
Power supply	BioRad
Cauter set	F-con
Table centrifuge (5417R)	Eppendorf
Thermocycler	Applied Biosystems
UV transluminator	Intas
Vortex	Neolab
Water bath	Julabo

5.13 Antibodies

5.13.1 Primary antibodies

Table 26. Primary antibodies

Antigen	Reactivity	Species	Dilution	Conjugate	Company	Cat. number
Tie2	human	rabbit		1:500 (WB)	Santa Cruz	sc-324
p-Tyr	-	mouse		1:1000 (WB)	Millippore	05-321
pAkt	human	rabbit		1:1000 (WB)	Cell Signaling	4060S
Akt	human	rabbit		1:1000 (WB)	Cell Signaling	9272S
CD45	mouse	rat	PE	1:200 (FACS)	BD Pharmingen	561087
Tyr119	mouse	rat	FITC	1:200 (FACS)	BD Pharmingen	561032
Lyve1	mouse	rat	FITC	1:250 (FACS)	e-bioscience	53-0443
Pdpn	mouse	hamster	Alexa-488	1:100 (FACS)	e-bioscience	53-5381-82
CD31	mouse	rat		1:100 (FACS)	BD Pharmingen	551262
CD34	mouse	rat	Pacific-Blue	1:50 (FACS)	BD Pharmingen	560230
Vegfr2	human	rabbit		1:1000 (WB)	Cell signaling	2479
Tagln	human	rabbit		1:1000 (WB)	Protein Tech Group	10493-1-AP
Mac3	mouse	rat		1:100 (IF)	BD Pharmingen	550292
αSMA	-	mouse	Cy3	1:250 (IF)	Sigma-Aldrich	C6198-2ML
CD31	mouse	rat		1:100 (IF)	BD Pharmingen	553370
Calponin	mouse	rabbit		1:100 (IF)	Millipore	04-589
GFP	mouse	rabbit		1:100 (IF)	Life Technology	A11122
Tubulin	mouse	mouse		1:5000 (WB)	Sigma	T8203
Des	mouse	rabbit		1:100 (IF)	Abcam	Ab15200-1

WB= Western blot, IF= Immunofluorescence, FACS= Fluorescence activated cell sorting

5.13.2 Secondary antibodies

Table 27. Secondary antibodies

Reactivity	Host	Conjugate	Dilution	Application	Source & Cat. no.
Mouse IgG	Rabbit	HRP	1:1000	WB	DAKO P0260
Rabbit IgG	Goat	AF 647	1:500	IF	Life Technologies A21246
Rabbit IgG	Goat	HRP	1:5000	WB	DAKO P0448
Rat IgG	Goat	AF546	1:500	IF	Life Technologies A11081
Rat IgG	Goat	AF488	1:500	IF	Life Technologies A11006

5.14 Additional staining reagents

Table 28. Staining reagents

Antigen	Reactivity
Avidin/Biotin blocking solution	DAKO
BSA	Gerbu
Eosin Y solution	Sigma-Aldrich
Fluorescent mounting medium	DAKO
Histomount	Invitrogen
Hoechst Dye 33258, 1mg/ml	Sigma-Aldrich
Liquid DAB Substrate Chromogen System	DAKO
Mayer's Hematoxylin solution	Sigma-Aldrich
Normal goat serum	DAKO
Normal goat serum ready-to-use (10%)	Zymed
Roti-Histofix 4% (pH 7)	Carl Roth

5.15 Solutions and buffers

Solutions and buffers for agarose-gels, FACS and Western blotting were prepared according to standard methods.

Table 29. Solutions and buffers

Antigen	Reactivity	Species
Blotting buffer (1x)	192mM 25mM	Glycine Trizma Base
Digestion mix	150mg 0.20% 50mL	Collagenase 1A DNaseI serum free medium
FACS	5%FCS	FCS in PBS

Antigen	Reactivity	Species
Modified RIPA lysis buffer	50mM T	Tris-HCl pH 7.5
	150mM	NaCl
	1mM	EDTA
	1%	NP-40
	0.25%	Na-deoxycholate
	100mM	Na-orthovanadate
PBS-T	1x	Protease inhibitor Mix G
	1% [v/v]	Tween-20 in 1x PBS
Running buffer (1x)	192mM	Glycine
	25mM	Trizma Base
	0.10%	SDS
Tris-Borate-EDTA buffer (TBE)	89mM	Tris/HCl, pH 8.0
	89mM	H_3BO_3
	1mM	EDTA
Tris-Buffered Saline Tween-20 (TBS-T)	10mM	Tris/HCl, pH 7.5
	100mM	NaCl
	0.10%	Tween-20
Zinc fixative	3mM	$Ca(C_2H_3O_2)_2$
	2.2mM	$Zn(C_2H_3O_2)_2$
	3.6mM	$ZnCl_2$
	0.1M	Tris-HCl (pH 7.4)

5.16 Software

Table 30. Software

Software	Company
Fiji	ImageJ
FlowJo	Miltenyi Biotec
Light Cycler 480 software	Roche
Living Image software 4.0	PerkinElmer
ZEN blue	Zeiss
Molecular Signature Database	http://software.broadinstitute.org/gsea/index.jsp
Genepattern	http://software.broadinstitute.org/cancer/software/genepattern/
Vevo 2100	VisualSonics

6 Abbreviations

ACE	Angiotensin converting enzyme
Angpt1	Angoipoietin 1
Angpt2	Angiopoietin 2
AngI	Angiotensin 1
AngII	Angiotensin 2
ANF/ANP	Atrial natriuretic factor
$ApoE^{KO}$	Apolipoprotein E KO
AO	Aortas
αSMA/ACTA2	Smooth muscle actin 2
bFGF	Basic fibroblast growth factor
BM	Basement membrane
β-MHC	Beta-myosin heavy chain
BP	Blood pressure
Ca^{2+}	Calcium
CAD	Coronary artery disease
CALD1	Caldesmon
CArG box	CC(A/T6GG
CM	Cardiomyocyte
CMs	Cardiomyocytes
CNN1	Calponin
COX	Cyclooxygenase
CVD	Cardiovascular diseases
Col 1	Collagen 1
CO	Cardiac Output
Coup-TFII	Chicken ovalbumin upstream promoter-transcription factor II
DAG	Diacylglycerol
DBP	Diastolic blood pressure
Des	Desmin
DMEM	Dulbecco's Modified Eagle's medium
DLL1	Delta-like 1
DOCA	Deoxycorticosterone acetate
EC	Endothelial cells
ECM	Extracellular matrix

ECG	Echocardiography
EdU	5-ethynyl-2′-deoxyuridine
EGFR	Epidermal growth factor receptor
eNOS	Endothelial nitric oxide synthase
ET1	Endothelin 1
FACS	Fluorescent-activated cell sorting
FAK	Focal adhesion kinase
FA	Femoral arteries
FOXO1	Forkhead box protein O1
GRB2	Receptor-bound protein 2
GSEA	Gene Set Enrichment Analysis
H_2O_2	Hydrogen peroxide
HAoEC	Human aortic endothelial cells
HAoSMC	Human aortic smooth muscle cells
HB-EGF	Heparin binding EGF-like growth factor
HDL	Low levels of high-density lipoprotein
HE	Hearts
H&E	Hematoxylin and eosin
HGF	Hepatocyte growth factor
HIF1	Hypoxia inducible factor 1
$\bullet HO^-$	Hydroxyl radical
HSC	Hematopoietic stem cells
HUaSMC	Human umbilical artery smooth muscle cells
HR	Heart rate
HUVEC	Human umbilical vein endothelial cells
HW	Heart weight
IB-4	Isolectin B-4
Ig	Immunoglobuline
IHC	Immunohistochemistry
IP_3	Inositol trisphosphate
IVS	Interventricular septum
KO	Knockout
KW	Kidney weight
LDL	Low-density lipoprotein
LDLR	Low-density lipoprotein receptor

LMOD1	Leiomodin 1
LTCCs	L-type Ca^{2+} channels
LVH	Left ventricular hypertrophy
LVID	Left ventricular internal diameter
LVPW	Left ventricular posterior wall
MΦ	Macrophages
MA	Mesenteric arteries
MAP	Mean arterial pressure
MAPK	Mitogen-activated protein kinase
MCM	MerCreMer
MCP	Monocyte chemotactic protein
MEF2	Myocyte enhancer factor 2
MGP	Matrix g1a protein
M/L	Media to lumen
MLC	Myosin light chain
MLCP	Myosin phosphatase
MLCK	Myosin light chain kinase
M-mode	Motion-mode
MMPs	Matrix metalloproteinases
MYH10	Myosin heavy chain 10
MYH11	Myosin heavy chain 11
Myl6	Myosin light chain 6
MYL9	Myosin light chain 9
MYOCD	Myocardin
NF-κB	Nuclear factor κB
nNOS	Neuronal nitric oxide
iNOS	Inducible NO synthase
NO	Nitric oxide
$\bullet O_2^-$	Superoxide anion
ORO	Oil red O
oxLDL	Oxidized low-density lipoprotein
P1	Postnatal day 1
PAH	Pulmonary arterial hypertension
Pcna	Proliferating cell nuclear antigen
PDGFRβ	Platelet derived growth factor receptor β

PFA	Paraformaldehyde
PIP2	Phosphoinositide 4, 5- bisphosphate
PI3K	Phosphoinositide 3-kinase
PKC	Protein kinase C
PLCγ	Phospholipase Cγ
PLC	Phospholipase C
RAS	Renin angiotensin system
ROS	Reactive oxygen species
RBP1	Retinol-binding protein 1
RPMI	Roswell Park Memorial Institute medium
SM22α/TAGLN	Transgelin
SBE	Smad binding elements
SBP	Baseline systolic blood pressure
SKA	Skeletal alpha actin
SMMHC	Smooth muscle myosin heavy chain
SMTN	Smoothelin
SRF	Serum response factor
SV	Stroke volume
TCFs	Transcription factors
TE	Tris-EDTA
TGFβ	Transforming growth factor beta
TL	Tibia lenght
Tnnt2	Troponin 2
TPM1	Tropomyosin 1
TPM4	Tropomyosin 4
VE-cadherin	Vascular endothelial cadherin
VEGFA	Vascular endothelial growth factor-a
VIM	Vimentin
VE-PTP	PhosphoTyr phosphatase
VSMC	Vascular smooth muscle cells
WHO	World Health Organization
YFP	Yellow fluorescent protein

7 Publications

1. **Kapel SS**, Shi J, Hasanov Z, Appak-Baskoy S, Singhal M, Wojtarowicz J, Hertel S, Krunic D, Korn C, Hu J, Arnold C, Robciuc M, Korff T, Augustin HG. Vascular smooth muscle cell-expressed Tie2 controls atherosclerosis progression. Submitted.

2. Hasanov Z, Ruckdeschel T, König C, Mogler C, **Kapel SS**, Korn C, Spegg C, Eichwald V, Wieland M, Appak S and Augustin HG. Endosialin promotes atherosclerosis through phenotypic remodeling of vascular smooth muscle cells. *Arterioscler Thromb Vasc Biol*. 2017;37:495-505. doi: 10.1161/ATVBAHA.116.308455.

3. Srivastava K, Hu J, Korn C, Savant S, Teichert M, **Kapel SS**, Jugold M, Besemfelder E, Thomas M, Pasparakis M and Augustin HG. Postsurgical adjuvant tumor therapy by combining anti-angiopoietin-2 and metronomic chemotherapy limits metastatic growth. *Cancer Cell*. 2014;26:880-895. doi: 10.1016/j.ccell.2014.11.005.

8 References

1. Augustin HG, Koh GY, Thurston G and Alitalo K. Control of vascular morphogenesis and homeostasis through the angiopoietin-Tie system. *Nat Rev Mol Cell Biol*. 2009;10:165-177. doi: 10.1038/nrm2639.
2. Thomas M and Augustin HG. The role of the Angiopoietins in vascular morphogenesis. *Angiogenesis*. 2009;12:125-137. doi: 10.1007/s10456-009-9147-3.
3. Adams RH and Alitalo K. Molecular regulation of angiogenesis and lymphangiogenesis. *Nat Rev Mol Cell Biol*. 2007;8:464-78. doi: 10.1038/nrm2183.
4. Herbert SP and Stainier DY. Molecular control of endothelial cell behaviour during blood vessel morphogenesis. *Nat Rev Mol Cell Biol*. 2011;12:551-64. doi: 10.1038/nrm3176.
5. Alitalo K. The lymphatic vasculature in disease. *Nat Med*. 2011;17:1371-80. doi: 10.1038/nm.2545.
6. Neufeld S, Planas-Paz L and Lammert E. Blood and lymphatic vascular tube formation in mouse. *Semin Cell Dev Biol*. 2014;31:115-23. doi: 10.1016/j.semcdb.2014.02.013.
7. Carmeliet P. Angiogenesis in health and disease. *Nat Med*. 2003;9:653-60. doi: 10.1038/nm0603-653.
8. Folkman J. Angiogenesis: an organizing principle for drug discovery? *Nat Rev Drug Discov*. 2007;6:273-86. doi: 10.1038/nrd2115.
9. Nolan DJ, Ginsberg M, Israely E, Palikuqi B, Poulos MG, James D, Ding BS, Schachterle W, Liu Y, Rosenwaks Z, Butler JM, Xiang J, Rafii A, Shido K, Rabbany SY, Elemento O and Rafii S. Molecular signatures of tissue-specific microvascular endothelial cell heterogeneity in organ maintenance and regeneration. *Dev Cell*. 2013;26:204-19. doi: 10.1016/j.devcel.2013.06.017.
10. Cleaver O and Melton DA. Endothelial signaling during development. *Nat Med*. 2003;9:661-8. doi: 10.1038/nm0603-661.
11. Lammert E and Axnick J. Vascular lumen formation. *Cold Spring Harb Perspect Med*. 2012;2:a006619. doi: 10.1101/cshperspect.a006619.
12. Jin SW and Patterson C. The opening act: vasculogenesis and the origins of circulation. *Arterioscler Thromb Vasc Biol*. 2009;29:623-9. doi: 10.1161/ATVBAHA.107.161539.
13. Risau W. Mechanisms of angiogenesis. *Nature*. 1997;386:671-4. doi: 10.1038/386671a0.
14. Swift MR and Weinstein BM. Arterial-venous specification during development. *Circ Res*. 2009;104:576-88. doi: 10.1161/CIRCRESAHA.108.188805.
15. Potente M, Gerhardt H and Carmeliet P. Basic and therapeutic aspects of angiogenesis. *Cell*. 2011;146:873-887. doi: 10.1016/j.cell.2011.08.039.
16. Carmeliet P. Angiogenesis in life, disease and medicine. *Nature*. 2005;438:932-6. doi: 10.1038/nature04478.
17. Fagiani E and Christofori G. Angiopoietins in angiogenesis. *Cancer Lett*. 2013;328:18-26. doi: 10.1016/j.canlet.2012.08.018.
18. Folkman J. Angiogenesis. *Annu Rev Med*. 2006;57:1-18. doi: 10.1146/annurev.med.57.121304.131306.
19. Ferrara N, Gerber HP and LeCouter J. The biology of VEGF and its receptors. *Nat Med*. 2003;9:669-76. doi: 10.1038/nm0603-669.
20. Fraisl P, Mazzone M, Schmidt T and Carmeliet P. Regulation of angiogenesis by oxygen and metabolism. *Dev Cell*. 2009;16:167-79. doi: 10.1016/j.devcel.2009.01.003.

21. Distler JH, Hirth A, Kurowska-Stolarska M, Gay RE, Gay S and Distler O. Angiogenic and angiostatic factors in the molecular control of angiogenesis. *Q J Nucl Med*. 2003;47:149-61.
22. Gerhardt H, Golding M, Fruttiger M, Ruhrberg C, Lundkvist A, Abramsson A, Jeltsch M, Mitchell C, Alitalo K, Shima D and Betsholtz C. VEGF guides angiogenic sprouting utilizing endothelial tip cell filopodia. *J Cell Biol*. 2003;161:1163-77. doi: 10.1083/jcb.200302047.
23. Dejana E. Endothelial cell-cell junctions: happy together. *Nat Rev Mol Cell Biol*. 2004; 5:261-70. doi: 10.1038/nrm1357.
24. Baffert F, Le T, Sennino B, Thurston G, Kuo CJ, Hu-Lowe D and McDonald DM. Cellular changes in normal blood capillaries undergoing regression after inhibition of VEGF signaling. *Am J Physiol Heart Circ Physiol*. 2006;290:H547-59. doi: 10.1152/ajpheart. 00616.2005.
25. Wacker A and Gerhardt H. Endothelial development taking shape. *Curr Opin Cell Biol*. 2011;23:676-85. doi: 10.1016/j.ceb.2011.10.002.
26. Carmeliet P, Ferreira V, Breier G, Pollefeyt S, Kieckens L, Gertsenstein M, Fahrig M, Vandenhoeck A, Harpal K, Eberhardt C, Declercq C, Pawling J, Moons L, Collen D, Risau W and Nagy A. Abnormal blood vessel development and lethality in embryos lacking a single VEGF allele. *Nature*. 1996;380:435-9. doi: 10.1038/380435a0.
27. Senger DR, Galli SJ, Dvorak AM, Perruzzi CA, Harvey VS and Dvorak HF. Tumor cells secrete a vascular permeability factor that promotes accumulation of ascites fluid. *Science*. 1983;219:983-5.
28. Keck PJ, Hauser SD, Krivi G, Sanzo K, Warren T, Feder J and Connolly DT. Vascular permeability factor, an endothelial cell mitogen related to PDGF. *Science*. 1989; 246:1309-12.
29. Sun Z, Li X, Massena S, Kutschera S, Padhan N, Gualandi L, Sundvold-Gjerstad V, Gustafsson K, Choy WW, Zang G, Quach M, Jansson L, Phillipson M, Abid MR, Spurkland A and Claesson-Welsh L. VEGFR2 induces c-Src signaling and vascular permeability in vivo via the adaptor protein TSAd. *J Exp Med*. 2012;209:1363-77. doi: 10.1084/jem.20111343.
30. Bernatchez PN, Soker S and Sirois MG. Vascular endothelial growth factor effect on endothelial cell proliferation, migration, and platelet-activating factor synthesis is Flk-1-dependent. *J Biol Chem*. 1999;274:31047-54.
31. dela Paz NG, Walshe TE, Leach LL, Saint-Geniez M and D'Amore PA. Role of shear-stress-induced VEGF expression in endothelial cell survival. *J Cell Sci*. 2012;125:831-43. doi: 10.1242/jcs.084301.
32. Simons M, Gordon E and Claesson-Welsh L. Mechanisms and regulation of endothelial VEGF receptor signalling. *Nat Rev Mol Cell Biol*. 2016;17:611-25. doi: 10.1038/ nrm.2016.87.
33. Koch S and Claesson-Welsh L. Signal transduction by vascular endothelial growth factor receptors. *Cold Spring Harb Perspect Med*. 2012;2:a006502. doi: 10.1101/cshperspect. a006502.
34. Neufeld G, Kessler O and Herzog Y. The interaction of Neuropilin-1 and Neuropilin-2 with tyrosine-kinase receptors for VEGF. *Adv Exp Med Biol*. 2002;515:81-90.
35. Roth L, Prahst C, Ruckdeschel T, Savant S, Westrom S, Fantin A, Riedel M, Heroult M, Ruhrberg C and Augustin HG. Neuropilin-1 mediates vascular permeability independently of vascular endothelial growth factor receptor-2 activation. *Sci Signal*. 2016;9:ra42. doi: 10.1126/scisignal.aad3812.
36. Hiratsuka S, Minowa O, Kuno J, Noda T and Shibuya M. Flt-1 lacking the tyrosine kinase domain is sufficient for normal development and angiogenesis in mice. *Proc Natl Acad Sci U S A*. 1998;95:9349-54.

37. Chappell JC, Taylor SM, Ferrara N and Bautch VL. Local guidance of emerging vessel sprouts requires soluble Flt-1. *Dev Cell*. 2009;17:377-86. doi: 10.1016/j.devcel. 2009. 07.011.

38. Kaipainen A, Korhonen J, Mustonen T, van Hinsbergh VW, Fang GH, Dumont D, Breitman M and Alitalo K. Expression of the fms-like tyrosine kinase 4 gene becomes restricted to lymphatic endothelium during development. *Proc Natl Acad Sci U S A*. 1995;92:3566-70.

39. Wu J, Iwata F, Grass JA, Osborne CS, Elnitski L, Fraser P, Ohneda O, Yamamoto M and Bresnick EH. Molecular determinants of NOTCH4 transcription in vascular endothelium. *Mol Cell Biol*. 2005;25:1458-74. doi: 10.1128/MCB.25.4.1458-1474.2005.

40. Roca C and Adams RH. Regulation of vascular morphogenesis by Notch signaling. *Genes Dev*. 2007;21:2511-24. doi: 10.1101/gad.1589207.

41. Beckers J, Clark A, Wunsch K, Hrabe De Angelis M and Gossler A. Expression of the mouse Delta1 gene during organogenesis and fetal development. *Mech Dev*. 1999;84:165-8.

42. Villa N, Walker L, Lindsell CE, Gasson J, Iruela-Arispe ML and Weinmaster G. Vascular expression of Notch pathway receptors and ligands is restricted to arterial vessels. *Mech Dev*. 2001;108:161-4.

43. Phng LK and Gerhardt H. Angiogenesis: a team effort coordinated by notch. *Dev Cell*. 2009;16:196-208. doi: 10.1016/j.devcel.2009.01.015.

44. Benedito R, Roca C, Sorensen I, Adams S, Gossler A, Fruttiger M and Adams RH. The notch ligands Dll4 and Jagged1 have opposing effects on angiogenesis. *Cell*. 2009;137:1124-35.doi: 10.1016/j.cell.2009.03.025.

45. Dumont DJ, Yamaguchi TP, Conlon RA, Rossant J and Breitman ML. tek, a novel tyrosine kinase gene located on mouse chromosome 4, is expressed in endothelial cells and their presumptive precursors. *Oncogene*. 1992;7:1471-80.

46. Korhonen J, Partanen J, Armstrong E, Vaahtokari A, Elenius K, Jalkanen M and Alitalo K. Enhanced expression of the tie receptor tyrosine kinase in endothelial cells during neovascularization. *Blood*. 1992;80:2548-55.

47. Partanen J, Armstrong E, Makela TP, Korhonen J, Sandberg M, Renkonen R, Knuutila S, Huebner K and Alitalo K. A novel endothelial cell surface receptor tyrosine kinase with extracellular epidermal growth factor homology domains. *Mol Cell Biol*. 1992;12:1698-707.

48. Maisonpierre PC, Goldfarb M, Yancopoulos GD and Gao G. Distinct rat genes with related profiles of expression define a TIE receptor tyrosine kinase family. *Oncogene*. 1993;8:1631-7.

49. Sato TN, Qin Y, Kozak CA and Audus KL. Tie-1 and tie-2 define another class of putative receptor tyrosine kinase genes expressed in early embryonic vascular system. *Proc Natl Acad Sci U S A*. 1993;90:9355-8.

50. Eklund L, Kangas J and Saharinen P. Angiopoietin-Tie signalling in the cardiovascular and lymphatic systems. *Clin Sci*. 2017;131:87-103. doi: 10.1042/CS20160129.

51. Thurston G. Role of Angiopoietins and Tie receptor tyrosine kinases in angiogenesis and lymphangiogenesis. *Cell Tissue Res*. 2003;314:61-8. doi: 10.1007/s00441-003-0749-6.

52. Procopio WN, Pelavin PI, Lee WM and Yeilding NM. Angiopoietin-1 and -2 coiled coil domains mediate distinct homo-oligomerization patterns, but fibrinogen-like domains mediate ligand activity. *J Biol Chem*. 1999;274:30196-201.

53. Davis S, Papadopoulos N, Aldrich TH, Maisonpierre PC, Huang T, Kovac L, Xu A, Leidich R, Radziejewska E, Rafique A, Goldberg J, Jain V, Bailey K, Karow M, Fandl J, Samuelsson SJ, Ioffe E, Rudge JS, Daly TJ, Radziejewski C and Yancopoulos GD. Angiopoietins have distinct modular domains essential for receptor binding, dimerization and superclustering. *Nat Struct Biol*. 2003;10:38-44. doi: 10.1038/nsb880.

54. Kim KT, Choi HH, Steinmetz MO, Maco B, Kammerer RA, Ahn SY, Kim HZ, Lee GM and Koh GY. Oligomerization and multimerization are critical for angiopoietin-1 to bind and phosphorylate Tie2. *J Biol Chem*. 2005;280:20126-31. doi: 10.1074/jbc.M500292200.

55. Leppanen VM, Saharinen P and Alitalo K. Structural basis of Tie2 activation and Tie2/Tie1 heterodimerization. *Proc Natl Acad Sci U S A*. 2017;114:4376-4381. doi: 10.1073/pnas. 1616166114.

56. Loughna S and Sato TN. Angiopoietin and Tie signaling pathways in vascular development. *Matrix Biol*. 2001;20:319-25.

57. Woo KV, Qu X, Babaev VR, Linton MF, Guzman RJ, Fazio S and Baldwin HS. Tie1 attenuation reduces murine atherosclerosis in a dose-dependent and shear stress-specific manner. *J Clin Invest*. 2011;121:1624-35. doi: 10.1172/JCI42040.

58. Dumont DJ, Fong GH, Puri MC, Gradwohl G, Alitalo K and Breitman ML. Vascularization of the mouse embryo: a study of flk-1, tek, tie, and vascular endothelial growth factor expression during development. *Dev Dyn*. 1995;203:80-92. doi: 10.1002/aja. 1002030109.

59. Arai F, Hirao A, Ohmura M, Sato H, Matsuoka S, Takubo K, Ito K, Koh GY and Suda T. Tie2/angiopoietin-1 signaling regulates hematopoietic stem cell quiescence in the bone marrow niche. *Cell*. 2004;118:149-161. doi: 10.1016/j.cell.2004.07.004.

60. Hamaguchi I, Morisada T, Azuma M, Murakami K, Kuramitsu M, Mizukami T, Ohbo K, Yamaguchi K, Oike Y, Dumont DJ and Suda T. Loss of Tie2 receptor compromises embryonic stem cell-derived endothelial but not hematopoietic cell survival. *Blood*. 2006;107:1207-13. doi: 10.1182/blood-2005-05-1823.

61. Chen L, Li J, Wang F, Dai C, Wu F, Liu X, Li T, Glauben R, Zhang Y, Nie G, He Y and Qin Z. Tie2 expression on macrophages is required for blood vessel reconstruction and tumor relapse after chemotherapy. *Cancer Res*. 2016;76:6828-6838. doi: 10.1158/0008-5472.CAN-16-1114.

62. Coffelt SB, Chen Y-Y, Muthana M, Welford AF, Tal AO, Scholz A, Plate KH, Reiss Y, Murdoch C, De Palma M and Lewis CE. Angiopoietin 2 stimulates TIE2-expressing monocytes to suppress T cell activation and to promote regulatory T cell expansion. *J Immunol*. 2011;186:4183-4190. doi: 10.4049/jimmunol.1002802.

63. He Y-F, Wang C-Q, Yu Y, Qian J, Song K, Sun Q-M and Zhou J. Tie2-expressing monocytes are associated with identification and prognoses of hepatitis B virus related hepatocellular carcinoma after resection. *PLOS ONE*. 2015;10:e0143657. doi: 10.1371/ journal.pone.0143657.

64. Venneri MA, De Palma M, Ponzoni M, Pucci F, Scielzo C, Zonari E, Mazzieri R, Doglioni C and Naldini L. Identification of proangiogenic TIE2-expressing monocytes (TEMs) in human peripheral blood and cancer. *Blood*. 2007;109:5276-5285. doi: 10.1182/blood-2006-10-053504.

65. Abou-Khalil R, Le Grand F, Pallafacchina G, Valable S, Authier F-J, Rudnicki MA, Gherardi RK, Germain S, Chretien F, Sotiropoulos A, Lafuste P, Montarras D and Chazaud B. Autocrine and paracrine angiopoietin 1/Tie-2 signaling promotes muscle satellite cell self-renewal. *Cell Stem Cell*. 2009;5:298-309. doi: 10.1016/j.stem.2009.06.001.

66. Androutsellis-Theotokis A, Rueger MA, Park DM, Mkhikian H, Korb E, Poser SW, Walbridge S, Munasinghe J, Koretsky AP, Lonser RR and McKay RD. Targeting neural precursors in the adult brain rescues injured dopamine neurons. *Proc Natl Acad Sci U S A*. 2009;106:13570-13575. doi: 10.1073/pnas.0905125106.

67. Lee O-H, Xu J, Fueyo J, Fuller GN, Aldape KD, Alonso MM, Piao Y, Liu T-J, Lang FF, Bekele BN and Gomez-Manzano C. Expression of the receptor tyrosine kinase Tie2 in neoplastic glial cells Is associated with integrin β1-dependent adhesion to the extracellular Matrix. *Mol Cancer Res*. 2006;4:915-926. doi: 10.1158/1541-7786.MCR-06-0184.

68. Tang K-D, Holzapfel BM, Liu J, Lee TK-W, Ma S, Jovanovic L, An J, Russell PJ, Clements JA, Hutmacher DW and Ling M-T. Tie-2 regulates the stemness and metastatic properties of prostate cancer cells. *Oncotarget*. 2016;7:2572-2584. doi: 10.18632/oncotarget.3950.

69. Teichert M, Milde L, Holm A, Stanicek L, Gengenbacher N, Savant S, Ruckdeschel T, Hasanov Z, Srivastava K, Hu J, Hertel S, Bartol A, Schlereth K and Augustin HG. Pericyte-expressed Tie2 controls angiogenesis and vessel maturation. *Nat Commun*. 2017; 8:16106. doi: 10.1038/ncomms16106.

70. Felcht M, Luck R, Schering A, Seidel P, Srivastava K, Hu J, Bartol A, Kienast Y, Vettel C, Loos EK, Kutschera S, Bartels S, Appak S, Besemfelder E, Terhardt D, Chavakis E, Wieland T, Klein C, Thomas M, Uemura A, Goerdt S and Augustin HG. Angiopoietin-2 differentially regulates angiogenesis through TIE2 and integrin signaling. *J Clin Invest*. 2012;122:1991-2005. doi: 10.1172/JCI58832.

71. Savant S, La Porta S, Budnik A, Busch K, Hu J, Tisch N, Korn C, Valls AF, Benest AV, Terhardt D, Qu X, Adams RH, Baldwin HS, Ruiz de Almodóvar C, Rodewald H-R and Augustin HG. The orphan receptor Tie1 controls angiogenesis and vascular remodeling by differentially regulating Tie2 in tip and stalk cells. *Cell Rep*. 2015;12:1761-1773. doi: 10.1016/j.celrep.2015.08.024.

72. Marron MB, Hughes DP, Edge MD, Forder CL and Brindle NP. Evidence for heterotypic interaction between the receptor tyrosine kinases TIE-1 and TIE-2. *J Biol Chem*. 2000; 275:39741-6. doi: 10.1074/jbc.M007189200.

73. Marron MB, Singh H, Tahir TA, Kavumkal J, Kim HZ, Koh GY and Brindle NP. Regulated proteolytic processing of Tie1 modulates ligand responsiveness of the receptor-tyrosine kinase Tie2. *J Biol Chem*. 2007;282:30509-17. doi: 10.1074/jbc.M702535200.

74. Tsiamis AC, Morris PN, Marron MB and Brindle NP. Vascular endothelial growth factor modulates the Tie-2:Tie-1 receptor complex. *Microvasc Res*. 2002;63:149-58. doi: 10. 1006/mvre.2001.2377.

75. Korhonen EA, Lampinen A, Giri H, Anisimov A, Kim M, Allen B, Fang S, D'Amico G, Sipila TJ, Lohela M, Strandin T, Vaheri A, Yla-Herttuala S, Koh GY, McDonald DM, Alitalo K and Saharinen P. Tie1 controls angiopoietin function in vascular remodeling and inflammation. *J Clin Invest*. 2016;126:3495-510. doi: 10.1172/JCI84923.

76. Yano M, Iwama A, Nishio H, Suda J, Takada G and Suda T. Expression and function of murine receptor tyrosine kinases, TIE and TEK, in hematopoietic stem cells. *Blood*. 1997;89:4317-26.

77. Suri C, Jones PF, Patan S, Bartunkova S, Maisonpierre PC, Davis S, Sato TN and Yancopoulos GD. Requisite role of angiopoietin-1, a ligand for the TIE2 receptor, during embryonic angiogenesis. *Cell*. 1996;87:1171-80.

78. Stratmann A, Risau W and Plate KH. Cell type-specific expression of angiopoietin-1 and angiopoietin-2 suggests a role in glioblastoma angiogenesis. *Am J Pathol*. 1998; 153: 1459-66. doi: 10.1016/S0002-9440(10)65733-1.

79. Sugimachi K, Tanaka S, Taguchi K, Aishima S, Shimada M and Tsuneyoshi M. Angiopoietin switching regulates angiogenesis and progression of human hepatocellular carcinoma. *J Clin Pathol*. 2003;56:854-60.

80. Xu Y and Yu Q. Angiopoietin-1, unlike angiopoietin-2, is incorporated into the extracellular matrix via its linker peptide region. *J Biol Chem*. 2001;276:34990-8. doi: 10.1074/jbc. M103661200.

81. Benest AV, Kruse K, Savant S, Thomas M, Laib AM, Loos EK, Fiedler U and Augustin HG. Angiopoietin-2 is critical for cytokine-induced vascular leakage. *PLOS ONE*. 2013; 8:e70459. doi: 10.1371/journal.pone.0070459.

82. Daly C, Pasnikowski E, Burova E, Wong V, Aldrich TH, Griffiths J, Ioffe E, Daly TJ, Fandl JP, Papadopoulos N, McDonald DM, Thurston G, Yancopoulos GD and Rudge JS. Angiopoietin-2 functions as an autocrine protective factor in stressed endothelial cells. *Proc Natl Acad Sci U S A*. 2006;103:15491-15496. doi: 10.1073/pnas.0607538103.

83. Yuan HT, Khankin EV, Karumanchi SA and Parikh SM. Angiopoietin 2 Is a partial agonist/antagonist of Tie2 signaling in the endothelium. *Mol Cell Biol*. 2009;29:2011-2022. doi: 10.1128/MCB.01472-08.

84. Kim M, Allen B, Korhonen EA, Nitschké M, Yang HW, Baluk P, Saharinen P, Alitalo K, Daly C, Thurston G and McDonald DM. Opposing actions of angiopoietin-2 on Tie2 signaling and FOXO1 activation. *J Clin Invest*. 2016;126:3511-3525. doi: 10.1172/JCI84871.

85. Orfanos SE, Kotanidou A, Glynos C, Athanasiou C, Tsigkos S, Dimopoulou I, Sotiropoulou C, Zakynthinos S, Armaganidis A, Papapetropoulos A and Roussos C. Angiopoietin-2 is increased in severe sepsis: correlation with inflammatory mediators. *Crit Care Med*. 2007;35:199-206. doi: 10.1097/01.CCM.0000251640.77679.D7.

86. Fiedler U and Augustin HG. Angiopoietins: a link between angiogenesis and inflammation. *Trends Immunol*. 2006;27:552-8. doi: 10.1016/j.it.2006.10.004.

87. Fiedler U, Reiss Y, Scharpfenecker M, Grunow V, Koidl S, Thurston G, Gale NW, Witzenrath M, Rosseau S, Suttorp N, Sobke A, Herrmann M, Preissner KT, Vajkoczy P and Augustin HG. Angiopoietin-2 sensitizes endothelial cells to TNF-alpha and has a crucial role in the induction of inflammation. *Nat Med*. 2006;12:235-9. doi: 10.1038/nm1351.

88. Parmar KM, Larman HB, Dai G, Zhang Y, Wang ET, Moorthy SN, Kratz JR, Lin Z, Jain MK, Gimbrone MA, Jr. and Garcia-Cardena G. Integration of flow-dependent endothelial phenotypes by Kruppel-like factor 2. *J Clin Invest*. 2006;116:49-58. doi: 10.1172/JCI24787.

89. Dumont DJ, Gradwohl G, Fong GH, Puri MC, Gertsenstein M, Auerbach A and Breitman ML. Dominant-negative and targeted null mutations in the endothelial receptor tyrosine kinase, tek, reveal a critical role in vasculogenesis of the embryo. *Genes Dev*. 1994;8:1897-909.

90. Sato TN, Tozawa Y, Deutsch U, Wolburg-Buchholz K, Fujiwara Y, Gendron-Maguire M, Gridley T, Wolburg H, Risau W and Qin Y. Distinct roles of the receptor tyrosine kinases Tie-1 and Tie-2 in blood vessel formation. *Nature*. 1995;376:70-4. doi: 10.1038/376070a0.

91. Takakura N, Huang XL, Naruse T, Hamaguchi I, Dumont DJ, Yancopoulos GD and Suda T. Critical role of the TIE2 endothelial cell receptor in the development of definitive hematopoiesis. *Immunity*. 1998;9:677-86.

92. Thomas M, Felcht M, Kruse K, Kretschmer S, Deppermann C, Biesdorf A, Rohr K, Benest AV, Fiedler U and Augustin HG. Angiopoietin-2 stimulation of endothelial cells induces alphavbeta3 integrin internalization and degradation. *J Biol Chem*. 2010;285:23842-9. doi: 10.1074/jbc.M109.097543.

93. Voskas D, Jones N, Van Slyke P, Sturk C, Chang W, Haninec A, Babichev YO, Tran J, Master Z, Chen S, Ward N, Cruz M, Jones J, Kerbel RS, Jothy S, Dagnino L, Arbiser J, Klement G and Dumont DJ. A cyclosporine-sensitive psoriasis-like disease produced in Tie2 transgenic mice. *Am J Pathol*. 2005;166:843-55. doi: 10.1016/S0002-9440(10) 62305-X.

94. Puri MC, Partanen J, Rossant J and Bernstein A. Interaction of the TEK and TIE receptor tyrosine kinases during cardiovascular development. *Development*. 1999;126:4569-80.

95. Rodewald HR and Sato TN. Tie1, a receptor tyrosine kinase essential for vascular endothelial cell integrity, is not critical for the development of hematopoietic cells. *Oncogene*. 1996;12:397-404.

96. Ward NL, Van Slyke P, Sturk C, Cruz M and Dumont DJ. Angiopoietin 1 expression levels in the myocardium direct coronary vessel development. *Dev Dyn*. 2004;229:500-9. doi: 10. 1002/dvdy.10479.

97. Suri C, McClain J, Thurston G, McDonald DM, Zhou H, Oldmixon EH, Sato TN and Yancopoulos GD. Increased vascularization in mice overexpressing angiopoietin-1. *Science*. 1998;282:468-71.

98. Thurston G, Suri C, Smith K, McClain J, Sato TN, Yancopoulos GD and McDonald DM. Leakage-resistant blood vessels in mice transgenically overexpressing angiopoietin-1. *Science*. 1999;286:2511-4.

99. Gale NW, Thurston G, Hackett SF, Renard R, Wang Q, McClain J, Martin C, Witte C, Witte MH, Jackson D, Suri C, Campochiaro PA, Wiegand SJ and Yancopoulos GD. Angiopoietin-2 is required for postnatal angiogenesis and lymphatic patterning, and only the latter role is rescued by Angiopoietin-1. *Dev Cell*. 2002;3:411-23.

100. Maisonpierre PC, Suri C, Jones PF, Bartunkova S, Wiegand SJ, Radziejewski C, Compton D, McClain J, Aldrich TH, Papadopoulos N, Daly TJ, Davis S, Sato TN and Yancopoulos GD. Angiopoietin-2, a natural antagonist for Tie2 that disrupts in vivo angiogenesis. *Science*. 1997;277:55-60.

101. DeBusk LM, Hallahan DE and Lin PC. Akt is a major angiogenic mediator downstream of the Ang1/Tie2 signaling pathway. *Exp Cell Res*. 2004;298:167-77. doi: 10.1016/ j.yexcr. 2004.04.013.

102. Kim I, Kim HG, So JN, Kim JH, Kwak HJ and Koh GY. Angiopoietin-1 regulates endothelial cell survival through the phosphatidylinositol 3'-Kinase/Akt signal transduction pathway. *Circ Res*. 2000;86:24-29.

103. Kwak HJ, So JN, Lee SJ, Kim I and Koh GY. Angiopoietin-1 is an apoptosis survival factor for endothelial cells. *FEBS Lett*. 1999;448:249-53.

104. Papapetropoulos A, Fulton D, Mahboubi K, Kalb RG, O'Connor DS, Li F, Altieri DC and Sessa WC. Angiopoietin-1 inhibits endothelial cell apoptosis via the Akt/survivin pathway. *J Biol Chem*. 2000;275:9102-5.

105. Daly C, Wong V, Burova E, Wei Y, Zabski S, Griffiths J, Lai KM, Lin HC, Ioffe E, Yancopoulos GD and Rudge JS. Angiopoietin-1 modulates endothelial cell function and gene expression via the transcription factor FKHR (FOXO1). *Genes Dev*. 2004;18:1060-71. doi: 10.1101/ gad.1189704.

106. Tsigkos S, Zhou Z, Kotanidou A, Fulton D, Zakynthinos S, Roussos C and Papapetropoulos A. Regulation of Ang2 release by PTEN/PI3-kinase/Akt in lung microvascular endothelial cells. *J Cell Physiol*. 2006;207:506-11. doi: 10.1002/jcp.20592.

107. Dejana E, Orsenigo F and Lampugnani MG. The role of adherens junctions and VE-cadherin in the control of vascular permeability. *J Cell Sci*. 2008;121:2115-22. doi: 10.1242/jcs.017897.

108. Kim I, Kim HG, Moon SO, Chae SW, So JN, Koh KN, Ahn BC and Koh GY. Angiopoietin-1 induces endothelial cell sprouting through the activation of focal adhesion kinase and plasmin secretion. *Circ Res*. 2000;86:952-9.

109. Hughes DP, Marron MB and Brindle NP. The antiinflammatory endothelial tyrosine kinase Tie2 interacts with a novel nuclear factor-kappaB inhibitor ABIN-2. *Circ Res*. 2003;92:630-6. doi: 10.1161/01.RES.0000063422.38690.DC.

110. Tadros A, Hughes DP, Dunmore BJ and Brindle NP. ABIN-2 protects endothelial cells from death and has a role in the antiapoptotic effect of angiopoietin-1. *Blood*. 2003;102:4407-9. doi: 10.1182/blood-2003-05-1602.

111. Iivanainen E, Kahari VM, Heino J and Elenius K. Endothelial cell-matrix interactions. *Microsc Res Tech*. 2003;60:13-22. doi: 10.1002/jemt.10238.

112. Kobayashi H, DeBusk LM, Babichev YO, Dumont DJ and Lin PC. Hepatocyte growth factor mediates angiopoietin-induced smooth muscle cell recruitment. *Blood*. 2006;108:1260-6. doi: 10.1182/blood-2005-09-012807.

113. Sullivan CC, Du L, Chu D, Cho AJ, Kido M, Wolf PL, Jamieson SW and Thistlethwaite PA. Induction of pulmonary hypertension by an angiopoietin 1/TIE2/serotonin pathway. *Proc Natl Acad Sci U S A*. 2003;100:12331-6. doi: 10.1073/pnas.1933740100.

114. Nishishita T and Lin PC. Angiopoietin 1, PDGF-B, and TGF-beta gene regulation in endothelial cell and smooth muscle cell interaction. *J Cell Biochem*. 2004;91:584-93. doi: 10.1002/jcb.10718.

115. Lee J, Kim KE, Choi DK, Jang JY, Jung JJ, Kiyonari H, Shioi G, Chang W, Suda T, Mochizuki N, Nakaoka Y, Komuro I, Yoo OJ and Koh GY. Angiopoietin-1 guides directional angiogenesis through integrin alphavbeta5 signaling for recovery of ischemic retinopathy. *Sci Transl Med*. 2013;5:203ra127. doi: 10.1126/scitranslmed.3006666.

116. Daly C, Eichten A, Castanaro C, Pasnikowski E, Adler A, Lalani AS, Papadopoulos N, Kyle AH, Minchinton AI, Yancopoulos GD and Thurston G. Angiopoietin-2 functions as a Tie2 agonist in tumor models, where it limits the effects of VEGF inhibition. *Cancer Res*. 2013;73:108-18. doi: 10.1158/0008-5472.CAN-12-2064.

117. Ahmed A, Fujisawa T, Niu X-L, Ahmad S, Al-Ani B, Chudasama K, Abbas A, Potluri R, Bhandari V, Findley CM, Lam GKW, Huang J, Hewett PW, Cudmore M and Kontos CD. Angiopoietin-2 confers atheroprotection in apoE−/− mice by inhibiting LDL oxidation via nitric oxide. *Circ Res*. 2009;104:1333-1336. doi: 10.1161/CIRCRESAHA.109.196154.

118. Yu H, Moran CS, Trollope AF, Woodward L, Kinobe R, Rush CM and Golledge J. Angiopoietin-2 attenuates angiotensin II-induced aortic aneurysm and atherosclerosis in apolipoprotein E-deficient mice. *Sci Rep*. 2016;6:35190. doi: 10.1038/srep35190.

119. del Toro R, Prahst C, Mathivet T, Siegfried G, Kaminker JS, Larrivee B, Breant C, Duarte A, Takakura N, Fukamizu A, Penninger J and Eichmann A. Identification and functional analysis of endothelial tip cell-enriched genes. *Blood*. 2010;116:4025-33. doi: 10.1182/blood-2010-02-270819.

120. Hammes HP, Lin J, Renner O, Shani M, Lundqvist A, Betsholtz C, Brownlee M and Deutsch U. Pericytes and the pathogenesis of diabetic retinopathy. *Diabetes*. 2002; 51:3107-12.

121. Park SW, Yun JH, Kim JH, Kim KW, Cho CH and Kim JH. Angiopoietin 2 induces pericyte apoptosis via alpha3beta1 integrin signaling in diabetic retinopathy. *Diabetes*. 2014; 63: 3057-68. doi: 10.2337/db13-1942.

122. Wissler RW. The arterial medial cell, smooth muscle, or multifunctional mesenchyme? *Circulation*. 1967;36:1-4.

123. Pease DC and Paule WJ. Electron microscopy of elastic arteries; the thoracic aorta of the rat. *J Ultrastruct Res*. 1960;3:469-83.

124. Owens GK. Regulation of differentiation of vascular smooth muscle cells. *Physiol Rev*. 1995;75:487-517.

125. Owens GK. Molecular control of vascular smooth muscle cell differentiation and phenotypic plasticity. *Novartis Found Symp*. 2007;283:174-191; discussion 191-193, 238-241.

126. Owens GK, Kumar MS and Wamhoff BR. Molecular regulation of vascular smooth muscle cell differentiation in development and disease. *Physiol Rev*. 2004;84:767-801. doi: 10.1152/physrev.00041.2003.

127. van Dijk CG, Nieuweboer FE, Pei JY, Xu YJ, Burgisser P, van Mulligen E, el Azzouzi H, Duncker DJ, Verhaar MC and Cheng C. The complex mural cell: pericyte function in health and disease. *Int J Cardiol*. 2015;190:75-89. doi: 10.1016/j.ijcard.2015.03.258.

128. Gittenberger-de Groot AC, DeRuiter MC, Bergwerff M and Poelmann RE. Smooth muscle cell origin and its relation to heterogeneity in development and disease. *Arterioscler Thromb Vasc Biol*. 1999;19:1589-94.

129. Rensen SS, Doevendans PA and van Eys GJ. Regulation and characteristics of vascular smooth muscle cell phenotypic diversity. *Neth Heart J*. 2007;15:100-8.

130. Jiang X, Rowitch DH, Soriano P, McMahon AP and Sucov HM. Fate of the mammalian cardiac neural crest. *Development*. 2000;127:1607-16.

131. Wasteson P, Johansson BR, Jukkola T, Breuer S, Akyurek LM, Partanen J and Lindahl P. Developmental origin of smooth muscle cells in the descending aorta in mice. *Development*. 2008;135:1823-32. doi: 10.1242/dev.020958.

132. Mikawa T and Gourdie RG. Pericardial mesoderm generates a population of coronary smooth muscle cells migrating into the heart along with ingrowth of the epicardial organ. *Dev Biol*. 1996;174:221-32. doi: 10.1006/dbio.1996.0068.

133. Waldo KL, Hutson MR, Ward CC, Zdanowicz M, Stadt HA, Kumiski D, Abu-Issa R and Kirby ML. Secondary heart field contributes myocardium and smooth muscle to the arterial pole of the developing heart. *Dev Biol*. 2005;281:78-90. doi: 10.1016/j.ydbio.2005.02.012.

134. Maeda J, Yamagishi H, McAnally J, Yamagishi C and Srivastava D. Tbx1 is regulated by forkhead proteins in the secondary heart field. *Dev Dyn*. 2006;235:701-10. doi: 10.1002/dvdy.20686.

135. Cheung C and Sinha S. Human embryonic stem cell-derived vascular smooth muscle cells in therapeutic neovascularisation. *J Mol Cell Cardiol*. 2011;51:651-64. doi: 10.1016/j.yjmcc.2011.07.014.

136. Hu Y, Zhang Z, Torsney E, Afzal AR, Davison F, Metzler B and Xu Q. Abundant progenitor cells in the adventitia contribute to atherosclerosis of vein grafts in ApoE-deficient mice. *J Clin Invest*. 2004;113:1258-65. doi: 10.1172/JCI19628.

137. Sone M, Itoh H, Yamahara K, Yamashita JK, Yurugi-Kobayashi T, Nonoguchi A, Suzuki Y, Chao TH, Sawada N, Fukunaga Y, Miyashita K, Park K, Oyamada N, Sawada N, Taura D, Tamura N, Kondo Y, Nito S, Suemori H, Nakatsuji N, Nishikawa S and Nakao K. Pathway for differentiation of human embryonic stem cells to vascular cell components and their potential for vascular regeneration. *Arterioscler Thromb Vasc Biol*. 2007;27:2127-34. doi: 10.1161/ATVBAHA.107.143149.

138. Xiao Q, Zeng L, Zhang Z, Hu Y and Xu Q. Stem cell-derived Sca-1+ progenitors differentiate into smooth muscle cells, which is mediated by collagen IV-integrin alpha1/beta1/alphav and PDGF receptor pathways. *Am J Physiol Cell Physiol*. 2007;292:C342-52. doi: 10.1152/ajpcell.00341.2006.

139. Andreeva ER, Pugach IM, Gordon D and Orekhov AN. Continuous subendothelial network formed by pericyte-like cells in human vascular bed. *Tissue Cell*. 1998;30:127-35.

140. Gerhardt H and Betsholtz C. Endothelial-pericyte interactions in angiogenesis. *Cell Tissue Res*. 2003;314:15-23. doi: 10.1007/s00441-003-0745-x.

141. Frid MG, Moiseeva EP and Stenmark KR. Multiple phenotypically distinct smooth muscle cell populations exist in the adult and developing bovine pulmonary arterial media in vivo. *Circ Res*. 1994;75:669-81.

142. Schwartz SM. Smooth muscle migration in atherosclerosis and restenosis. *J Clin Invest*. 1997;100:S87-9.

143. Schwartz SM. The intima: A new soil. *Circ Res*. 1999;85:877-9.

144. Adams LD, Geary RL, McManus B and Schwartz SM. A comparison of aorta and vena cava medial message expression by cDNA array analysis identifies a set of 68 consistently differentially expressed genes, all in aortic media. *Circ Res*. 2000;87:623-31.

145. Moiseeva EP. Adhesion receptors of vascular smooth muscle cells and their functions. *Cardiovasc Res*. 2001;52:372-86.

146. Beamish JA, He P, Kottke-Marchant K and Marchant RE. Molecular regulation of contractile smooth muscle cell phenotype: implications for vascular tissue engineering. *Tissue Eng Part B Rev*. 2010;16:467-91. doi: 10.1089/ten.TEB.2009.0630.

147. Miano JM, Cserjesi P, Ligon KL, Periasamy M and Olson EN. Smooth muscle myosin heavy chain exclusively marks the smooth muscle lineage during mouse embryogenesis. *Circ Res*. 1994;75:803-12.

148. Kuro-o M, Nagai R, Nakahara K, Katoh H, Tsai RC, Tsuchimochi H, Yazaki Y, Ohkubo A and Takaku F. cDNA cloning of a myosin heavy chain isoform in embryonic smooth muscle and its expression during vascular development and in arteriosclerosis. *J Biol Chem*. 1991; 266:3768-73.

149. Neuville P, Geinoz A, Benzonana G, Redard M, Gabbiani F, Ropraz P and Gabbiani G. Cellular retinol-binding protein-1 is expressed by distinct subsets of rat arterial smooth muscle cells in vitro and in vivo. *Am J Pathol*. 1997;150:509-21.

150. Alexander MR and Owens GK. Epigenetic control of smooth muscle cell differentiation and phenotypic switching in vascular development and disease. *Annu Rev Physiol*. 2012;74:13-40. doi: 10.1146/annurev-physiol-012110-142315.

151. Hellstrom M, Kalen M, Lindahl P, Abramsson A and Betsholtz C. Role of PDGF-B and PDGFR-beta in recruitment of vascular smooth muscle cells and pericytes during embryonic blood vessel formation in the mouse. *Development*. 1999;126:3047-55.

152. Armulik A, Abramsson A and Betsholtz C. Endothelial/pericyte interactions. *Circ Res*. 2005;97:512-23. doi: 10.1161/01.RES.0000182903.16652.d7.

153. Betsholtz C, Lindblom P and Gerhardt H. Role of pericytes in vascular morphogenesis. *EXS*. 2005:115-25.

154. Andrae J, Gallini R and Betsholtz C. Role of platelet-derived growth factors in physiology and medicine. *Genes Dev*. 2008;22:1276-312. doi: 10.1101/gad.1653708.

155. Leveen P, Pekny M, Gebre-Medhin S, Swolin B, Larsson E and Betsholtz C. Mice deficient for PDGF B show renal, cardiovascular, and hematological abnormalities. *Genes Dev*. 1994;8:1875-87.

156. Soriano P. Abnormal kidney development and hematological disorders in PDGF beta-receptor mutant mice. *Genes Dev*. 1994;8:1888-96.

157. Lindahl P, Johansson BR, Leveen P and Betsholtz C. Pericyte loss and microaneurysm formation in PDGF-B-deficient mice. *Science*. 1997;277:242-5.

158. Winkler EA, Bell RD and Zlokovic BV. Pericyte-specific expression of PDGF beta receptor in mouse models with normal and deficient PDGF beta receptor signaling. *Mol Neurodegener*. 2010;5:32. doi: 10.1186/1750-1326-5-32.

159. Bergers G and Song S. The role of pericytes in blood-vessel formation and maintenance. *Neuro Oncol*. 2005;7:452-64. doi: 10.1215/S1152851705000232.

160. Li L, Miano JM, Cserjesi P and Olson EN. SM22 alpha, a marker of adult smooth muscle, is expressed in multiple myogenic lineages during embryogenesis. *Circ Res*. 1996;78:188-95.

161. Frid MG, Shekhonin BV, Koteliansky VE and Glukhova MA. Phenotypic changes of human smooth muscle cells during development: late expression of heavy caldesmon and calponin. *Dev Biol*. 1992;153:185-93.

162. Hungerford JE, Owens GK, Argraves WS and Little CD. Development of the aortic vessel wall as defined by vascular smooth muscle and extracellular matrix markers. *Dev Biol*. 1996;178:375-92. doi: 10.1006/dbio.1996.0225.

163. Schildmeyer LA, Braun R, Taffet G, Debiasi M, Burns AE, Bradley A and Schwartz RJ. Impaired vascular contractility and blood pressure homeostasis in the smooth muscle alpha-actin null mouse. *FASEB J*. 2000;14:2213-20. doi: 10.1096/fj.99-0927com.

164. Fatigati V and Murphy RA. Actin and tropomyosin variants in smooth muscles. Dependence on tissue type. *J Biol Chem*. 1984;259:14383-8.

165. Solway J, Seltzer J, Samaha FF, Kim S, Alger LE, Niu Q, Morrisey EE, Ip HS and Parmacek MS. Structure and expression of a smooth muscle cell-specific gene, SM22 alpha. *J Biol Chem*. 1995;270:13460-9.

166. Zhang JC, Kim S, Helmke BP, Yu WW, Du KL, Lu MM, Strobeck M, Yu Q and Parmacek MS. Analysis of SM22alpha-deficient mice reveals unanticipated insights into smooth muscle cell differentiation and function. *Mol Cell Biol*. 2001;21:1336-44. doi: 10.1128/ MCB.2001. 21.4.1336-1344.2001.

167. Shen Z, Li C, Frieler RA, Gerasimova AS, Lee SJ, Wu J, Wang MM, Lumeng CN, Brosius FC, 3rd, Duan SZ and Mortensen RM. Smooth muscle protein 22 alpha-Cre is expressed in myeloid cells in mice. *Biochem Biophys Res Commun*. 2012;422:639-42. doi: 10.1016/ j.bbrc.2012.05.041.

168. Small JV and Gimona M. The cytoskeleton of the vertebrate smooth muscle cell. *Acta Physiol Scand*. 1998;164:341-8. doi: 10.1046/j.1365-201X.1998.00441.x.

169. Shapland C, Lowings P and Lawson D. Identification of new actin-associated polypeptides that are modified by viral transformation and changes in cell shape. *J Cell Biol*. 1988; 107: 153-61.

170. Shapland C, Hsuan JJ, Totty NF and Lawson D. Purification and properties of transgelin: a transformation and shape change sensitive actin-gelling protein. *J Cell Biol*. 1993; 121: 1065-73.

171. Shanahan CM, Weissberg PL and Metcalfe JC. Isolation of gene markers of differentiated and proliferating vascular smooth muscle cells. *Circ Res*. 1993;73:193-204.

172. Shanahan CM, Cary NR, Metcalfe JC and Weissberg PL. High expression of genes for calcification-regulating proteins in human atherosclerotic plaques. *J Clin Invest*. 1994; 93: 2393-402. doi: 10.1172/JCI117246.

173. Je HD and Sohn UD. SM22alpha is required for agonist-induced regulation of contractility: evidence from SM22alpha knockout mice. *Mol Cells*. 2007;23:175-81.

174. Low R, Leguillette R and Lauzon AM. (+)Insert smooth muscle myosin heavy chain (SM-B): from single molecule to human. *Int J Biochem Cell Biol*. 2006;38:1862-74. doi: 10.1016/ j.biocel.2006.03.014.

175. Carmeliet P. Mechanisms of angiogenesis and arteriogenesis. *Nat Med*. 2000;6:389-395. doi: 10.1038/74651.

176. Folkman J and D'Amore PA. Blood vessel formation: What is its molecular basis? *Cell*. 1996;87:1153-1155. doi: 10.1016/S0092-8674(00)81810-3.

177. Jones N, Iljin K, Dumont DJ and Alitalo K. Tie receptors: new modulators of angiogenic and lymphangiogenic responses. *Nat Rev Mol Cell Biol*. 2001;2:257-67. doi: 10.1038/ 35067005.

178. Dora KA. Cell-cell communication in the vessel wall. *Vasc Med*. 2001;6:43-50.

179. Triggle CR, Samuel SM, Ravishankar S, Marei I, Arunachalam G and Ding H. The endothelium: influencing vascular smooth muscle in many ways. *Can J Physiol Pharmacol*. 2012;90:713-38. doi: 10.1139/y2012-073.

180. Kohler N and Lipton A. Platelets as a source of fibroblast growth-promoting activity. *Exp Cell Res*. 1974;87:297-301.

181. Ross R, Glomset J, Kariya B and Harker L. A platelet-dependent serum factor that stimulates the proliferation of arterial smooth muscle cells in vitro. *Proc Natl Acad Sci U S A*. 1974;71:1207-10.

182. Westermark B and Wasteson A. A platelet factor stimulating human normal glial cells. *Exp Cell Res*. 1976;98:170-4.

183. Betsholtz C, Karlsson L and Lindahl P. Developmental roles of platelet-derived growth factors. *Bioessays*. 2001;23:494-507. doi: 10.1002/bies.1069.

184. Heldin CH and Westermark B. Mechanism of action and in vivo role of platelet-derived growth factor. *Phys Rev*. 1999;79:1283-316. doi: 10.1152/physrev.1999.79.4.1283.

185. Ostman A, Andersson M, Betsholtz C, Westermark B and Heldin CH. Identification of a cell retention signal in the B-chain of platelet-derived growth factor and in the long splice version of the A-chain. *Cell Regul*. 1991;2:503-12.

186. Gaengel K, Niaudet C, Hagikura K, Lavina B, Muhl L, Hofmann JJ, Ebarasi L, Nystrom S, Rymo S, Chen LL, Pang MF, Jin Y, Raschperger E, Roswall P, Schulte D, Benedito R, Larsson J, Hellstrom M, Fuxe J, Uhlen P, Adams R, Jakobsson L, Majumdar A, Vestweber D, Uv A and Betsholtz C. The sphingosine-1-phosphate receptor S1PR1 restricts sprouting angiogenesis by regulating the interplay between VE-cadherin and VEGFR2. *Dev Cell*. 2012;23:587-99. doi: 10.1016/j.devcel.2012.08.005.

187. Lindblom P, Gerhardt H, Liebner S, Abramsson A, Enge M, Hellstrom M, Backstrom G, Fredriksson S, Landegren U, Nystrom HC, Bergstrom G, Dejana E, Ostman A, Lindahl P and Betsholtz C. Endothelial PDGF-B retention is required for proper investment of pericytes in the microvessel wall. *Genes Dev*. 2003;17:1835-40. doi: 10.1101/gad. 266803.

188. Enge M, Bjarnegard M, Gerhardt H, Gustafsson E, Kalen M, Asker N, Hammes HP, Shani M, Fassler R and Betsholtz C. Endothelium-specific platelet-derived growth factor-B ablation mimics diabetic retinopathy. *EMBO J*. 2002;21:4307-16.

189. Onimaru M, Yonemitsu Y, Fujii T, Tanii M, Nakano T, Nakagawa K, Kohno R, Hasegawa M, Nishikawa S and Sueishi K. VEGF-C regulates lymphangiogenesis and capillary stability by regulation of PDGF-B. *Am J Physiol Heart Circ Physiol*. 2009;297:H1685-96. doi: 10.1152/ajpheart.00015.2009.

190. Greenberg JI, Shields DJ, Barillas SG, Acevedo LM, Murphy E, Huang J, Scheppke L, Stockmann C, Johnson RS, Angle N and Cheresh DA. A role for VEGF as a negative regulator of pericyte function and vessel maturation. *Nature*. 2008;456:809-13. doi: 10.1038/nature07424.

191. Dong A, Seidel C, Snell D, Ekawardhani S, Ahlskog JK, Baumann M, Shen J, Iwase T, Tian J, Stevens R, Hackett SF, Stumpp MT and Campochiaro PA. Antagonism of PDGF-BB suppresses subretinal neovascularization and enhances the effects of blocking VEGF-A. *Angiogenesis*. 2014;17:553-62. doi: 10.1007/s10456-013-9402-5.

192. Goumans MJ and Mummery C. Functional analysis of the TGFbeta receptor/Smad pathway through gene ablation in mice. *Int J Dev Biol*. 2000;44:253-65.

193. Dandre F and Owens GK. Platelet-derived growth factor-BB and Ets-1 transcription factor negatively regulate transcription of multiple smooth muscle cell differentiation marker genes. *Am J Physiol Heart Circ Physiol*. 2004;286:H2042-51. doi: 10.1152/ajpheart.00625.2003.

194. Hao H, Gabbiani G and Bochaton-Piallat ML. Arterial smooth muscle cell heterogeneity: implications for atherosclerosis and restenosis development. *Arterioscler Thromb Vasc Biol*. 2003;23:1510-20. doi: 10.1161/01.ATV.0000090130.85752.ED.

195. Mack CP. Signaling mechanisms that regulate smooth muscle cell differentiation. *Arterioscler Thromb Vasc Biol*. 2011;31:1495-505. doi: 10.1161/ATVBAHA.110.221135.

196. Wamhoff BR, Bowles DK, McDonald OG, Sinha S, Somlyo AP, Somlyo AV and Owens GK. L-type voltage-gated Ca2+ channels modulate expression of smooth muscle differentiation marker genes via a rho kinase/myocardin/SRF-dependent mechanism. *Circ Res*. 2004;95:406-14. doi: 10.1161/01.RES.0000138582.36921.9e.

197. Yoshida T, Hoofnagle MH and Owens GK. Myocardin and Prx1 contribute to angiotensin II-induced expression of smooth muscle alpha-actin. *Circ Res*. 2004;94:1075-82. doi: 10.1161/01.RES.0000125622.46280.95.

198. Tang Y LZ, Xu Z, Han L. Upregulation of autophagy by angiotensin II triggers phenotypic switching of aortic vascular smooth muscle cells. *J Clin Exp Cardiolog* 2014;5:1-5. doi: 10.4172/2155-9880.1000308.

199. Dong X, Yu LG, Sun R, Cheng YN, Cao H, Yang KM, Dong YN, Wu Y and Guo XL. Inhibition of PTEN expression and activity by angiotensin II induces proliferation and migration of vascular smooth muscle cells. *J Cell Biochem*. 2013;114:174-82. doi: 10.1002/jcb.24315.

200. Hilgers RH, Todd J, Jr. and Webb RC. Increased PDZ-RhoGEF/RhoA/Rho kinase signaling in small mesenteric arteries of angiotensin II-induced hypertensive rats. *J Hypertens*. 2007; 25:1687-97. doi: 10.1097/HJH.0b013e32816f778d.

201. Shore P and Sharrocks AD. The MADS-box family of transcription factors. *Eur J Biochem*. 1995;229:1-13.

202. Wang Z, Castresana MR and Newman WH. NF-kappaB is required for TNF-alpha-directed smooth muscle cell migration. *FEBS Lett*. 2001;508:360-4.

203. Wang D, Chang PS, Wang Z, Sutherland L, Richardson JA, Small E, Krieg PA and Olson EN. Activation of cardiac gene expression by myocardin, a transcriptional cofactor for serum response factor. *Cell*. 2001;105:851-62.

204. Wang DZ, Li S, Hockemeyer D, Sutherland L, Wang Z, Schratt G, Richardson JA, Nordheim A and Olson EN. Potentiation of serum response factor activity by a family of myocardin-related transcription factors. *Proc Natl Acad Sci U S A*. 2002;99:14855-60. doi: 10.1073/pnas.222561499.

205. Liu Y, Sinha S, McDonald OG, Shang Y, Hoofnagle MH and Owens GK. Kruppel-like factor 4 abrogates myocardin-induced activation of smooth muscle gene expression. *J Biol Chem*. 2005;280:9719-27. doi: 10.1074/jbc.M412862200.

206. McDonald OG, Wamhoff BR, Hoofnagle MH and Owens GK. Control of SRF binding to CArG box chromatin regulates smooth muscle gene expression in vivo. *J Clin Invest*. 2006;116:36-48. doi: 10.1172/JCI26505.

207. Yoshida T and Owens GK. Molecular determinants of vascular smooth muscle cell diversity. *Circ Res*. 2005;96:280-91. doi: 10.1161/01.RES.0000155951.62152.2e.

208. Wang Z, Wang DZ, Hockemeyer D, McAnally J, Nordheim A and Olson EN. Myocardin and ternary complex factors compete for SRF to control smooth muscle gene expression. *Nature*. 2004;428:185-9. doi: 10.1038/nature02382.

209. Schwartz MA. Integrin signaling revisited. *Trends Cell Biol*. 2001;11:466-70.

210. Hao H, Ropraz P, Verin V, Camenzind E, Geinoz A, Pepper MS, Gabbiani G and Bochaton-Piallat ML. Heterogeneity of smooth muscle cell populations cultured from pig coronary artery. *Arterioscler Thromb Vasc Biol*. 2002;22:1093-9.

211. Hedin U, Bottger BA, Forsberg E, Johansson S and Thyberg J. Diverse effects of fibronectin and laminin on phenotypic properties of cultured arterial smooth muscle cells. *J Cell Biol*. 1988;107:307-19.

212. Ichii T, Koyama H, Tanaka S, Kim S, Shioi A, Okuno Y, Raines EW, Iwao H, Otani S and Nishizawa Y. Fibrillar collagen specifically regulates human vascular smooth muscle cell genes involved in cellular responses and the pericellular matrix environment. *Circ Res*. 2001;88:460-7.

213. Lehoux S and Tedgui A. Signal transduction of mechanical stresses in the vascular wall. *Hypertension*. 1998;32:338-45.

214. Halka AT, Turner NJ, Carter A, Ghosh J, Murphy MO, Kirton JP, Kielty CM and Walker MG. The effects of stretch on vascular smooth muscle cell phenotype in vitro. *Cardiovasc Pathol*. 2008;17:98-102. doi: 10.1016/j.carpath.2007.03.001.

215. Owens GK. Role of mechanical strain in regulation of differentiation of vascular smooth muscle cells. *Circ Res*. 1996;79:1054-5.

216. Reusch P, Wagdy H, Reusch R, Wilson E and Ives HE. Mechanical strain increases smooth muscle and decreases nonmuscle myosin expression in rat vascular smooth muscle cells. *Circ Res*. 1996;79:1046-53.

217. Birukov KG, Bardy N, Lehoux S, Merval R, Shirinsky VP and Tedgui A. Intraluminal pressure is essential for the maintenance of smooth muscle caldesmon and filamin content in aortic organ culture. *Arterioscler Thromb Vasc Biol*. 1998;18:922-7.

218. Williams B. Mechanical influences on vascular smooth muscle cell function. *J Hypertens*. 1998;16:1921-9.

219. Wilson E, Mai Q, Sudhir K, Weiss RH and Ives HE. Mechanical strain induces growth of vascular smooth muscle cells via autocrine action of PDGF. *J Cell Biol*. 1993;123:741-7.

220. Pukac L, Huangpu J and Karnovsky MJ. Platelet-derived growth factor-BB, insulin-like growth factor-I, and phorbol ester activate different signaling pathways for stimulation of vascular smooth muscle cell migration. *Exp Cell Res*. 1998;242:548-60. doi:10.1006/excr.1998.4138.

221. Rauch BH, Millette E, Kenagy RD, Daum G and Clowes AW. Thrombin- and factor Xa-induced DNA synthesis is mediated by transactivation of fibroblast growth factor receptor-1 in human vascular smooth muscle cells. *Circ Res*. 2004;94:340-5. doi: 10.1161/01.RES.0000111805.09592.D8.

222. Kim JS, Kim IK, Lee SY, Song BW, Cha MJ, Song H, Choi E, Lim S, Ham O, Jang Y and Hwang KC. Anti-proliferative effect of rosiglitazone on angiotensin II-induced vascular smooth muscle cell proliferation is mediated by the mTOR pathway. *Cell Biol Int*. 2012;36:305-10. doi: 10.1042/CBI20100524.

223. Wynne BM, Chiao CW and Webb RC. Vascular smooth muscle cell signaling mechanisms for contraction to angiotensin II and endothelin-1. *J Am Soc Hypertens*. 2009;3:84-95. doi: 10.1016/j.jash.2008.09.002.

224. Greenwald SE. Ageing of the conduit arteries. *J Pathol*. 2007;211:157-72. doi: 10.1002/path.2101.

225. Lacolley P, Regnault V, Nicoletti A, Li Z and Michel J-B. The vascular smooth muscle cell in arterial pathology: a cell that can take on multiple roles. *Cardiovasc Res*. 2012;95:194-204. doi: 10.1093/cvr/cvs135.

226. Neylon CB. Vascular biology of endothelin signal transduction. *Clin Exp Pharmacol Physiol*. 1999;26:149-53.

227. Ohtsu H, Suzuki H, Nakashima H, Dhobale S, Frank GD, Motley ED and Eguchi S. Angiotensin II signal transduction through small GTP-binding proteins: mechanism and significance in vascular smooth muscle cells. *Hypertension*. 2006;48:534-40. doi: 10.1161/01.HYP.0000237975.90870.eb.

228. Robin P, Boulven I, Desmyter C, Harbon S and Leiber D. ET-1 stimulates ERK signaling pathway through sequential activation of PKC and Src in rat myometrial cells. *Am J Physiol Cell Physiol*. 2002;283:C251-60. doi: 10.1152/ajpcell.00601.2001.

229. Drexler H. Nitric oxide synthases in the failing human heart: a doubled-edged sword? *Circulation*. 1999;99:2972-5.

230. Luoma JS and Yla-Herttuala S. Expression of inducible nitric oxide synthase in macrophages and smooth muscle cells in various types of human atherosclerotic lesions. *Virchows Arch*. 1999;434:561-8.

231. Zhang M and Shah AM. ROS signalling between endothelial cells and cardiac cells. *Cardiovasc Res*. 2014;102:249-57. doi: 10.1093/cvr/cvu050.

232. Jeremy JY, Rowe D, Emsley AM and Newby AC. Nitric oxide and the proliferation of vascular smooth muscle cells. *Cardiovasc Res*. 1999;43:580-94.

233. Landmesser U, Dikalov S, Price SR, McCann L, Fukai T, Holland SM, Mitch WE and Harrison DG. Oxidation of tetrahydrobiopterin leads to uncoupling of endothelial cell nitric oxide synthase in hypertension. *J Clin Invest*. 2003;111:1201-9. doi: 10.1172/ JCI14172.

234. Moens AL, Takimoto E, Tocchetti CG, Chakir K, Bedja D, Cormaci G, Ketner EA, Majmudar M, Gabrielson K, Halushka MK, Mitchell JB, Biswal S, Channon KM, Wolin MS, Alp NJ, Paolocci N, Champion HC and Kass DA. Reversal of cardiac hypertrophy and fibrosis from pressure overload by tetrahydrobiopterin: efficacy of recoupling nitric oxide synthase as a therapeutic strategy. *Circulation*. 2008;117:2626-36. doi: 10.1161/CIRCULATIONAHA. 107.737031.

235. Silberman GA, Fan TH, Liu H, Jiao Z, Xiao HD, Lovelock JD, Boulden BM, Widder J, Fredd S, Bernstein KE, Wolska BM, Dikalov S, Harrison DG and Dudley SC, Jr. Uncoupled cardiac nitric oxide synthase mediates diastolic dysfunction. *Circulation*. 2010;121:519-28. doi: 10.1161/CIRCULATIONAHA.109.883777.

236. Liu T, Castro S, Brasier AR, Jamaluddin M, Garofalo RP and Casola A. Reactive oxygen species mediate virus-induced STAT activation: role of tyrosine phosphatases. *J Biol Chem*. 2004;279:2461-9. doi: 10.1074/jbc.M307251200.

237. Schulz E, Gori T and Munzel T. Oxidative stress and endothelial dysfunction in hypertension. *Hypertens Res*. 2011;34:665-73. doi: 10.1038/hr.2011.39.

238. Virdis A, Duranti E and Taddei S. Oxidative stress and vascular damage in hypertension: role of angiotensin II. *Int J Hypertens*. 2011;2011:916310. doi: 10.4061/2011/916310.

239. Murdoch CE, Chaubey S, Zeng L, Yu B, Ivetic A, Walker SJ, Vanhoutte D, Heymans S, Grieve DJ, Cave AC, Brewer AC, Zhang M and Shah AM. Endothelial NADPH oxidase-2 promotes interstitial cardiac fibrosis and diastolic dysfunction through proinflammatory effects and endothelial-mesenchymal transition. *J Am Coll Cardiol*. 2014;63:2734-41. doi: 10.1016/j.jacc.2014.02.572.

240. Zhang M, Brewer AC, Schroder K, Santos CX, Grieve DJ, Wang M, Anilkumar N, Yu B, Dong X, Walker SJ, Brandes RP and Shah AM. NADPH oxidase-4 mediates protection against chronic load-induced stress in mouse hearts by enhancing angiogenesis. *Proc Natl Acad Sci U S A*. 2010;107:18121-6. doi: 10.1073/pnas.1009700107.

241. Mayet J and Hughes A. Cardiac and vascular pathophysiology in hypertension. *Heart*. 2003;89:1104-9.

242. Yemane H, Busauskas M, Burris SK and Knuepfer MM. Neurohumoral mechanisms in deoxycorticosterone acetate (DOCA)-salt hypertension in rats. *Exp Physiol*. 2010;95:51-5. doi: 10.1113/expphysiol.2008.046334.

243. Kempf T and Wollert KC. Nitric oxide and the enigma of cardiac hypertrophy. *Bioessays*. 2004;26:608-15. doi: 10.1002/bies.20049.

244. Intengan HD and Schiffrin EL. Vascular remodeling in hypertension: roles of apoptosis, inflammation, and fibrosis. *Hypertension*. 2001;38:581-7.

245. Renna NF, de Las Heras N and Miatello RM. Pathophysiology of vascular remodeling in hypertension. *Int J Hypertens*. 2013;2013:808353. doi: 10.1155/2013/808353.

246. Zeiher AM, Schachlinger V, Hohnloser SH, Saurbier B and Just H. Coronary atherosclerotic wall thickening and vascular reactivity in humans. Elevated high-density lipoprotein levels

ameliorate abnormal vasoconstriction in early atherosclerosis. *Circulation*. 1994;89:2525-32.

247. Libby P and Theroux P. Pathophysiology of coronary artery disease. *Circulation*. 2005; 111:3481-8. doi: 10.1161/CIRCULATIONAHA.105.537878.

248. Schiffrin EL. Remodeling of resistance arteries in essential hypertension and effects of antihypertensive treatment. *Am J Hypertens*. 2004;17:1192-200. doi: 10.1016/j. amjhyper.2004.05.023.

249. Heerkens EH, Izzard AS and Heagerty AM. Integrins, vascular remodeling, and hypertension. *Hypertension*. 2007;49:1-4. doi: 10.1161/01.HYP.0000252753.63224.3b.

250. Korshunov VA, Schwartz SM and Berk BC. Vascular remodeling: hemodynamic and biochemical mechanisms underlying Glagov's phenomenon. *Arterioscler Thromb Vasc Biol*. 2007;27:1722-8. doi: 10.1161/ATVBAHA.106.129254.

251. Feihl F, Liaudet L, Levy BI and Waeber B. Hypertension and microvascular remodelling. *Cardiovasc Res*. 2008;78:274-85. doi: 10.1093/cvr/cvn022.

252. Schiffrin EL, Deng LY and Larochelle P. Morphology of resistance arteries and comparison of effects of vasoconstrictors in mild essential hypertensive patients. *Clin Invest Med*. 1993;16:177-86.

253. Rizzoni D, Porteri E, Castellano M, Bettoni G, Muiesan ML, Muiesan P, Giulini SM and Agabiti-Rosei E. Vascular hypertrophy and remodeling in secondary hypertension. *Hypertension*. 1996;28:785-90.

254. Delbosc S, Haloui M, Louedec L, Dupuis M, Cubizolles M, Podust VN, Fung ET, Michel JB and Meilhac O. Proteomic analysis permits the identification of new biomarkers of arterial wall remodeling in hypertension. *Mol Med*. 2008;14:383-94. doi: 10.2119/2008-00030.Delbosc.

255. Kahan T and Bergfeldt L. Left ventricular hypertrophy in hypertension: its arrhythmogenic potential. *Heart*. 2005;91:250-6. doi: 10.1136/hrt.2004.042473.

256. Katholi RE and Couri DM. Left ventricular hypertrophy: major risk factor in patients with hypertension: update and practical clinical applications. *Int J Hypertens*. 2011;2011: 495349. doi: 10.4061/2011/495349.

257. Ahuja P, Sdek P and MacLellan WR. Cardiac myocyte cell cycle control in development, disease, and regeneration. *Phys Rev*. 2007;87:521-44. doi: 10.1152/physrev.00032.2006.

258. Carreno JE, Apablaza F, Ocaranza MP and Jalil JE. Cardiac hypertrophy: molecular and cellular events. *Rev Esp Cardiol*. 2006;59:473-86.

259. Takeuchi T. Regulation of cardiomyocyte proliferation during development and regeneration. *Dev Growth Differ*. 2014;56:402-9. doi: 10.1111/dgd.12134.

260. S. TPSaT. Regulation of phospholipase C in cardiac hypertrophy. *Clin Lipidol*. 2009;4:79-90. doi: 10.2217/17584299.4.1.79.

261. Kanda M and Nagai T. Neonatal Rat Heart Response to Pressure Overload. *Int Heart J*. 2017;58:155-157. doi: 10.1536/ihj.17-006.

262. Orlic D, Kajstura J, Chimenti S, Jakoniuk I, Anderson SM, Li B, Pickel J, McKay R, Nadal-Ginard B, Bodine DM, Leri A and Anversa P. Bone marrow cells regenerate infarcted myocardium. *Nature*. 2001;410:701-5. doi: 10.1038/35070587.

263. Balsam LB, Wagers AJ, Christensen JL, Kofidis T, Weissman IL and Robbins RC. Haematopoietic stem cells adopt mature haematopoietic fates in ischaemic myocardium. *Nature*. 2004;428:668-73. doi: 10.1038/nature02460.

264. Schachinger V, Assmus B, Britten MB, Honold J, Lehmann R, Teupe C, Abolmaali ND, Vogl TJ, Hofmann WK, Martin H, Dimmeler S and Zeiher AM. Transplantation of progenitor cells and regeneration enhancement in acute myocardial infarction: final one-year results

of the TOPCARE-AMI Trial. *J Am Coll Cardiol*. 2004;44:1690-9. doi: 10.1016/j.jacc.2004.08.014.

265. Strauer BE, Brehm M, Zeus T, Kostering M, Hernandez A, Sorg RV, Kogler G and Wernet P. Repair of infarcted myocardium by autologous intracoronary mononuclear bone marrow cell transplantation in humans. *Circulation*. 2002;106:1913-8.

266. Meyer GP, Wollert KC, Lotz J, Steffens J, Lippolt P, Fichtner S, Hecker H, Schaefer A, Arseniev L, Hertenstein B, Ganser A and Drexler H. Intracoronary bone marrow cell transfer after myocardial infarction: eighteen months' follow-up data from the randomized, controlled BOOST (Bone marrow transfer to enhance ST-elevation infarct regeneration) trial. *Circulation*. 2006;113:1287-94. doi: 10.1161/CIRCULATIONAHA.105.575118.

267. Braun T and Martire A. Cardiac stem cells: paradigm shift or broken promise? A view from developmental biology. *Trends Biotechnol*. 2007;25:441-7. doi: 10.1016/j.tibtech.2007.08.004.

268. Brockes JP and Kumar A. Plasticity and reprogramming of differentiated cells in amphibian regeneration. *Nat Rev Mol Cell Biol*. 2002;3:566-74. doi: 10.1038/nrm881.

269. Oberpriller JO and Oberpriller JC. Response of the adult newt ventricle to injury. *J Exp Zool*. 1974;187:249-53. doi: 10.1002/jez.1401870208.

270. Sanchez Alvarado A and Tsonis PA. Bridging the regeneration gap: genetic insights from diverse animal models. *Nat Rev Genet*. 2006;7:873-84. doi: 10.1038/nrg1923.

271. Ruwhof C and van der Laarse A. Mechanical stress-induced cardiac hypertrophy: mechanisms and signal transduction pathways. *Cardiovasc Res*. 2000;47:23-37.

272. Brand K, Page S, Rogler G, Bartsch A, Brandl R, Knuechel R, Page M, Kaltschmidt C, Baeuerle PA and Neumeier D. Activated transcription factor nuclear factor-kappa B is present in the atherosclerotic lesion. *J Clin Invest*. 1996;97:1715-22. doi: 10.1172/JCI118598.

273. Brancaccio M, Hirsch E, Notte A, Selvetella G, Lembo G and Tarone G. Integrin signalling: the tug-of-war in heart hypertrophy. *Cardiovasc Res*. 2006;70:422-33. doi: 10.1016/j.cardiores.2005.12.015.

274. Babbitt CJ, Shai SY, Harpf AE, Pham CG and Ross RS. Modulation of integrins and integrin signaling molecules in the pressure-loaded murine ventricle. *Histochem Cell Biol*. 2002;118:431-9. doi: 10.1007/s00418-002-0476-1.

275. Willey CD, Balasubramanian S, Rodriguez Rosas MC, Ross RS and Kuppuswamy D. Focal complex formation in adult cardiomyocytes is accompanied by the activation of beta3 integrin and c-Src. *J Mol Cell Cardiol*. 2003;35:671-83.

276. Martinez-Lemus LA, Crow T, Davis MJ and Meininger GA. alphavbeta3- and alpha5beta1-integrin blockade inhibits myogenic constriction of skeletal muscle resistance arterioles. *Am J Physiol Heart Circ Physiol*. 2005;289:H322-9. doi: 10.1152/ajpheart.00923.2003.

277. Haq S, Choukroun G, Lim H, Tymitz KM, del Monte F, Gwathmey J, Grazette L, Michael A, Hajjar R, Force T and Molkentin JD. Differential activation of signal transduction pathways in human hearts with hypertrophy versus advanced heart failure. *Circulation*. 2001;103:670-7.

278. Purcell NH, Wilkins BJ, York A, Saba-El-Leil MK, Meloche S, Robbins J and Molkentin JD. Genetic inhibition of cardiac ERK1/2 promotes stress-induced apoptosis and heart failure but has no effect on hypertrophy in vivo. *Proc Natl Acad Sci U S A*. 2007;104: 14074-9. doi: 10.1073/pnas.0610906104.

279. Esposito G, Prasad SV, Rapacciuolo A, Mao L, Koch WJ and Rockman HA. Cardiac overexpression of a G(q) inhibitor blocks induction of extracellular signal-regulated kinase

and c-Jun NH(2)-terminal kinase activity in in vivo pressure overload. *Circulation*. 2001;103:1453-8.

280. Wilkie N, Ng LL and Boarder MR. Angiotensin II responses of vascular smooth muscle cells from hypertensive rats: enhancement at the level of p42 and p44 mitogen activated protein kinase. *Br J Pharmacol*. 1997;122:209-16. doi: 10.1038/sj.bjp.0701366.
281. Rich S and McLaughlin VV. Endothelin receptor blockers in cardiovascular disease. *Circulation*. 2003;108:2184-90. doi: 10.1161/01.CIR.0000094397.19932.78.
282. Dhaun N, Goddard J, Kohan DE, Pollock DM, Schiffrin EL and Webb DJ. Role of endothelin-1 in clinical hypertension: 20 years on. *Hypertension*. 2008;52:452-9. doi: 10.1161/HYPERTENSIONAHA.108.117366.
283. Schiffrin EL. State-of-the-Art lecture. Role of endothelin-1 in hypertension. *Hypertension*. 1999;34:876-81.
284. Schiffrin EL. Role of endothelin-1 in hypertension and vascular disease. *Am J Hypertens*. 2001;14:83S-89S.
285. Louis SF and Zahradka P. Vascular smooth muscle cell motility: From migration to invasion. *Exp Clin Cardiol*. 2010;15:e75-85.
286. De Mello WC and Danser AH. Angiotensin II and the heart : on the intracrine renin-angiotensin system. *Hypertension*. 2000;35:1183-8.
287. Xue B, Beltz TG, Yu Y, Guo F, Gomez-Sanchez CE, Hay M and Johnson AK. Central interactions of aldosterone and angiotensin II in aldosterone- and angiotensin II-induced hypertension. *Am J Physiol Heart Circ Physiol*. 2011;300:H555-64. doi: 10.1152/ajpheart.00847.2010.
288. DiBona GF. Sympathetic nervous system and hypertension. *Hypertension*. 2013;61:556-60. doi: 10.1161/HYPERTENSIONAHA.111.00633.
289. Tsuda K. Renin-Angiotensin system and sympathetic neurotransmitter release in the central nervous system of hypertension. *Int J Hypertens*. 2012;2012:474870. doi: 10.1155/2012/474870.
290. Rosenkranz S, Flesch M, Amann K, Haeuseler C, Kilter H, Seeland U, Schluter KD and Bohm M. Alterations of beta-adrenergic signaling and cardiac hypertrophy in transgenic mice overexpressing TGF-beta(1). *Am J Physiol Heart Circ Physiol*. 2002;283:H1253-62. doi: 10.1152/ajpheart.00578.2001.
291. Ohta K, Kim S, Wanibuchi H, Ganten D and Iwao H. Contribution of local renin-angiotensin system to cardiac hypertrophy, phenotypic modulation, and remodeling in TGR (mRen2)27 transgenic rats. *Circulation*. 1996;94:785-91.
292. Yamazaki T, Komuro I and Yazaki Y. Role of the renin-angiotensin system in cardiac hypertrophy. *Am J Cardiol*. 1999;83:53H-57H.
293. Nakamura Y, Yoshiyama M, Omura T, Yoshida K, Izumi Y, Takeuchi K, Kim S, Iwao H and Yoshikawa J. Beneficial effects of combination of ACE inhibitor and angiotensin II type 1 receptor blocker on cardiac remodeling in rat myocardial infarction. *Cardiovasc Res*. 2003;57:48-54.
294. Kim S, Yoshiyama M, Izumi Y, Kawano H, Kimoto M, Zhan Y and Iwao H. Effects of combination of ACE inhibitor and angiotensin receptor blocker on cardiac remodeling, cardiac function, and survival in rat heart failure. *Circulation*. 2001;103:148-54.
295. Liu YH, Yang XP, Sharov VG, Nass O, Sabbah HN, Peterson E and Carretero OA. Effects of angiotensin-converting enzyme inhibitors and angiotensin II type 1 receptor antagonists in rats with heart failure. Role of kinins and angiotensin II type 2 receptors. *J Clin Invest*. 1997;99:1926-35. doi: 10.1172/JCI119360.
296. Schieffer B, Wirger A, Meybrunn M, Seitz S, Holtz J, Riede UN and Drexler H. Comparative effects of chronic angiotensin-converting enzyme inhibition and angiotensin II type 1

receptor blockade on cardiac remodeling after myocardial infarction in the rat. *Circulation*. 1994;89:2273-82.

297. Pfeffer MA, McMurray JJ, Velazquez EJ, Rouleau JL, Kober L, Maggioni AP, Solomon SD, Swedberg K, Van de Werf F, White H, Leimberger JD, Henis M, Edwards S, Zelenkofske S, Sellers MA and Califf RM. Valsartan, captopril, or both in myocardial infarction complicated by heart failure, left ventricular dysfunction, or both. *N Engl J Med*. 2003; 349:1893-906. doi: 10.1056/NEJMoa032292.
298. Pfeffer MA, Swedberg K, Granger CB, Held P, McMurray JJ, Michelson EL, Olofsson B, Ostergren J, Yusuf S, Pocock S, Investigators C and Committees. Effects of candesartan on mortality and morbidity in patients with chronic heart failure: the CHARM-Overall programme. *Lancet*. 2003;362:759-66.
299. Sparks MA, Parsons KK, Stegbauer J, Gurley SB, Vivekanandan-Giri A, Fortner CN, Snouwaert J, Raasch EW, Griffiths RC, Haystead TA, Le TH, Pennathur S, Koller B and Coffman TM. Angiotensin II type 1A receptors in vascular smooth muscle cells do not influence aortic remodeling in hypertension. *Hypertension*. 2011;57:577-85. doi: 10.1161/HYPERTENSIONAHA.110.165274.
300. Schiffrin EL, Park JB, Intengan HD and Touyz RM. Correction of arterial structure and endothelial dysfunction in human essential hypertension by the angiotensin receptor antagonist losartan. *Circulation*. 2000;101:1653-9.
301. Lusis AJ. Atherosclerosis. *Nature*. 2000;407:233-41. doi: 10.1038/35025203.
302. Bennett MR, Sinha S and Owens GK. Vascular Smooth Muscle Cells in Atherosclerosis. *Circ Res*. 2016;118:692-702. doi: 10.1161/CIRCRESAHA.115.306361.
303. Rudijanto A. The role of vascular smooth muscle cells on the pathogenesis of atherosclerosis. *Acta Med Indones*. 2007;39:86-93.
304. Hansson GK and Libby P. The immune response in atherosclerosis: a double-edged sword. *Nat Rev Immunol*. 2006;6:508-19. doi: 10.1038/nri1882.
305. Hansson GK, Robertson AK and Soderberg-Naucler C. Inflammation and atherosclerosis. *Annu Rev Pathol*. 2006;1:297-329. doi: 10.1146/annurev.pathol.1.110304.100100.
306. Libby P, Ridker PM and Hansson GK. Progress and challenges in translating the biology of atherosclerosis. *Nature*. 2011;473:317-25. doi: 10.1038/nature10146.
307. Libby P, Ridker PM and Maseri A. Inflammation and atherosclerosis. *Circulation*. 2002; 105:1135-43.
308. Cochain C and Zernecke A. Macrophages in vascular inflammation and atherosclerosis. *Pflugers Arch*. 2017;469:485-499. doi: 10.1007/s00424-017-1941-y.
309. Ross R. The pathogenesis of atherosclerosis: a perspective for the 1990s. *Nature*. 1993;362:801-9. doi: 10.1038/362801a0.
310. Ross R. Atherosclerosis--an inflammatory disease. *N Engl J Med*. 1999;340:115-26. doi: 10.1056/NEJM199901143400207.
311. Geng YJ, Wu Q, Muszynski M, Hansson GK and Libby P. Apoptosis of vascular smooth muscle cells induced by in vitro stimulation with interferon-gamma, tumor necrosis factor-alpha, and interleukin-1 beta. *Arterioscler Thromb Vasc Biol*. 1996;16:19-27.
312. Rosner D, Stoneman V, Littlewood T, McCarthy N, Figg N, Wang Y, Tellides G and Bennett M. Interferon-gamma induces Fas trafficking and sensitization to apoptosis in vascular smooth muscle cells via a PI3K- and Akt-dependent mechanism. *Am J Pathol*. 2006;168:2054-63.
313. Tang M and Fang J. TNFalpha regulates apoptosis of human vascular smooth muscle cells through gap junctions. *Mol Med Rep*. 2017;15:1407-1411. doi: 10.3892/mmr.2017. 6106.
314. Davignon J and Ganz P. Role of endothelial dysfunction in atherosclerosis. *Circulation*. 2004;109:III27-32. doi: 10.1161/01.CIR.0000131515.03336.f8.

315. Wang Y, Chun OK and Song WO. Plasma and dietary antioxidant status as cardiovascular disease risk factors: a review of human studies. *Nutrients*. 2013;5:2969-3004. doi: 10.3390/nu5082969.

316. van der Zwan LP, Teerlink T, Dekker JM, Henry RM, Stehouwer CD, Jakobs C, Heine RJ and Scheffer PG. Circulating oxidized LDL: determinants and association with brachial flow-mediated dilation. *J Lipid Res*. 2009;50:342-9. doi: 10.1194/jlr.P800030-JLR200.

317. Celermajer DS, Sorensen KE, Bull C, Robinson J and Deanfield JE. Endothelium-dependent dilation in the systemic arteries of asymptomatic subjects relates to coronary risk factors and their interaction. *J Am Coll Cardiol*. 1994;24:1468-74.

318. Cox DA, Vita JA, Treasure CB, Fish RD, Alexander RW, Ganz P and Selwyn AP. Atherosclerosis impairs flow-mediated dilation of coronary arteries in humans. *Circulation*. 1989;80:458-65.

319. Ludmer PL, Selwyn AP, Shook TL, Wayne RR, Mudge GH, Alexander RW and Ganz P. Paradoxical vasoconstriction induced by acetylcholine in atherosclerotic coronary arteries. *N Engl J Med*. 1986;315:1046-51. doi: 10.1056/NEJM198610233151702.

320. Reddy KG, Nair RN, Sheehan HM and Hodgson JM. Evidence that selective endothelial dysfunction may occur in the absence of angiographic or ultrasound atherosclerosis in patients with risk factors for atherosclerosis. *J Am Coll Cardiol*. 1994;23:833-43.

321. Swirski FK, Libby P, Aikawa E, Alcaide P, Luscinskas FW, Weissleder R and Pittet MJ. Ly-6Chi monocytes dominate hypercholesterolemia-associated monocytosis and give rise to macrophages in atheromata. *J Clin Invest*. 2007;117:195-205. doi: 10.1172/JCI29950.

322. Tacke F, Alvarez D, Kaplan TJ, Jakubzick C, Spanbroek R, Llodra J, Garin A, Liu J, Mack M, van Rooijen N, Lira SA, Habenicht AJ and Randolph GJ. Monocyte subsets differentially employ CCR2, CCR5, and CX3CR1 to accumulate within atherosclerotic plaques. *J Clin Invest*. 2007;117:185-194. doi: 10.1172/JCI28549.

323. Bouhlel MA, Derudas B, Rigamonti E, Dievart R, Brozek J, Haulon S, Zawadzki C, Jude B, Torpier G, Marx N, Staels B and Chinetti-Gbaguidi G. PPARgamma activation primes human monocytes into alternative M2 macrophages with anti-inflammatory properties. *Cell Metab*. 2007;6:137-43. doi: 10.1016/j.cmet.2007.06.010.

324. Libby P. Molecular and cellular mechanisms of the thrombotic complications of atherosclerosis. *J Lipid Res*. 2009;50 Suppl:S352-7. doi: 10.1194/jlr.R800099-JLR200.

325. Szaba FM and Smiley ST. Roles for thrombin and fibrin(ogen) in cytokine/chemokine production and macrophage adhesion in vivo. *Blood*. 2002;99:1053-9.

326. McDonald OG and Owens GK. Programming smooth muscle plasticity with chromatin dynamics. *Circ Res*. 2007;100:1428-41. doi: 10.1161/01.RES.0000266448.30370.a0.

327. Regan CP, Adam PJ, Madsen CS and Owens GK. Molecular mechanisms of decreased smooth muscle differentiation marker expression after vascular injury. *J Clin Invest*. 2000;106:1139-47. doi: 10.1172/JCI10522.

328. Wamhoff BR, Hoofnagle MH, Burns A, Sinha S, McDonald OG and Owens GK. A G/C element mediates repression of the SM22alpha promoter within phenotypically modulated smooth muscle cells in experimental atherosclerosis. *Circ Res*. 2004;95:981-8. doi: 10.1161/01.RES.0000147961.09840.fb.

329. Chen J, Kitchen CM, Streb JW and Miano JM. Myocardin: a component of a molecular switch for smooth muscle differentiation. *J Mol Cell Cardiol*. 2002;34:1345-56.

330. Long X, Bell RD, Gerthoffer WT, Zlokovic BV and Miano JM. Myocardin is sufficient for a smooth muscle-like contractile phenotype. *Arterioscler Thromb Vasc Biol*. 2008;28:1505-10. doi: 10.1161/ATVBAHA.108.166066.

331. Sun Q, Taurin S, Sethakorn N, Long X, Imamura M, Wang DZ, Zimmer WE, Dulin NO and Miano JM. Myocardin-dependent activation of the CArG box-rich smooth muscle gamma-

actin gene: preferential utilization of a single CArG element through functional association with the NKX3.1 homeodomain protein. *J Biol Chem*. 2009;284:32582-90. doi: 10.1074/jbc.M109.033910.

332. Wang Z, Wang DZ, Pipes GC and Olson EN. Myocardin is a master regulator of smooth muscle gene expression. *Proc Natl Acad Sci U S A*. 2003;100:7129-34. doi: 10.1073/pnas.1232341100.
333. Xia XD, Zhou Z, Yu XH, Zheng XL and Tang CK. Myocardin: A novel player in atherosclerosis. *Atherosclerosis*. 2017;257:266-278. doi: 10.1016/j.atherosclerosis.2016.12.002.
334. Kozaki K, Kaminski WE, Tang J, Hollenbach S, Lindahl P, Sullivan C, Yu JC, Abe K, Martin PJ, Ross R, Betsholtz C, Giese NA and Raines EW. Blockade of platelet-derived growth factor or its receptors transiently delays but does not prevent fibrous cap formation in ApoE null mice. *Am J Pathol*. 2002;161:1395-407. doi: 10.1016/S0002-9440(10)64415-X.
335. Sano H, Sudo T, Yokode M, Murayama T, Kataoka H, Takakura N, Nishikawa S, Nishikawa SI and Kita T. Functional blockade of platelet-derived growth factor receptor-beta but not of receptor-alpha prevents vascular smooth muscle cell accumulation in fibrous cap lesions in apolipoprotein E-deficient mice. *Circulation*. 2001;103:2955-60.
336. He C, Medley SC, Hu T, Hinsdale ME, Lupu F, Virmani R and Olson LE. PDGFRbeta signalling regulates local inflammation and synergizes with hypercholesterolaemia to promote atherosclerosis. *Nat Commun*. 2015;6:7770. doi: 10.1038/ncomms8770.
337. Katsuda S and Kaji T. Atherosclerosis and extracellular matrix. *J Atheroscler Thromb*. 2003;10:267-74.
338. Barnes MJ and Farndale RW. Collagens and atherosclerosis. *Exp Gerontol*. 1999;34:513-25.
339. Orr AW, Lee MY, Lemmon JA, Yurdagul A, Jr., Gomez MF, Bortz PD and Wamhoff BR. Molecular mechanisms of collagen isotype-specific modulation of smooth muscle cell phenotype. *Arterioscler Thromb Vasc Biol*. 2009;29:225-31. doi: 10.1161/ATVBAHA.108.178749.
340. Lim S and Park S. Role of vascular smooth muscle cell in the inflammation of atherosclerosis. *BMB Rep*. 2014;47:1-7.
341. Braun M, Pietsch P, Felix SB and Baumann G. Modulation of intercellular adhesion molecule-1 and vascular cell adhesion molecule-1 on human coronary smooth muscle cells by cytokines. *J Mol Cell Cardiol*. 1995;27:2571-9. doi: 10.1006/jmcc.1995.0044.
342. Cherepanova OA, Pidkovka NA, Sarmento OF, Yoshida T, Gan Q, Adiguzel E, Bendeck MP, Berliner J, Leitinger N and Owens GK. Oxidized phospholipids induce type VIII collagen expression and vascular smooth muscle cell migration. *Circ Res*. 2009;104:609-18. doi: 10.1161/CIRCRESAHA.108.186064.
343. Landry DB, Couper LL, Bryant SR and Lindner V. Activation of the NF-kappa B and I kappa B system in smooth muscle cells after rat arterial injury. Induction of vascular cell adhesion molecule-1 and monocyte chemoattractant protein-1. *Am J Pathol*. 1997;151:1085-95.
344. Li H, Cybulsky MI, Gimbrone MA, Jr. and Libby P. Inducible expression of vascular cell adhesion molecule-1 by vascular smooth muscle cells in vitro and within rabbit atheroma. *Am J Pathol*. 1993;143:1551-9.
345. Freis ED. Hypertension and atherosclerosis. *Am J Med*. 1969;46:735-40.
346. Hollander W. Role of hypertension in atherosclerosis and cardiovascular disease. *Am J Cardiol*. 1976;38:786-800.
347. Stamler J, Neaton JD and Wentworth DN. Blood pressure (systolic and diastolic) and risk of fatal coronary heart disease. *Hypertension*. 1989;13:I2-12.

348. Kannel WB, Neaton JD, Wentworth D, Thomas HE, Stamler J, Hulley SB and Kjelsberg MO. Overall and coronary heart disease mortality rates in relation to major risk factors in 325,348 men screened for the MRFIT. Multiple Risk Factor Intervention Trial. *Am Heart J*. 1986;112:825-36.

349. Robertson WB and Strong JP. Atherosclerosis in persons with hypertension and diabetes mellitus. *Lab Invest*. 1968;18:538-51.

350. Wilens SL. The experimental production of lipid deposition in excised arteries. *Science*. 1951;114:389-93.

351. Fisher ER and Geller JH. Effect of cholesterol atherosclerosis, hypertension and cortisone on aortic oxygen consumption in rabbit. *Circ Res*. 1960;8:820-4.

352. Schiffrin EL and Canadian Institutes of Health Research Multidisciplinary Research Group on H. Beyond blood pressure: the endothelium and atherosclerosis progression. *Am J Hypertens*. 2002;15:115S-122S.

353. Li JJ and Chen JL. Inflammation may be a bridge connecting hypertension and atherosclerosis. *Med Hypotheses*. 2005;64:925-9. doi: 10.1016/j.mehy.2004.10.016.

354. Nadar SK, Blann A, Beevers DG and Lip GY. Abnormal angiopoietins 1&2, angiopoietin receptor Tie-2 and vascular endothelial growth factor levels in hypertension: relationship to target organ damage [a sub-study of the Anglo-Scandinavian Cardiac Outcomes Trial (ASCOT)]. *J Intern Med*. 2005;258:336-43. doi: 10.1111/j.1365-2796. 2005.01550.x.

355. David S, Kumpers P, Lukasz A, Kielstein JT, Haller H and Fliser D. Circulating angiopoietin-2 in essential hypertension: relation to atherosclerosis, vascular inflammation, and treatment with olmesartan/pravastatin. *J Hypertens*. 2009;27:1641-7. doi: 10.1097/HJH. 0b013e32832be575.

356. Patel JV, Lim HS, Varughese GI, Hughes EA and Lip GY. Angiopoietin-2 levels as a biomarker of cardiovascular risk in patients with hypertension. *Ann Med*. 2008;40:215-22. doi: 10.1080/07853890701779586.

357. Kumpers P, Nickel N, Lukasz A, Golpon H, Westerkamp V, Olsson KM, Jonigk D, Maegel L, Bockmeyer CL, David S and Hoeper MM. Circulating angiopoietins in idiopathic pulmonary arterial hypertension. *Eur Heart J*. 2010;31:2291-300. doi: 10.1093/ eurheartj/ehq226.

358. Chu D, Sullivan CC, Du L, Cho AJ, Kido M, Wolf PL, Weitzman MD, Jamieson SW and Thistlethwaite PA. A new animal model for pulmonary hypertension based on the overexpression of a single gene, angiopoietin-1. *Ann Thorac Surg*. 2004;77:449-56; discussion 456-7. doi: 10.1016/S0003-4975(03)01350-X.

359. Dewachter L, Adnot S, Fadel E, Humbert M, Maitre B, Barlier-Mur AM, Simonneau G, Hamon M, Naeije R and Eddahibi S. Angiopoietin/Tie2 pathway influences smooth muscle hyperplasia in idiopathic pulmonary hypertension. *Am J Respir Crit Care Med*. 2006;174:1025-33. doi: 10.1164/rccm.200602-304OC.

360. Zhao YD, Campbell AI, Robb M, Ng D and Stewart DJ. Protective role of angiopoietin-1 in experimental pulmonary hypertension. *Circ Res*. 2003;92:984-91. doi: 10.1161/01.RES. 0000070587.79937.F0.

361. Kugathasan L, Ray JB, Deng Y, Rezaei E, Dumont DJ and Stewart DJ. The angiopietin-1-Tie2 pathway prevents rather than promotes pulmonary arterial hypertension in transgenic mice. *J Exp Med*. 2009;206:2221-34. doi: 10.1084/jem.20090389.

362. David Sa, Kumpers Pa, Lukasz Aa, Kielstein JTa, Haller Ha and Fliser Db. Circulating angiopoietin-2 in essential hypertension: relation to atherosclerosis, vascular inflammation, and treatment with olmesartan/pravastatin. *J Hypertens*. 2009;27:1641-1647. doi: 10.1097/HJH.0b013e32832be575.

363. Fujisawa T, Wang K, Niu X-L, Egginton S, Ahmad S, Hewett P, Kontos CD and Ahmed A. Angiopoietin-1 promotes atherosclerosis by increasing the proportion of circulating Gr1+ monocytes. *Cardiovasc Res*. 2017;113:81-89. doi: 10.1093/cvr/cvw223.

364. Hauer AD, Habets KL, van Wanrooij EJ, de Vos P, Krueger J, Reisfeld RA, van Berkel TJ and Kuiper J. Vaccination against TIE2 reduces atherosclerosis. *Atherosclerosis*. 2009;204:365-371. doi: 10.1016/j.atherosclerosis.2008.09.039.

365. Post S, Peeters W, Busser E, Lamers D, Sluijter JPG, Goumans MJ, de Weger RA, Moll FL, Doevendans PA, Pasterkamp G and Vink A. Balance between angiopoietin-1 and angiopoietin-2 is in favor of angiopoietin-2 in atherosclerotic plaques with high microvessel density. *J Vasc Res*. 2008;45:244-250. doi: 10.1159/000112939.

366. Theelen TL, Lappalainen JP, Sluimer JC, Gurzeler E, Cleutjens JP, Gijbels MJ, Biessen EAL, Daemen MJAP, Alitalo K and Ylä-Herttuala S. Angiopoietin-2 blocking antibodies reduce early atherosclerotic plaque development in mice. *Atherosclerosis*. 2015;241:297-304. doi: 10.1016/j.atherosclerosis.2015.05.018.

367. Woo KV, Qu X, Babaev VR, Linton MF, Guzman RJ, Fazio S and Baldwin HS. Tie1 attenuation reduces murine atherosclerosis in a dose-dependent and shear stress-specific manner. *J Clin Invest*. 2011;121:1624-1635. doi: 10.1172/JCI42040.

368. Woo KV and Baldwin HS. Role of Tie1 in shear stress and atherosclerosis. *Trends Cardiovasc Med*. 2011;21:118-23. doi: 10.1016/j.tcm.2012.03.009.

369. Nykänen AI, Krebs R, Saaristo A, Turunen P, Alitalo K, Ylä-Herttuala S, Koskinen PK and Lemström KB. Angiopoietin-1 protects against the development of cardiac allograft arteriosclerosis. *Circulation*. 2003;107:1308-1314. doi: 10.1161/01.CIR.0000054623.35669.3F.

370. Iurlaro M, Scatena M, Zhu W-H, Fogel E, Wieting SL and Nicosia RF. Rat aorta-derived mural precursor cells express the Tie2 receptor and respond directly to stimulation by angiopoietins. *J Cell Sci*. 2003;116:3635-3643. doi: 10.1242/jcs.00629.

371. Shahrara S, Volin MV, Connors MA, Haines GK and Koch AE. Differential expression of the angiogenic Tie receptor family in arthritic and normal synovial tissue. *Arthritis Res*. 2002;4:201-208.

372. Tian S, Hayes AJ, Metheny-Barlow LJ and Li LY. Stabilization of breast cancer xenograft tumour neovasculature by angiopoietin-1. *Br J Cancer*. 2002;86:645-651. doi: 10.1038/sj.bjc.6600082.

373. Srinivas S, Watanabe T, Lin CS, William CM, Tanabe Y, Jessell TM and Costantini F. Cre reporter strains produced by targeted insertion of EYFP and ECFP into the ROSA26 locus. *BMC Dev Biol*. 2001;1:4.

374. Tachibana K, Jones N, Dumont DJ, Puri MC and Bernstein A. Selective role of a distinct tyrosine residue on Tie2 in heart development and early hematopoiesis. *Mol Cell Biol*. 2005;25:4693-4702. doi: 10.1128/MCB.25.11.4693-4702.2005.

375. Bowers CW and Dahm LM. Maintenance of contractility in dissociated smooth muscle: low-density cultures in a defined medium. *Am J Pathol- Cell Phys*. 1993;264:C229-C236.

376. Chamley-Campbell J, Campbell GR and Ross R. The smooth muscle cell in culture. *Physiol Rev*. 1979;59:1-61.

377. Licht AH, Nubel T, Feldner A, Jurisch-Yaksi N, Marcello M, Demicheva E, Hu JH, Hartenstein B, Augustin HG, Hecker M, Angel P, Korff T and Schorpp-Kistner M. Junb regulates arterial contraction capacity, cellular contractility, and motility via its target Myl9 in mice. *J Clin Invest*. 2010;120:2307-18. doi: 10.1172/JCI41749.

378. Kramer K and Kinter LB. Evaluation and applications of radiotelemetry in small laboratory animals. *Physiol Genomics*. 2003;13:197-205. doi: 10.1152/physiolgenomics. 00164.2002.

379. Kramer K and Remie R. Measuring blood pressure in small laboratory animals. *Methods Mol Med*. 2005;108:51-62.

380. Porth CM. Essentials of pathophysiology: concepts of altered health states 2nd Edition. *Lippincott Williams & Wilkins*. 2007.

381. Zoccali C. Arterial pressure components and cardiovascular risk in end-stage renal disease. *Nephrol Dial Transplant*. 2003;18:249-52.

382. Guyton AC, Coleman TG and Granger HJ. Circulation: overall regulation. *Annu Rev Physiol*. 1972;34:13-46. doi: 10.1146/annurev.ph.34.030172.000305.

383. Kojda G and Hambrecht R. Molecular mechanisms of vascular adaptations to exercise. Physical activity as an effective antioxidant therapy? *Cardiovasc Res*. 2005;67:187-97. doi: 10.1016/j.cardiores.2005.04.032.

384. Woodcock EA and Matkovich SJ. Cardiomyocytes structure, function and associated pathologies. *Int J Biochem Cell Biol*. 2005;37:1746-51. doi: 10.1016/j.biocel.2005.04.011.

385. Abe T and Fujimori T. Reporter mouse lines for fluorescence imaging. *Dev Growth Differ*. 2013;55:390-405. doi: 10.1111/dgd.12062.

386. Busch K, Klapproth K, Barile M, Flossdorf M, Holland-Letz T, Schlenner SM, Reth M, Hofer T and Rodewald HR. Fundamental properties of unperturbed haematopoiesis from stem cells in vivo. *Nature*. 2015;518:542-6. doi: 10.1038/nature14242.

387. Lee YT, Lin HY, Chan YW, Li KH, To OT, Yan BP, Liu T, Li G, Wong WT, Keung W and Tse G. Mouse models of atherosclerosis: a historical perspective and recent advances. *Lipids in health and disease*. 2017;16:12. doi: 10.1186/s12944-016-0402-5.

388. Lacolley P, Regnault V, Nicoletti A, Li Z and Michel JB. The vascular smooth muscle cell in arterial pathology: a cell that can take on multiple roles. *Cardiovasc Res*. 2012;95:194-204. doi: 10.1093/cvr/cvs135.

389. Lafeber M, Spiering W, Visseren FL and Grobbee DE. Multifactorial Prevention of Cardiovascular Disease in Patients with Hypertension: the Cardiovascular Polypill. *Curr Hypertens Rep*. 2016;18:40. doi: 10.1007/s11906-016-0648-3.

390. Teichert M, Stumpf C, Booken N, Wobser M, Nashan D, Hallermann C, Mogler C, Muller CS, Becker JC, Moritz RK, Andrulis M, Nicolay JP, Goerdt S, Thomas M, Klemke CD, Augustin HG and Felcht M. Aggressive primary cutaneous B-cell lymphomas show increased Angiopoietin-2-induced angiogenesis. *Exp Dermatol*. 2015;24:424-9. doi: 10.1111/exd.12688.

391. Rzucidlo EM, Martin KA and Powell RJ. Regulation of vascular smooth muscle cell differentiation. *J Vasc Surg*. 2007;45:A25-A32. doi: 10.1016/j.jvs.2007. 03.001.

392. Wang N, Symons JD, Zhang H, Jia Z, Gonzalez FJ and Yang T. Distinct functions of vascular endothelial and smooth muscle PPARgamma in regulation of blood pressure and vascular tone. *Toxicol Pathol*. 2009;37:21-7. doi: 10.1177/0192623308328545.

393. Schreier B, Rabe S, Schneider B, Bretschneider M, Rupp S, Ruhs S, Neumann J, Rueckschloss U, Sibilia M, Gotthardt M, Grossmann C and Gekle M. Loss of epidermal growth factor receptor in vascular smooth muscle cells and cardiomyocytes causes arterial hypotension and cardiac hypertrophy. *Hypertension*. 2013;61:333-40. doi: 10. 1161/HYPERTENSIONAHA.112.196543.

394. Henry JB, Miller MC, Kelly KC and Champney D. Mean arterial pressure (MAP): an alternative and preferable measurement to systolic blood pressure (SBP) in patients for hypotension detection during hemapheresis. *J Clin Apher*. 2002;17:55-64. doi: 10. 1002/jca.10022.

395. Yin FC, Spurgeon HA, Rakusan K, Weisfeldt ML and Lakatta EG. Use of tibial length to quantify cardiac hypertrophy: application in the aging rat. *Am J Physiol*. 1982;243:H941-7.

396. Lyons GE, Schiaffino S, Sassoon D, Barton P and Buckingham M. Developmental regulation of myosin gene expression in mouse cardiac muscle. *J Cell Biol*. 1990;111: 2427-36.

397. Paulin D and Li Z. Desmin: a major intermediate filament protein essential for the structural integrity and function of muscle. *Exp Cell Res*. 2004;301:1-7. doi: 10.1016/j.yexcr.2004.08.004.

398. Toko H, Zhu W, Takimoto E, Shiojima I, Hiroi Y, Zou Y, Oka T, Akazawa H, Mizukami M, Sakamoto M, Terasaki F, Kitaura Y, Takano H, Nagai T, Nagai R and Komuro I. Csx/Nkx2-5 is required for homeostasis and survival of cardiac myocytes in the adult heart. *J Biol Chem*. 2002;277:24735-43. doi: 10.1074/jbc.M107669200.

399. Iyer A, Chan V and Brown L. The DOCA-Salt Hypertensive Rat as a Model of Cardiovascular Oxidative and Inflammatory Stress. *Curr Cardiol Rev*. 2010;6:291-7. doi: 10.2174/157340310793566109.

400. Karatas A, Hegner B, de Windt LJ, Luft FC, Schubert C, Gross V, Akashi YJ, Gurgen D, Kintscher U, da Costa Goncalves AC, Regitz-Zagrosek V and Dragun D. Deoxycorticosterone acetate-salt mice exhibit blood pressure-independent sexual dimorphism. *Hypertension*. 2008;51:1177-83. doi: 10.1161/HYPERTENSIONAHA.107.107938.

401. Pfisterer L, Feldner A, Hecker M and Korff T. Hypertension impairs myocardin function: a novel mechanism facilitating arterial remodelling. *Cardiovasc Res*. 2012;96:120-9. doi: 10.1093/cvr/cvs247.

402. Sadoshima J and Izumo S. Molecular characterization of angiotensin II--induced hypertrophy of cardiac myocytes and hyperplasia of cardiac fibroblasts. Critical role of the AT1 receptor subtype. *Circ Res*. 1993;73:413-23.

403. Moran CM, Thomson AJ, Rog-Zielinska E and Gray GA. High-resolution echocardiography in the assessment of cardiac physiology and disease in preclinical models. *Exp Physiol*. 2013;98:629-44. doi: 10.1113/expphysiol.2012.068577.

404. Stypmann J, Engelen MA, Troatz C, Rothenburger M, Eckardt L and Tiemann K. Echocardiographic assessment of global left ventricular function in mice. *Lab Anim*. 2009;43:127-37. doi: 10.1258/la.2007.06001e.

405. Zadelaar S, Kleemann R, Verschuren L, de Vries-Van der Weij J, van der Hoorn J, Princen HM and Kooistra T. Mouse models for atherosclerosis and pharmaceutical modifiers. *Arterioscler Thromb Vasc Biol*. 2007;27:1706-21. doi: 10.1161/ATVBAHA.107.142570.

406. Nakashima Y, Plump AS, Raines EW, Breslow JL and Ross R. ApoE-deficient mice develop lesions of all phases of atherosclerosis throughout the arterial tree. *Arterioscler Thromb*. 1994;14:133-40.

407. Ishibashi S, Brown MS, Goldstein JL, Gerard RD, Hammer RE and Herz J. Hypercholesterolemia in low density lipoprotein receptor knockout mice and its reversal by adenovirus-mediated gene delivery. *J Clin Invest*. 1993;92:883-93. doi: 10.1172/JCI116663.

408. Plump AS, Scott CJ and Breslow JL. Human apolipoprotein A-I gene expression increases high density lipoprotein and suppresses atherosclerosis in the apolipoprotein E-deficient mouse. *Proc Natl Acad Sci U S A*. 1994;91:9607-11.

409. Steinberg D. Atherogenesis in perspective: hypercholesterolemia and inflammation as partners in crime. *Nat Med*. 2002;8:1211-1217. doi: 10.1038/nm1102-1211.

410. Gomez D and Owens GK. Smooth muscle cell phenotypic switching in atherosclerosis. *Cardiovasc Res*. 2012;95:156-64. doi: 10.1093/cvr/cvs115.

411. Woollard KJ and Geissmann F. Monocytes in atherosclerosis: subsets and functions. *Nat Rev Cardiol*. 2010;7:77-86. doi: 10.1038/nrcardio.2009.228.

412. Saharinen P, Eklund L and Alitalo K. Therapeutic targeting of the angiopoietin-TIE pathway. *Nat Rev Drug Discov*. 2017. doi: 10.1038/nrd.2016.278.

413. Daly C, Pasnikowski E, Burova E, Wong V, Aldrich TH, Griffiths J, Ioffe E, Daly TJ, Fandl JP, Papadopoulos N, McDonald DM, Thurston G, Yancopoulos GD and Rudge JS. Angiopoietin-2 functions as an autocrine protective factor in stressed endothelial cells. *Proc Natl Acad Sci U S A*. 2006;103:15491-6. doi: 10.1073/pnas.0607538103.

414. Scholz A, Lang V, Henschler R, Czabanka M, Vajkoczy P, Chavakis E, Drynski J, Harter PN, Mittelbronn M, Dumont DJ, Plate KH and Reiss Y. Angiopoietin-2 promotes myeloid cell infiltration in a beta(2)-integrin-dependent manner. *Blood*. 2011;118:5050-9. doi: 10.1182/blood-2011-03-343293.

415. Shimoda H, Bernas MJ, Witte MH, Gale NW, Yancopoulos GD and Kato S. Abnormal recruitment of periendothelial cells to lymphatic capillaries in digestive organs of angiopoietin-2-deficient mice. *Cell Tissue Res*. 2007;328:329-37. doi: 10.1007/s00441-006-0360-8.

416. Yla-Herttuala S, Bentzon JF, Daemen M, Falk E, Garcia-Garcia HM, Herrmann J, Hoefer I, Jauhiainen S, Jukema JW, Krams R, Kwak BR, Marx N, Naruszewicz M, Newby A, Pasterkamp G, Serruys PW, Waltenberger J, Weber C, Tokgozoglu L, Atherosclerosis ESCWGo and Vascular B. Stabilization of atherosclerotic plaques: an update. *Eur Heart J*. 2013;34:3251-8. doi: 10.1093/eurheartj/eht301.

417. Baumer Y, McCurdy S, Alcala M, Mehta N, Lee BH, Ginsberg MH and Boisvert WA. CD98 regulates vascular smooth muscle cell proliferation in atherosclerosis. *Atherosclerosis*. 2017;256:105-114. doi: 10.1016/j.atherosclerosis.2016.11.017.

418. Cascone I, Audero E, Giraudo E, Napione L, Maniero F, Philips MR, Collard JG, Serini G and Bussolino F. Tie-2-dependent activation of RhoA and Rac1 participates in endothelial cell motility triggered by angiopoietin-1. *Blood*. 2003;102:2482-90. doi: 10.1182/blood-2003-03-0670.

419. Lee JS, Song SH, Kim JM, Shin IS, Kim KL, Suh YL, Kim HZ, Koh GY, Byun J, Jeon ES, Suh W and Kim DK. Angiopoietin-1 prevents hypertension and target organ damage through its interaction with endothelial Tie2 receptor. *Cardiovasc Res*. 2008;78:572-80. doi: 10.1093/cvr/cvn048.

420. Hasanov Z, Ruckdeschel T, König C, Mogler C, Kapel SS, Korn C, Spegg C, Eichwald V, Wieland M, Appak S and Augustin HG. Endosialin promotes atherosclerosis through phenotypic remodeling of vascular smooth muscle cells. *Arterioscler Thromb Vasc Biol*. 2017;37:495-505. doi: 10.1161/ATVBAHA.116.308455.

421. Livak KJ and Schmittgen TD. Analysis of relative gene expression data using real-time quantitative PCR and the 2(-Delta Delta C(T)) Method. *Methods*. 2001;25:402-8. doi: 10.1006/meth.2001.1262.

422. Korn C, Scholz B, Hu J, Srivastava K, Wojtarowicz J, Arnsperger T, Adams RH, Boutros M, Augustin HG and Augustin I. Endothelial cell-derived non-canonical Wnt ligands control vascular pruning in angiogenesis. *Development*. 2014;141:1757-66. doi: 10.1242/dev.104422.